STUDIES IN MARINE PROPULSION

VIBRATION

by

DOUGLAS HECTOR NORRIE, B.E.(HONS.)., B.Sc.

Submitted to the Board of Research Studies at the University of Adelaide to fulfil the requirements for the degree of Doctor of Philosophy.

Department of Mechanical Engineering.

July, 1964.

TABLE OF CONTENTS

SUMMARY		i
STATEMENT BY AUTHOR		ii
ACKNOWLEDGEMENTS		iii
INTRODUCTION		1
PART I.	THE PROPULSION VIBRATION PROBLEM	5
Chapter 1.	The Propulsion Vibration Problem	6
PART II.	MODEL RESEARCH - THE RESEARCH WATER TUNNEL AND PROPELLER DYNAMOMETER	29
Chapter 2.	The Research Water Tunnel Facility	30
Chapter 3.	The Model Propeller Dynamometer	39
Chapter 4.	The Characteristics of the Dynamometer	44
Chapter 5.	The Analysis of Dynamic Records from the Dynamometer	59
PART III.	MODEL RESEARCH - THE VIRTUAL INERTIA OF PROPELLERS UNDER LOAD	69
Chapter 6.	The Importance of Virtual Inertia	70
Chapter 7.	The Ideal Hydrodynamic Mass and Inertia	72
Chapter 8.	Factors influencing the Actual Hydrodynamic Inertia of Propeller	78
Chapter 9.	Dimensional Analysis of the Propeller Virtual Inertia Problem	90
Chapter 10.	Experimental Methods for Determining the Virtual Inertia	98

Chapter 11.	The Experimental Equipment and Procedure	102
Chapter 12.	Hydrodynamic Inertia Results	112
Chapter 13.	Conclusions and Recommendations	130
PART IV.	FULL SCALE RESEARCH - EXPERIMENTAL EQUIPMENT AND TECHNIQUES	133
Chapter 14.	Strain-Gauge Instrumentation for Simultaneous Measurement of Torque and Thrust	134
Chapter 15.	The Development of a D.C.Strain-Gauge System for Ship Tail-Shaft Measurements	144
Chapter 16.	An Automatic Digital Curve Reader	156
Chapter 17.	The Digital Computer Programmes for the Analysis of Results-(Forced Vibration)	170
Chapter 18.	The Digital Computer Programmes for the Analysis of Results - Free and Resonance Vibrations	189
PART V.	FULL SCALE RESEARCH - MEASUREMENT OF FORCE FLUCTUATIONS AND VIRTUAL INERTIA OF PROPELLERS	194
Chapter 19.	The Scope of the Full-Scale Ship Tests	195
Chapter 20.	The Results of the Full-Scale Tests	199
Chapter 21.	Conclusions and Recommendations	215
PART VI.	RESEARCH ON LOW-VIBRATION PROPULSION	219
Chapter 22.	Research on Low-Vibration Propulsion	220
APPENDIX I.	THE STEADY TORQUE AND THRUST CHARACTERISTICS OF THE VARIABLE -PITCH PROPELLER	231

APPENDIX II. GRAPHICAL CONSTRUCTION FOR PROPELLER REYNOLDS NUMBER 232

APPENDIX III. DIMENSIONLESS COEFFICIENTS OF TORQUE AND THRUST FLUCTUATIONS 235

APPENDIX IV. STEADY - STATE PERFORMANCE OF SHIP B 239

APPENDIX V. PUBLICATIONS SUBMITTED AS ADDITIONAL EVIDENCE 240

BIBLIOGRAPHY iv

SUMMARY

This thesis describes the various investigations into aspects of the propulsion vibration problem, which have been carried out under the direction of the author in the Department of Mechanical Engineering at the University of Adelaide, over a period of almost seven years.

The various sections of the propulsion vibration project are briefly summarised below:-

(1) A survey of the literature, and correlation of the then available data.

(2) The development of the research water tunnel.

(3) The development of a propeller dynamometer for the water tunnel, to measure instantaneous torque and thrust.

(4) The determination of the virtual inertia of a propeller under various operating conditions, by model studies in the water tunnel.

(5) The development of a technique to measure propeller force fluctuations on full-scale ships.

(6) The measurement of propeller unsteady forces on full-scale ships under various conditions of operation.

(7) The determination of the virtual inertia of a propeller under full-scale conditions.

(8) The investigation of possible configurations of propulsion system which would have inherently low vibration characteristics.

STATEMENT

This thesis contains no material which has been accepted for the award to the author of any other degree or diploma by any University. To the best of the author's knowledge and belief, this thesis contains no material previously published or written by another person, except where due reference is made in the text.

(Signed)

D.H.Norrie

July, 1964.

ACKNOWLEDGEMENTS

The author wishes to gratefully acknowledge the assistance of the following during the course of the work described in this thesis:-

Professor H.H.Davis, Head of the Department of Mechanical Engineering, under whose general supervision the research described in this thesis has been carried out. Without his encouragement and help this work would never have been completed.

Professor F.B.Bull, Head of the Department of Civil Engineering, for encouragement and assistance on numerous occasions.

Dr.J.Mannam, Reader in Mechanical Engineering, for assistance on many occasions, particularly with the design and development of the slipring unit for the ship tests. Also for invaluable support as a member of the team which carried out the investigations on Ship B, during sea trials and a voyage around the coast of Australia.

Mr.W.D.Doble, Senior Lecturer in Mechanical Engineering, for valuable suggestions and discussions on the dynamics of the propeller dynamometer.

Mr.J.H.Fowler, Lecturer in Mechanical Engineering, for assistance with instrumentation for the ship tests, particularly with the design of the intercommunication system and the automatic digital curve reader. Also for major contributions in the analysis of the data from the ship tests, using numerical analysis and digital computer techniques. In particular, for the development of the data-preconditioning, the harmonic analysis and the Holzer analysis computer programmes.

Mr.R.Culver, Senior Lecturer in Civil Engineering, for co-operation and assistance on numerous occasions. In particular, for the procurement and installation in a below-ground pit of the 125 H.P.pumps and motors later incorporated in the research water tunnel.

Mr.M.R.Hale, post-graduate student, for assistance in development of the water tunnel and propeller dynamometer and for carrying out one of the early investigations on virtual inertia in the water tunnel. Mr.Hale was an invaluable member of the team which carried out the investigations on ship B, during sea trials. Also for co-ordinating the systematic taking of data from the records of the ship tests, and for assisting with the correlation of much of this data. In addition, for help with the digital computer programmes, particularly for the development of the magnetic-component correction programme. Mr.Hale is continuing the low-vibration propulsion research, having been engaged on this project since its commencement in early 1962. His has been a major contribution.

Mr.I.Flower, post-graduate student, for assistance in the systematic taking of data from the records of the ship tests, and for assisting with its correlation. In addition, for help with the digital computer programme, particularly for the development of the applied hydrodynamic force and the modified Holzer analysis programmes.

Mr.G.Morgan, post-graduate student, for assistance in the systematic taking of data from the records of the ship tests and for assisting with its correlation. Also for operation of the automatic

digital curve reader. In addition, for assisting Mr.J.H.Fowler with the development of the Holzer-analysis digital computer programme.

Mr.G.Jansen, post-graduate student, for assistance in the systematic taking of data from the records of the ship tests and for assisting with its correlation. Also for operation of the curve reader.

Mr.E.H.Watkins, who as a post-graduate student further developed the propeller dynamometer, almost to its present stage. The development of much of the equipment for the tests on Ship A was carried out by Mr.Watkins. The actual tests were carried out in collaboration with the author. In the final stages of the virtual inertia work on model propellers, Mr.Watkins, as a Consultant Engineer was responsible for the experimental work, and the computation of results, and without his services (and that of his team of assistants) large sections of the work would have remained uncompleted.

Mr.R.Miller, who as an under-graduate student carried out one of the early investigations on virtual inertia in the water tunnel.

Messrs. Pfitzner, Dollan,Phillips, and Sawley, who as graduates or as post-graduate students, acted as Technical Assistants under the supervision of Mr.E.H.Watkins and the author, to carry out the analysis of data, the computation of results, and the preparation of diagrams for the final stages of the virtual inertia work on model propellers.

Mr.A.E.R.Wood, who as a post-graduate student carried out further development of the research water tunnel. As a Director of Eilco, Mr.Wood in collaboration with Mr.I.Wall, was responsible for the electronic design and development of the automatic digital curve reader, and of the amplifiers and pre-amplifiers for the 8 - channel recorder.

Mr.I.Wall, Director of Eilco, who with Mr.A.E.R.Wood, was responsible for the electronic design and development of the automatic digital curve reader, and of the amplifiers and pre-amplifiers for the 8 - channel recorder.

Mr.R.Wright, of the Engineering and Water Supply Department of South Australia, who with the author, carried out the design of the closed-circuit configuration of the water tunnel and supervised its construction.

Mr.S.Attwood, until 1962, Supervisor of the Mechanical Engineering Workshop, for valued assistance with the manufacture of precision equipment.

Mr.R.Fitton, since 1962, Supervisor of the Mechanical Engineering Workshop, for valued assistance with the manufacture of precision equipment.

Mr.R.Schumann, Senior Technician, who was responsible for the design and development of much of the electronic equipment used on the project, Also for invaluable support as a member of the team which carried out the investigations on Ship B, during sea trials and a voyage around the coast of Australia. His help was indispensable and greatly valued.

Mr.R.Trueman, Laboratory Technician, who developed (and manufactured) much of the mechanical equipment used in the proje t. His help (and encouragement) was indispensable and highly valued.

Messrs.A.Syme and D.Morrison, Laboratory Technicians, for valuable assistance in the manufacture of equipment.

Mr.J.Mathieson, for the skilled preparation of many of the tracings in this thesis.

The author also wishes to gratefully acknowledge the work carried out in the Department of Mechanical Engineering by the following, which although carried out before the project described in this thesis, formed a basis on which to build:-

Mr.J.P.Duncan, Senior Lecturer in Mechanical Engineering (now Professor of Mechanical Engineering, University of Sheffield), for the first ship tests (on auxiliary - powered schooners in 1954)

Dr. P.O.A.L.Davies, Senior Lecturer in Mechanical Engineering, (now of the University of Southampton), for the design and early development of the open-circuit configuration of the water tunnel.

Mr.G.M.Tostevin, who as a post-graduate student, developed the first propeller dynamometer, further developed the open-circuit configuration of the water tunnel and carried out the first virtual inertia tests.

Grateful acknowledgement is made of the assistance and co-operation on numerous occasions of the management and staff of the following firms or public bodies, without whose assistance the project would not have been completed:-

The Broken Hill Proprietary Co.Ltd.

The Broken Hill Associated Smelters Proprietary Company Ltd.

The Engineering and Water Supply Department of South Australia.

The Electronics,Instruments and Lighting Proprietary Co.Ltd (Eilco)

The Both Equipment Company Ltd.

The Digital Machines Section of the Weapons Research Establishment

(Salisbury. S.A.)

The only persons who have submitted or who will be submitting for post-graduate degrees, material based on sections of the project described in this thesis, are the following :-

(1) E.H.Watkins, who in 1959 submitted a thesis for the degree of Master of Engineering, based on the design and development of the propeller dynamometer and entitled "Studies in Marine Propeller Vibrations". The author was Watkin's supervisor.

(2) M.R.Hale, who since early 1962 has been engaged, as a post-graduate student for the degree of Doctor of Philosophy, on low-vibration propulsion research. The work described by the author in the present thesis, on this low-vibration research, only covers the introductory work, and does not include any work carried out subsequent to early 1963. The author is Hale's supervisor.

INTRODUCTION

This thesis describes the various investigations into aspects of the propulsion vibration problem, which have been carried out under the direction of the author in the Department of Mechanical Engineering at the University of Adelaide, over a period of almost seven years.

When this research project was first begun, it was difficult to decide where to begin. The problem could be stated very briefly: "The vibration level in ships caused by the propeller is becoming excessive as the speed and power of ships is increasing, and needs to be reduced". The phenomena associated with the vibrations, however, are extremely complex, as will be seen later. At the commencement of the project, there was no way of deciding which of the many possible research avenues would prove rewarding, and which would turn out to be blind alleys. It was therefore decided to attack the problem on a broad front i.e. to pursue, concurrently, investigations into a range of selected aspects. As the picture became clearer, it was intended to concentrate on the more rewarding lines of investigation.

The various sections of the project (which are described in detail, later) are briefly summarised below:-

1. A survey of the literature, and correlation of the then available data.

2. The development of the research water tunnel.

3. The development of a propeller dynamometer for the water tunnel, to measure instantaneous torque and thrust.

4. The determination of the virtual inertia of a propeller under

various operating conditions, by model studies in the water tunnel.

5. The development of a technique to measure propeller force fluctuations on full-scale ships.

6. The measurement of propeller unsteady forces on full-scale ships under various conditions of operation.

7. The determination of the virtual inertia of a propeller under full-scale conditions.

8. The investigation of possible configurations of propulsion system which would have inherently low vibration characteristics.

It was also intended that towed-model tests be carried out on a model of the vessel which was tested under full-scale conditions. It was also proposed to obtain from mirror-image model tests of the same ship in a wind-tunnel, the wake profile in the plane of the propeller disc. This profile was then to be used in a calculation of the unsteady torque and thrust for correlation with the full-scale measurements. The towed model testing proceeded to the stage of developing a small-model towing tank, using what is believed to be a unique method of measuring the model resistance (Ref. 0.1). The ship model was manufactured, and some work was carried out on the determination of its resistance. A number of tests were carried out in the wind tunnel on the mirror-image model of the ship, and the results were used in an endeavour to determine a resistance form-factor for the vessel, in conjunction with the towed-model tests (Ref. 0.2,0.3,0.4). The other aspects of the research project were early found to be more extensive than originally envisaged,. however, and the towed-model and

mirror-image model tests were terminated at this preliminary stage, in order to concentrate on the remainder of the project.

The propulsion vibration project has now been in progress for a period of almost seven years. The various aspects of the research have all proved to be more extensive and complex than originally envisaged. Nevertheless, what has been accomplished is not greatly short of what was originally envisaged in the first phase of the investigation. That progress has been satisfactory despite the unexpected difficulties encountered is in considerable measure due to the support given to the project by those colleagues, undergraduate students, postgraduate students, technicians, and others who have taken part in the investigations over that period. At no time has there been fewer than three persons actively engaged on the project, and on several occasions the number has risen to as high as twelve. Tests have been carried out in three locations, as under:-

(1) Model tests in the Fluid Mechanics Laboratory of the Department of Mechanical Engineering, at the University of Adelaide.

(2) Full-scale investigations during the sea trials of two 19,000 ton capacity ore-carriers. The base for operations was at Whyalla, some 260 miles distant from Adelaide.

(3) Full-scale investigations during a 6,000 mile voyage of one of the ore-carriers, around the coast of Australia. The departure point was from Sydney, more than 900 miles distant from Adelaide.

The away-from-home tests were carried out by a team from the University of Adelaide varying in number from 3 to 4, led by the author, on expeditions varying in length from 1 1/2 to 3 1/2 weeks.

Under these circumstances, it would not only be untrue but also disloyal to state that the entire project was carried out by the author. It was rather, the work of a team which varied in size and composition over the period. The author freely and gratefully acknowledges the assistance which has been given often under difficult circumstances and at inconvenient times. A fuller acknowledgement is given elsewhere.

It is necessary to point out, however, that a not inconsiderable portion of the work was carried out personally by the author. In addition, the author was responsible for the initiation, direction and co-ordination of all phases of the project. He was also responsible for the correlation of the information obtained.

It may therefore be stated that the author is responsible for the work described in this thesis, and that this thesis may be properly submitted as evidence of work carried out towards the Degree of Doctor of Philosophy.

PART 1

THE PROPULSION VIBRATION PROBLEM

CHAPTER I

THE PROPULSION VIBRATION PROBLEM

1.1 INTRODUCTION

The first recorded reference to a fluctuating force being produced by a screw propeller is in John Bourne's treatise on screw propellers, published in 1845. Since that time, there has been an increasing number of references in the literature to the problems associated with such fluctuating forces.

Vibrations in ships can have two adverse effects; firstly on machinery, causing excess wear or failure, and secondly on personnel, inducing fatigue and loss of efficiency.

Until recently, the investigations associated with propeller vibrations had, perforce, emphasised the adverse effects on the various components of the propulsion system and hull of the vessel. There are many instances in the literature of failure to tail shafts due to excessive vibrational loads in the longitudinal, torsional or lateral directions, excited by the propeller forces. Failure of other components and excessive wear have also been recorded. Investigations showed that in almost every case the natural frequency of vibration of the component was of the same order as one of the exciting frequencies of the propeller, and the well-known phenomenon of mechanical resonance was occurring, with resulting excessive fluctuating stresses. Fortunately, the fluctuating propeller forces occur at discreet frequencies related to the shaft speed and number of propeller blades, and the solution to the problem is therefore to design the components in which trouble is likely to occur so that their natural frequencies are well away

from the frequencies of the exciting forces generated at normal operating speeds. In these days, calculations to ensure this are carried out as a routine matter for each new ship and the number of failures associated with propeller- excited vibrations has decreased to a very small percentage.

In recent years, however, the other aspect of vibration, that is, the adverse effect on personnel, has been steadily achieving increased prominence. Many ships now carry the equipment and instrumentation the performance and life of which can be impaired by excessive vibration. The level of vibration regarded as tolerable has thus been reduced in recent years. Unfortunately, over the same period, ship power, speed and size has been increasing, and this has resulted in increased levels of propeller exciting force. The vibration problem has thus been becoming increasingly acute and this trend can be expected to continue.

The prominence which the propulsion vibration problem has reached in recent times has been strikingly summarised by Voigt in Germany (Ref:1.1):- "Ever since the Second World War engine power has kept on increasing at an extraordinary rate in proportion to the size of ships, and as a result vibrations i.e. oscillations of the ship, have manifested themselves to an extent rarely observed in former times. Thus, vibrations have been called the latest fashionable disease of ships - - -. It is striking that in recent years, papers on vibrations have been presented in ever-increasing numbers at the meetings of foreign professional societies and that these reports indicate that extensive and costly investigations are being undertaken for the purpose of clearing up vibration problems. You may get an idea of the extent of these investigations by studying the

bibliography on ship vibrations". The bibliography (Ref. 1.2) referred to lists some 300 publications!

Investigations into various aspects of the ship vibration problem are proceeding in many establishments. These researches may be divided into the following groups:-

(a) Experimental investigations aimed at obtaining a better understanding of the physical phenomena which occur.

(b) The development of satisfactory theories so that the effect of changes in configuration can be estimated for any future design, and the levels of vibration which will occur can be calculated.

(c) Experimental investigations aimed towards obtaining, for design use, numerical data on the various parameters involved in the phenomena.

(d) Theoretical and experimental investigations of alternative propulsion systems which have inherently lower vibration levels.

1.2. RESEARCH ON PROPELLER VIBRATION

It is convenient to regard the fluctuating forces and moments associated with the propeller as being due to two separate mechanisms, operating independently, although in reality both mechanisms occur concurrently. Using this distinction the fluctuating (periodic) forces and moments can be divided into two groups; those in the first group having their origin in the variation of the wake, and those in the second group being caused by the movement of the pressure fields associated with the propeller blades. Forces in the first group are transmitted to the hull through the propeller shaft and are called bearing forces (and moments).

Those in the second group are transmitted directly to the hull surface by pressure forces and are known as surface forces (and moments). Many investigations are proceeding on various aspects of these two mechanisms, and on the effect of variations in various parameters on the forces in the two corresponding groups. Research in this field, up to the present is ably summarised in Ref: 1.3.

The aim of this research is directed towards ultimately being able to predict for a ship in the design stage, the frequencies and amplitudes of vibrations within the ship, at operating conditions. The corresponding stresses in the various members of the ship would then be calculable. The design could then be modified until the best compromise between all the factors was obtained. This desirable situation is still some distance off, but considerable progress has been made towards this end.

If the investigations concerned with forces (and moments) originating from wake variation are considered, the following general lines of approach may be distinguished:

(1) The measurement of wake distribution at the propeller disc from towed-model tests, by calculation, an estimate of the fluctuating forces and moments applied to the propeller is then obtained for a propeller of given shape. A reliable theory on which to base the calculation is clearly of importance.

(2) The development of more precise analyses by which the fluctuating forces and moments can be computed. These analyses are generally based on lifting-surface theories, using either line or surface-vortex methods.

(3) The verification of methods of calculating fluctuating forces and moments, by model tests with propellers operating in simple wake profiles (generated for example, by gauze patches - Ref: 1.4).

(4) The determination of the mechanical and hydrodynamic parameters involved in the phenomena.

Assuming that the hydrodynamic applied forces to the propeller can be calculated for any given design, it is necessary to know all the hydrodynamic parameters (such as virtual inertia, virtual mass, and damping) in order to calculate the dynamic behaviour of the shaft system. Research is therefore being carried out to relate these parameters with propeller configuration and operating conditions. It is also necessary to know the mechanical parameters which affect the vibration, such as the bearing and thrust-block damping, and rigidities.

(5) The measurement of fluctuating forces and moments on full-scale vessels. These tests can help provide interim design data. If sufficient configurations of ship and propeller are tested the resulting data when correlated should allow a reasonable prediction to be made of the fluctuating forces and moments applied to the propeller. Published reports of such tests often only give the fluctuating stresses in the tail shaft. It is very desirable for the fluctuating forces and moments applied to the propeller i.e. the applied hydrodynamic forces to be calculated and reported. In many cases, however, there are considerable difficulties in making reliable calculations (See Ref: 1.5).

In the research on pressure-field fluctuations the following lines of approach can be distinguished:

(1) The development of analytical methods of calculating the pressure field fluctuations under various conditions, both in the free-field case and in the presence of a body of known configuration.

(2) The measurement of the pressure field near propellers both at model - and full - scale.

Yet another approach to the problem of propeller vibration is the development of new types of propulsion system which would have inherently low vibration characteristics (Ref: 1.6).

1.3. THE ORIGIN OF THE VIBRATIONS

The vibrations which occur in a ship are due to exciting forces causing natural or forced vibrations of the hull and its contents. The exciting forces may be divided into those which are periodic and those which are transient, as shown in Fig. 1.1 .

The transient forces are associated with the seaway and the resultant unsteady motion of the ship. These forces can be of very high levels, the forces resulting when the hull "slams" into a heavy sea or when the propellers partly emerge from the water during rough conditions, being two examples.

The periodic forces are associated with either the propeller or the machinery of the ship. Such forces have a fundamental frequency proportional to the operating speed of the propeller or machine, with higher harmonics equal to multiples of this frequency. Vibrations

Fig. 1.1 Classification of ship vibration.

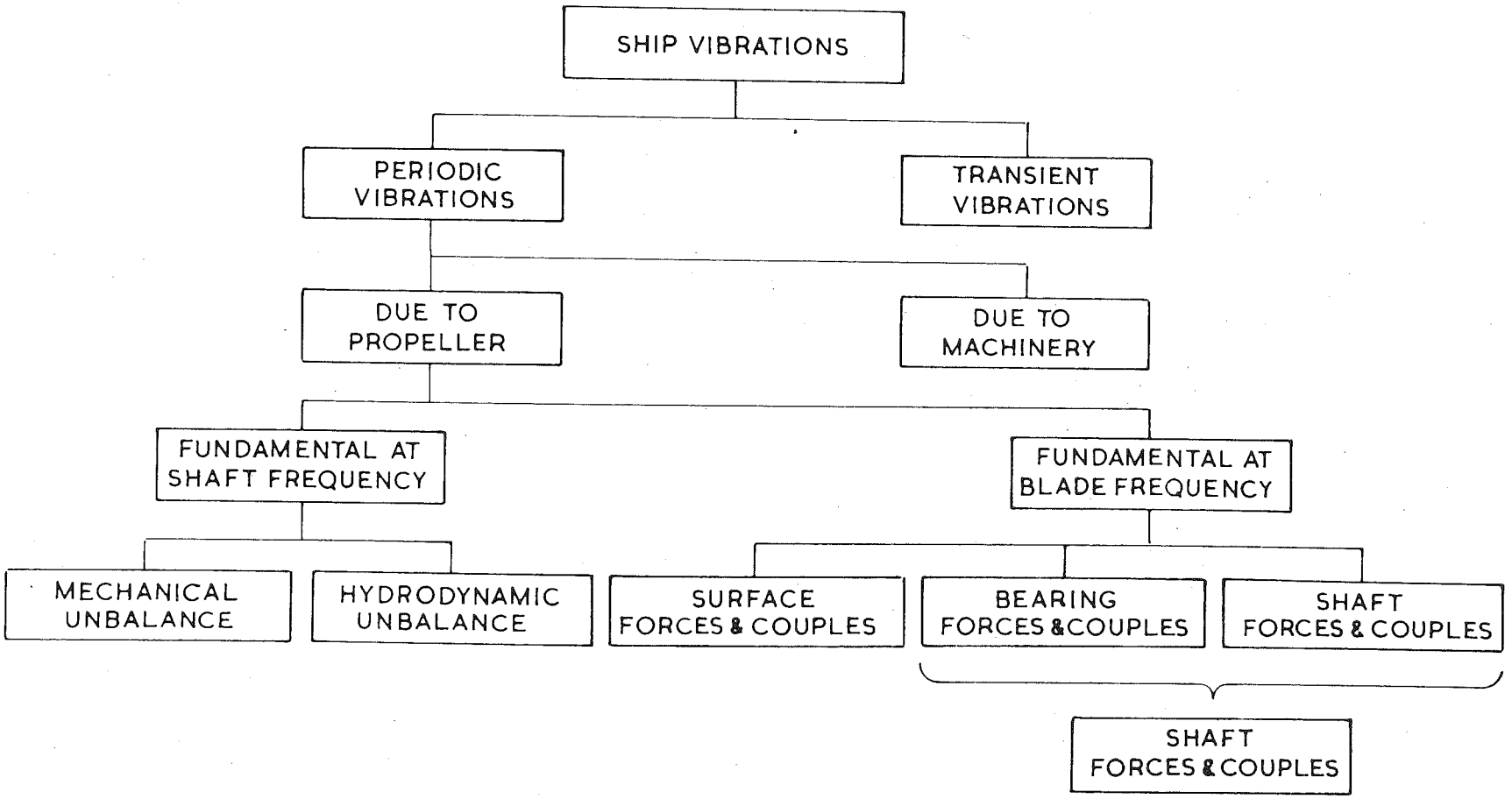
SHIP VIBRATIONS
PERIODIC VIBRATIONS
TRANSIENT VIBRATIONS
DUE TO PROPELLER
DUE TO MACHINERY
FUNDAMENTAL AT SHAFT FREQUENCY
FUNDAMENTAL AT BLADE FREQUENCY
MECHANICAL UNBALANCE
HYDRODYNAMIC UNBALANCE
SURFACE FORCES & COUPLES
BEARING FORCES & COUPLES
SHAFT FORCES & COUPLES
SHAFT FORCES & COUPLES

originating in machines are often due to static or dynamic unbalance.

Vibrations associated with the propeller may be divided into two groups. In the first group, the fundamental frequency is at shaft frequency, i.e. once per revolution. Such forces originate from either mechanical unbalance (static or dynamic) or hydrodynamic unbalance (due to each blade of the propeller not being identical). In the second group, the fundamental frequency is at blade frequency (number of blades times rotational speed).

Forces and moments in the second group may be arbitrarily divided on the basis of the mechanism of transmission to the hull, into "surface", "bearing", and "shaft", forces and moments. Surface forces and moments are those due to pressure forces on the hull surface. Bearing forces and moments are those transmitted to the ship via the propeller stern-tube bearing. Shaft forces and moments are those transmitted to the ship by the shaft after passing through the stern-tube bearing, and thus consists of an axial force and a torsional moment. An alternative classification of the second group retains the class of surface forces and moments as defined above, but groups the bearing and shaft forces (and moments) together under the heading "Shaft Forces and Moments". (Ref. Fig. 1.1)

It is often convenient to regard the fluctuating forces and moments associated with the propeller as due to two separate causes, although, in reality, both phenomena occur together and are inter-related. On this basis, the forces can be divided into two classes; those in the first class having their origin in the variation of the wake and those in the second class being caused by the presence of the hull after-body

(and appendages such as the rudder). These two classes will now be discussed separately.

1.3.1 Forces and Moments Originating from Wake Variation

These fluctuations are due to the propeller operating in a non-uniform flow stream, the wake of the vessel. This wake may be regarded as having two components, firstly, that due to the potential flow field around the ship, known as the potential wake, and secondly that due to the viscous forces acting in the boundary layer of the ship, called the frictional wake. Thus, because of the shape of the ship and the presence of viscosity, the velocity field at the propeller varies axially, radially and circumferentially. During rotation, therefore, an element of the propeller blading experiences a relative velocity which varies in magnitude and direction. The force on the element, in magnitude and direction, thus varies cyclically during each revolution. The sum of these blade-element forces, (when integrated over the whole propeller), can be resolved into component forces in three mutually perpendicular directions, and moments about these axes. These component forces and moments vary cyclically, with a periodicity of one revolution. The fundamental frequency is at blade frequency (number of blades times shaft speed) with higher harmonics of multiples of this frequency.

In general, the greater the assymetry of the wake, the larger will be the fluctuations in the forces and moments. The degree of

assymetry of the wake is dependent on the shape of the after-body of the ship and the position of the propeller in relation to the hull. If the vessel has more than one propeller, the shape and position of the stern brackets of A-frames, and the relative positions of the propellers, also influence the wake. When the vessel is turning, the wake pattern in the vicinity of the propeller disc changes considerably and the fluctuations in the forces and moments may be greatly increased, depending upon the amount of side slip, the position of other propellers, and the angle of the rudder.

As an example of the effect of after-body shape, the wake distribution behind a typical "V" section after-body and a typical "U" section after-body is shown in Fig. 1.2. It will be seen that in both cases (and this generally true for all single-screw configurations) there is a minimum wake velocity in the vertical positions above and below the propeller, at 6° and 180°. As a propeller blade passes through these positions, the angle of incidence of the relative velocity will thus increase, and the left force on blade elements will increase correspondingly. There will thus be a maximum in the resultant force on a blade at approximately 0° and 180°. If the propeller has an even number of blades, the maxima of blade forces for opposite blades will thus be in phase. Certain of the resulting propeller vibratory forces (e.g. thrust) will therefore be proportionately greater in this case than for a propeller with

Fig. 1.2 (a,b,c) Velocity variation over the propeller disc, for V- and U- shaped afterbodies. The numerical values give the local velocities, relative to the propeller disc, as a percentage of ship speed.

(Adapted from Ref. 1.7)

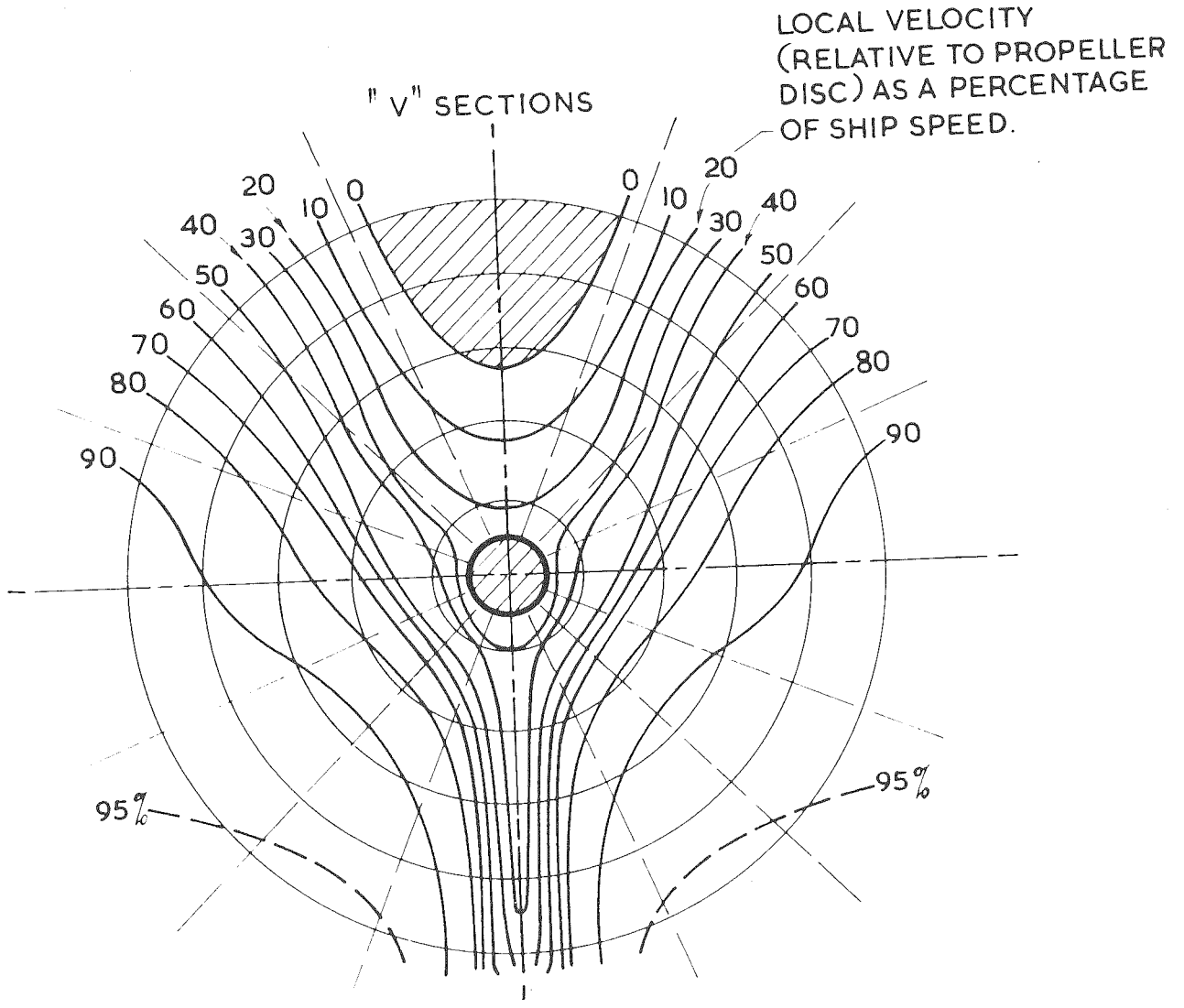
LOCAL VELOCITY
(RELATIVE TO PROPELLER
DISC) AS A PERCENTAGE
OF SHIP SPEED.
" V" SECTIONS
0
10
20
30
40
50
60
70
80
90
95%

(a)

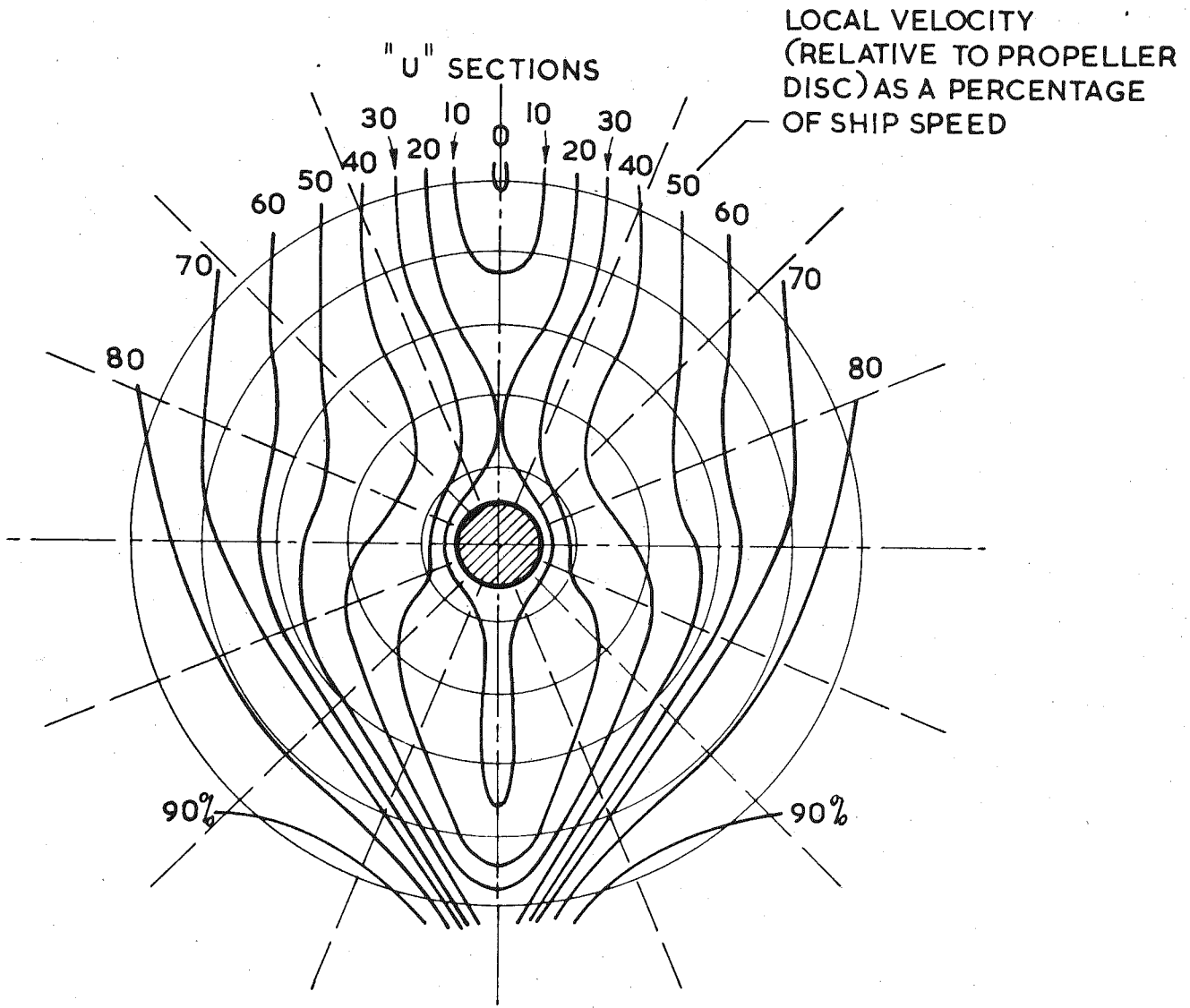
"U" SECTIONS
LOCAL VELOCITY (RELATIVE TO PROPELLER DISC) AS A PERCENTAGE OF SHIP SPEED
0
10
10
20
20
30
30
40
40
50
50
60
60
70
70
80
80
90%
90%

(b)

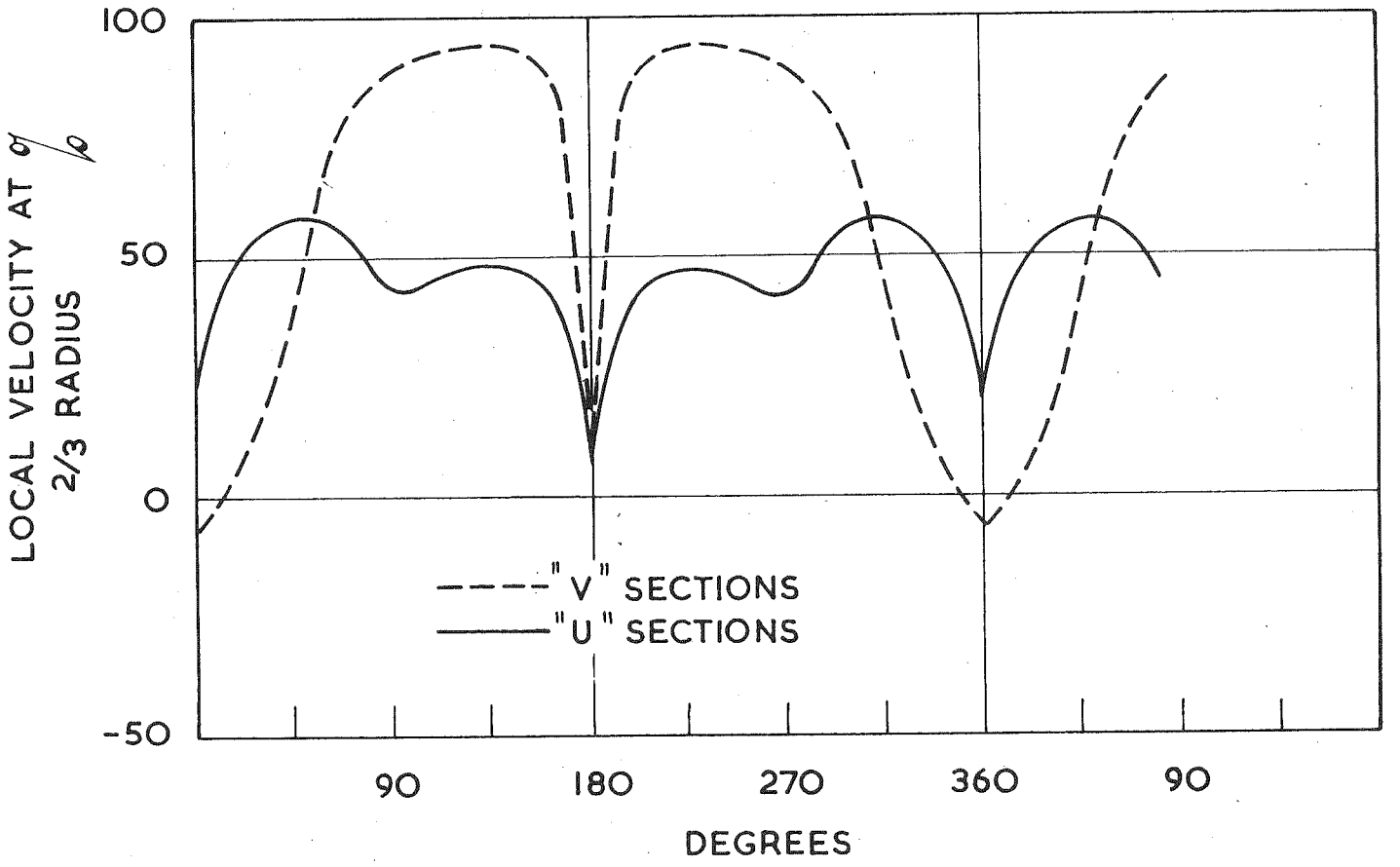
100
50
0
-50
LOCAL VELOCITY AT 2/3 RADIUS
"V" SECTIONS
"U" SECTIONS
90
180
270
360
90
DEGREES

(c)

an odd number of blades. This phasing effect is slightly modified depending on the skew and rake of the propeller blades.

The varying forces on each blade element can excite the blades themselves into various complex modes of vibration. These vibrations help to induce localised cavitation on the blades, especially those which are heavily loaded and located near the surface of the water. When cavitation of this type exists, it generates very-high-frequency vibrations which are usually insignificant, in so far as stresses are concerned, although the noise may be troublesome. Since in large prototype propellers, the natural frequencies of the various modes of vibration of the blades themselves are very high, compared with the natural frequency of the shaft system, this type of blade vibration does not have an appreciable effect on the dynamics of the complete system. In model studies, however, this effect can be significant and alter the characteristics of the system considerably.

1.3.2 Forces and Moments Originating from the Presence of the After-body and Appendages.

Associated with each blade of the propeller is a pressure and velocity field which rotates with the blade, and which varies as the blade force changes. If there is a solid surface near the rotating propeller, its presence will cause the pressure and velocity field to vary slightly as the blade changes its distance from the body during rotation. The effect will be greatest when the blade is in close proximity to the body. This small change in the pressure and velocity field due to the presence of the body

means a corresponding change in propeller force.

As each blade and its pressure field rotates around the shaft axis, the intensities of pressure at points on the nearby body will change. The resultant force on the body, obtained by integration of the surface pressure forces, will therefore vary in position, magnitude and direction as the propeller blades rotates. The total surface force due to the whole propeller will clearly be cyclic. It will have a fundamental frequency equal to blade frequency, and higher harmonics equal to multiples of the blade frequency.

1.4. THE LEVELS OF SHIP VIBRATIONS AND THEIR EFFECTS ON PERSONNEL.

Presented in Table 1.1 are results collected from various sources of the force and moment fluctuations for a variety of ship and propeller configurations. The predominant influence of after-body shape on the magnitude of the fluctuations will be clearly seen. It will also be noted that, on the model scale at least, the use of a wake-adapted propeller* reduces the magnitude of the fluctuations very considerably. Even for the most favourable configurations, however, it will be seen that the magnitude of fluctuations is still comparatively large.

* (A wake-adapted propeller is one which has been designed on the basis of a known wake distribution at the propeller, obtained from model tests. The shape and incidence of each blade element are chosen so that the best performance compromise is obtained as the blade element sweeps around its circumferential path passing through the known variation of relative velocity.)

Further information on the magnitude of the fluctuations is given in Table 1.2, for surface and bearing forces. It will be noted that the surface and bearing forces are of approximately equal magnitude.

Table 1.3 presents data on the frequency and amplitude of the vertical and athwartships vibrations for a number of vessels, mainly those for military application. It will be noted that in exceptional cases the vibration amplitude at the stern is equivalent to 1-2 millimetres. Even larger amplitudes have been recorded, one well-known passenger liner having amplitudes at the stern of 2-3 millimetres.

The effect of number of propeller blades on the type and magnitude of the vibrations is indicated in Table 1.4. In this table is shown a comparison of the vibration forces at both fundamental and second harmonic of blade frequency, for four and five-bladed propellers. It will be seen that although the four-bladed propeller has more severe torque and thrust fluctuations than the five-bladed propeller, it has very much smaller bending fluctuations.

Whether a certain vibration level is regarded as acceptable or not will depend upon the criterion used. This criterion will depend upon the use to which the ship is put, military applications usually allowing higher vibration levels than civilian uses. One set of criteria based on a single parameter, displacement amplitude is given in Table 1.5.

More refined criteria for vibration limits are available, based on two parameters, either acceleration and frequency, or amplitude and frequency. One set of such criteria in terms of allowable acceleration against frequency is shown in Fig. 1.3.

Fig. 1.3 Vibration tolerance criteria. Peak accelerations at which subjects perceive vibrations (I); find it unpleasant (II); or refuse to tolerate it further (III). The shaded areas are one standard deviation on either side of the mean. These curves are for subjects without any protection, exposure time 5-10 minutes. The short term tolerance curve is for subjects with standard U.S.Air Force lap belt and shoulder harness, exposure time approximately one minute. The Military Aircraft Tolerance Curve is used as the criterion for long term exposure in military aircraft.

(Adapted from Ref. 1.8)

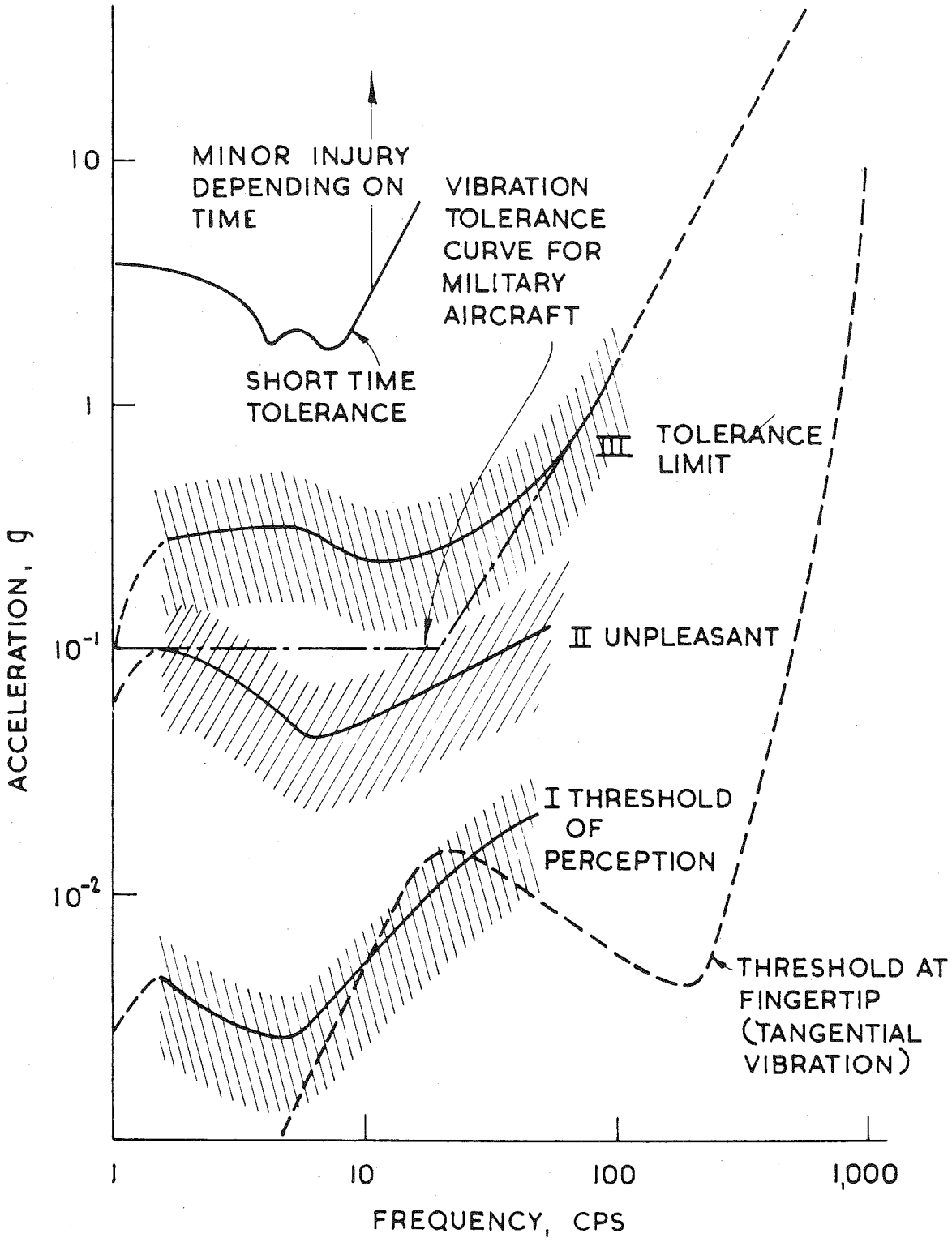
10
1
10^{-1}
10^{-2}
ACCELERATION, g
MINOR INJURY DEPENDING ON TIME
VIBRATION TOLERANCE CURVE FOR MILITARY AIRCRAFT
SHORT TIME TOLERANCE
III TOLERANCE LIMIT
II UNPLEASANT
I THRESHOLD OF PERCEPTION
THRESHOLD AT FINGERTIP (TANGENTIAL VIBRATION)
1
10
100
1,000
FREQUENCY, CPS

TABLE 1.1 VIBRATION EXCITING FORCES AND MOMENTS

SHIP	MODEL OR PROTOTYPE	PROTOTYPE						Number of Propellers	Blades per Propeller	* $\frac{\Delta T}{T}$ %	ϕ $\frac{\Delta Q}{Q}$ %	Vertical Force (Surface) % of mean thrust +	Athwartships Force (Surface) % of mean thrust +	Couple (About Prop. Axis % of mean torque +	REFERENCE	REMARKS
		Length (between Perpendiculers)	Displacement	S.H.P.	R.P.M.	Thrust (Ton)	Speed (kt)									
Mariner Model 4144	M	528ft	18,610 ton	13,180	96	85.5	20	1	4			6	16	70	1.10	Dry Cargo Ship
"Gopher Mariner"	M	528	18,610 tons	-	95	-	-	1	4			8			1.10	" "
	P	528	18,610 tons	-	95	-	-	1	4			1			1.10	" "
"Old Colony Mariner"	M	528ft	18,610 tons		103		21.3	1	4			10			1.10	" "
	P	528ft	18,610 tons		100		21.3	1	4			7			1.10	" "
"President Hoover	M							2	3		3.2	12.5			1.11	" "
	P										3.3				1.11	" "
Single Screw Vessel	M						14	1	4	16.0	7.4				1.12	Identical models but different measuring techniques.
	M						14	1.	4	16.8	10.2				1.12	

TABLE 1.1 VIBRATION EXCITING FORCES AND MOMENTS

SHIP	MODEL OR PROTOTYPE	PROTOTYPE						Number of Propellers	Blades per Propeller	* $\frac{\Delta T}{T}$%	ϕ $\frac{\Delta Q}{Q}$ %	Vertical Force (Surface) of mean thrust +	Athwartships Force (Surface) % of mean thrust +	Couple (About Prop. Axis % of mean torque +	REFERENCE	REMARKS
		Length (between Perpendiculers)	Displacement	S.H.P.	R.P.M.	Thrust (Ton)	Speed (kt)									
"Hadrian"	P	215 m	60,119 c.m.		103	145	17.5	1	4	7-8	3.8				1.13	Tanker (A.G. Weser Cigar shape stern)
Series 60 Models																
Extreme U-Section	M	400ft		96%			17.5	1	4	20.0					1.14	
Moderate U-section	M	400ft		100%			17.5	1	4	14.6					1.14	Parent model Power = 100%
Extreme V-section	M	400ft		96%			17.5	1	4	13.5	-				1.14	
Tanker Model series			39,000 ton d.w													
Extreme U-section III	M	205.5m		102%	108	139	16	1	4	22	11				1.13	

(Continued)

TABLE 1.1 VIBRATION EXCITING FORCES AND MOMENTS

SHIP	MODEL OR PROTOTYPE	PROTOTYPE						Number of Propellers	Blades per Propeller	* $\frac{\Delta T}{T}$ %	ϕ $\frac{\Delta Q}{Q}$ %	Vertical Force (Surface) % of mean thrust +	Athwartships Force (Surface) % of mean thrust +	Couple (About Prop. Axis % of mean torque +	REFERENCE	REMARKS
		Length (between Perpendiculars)	Displacement	S.H.P.	R.P.M.	Thrust (Ton)	Speed (kt)									
Moderate U - Section I	M	205.5m	39,000 ton d.w	100%	110	133	16	1	4	18	16				1.13	Parent model Power = 100%
Extreme V- Section II	M	"	"	106%	112	133	16	1	4	20	10				1.13	
Parent with Hogner Stern IV	M	"	"	103%	108	145	16	1	4	16	5				1.13	
III + Wake Adapted propeller	M	"	"	101%			16	1	4	9	2				1.13	
I + Wake Adapted Propeller	M	"	"	101%			16	1	4	6	3				1.13	

(Continued)

TABLE 1.1 VIBRATION EXCITING FORCES AND MOMENTS

SHIP	MODEL OR PROTOTYPE	PROTOTYPE						Number of Propellers	Blades per Propeller	* $\frac{\Delta T}{T}$ %	ϕ $\frac{\Delta Q}{Q}$ %	Vertical Force (Surface) % of mean thrust +	Athwartships Force (Surface) % of mean thrust +	Couple (About Prop. Axis % of mean torque	REFERENCE	REMARKS
		Length (between Perpendiculars)	Displacement	S.H.P.	R.P.M.	Thrust (Ton)	Speed (kt)									
II + Wake Adapted Propeller	M	205.5m	39,000 ton d.w	103%			16	1	4	6	3				1.13	
III + Propeller nozzle	M	"	"	101%			16	1)	4	16	12				1.13	

* peak-to-peak Thrust fluctuations, as a percentage of mean thrust.

ϕ peak-to-peak Torque fluctuations, as a percentage of mean torque.

\+ 1/2 (peak-to-peak fluctuations)

TABLE 1.2 - BEARING AND SURFACE FORCE FLUCTUATIONS ON A SINGLE - SCREW PROTOTYPE SHIP AS DETERMINED FROM A MODEL STUDY

(Adapted from Ref: 1.10)

SHAFT SPEED REV/MIN.	93	93	93
SHIP VELOCITY kt	16.9	20.0	23.0
MEAN SHAFT THRUST lbf	221,000	169,000	112,000
MEAN SHAFT TORQUE lbf-ft	840,000	677,000	497,000
TRANSVERSE FORCE			
Surface	23,800	18,000	21,000
Bearing	16,500	16,000	15,000
* Total	28,000	26,000	35,500
TRANSVERSE FORCE (% of total)			
Surface	85	69	59
Bearing	69	61	42
VERTICAL FORCE lbf			
Surface	9,500	4,500	6,500
Bearing	5,500	6,000	7,000
* Total	7,500	11,000	14,000
VERTICAL FORCE (% of Total)			
Surface	126	41	46.4
Bearing	73	54.5	50
COUPLE (ABOUT PROPELLER SHAFT) lbf-ft			
Surface	320,000	430,000	650,000
Total	680,000	420,000	1,020,000

(Continued)

TABLE 1.2 - BEARING AND SURFACE FORCE FLUCTUATIONS ON A SINGLE-SCREW PROTOTYPE SHIP AS DETERMINED FROM A MODEL STUDY

(Adapted from Ref: 1.10)

SURFACE COUPLE (% of Total)	47	102	64
FORCES AS % OF MEAN THRUST			
Transverse			
Surface	10.8	10.6	18.8
Bearing	7.5	9.45	13.4
Total	12.7	15.4	31.7
Vertical			
Surface	4.3	2.66	5.8
Bearing	2.5	3.56	6.25
Total	3.4	6.5	12.5
Total COUPLE AS % OF THE MEAN TORQUE	38.1	62.1	205

* Total Force = Surface Force + Bearing Force + Force on Rudder (Vectorial addition)

ϕ Total Couple = Surface Couple + Couple on Rudder (Vectorial addition)

N.B. Values of vibratory forces and couples are for peak-to-peak fluctuations.

TABLE 1.3 - HULL VIBRATION FREQUENCIES & AMPLITUDES (MEASURED VALUES)
(Adapted from Reference 1.8)

TYPE OF SHIP	NO. OF PROPS.	BLADES PER PROP.	LOCATION	SHAFT SPEED REV/MIN (NOMINAL)	VERTICAL VIBRATION		LOCATION	SHAFT SPEED REV/MIN (NOMINAL)	ATHWARTSHIP VIBRATION	
					FREQUENCY C/min	DISPLACEMENT AMPLITUDE, in			FREQUENCY c/min	DISPLACEMENT AMPLITUDE IN
Ammunition ship, maritime hull No.MC1575	1	4	Stern	95 45	95* 105-110+	0.014 0.013	Stern	40	40*	0.025
Refrigeration ship, maritime hull No. MA 36	1	4	Stern	100	400+	0.018	Stern	37	148+	0.019
Icebreaker	2	3	Stern	95	285+	0.040	-	-	-	-
Destroyer	2	3	-	-	-	-	Stern	180 240	540+ 240*	0.007 0.028
DESTROYER	2	4	Stern	220 310 240 60	74‡ 310* 960+ 461ϕ	0.180 0.021 0.004 0.002	Stern	300 123 310	120‡ 123* 1,300+	0.134 0.033 0.003

TABLE 1.3 - HULL VIBRATION FREQUENCIES & AMPLITUDES (MEASURED VALUES)
(Adapted from Reference 1.8)

TYPE OF SHIP	NO. OF PROPS.	BLADES PER PROP.	VERTICAL VIBRATION				ATHWARTSHIP VIBRATION			
			LOCATION	SHAFT SPEED REV/MIN (NOMINAL)	FREQUENCY C/min	DISPLACEMENT AMPLITUDE, in	LOCATION	SHAFT SPEED REV/MIN (NOMINAL)	FREQUENCY C/min	DISPLACEMENT AMPLITUDE in
Aircraft carrier	4	5	Stern	160	160*	0.008	Stern	165	165*	0.010
				153	765+	0.005		165	825+	0.003
			Island	153	153	0.003	Island	115	575+	0.002
				150	750+	0.002				
Heavy cruiser	2	4	Stern	330	60‡	0.009	Stern	300	90‡	0.017
				280	1,120*	0.002		300	1,200+	0.002

NOTE: * shaft frequency
+ blade frequency
ϕ double blade frequency
‡ hull natural frequency

TABLE 1.4

COMPARISON OF VIBRATION MAGNITUDES

FOR 4 - BLADED AND 5 - BLADED PROPELLERS

(Adapted from Ref. 1.15)

TYPE OF VIBRATION		4 - BLADES						5 - BLADES					
		Single-screw			Multi-screw			Single-screw			Multi-screw		
		L	M	S	L	M	S	L	M	S	L	M	S
HULL	Vertical			4N		4N			5N 10N			5N	
	Athwart-ships			4N			4N			5N 10N			5N
SHAFT	Torsional	4N		8N		4N				5N 10N			5N
	Axial	4N	8N			4N				5N 10N			5N
	Bending			4N			4N	5N		10N		5N	

L = Large M = Medium S = Small

N.B. N is the shaft speed in rev/min. The fundamental and second harmonic frequencies for the four and five-bladed propellers are 4N and 8N, 5N and 10N respectively.

TABLE 1.5

VIBRATION DISPLACEMENT CRITERIA

RATING	HULL DISPLACEMENT AMPLITUDE (AT SHAFT OR PROPELLER BLADE FREQUENCIES)
Excellent	Less than 0.010 in.
Satisfactory	Less than 0.020 in.
Unsatisfactory	Greater than 0.020 in.

In Fig: 1.4 is presented a set of curves based on vibration tests on more than 100 ships, and on comments from the persons on board. The limit of permissible vibrations shown on this curve, in terms of amplitude versus frequency, corresponds to the vibration level above which most people would feel irritated or annoyed. The author of the paper from which Fig: 1.4 is taken, Professor E.A.Kjaer, has defined a vibration-factor which may be used in conjunction with this curve. This vibration-factor is defined as the ratio of the actual amplitude to the maximum permissible amplitude as determined from Fig: 1.4, at the same frequency. Values of vibration-factor less than 1 are satisfactory, greater than 1 are unsatisfactory. In the same paper, Kjaer showed that in many cases, in ships, the vibration-factor considerably exceeds 1.

Fig. 1.4 Permissible vibration level on ships.

(Adapted from Ref. 1.9)

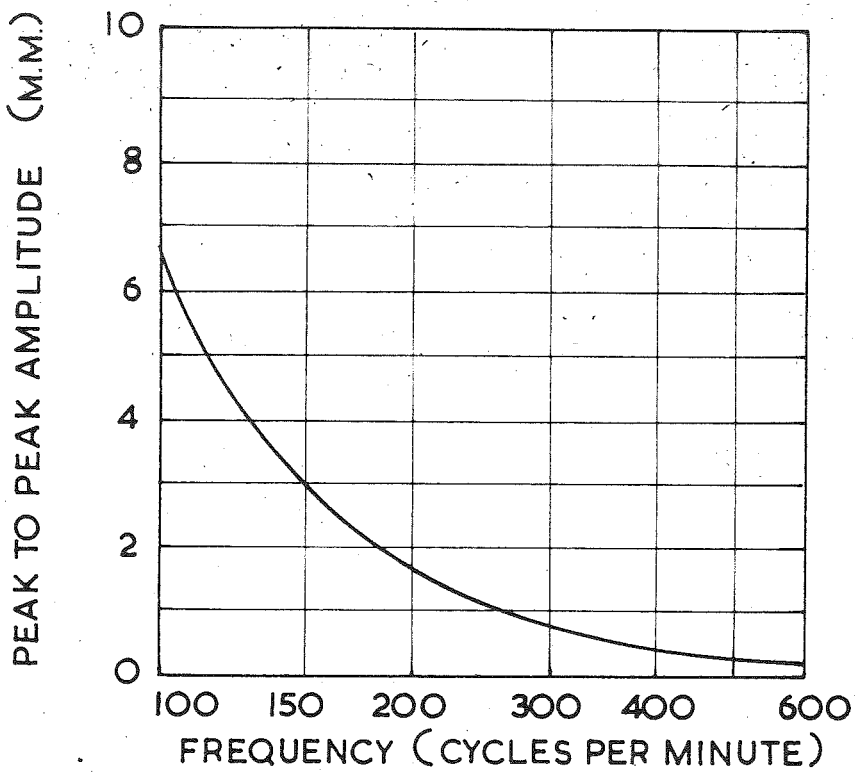
PEAK TO PEAK AMPLITUDE (M.M.)
10
8
6
4
2
0
100
150
200
300
400
600
FREQUENCY (CYCLES PER MINUTE)

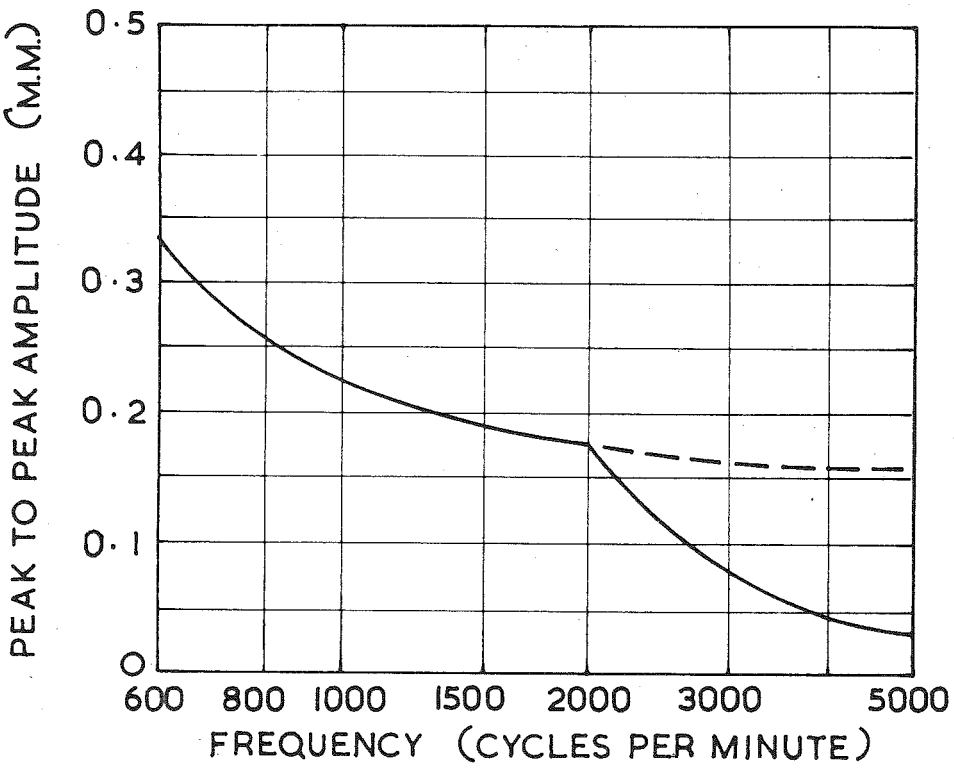
PEAK TO PEAK AMPLITUDE (M.M.)
0·5
0·4
0·3
0·2
0·1
0
600
800
1000
1500
2000
3000
5000
FREQUENCY (CYCLES PER MINUTE)

PART II

MODEL RESEARCH -

THE RESEARCH WATER TUNNEL

AND

PROPELLER DYNAMOMETER

CHAPTER 2

THE RESEARCH WATER TUNNEL FACILITY

2.1 INTRODUCTION

In 1951-2, Dr. P.O.A.L.Davies, then Senior Lecturer in the Department of Mechanical Engineering, proposed that the Department should build a research water tunnel suitable both for submerged model studies in a "full" working section, and for research on surface phenomena using an open-channel working section. The original proposal was for an open-circuit tunnel, i.e., of the non-circulating type, supplied from a gravity feed tank. The design of the tunnel (Ref. 2.1) was completed in 1953 by Dr. Davies and construction was begun in late 1953. The tunnel was in operation in the open-circuit configuration, fitted with a working section of circular cross-section by early 1955. Since that time a number of research investigations have been undertaken in the tunnel. Most of these have used a "full" working section, although a partly-full working section has been used on occasions when a flow with a free surface has been required.

Although the velocity profile in the working section, and the flow stability, were very satisfactory with the tunnel in the open circuit configuration, the maximum working section velocity was limited to 8 ft/s. Proposals were therefore put forward to convert the tunnel to a closed-circuit configuration, with a higher working section velocity. In 1957 Mr. R.Culver, of the Department of Civil Engineering, procured and installed in a below ground pit two 125- h.p. centrifugal pumps and motors. In early 1961, the author, with the collaboration of Mr.Culver, and Mr.R.Wright

of the Engineering and Water Supply Department of South Australia, completed the design for a closed-circuit configuration incorporating these pumps. Modifications to convert the tunnel to this configuration were begun in late 1961 and continued until May, 1963, the work being carried out in stages during period of minimum research activity. The tunnel was in operation in the new form by June, 1963.

2.2. THE WATER TUNNEL FACILITY (OPEN-CIRCUIT CONFIGURATION)

2.2.1 General Description:

The general arrangement of the tunnel in the open-circuit configuration is shown in Fig: 2.1. Water was supplied by three pumps with a total capacity of 15 cusecs to an elevated constant-head supply tank. From the tank, the flow was through a supply main, a stilling section, a 16 : 1 contraction, and an 18 in. dia. working section, finally discharging through a draft tube into the laboratory sump. (A description of the design of the circuit is given in Ref: 2.1) The potential energy of the water in the supply tank was converted to kinetic energy in the supply main, a portion of this kinetic being reconverted to pressure energy in the diffuser before the fluid entered the stilling-section. The stilling tank was designed to have above the water-surface a space, filled with air, the pressure of which could be controlled. The level of the free surface was fixed by a number of weirs, which under normal conditions carried about 10 per cent of the input flow. Three wire-mesh screens were fitted at the diffuser exit and four within the stilling tank, to reduce turbulence in the working section to a low value. The screens at the

Fig. 2.1 General arrangement of open-circuit configuration of research water tunnel.

(Adapted from Ref. 2.1)

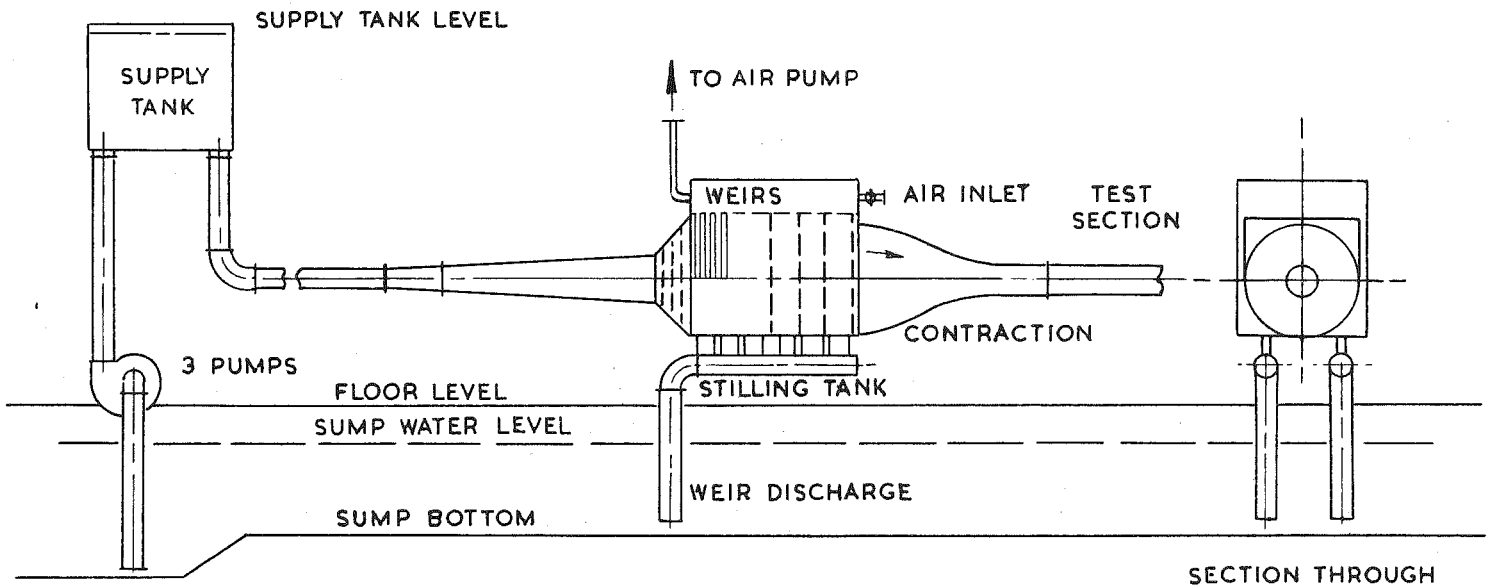

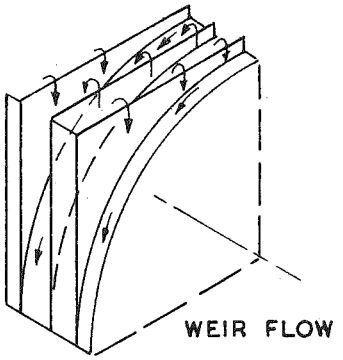

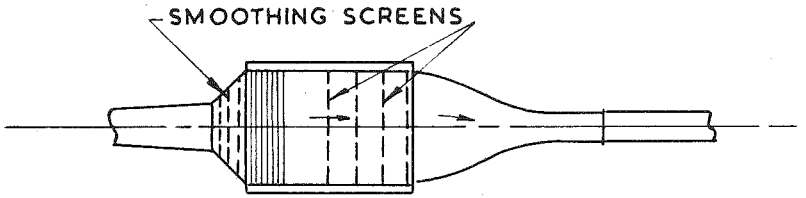

PLAN

5 0 5 10

FEET

diffuser exit also allowed a wide-angle flare to be used in this region without separation occurring, thus reducing the diffuser length. Water was accelerated from the stilling tank through the contraction to the working section, an area contraction ratio of 16 : 1 being used to reduce further the turbulence level in the working section.

The velocity in the working section depended only on the head difference between the contraction entrance and the draft tube exit. Since the water levelsat these stations were fixed, the head difference was determined only by pressure in the air space. A constant pressure was maintained in the air space by pumping from it at a constant rate with an ejector pump and allowing air to flow into it from the atmosphere through a variable constriction. The area of the constriction therefore controlled the air pressure in the air space, and under these conditions velocity control was obtained with a single variable.

2.2.2 Method of Achieving a Uniform Velocity Profile and Low Turbulence.

The use of screens and a large stilling tank enabled a flow of high uniformity to be obtained at the contraction entrance. The contraction was designed so that this uniformity would be preserved as far as possible in the flow into the test section. In a large contraction, there is a tendency for the boundary layer to separate near the start of the contraction, with subsequent increase in stream turbulence and non-uniformity of velocity profile. This

difficulty has received some attention in the literature, and in the present case the design method of Batchelor and Shaw (Ref. 2.2) was used. The pressure gradient along the contraction boundary was determined on the basis of potential flow. This pressure gradient is shown in Fig. 2.2, together with that for a conical diffuser of 7^{o} included angle. On the basis of these results, it was considered that separation at the start of the contraction would be most unlikely. This was subsequently borne out by tests on the contraction when the tunnel was in operation.

To ensure a low level of turbulence in the working section, the stilling chamber was fitted with spaced wire-mesh smoothing screens, followed by a contraction of large area-ratio (16:1). It was calculated by the method of Taylor and Batchelor (Ref. 2.3) that the magnitude of transverse disturbances passing through this screen system would be reduced by a factor of 1/9th. Screens were also used near the diffuser exit.

2.2.3 Method of Achieving Constant Velocity with Time

Flow variations in the supply main were reduced very considerably by the weir system, as is shown by the following argument. Suppose the supply main to slightly increase its flow. This would cause a small rise in head across the weirs, which, although of small absolute magnitude, would be large in relation to the pre-existing head on the weirs, thus causing a considerable flow increase over the weirs. The small change in weir head, however, would cause a negligible increase in head across the contraction, and the increase in test section flow would be correspondingly

Fig. 2.2 Contraction boundary pressure gradient

(From Ref. 2.1)

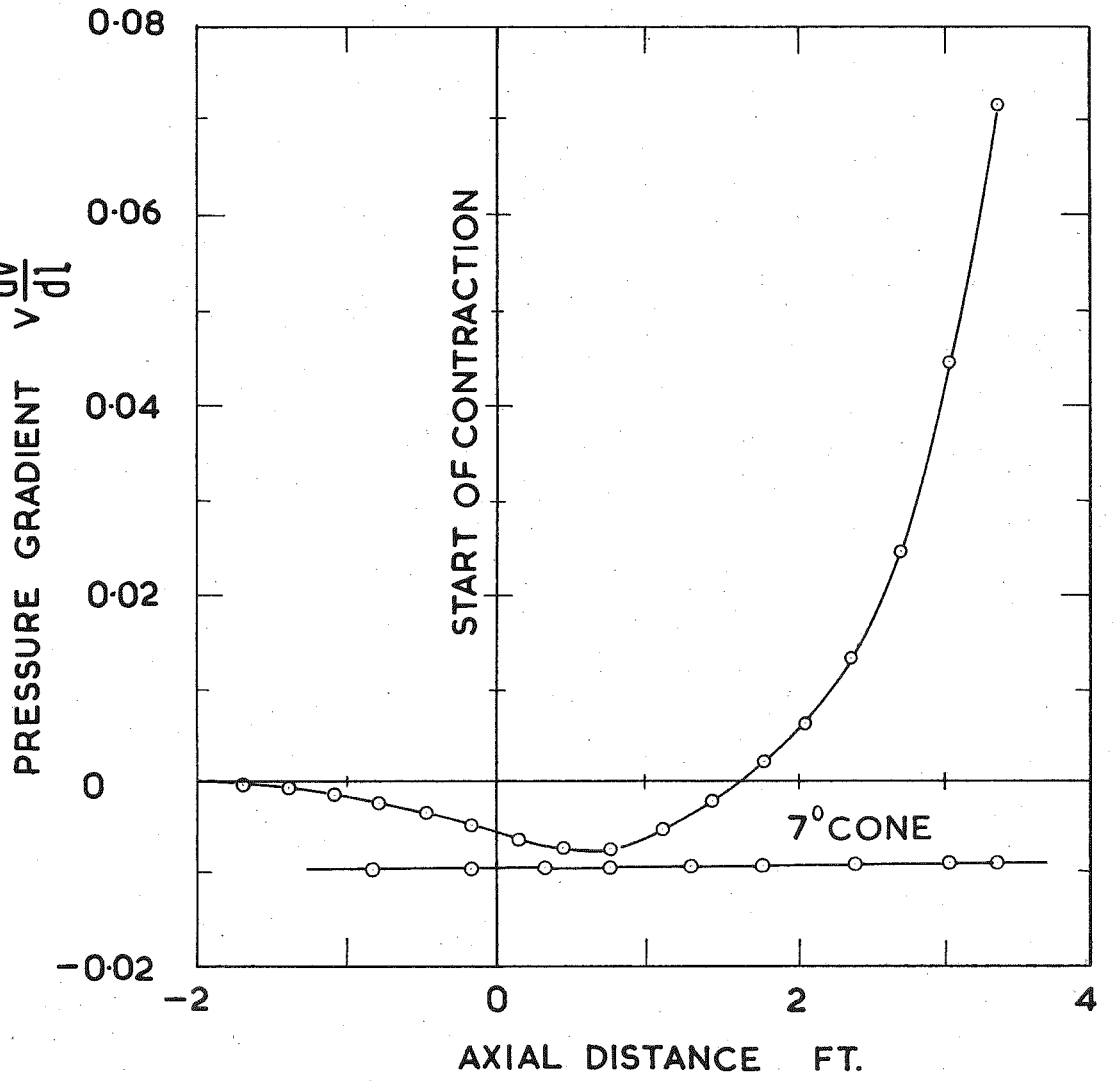
0·08
0·06
0·04
0·02
0
−0·02
PRESSURE GRADIENT $v\frac{dv}{dl}$
START OF CONTRACTION
7° CONE
−2
0
2
4
AXIAL DISTANCE FT.

small. A decrease in supply-main flow can similarly be shown to cause a considerable decrease in weir flow but a negligible decrease in the test section flow. Flow fluctuations in the supply main thus cause substantial variations in the waste flow over the weirs, while the working section velocity remains substantially constant.

The above argument is expanded in mathematical form in Ref: 2.1, where it is shown that the attenuation of flow disturbances by a weir system increases with the total length of the weirs. In the Adelaide tunnel, the total length of weirs was 204ft., made up of 34 weirs each 6 ft long across the stilling chamber. It should be noted that the analysis in Ref: 2.1 was based on the assumption that the flow over the weir was proportional to the 3/2 power of the head above the weir. For the sheet metal weirs used in the Adelaide tunnel, however, it was found experimentally (Ref: 2.4) that the flow followed the law:

$$Q = 1.06(h - 0.0108) \text{ for } .0108 > h < 0.06$$

where Q = flow in cu. ft/s per foot length of weir

h = head above weir in feet

(Due to surface tension effects, there was no flow below $h = 0.0108$)
The conclusion reached in Ref: 2.1 regarding the attenuation of flow disturbances are unchanged, however, if the analysis is modified according to the above law. Similar conclusions are reached in Ref: 2.4 by a somewhat different analysis.

2.3. THE WATER TUNNEL FACILITY (CLOSED-CIRCUIT CONFIGURATION).

2.3.1 General Description

The water tunnel in its present form is a closed-circuit configuration, as shown in Fig: 2.3. The original stilling tank, contraction, and test section have been retained, the remainder of the circuit being re-constructed in the conversion to the closed-circuit configuration. Two 125-h.p. double-inlet centrifugal pumps running at 405 rev./min. circulate the water around the tunnel circuit. In normal operation, the weirs are inoperative, the level of water being just up to the weir crests. The static pressure in the circuit can be controlled by varying the air pressure in the stilling chamber air-space in the same manner as for the open-circuit configuration.

The test section is 8 ft. long and 18 in. in internal diameter. It is provided with four perspex inspection doors, curved on the inside to be flush with the inside wall and flat on the outside to prevent optical distortion.

An operating platform has been built under the test section, so that operation and control can be carried out at a convenient level. The remote-control panel, for varying the flow through the tunnel and for controlling the charging and emptying cycles, is mounted on this platform, adjacent to the test section. The tunnel is at present instrumented for propeller vibration research, the propeller dynamometer being arranged in the working section, as shown in Fig: 2.4. The control panel for the dynamometer is

Fig. 2.3 General arrangement of closed-circuit configuration of research water tunnel.

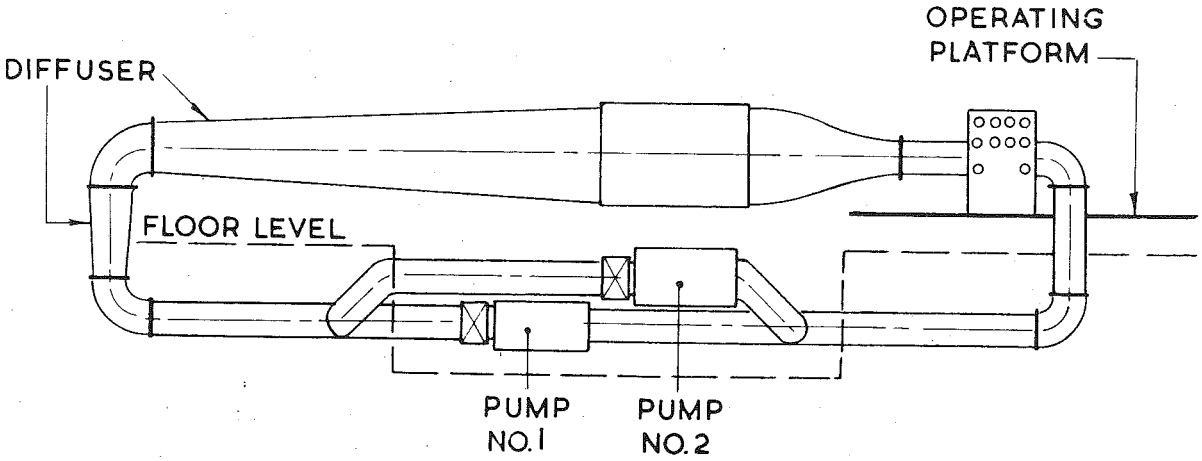

SIDE ELEVATION

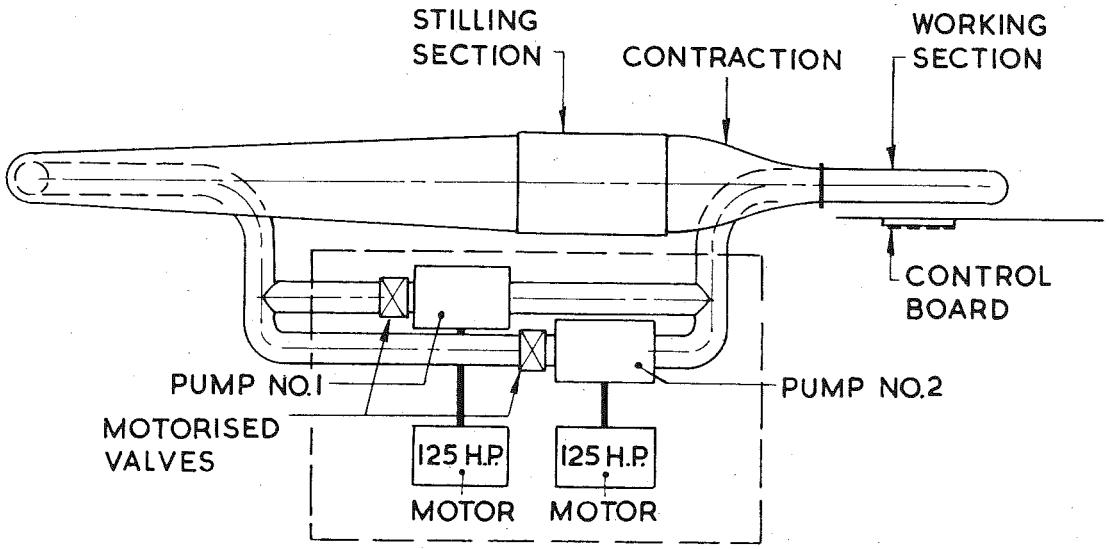

5 0 5 10

FEET

PLAN

Fig. 2.4 General arrangement of propeller dynamometer in tunnel.

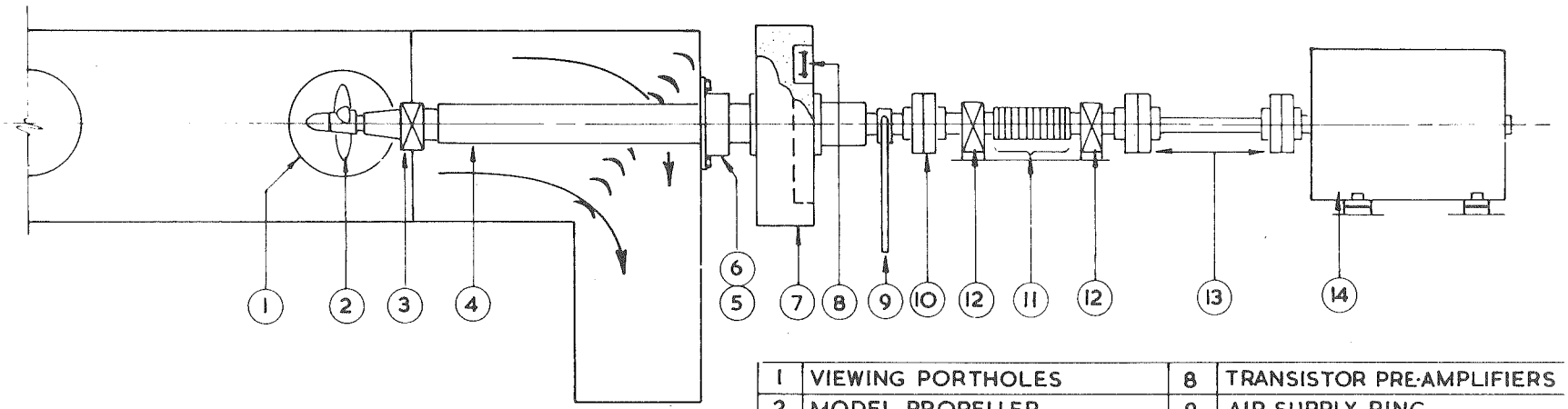

No.	DESCRIPTION	No.	DESCRIPTION
1	VIEWING PORTHOLES	8	TRANSISTOR PRE-AMPLIFIERS
2	MODEL PROPELLER	9	AIR SUPPLY RING
3	PRESSURISED WATER BEARING	10	RUBBER COUPLING
4	DYNAMOMETER	11	SLIP RINGS & BRUSHES
5	WATER SEAL	12	SPHERICAL ROLLER BEARING
6	DOUBLE CONICAL OIL BEARING	13	FLEXIBLE COUPLING
7	FLYWHEEL	14	VARIABLE SPEED D.C. MOTOR

next to the tunnel-control panel. Meters on an adjacent panel indicate the supply voltage both to strain-gauge bridges in the dynamometer and also to the transistor pre-amplifiers fitted in the fly-wheel. Meters indicating the mean torque and thrust of the model propeller, as well as output terminals for instrumentation to measure the fluctuating torque and thrust components, are also fitted to this panel. Against the laboratory wall, adjacent to the test section, are mounted pressure gauges and manometers, indicating the head before and after each pump, the head after the main stop-valves, the air-bearing pressure in the dynamometer, mains air pressure, and the air pressure in the charge-and-empty control circuit. Air-water and mercury-water manometers are mounted against the wall adjacent to the test section, for use as required.

2.3.2 Control

Flow through the circuit is controlled by actuating the motorised gate-valves fitted downstream of the pumps, from the remote-control panel. Fow low velocities, only one pump is used, whereas for higher velocities both pumps are in operation. When starting the pumps, the gate-valves are in the closed position, so that the pumps are started, as is normal practice, in the zero flow condition, this being the minimum power condition for the machines.

A single 5-in centrifugal pump is used for both charging and emptying the circuit, the flow being directed as required by setting the valves in a "cross-over" pipe network to the appropriate configuration. The operation of these valves, which are of the flap type, is by pneumatic rams. Supply air for these rams is controlled by two

single-toggle pneumatic valves of the multiport type on the control panel.

The two positions of the upper valve on the panel correspond to the "charge" and to the "empty" configurations of the flap valves. The lower valve is inoperative in one position, but in the other position sets the flap valves into a "hold" configuration which prevents water from being pumped into or being drained from the tunnel. After charging the tunnel, the "hold" configuration is used to prevent water draining back to the sump through the now stationary 5-in pump.

This control system is interlocked with the electrical circuit of the float switch in the pump pit, so that the flooding of the pit causes the flap valves to be switched into an emergency-pumping configuration. Water is then pumped directly into the laboratory sump from the drainage-sump in the pump pit. Starting of the pump is automatic if flooding of the pump pit occurs. This starting cycle can also be initiated by pushing a button on the control panel. Either event actuates an electrical timer which, in sequence, opens a solenoid valve on the pump air vent and a solenoid valve on the mains water-supply to the pump, allows sufficient time for the pump to prime completely, closes both valves, and then starts the pump motor.

2.3.3 Performance

The head-flow curve for one of the 125-h.p. pumps as determined by actual tests is shown in Fig: 2.5, as is also the head-flow characteristic for the two pumps operating in parallel. The system

Fig. 2.5 Pump and system characteristics.

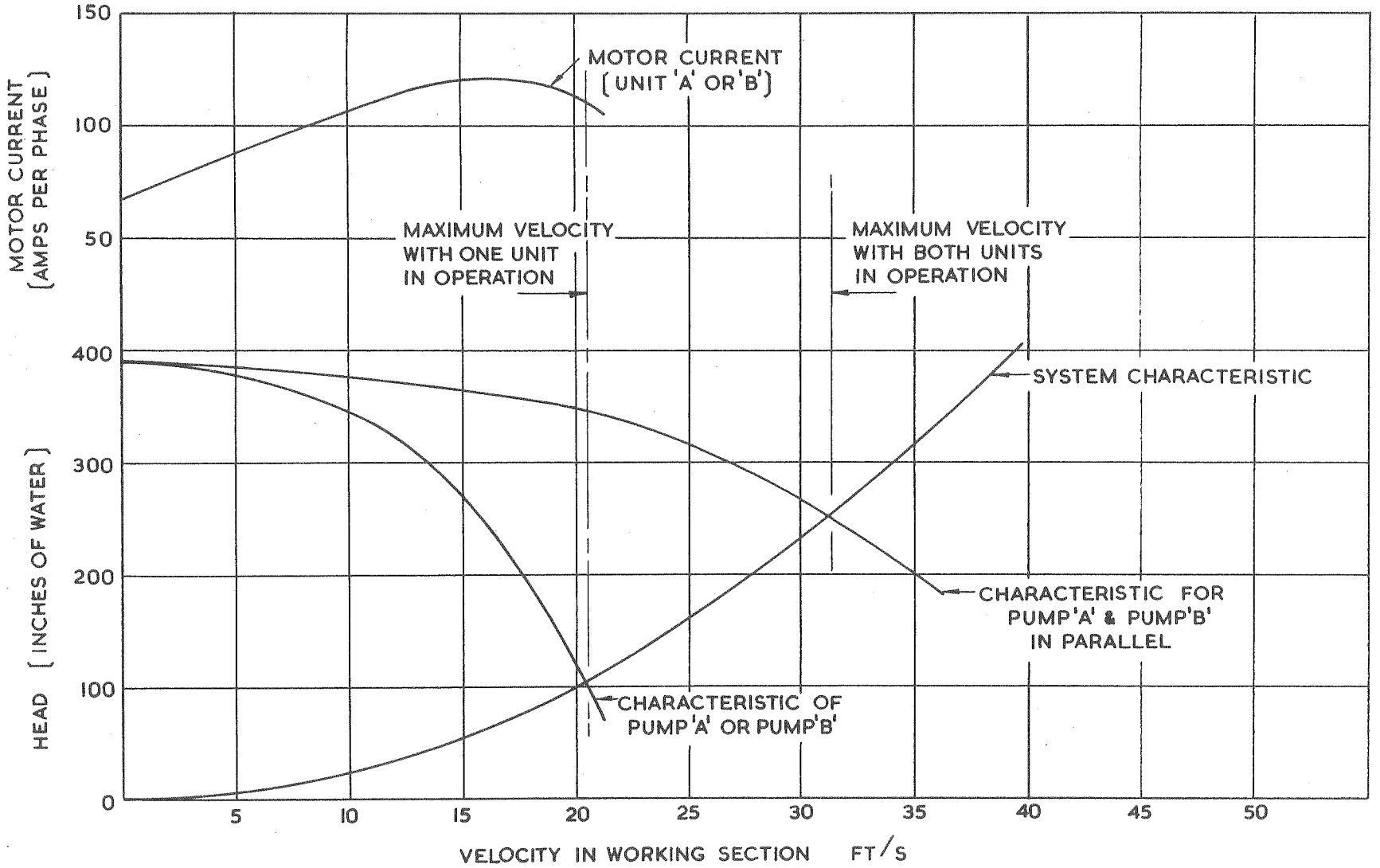
MOTOR CURRENT (AMPS PER PHASE)
HEAD (INCHES OF WATER)
VELOCITY IN WORKING SECTION FT/S
150
100
50
400
300
200
100
0
5
10
15
20
25
30
35
40
45
50
MOTOR CURRENT (UNIT 'A' OR 'B')
MAXIMUM VELOCITY WITH ONE UNIT IN OPERATION
MAXIMUM VELOCITY WITH BOTH UNITS IN OPERATION
SYSTEM CHARACTERISTIC
CHARACTERISTIC FOR PUMP 'A' & PUMP 'B' IN PARALLEL
CHARACTERISTIC OF PUMP 'A' OR PUMP 'B'

characteristic as determined by test is also shown in Fig. 2.5. It will be seen that with one and two pumps in operation, the maximum velocities in the test section are 20.5 and 31.0 ft./s. respectively.

The velocity profiles across the working section are shown in Fig. 2.6 for a flow velocity of 15 ft./s. It will be seen that, except for a wall boundary-layer region of approximately 2 in., the velocity profile is uniform to within $\pm$ 1 per cent. These measurements were made with one screen in the stilling section.

Fig. 2.6 Velocity profiles in the working section (at No. 2 cover) at approximately half the maximum tunnel velocity.

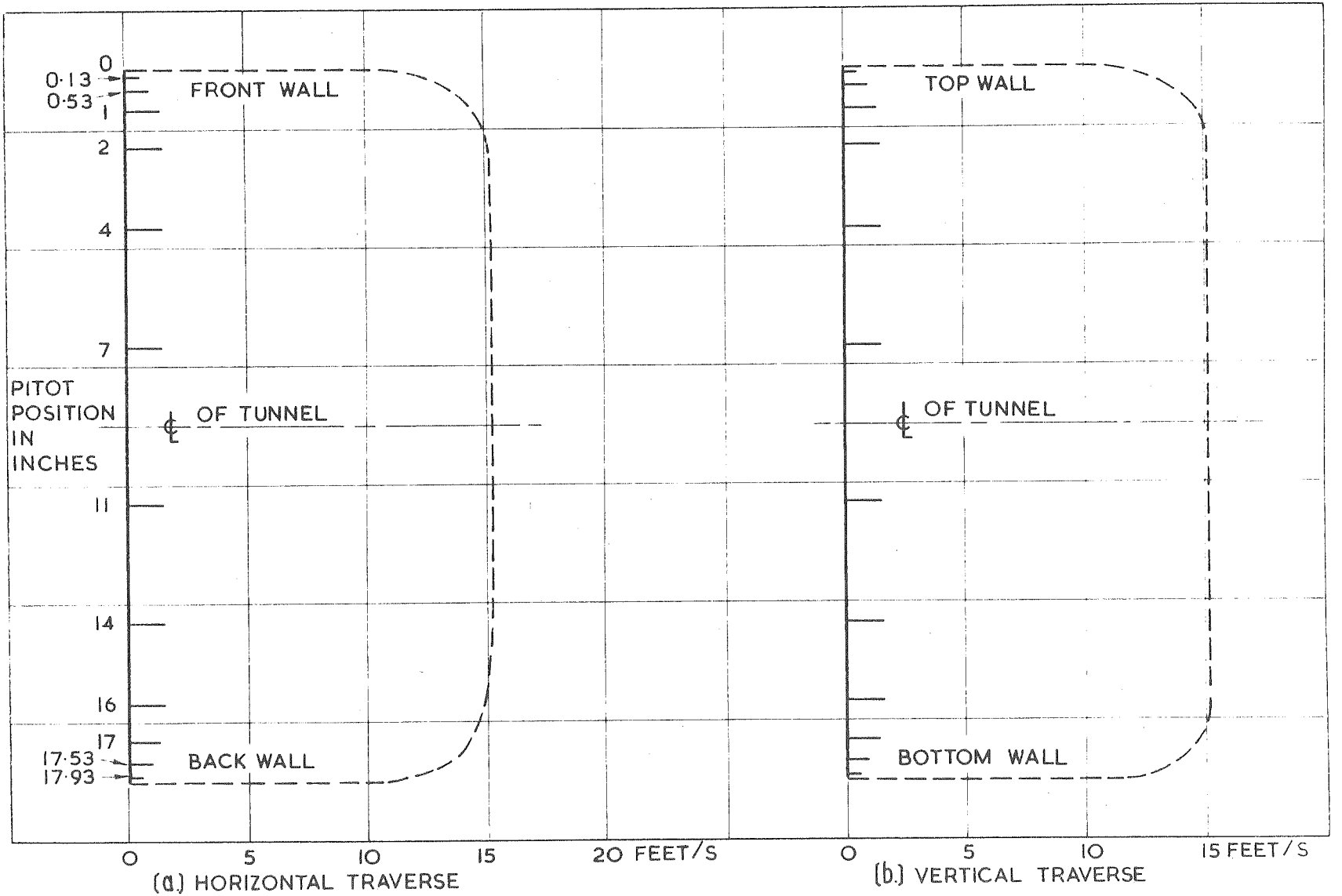
0
0·13
0·53
1
2
4
7
11
14
16
17
17·53
17·93
FRONT WALL
BACK WALL
PITOT POSITION IN INCHES
℄ OF TUNNEL
0
5
10
15
20 FEET/S
(a.) HORIZONTAL TRAVERSE
TOP WALL
BOTTOM WALL
℄ OF TUNNEL
0
5
10
15 FEET/S
(b.) VERTICAL TRAVERSE

CHAPTER 3

THE MODEL PROPELLER DYNAMOMETER

3.1. INTRODUCTION

Of the research investigations which have been undertaken in the research water tunnel since 1955, the most important has been the research on model propeller vibrations.

For the investigations on model propellers, a dynamometer driven by a variable speed motor has been developed. The first design of the dynamometer was by Tostevin (Ref. 3.1). This was of the strain-gauge type and incorporated a mechanical system using diaphragms to separate the torque and thrust. This was used successfully to measure mean values of torque and thrust, but because of the low natural frequencies of the dynamometer and also because of the high background tunnel noise, some difficulty was experienced in resolving torque and thrust fluctuations with sufficient accuracy. In 1958, an improved design of dynamometer was constructed by Watkins Ref. 3.2, which also incorporated a mechanical system to separate torque and thrust. Thin metal shells on which resistance strain-gauges were cemented were again used as measuring elements. Further development of the dynamometer has since taken place.

3.2. THE CONSTRUCTION OF THE PROPELLER DYNAMOMETER

3.2.1 General Description

Fig. 2.4 shows the general layout of the present design of propeller dynamometer. The model propeller is mounted on an inner dynamometer unit which is housed within the drive-shaft. Lateral support for the drive shaft is by means of a water-lubricated bearing at the propeller end, and by a double-conical oil-

lubricated bearing at the drive end. The oil-bearing also provides a longitudinal location of the drive shaft. Mounted on the drive shaft adjacent to the oil bearing is a fly-wheel the inertia of which is sufficiently large to fix the torsional and longitudinal nodes of the dynamometer at this point. Torque and thrust forces on the propeller are first separated mechanically within the dynamometer, and then measured electrically by the strain cells. The output from the strain cells is amplified by transistor pre-amplifiers in the fly-wheel and then transmitted through slip-rings to the recording equipment.

The construction of the inner dynamometer unit shown diagramatically in Fig. 3.1. The thrust force on the propeller is transmitted through the tension rod down to the thrust (tension) shells, two flexible diaphragms allowing the longitudinal motion but preventing lateral displacement. Since the tension rod has a very small torsional stiffness, torque applied to the propeller is transmitted almost entirely through the flexible diaphragm adjacent to the propeller to the torsion shell. The component sizes have been chosen so that negligible torsion is transmitted to the tension shells and negligible thrust is applied to the torsion shell. The dynamometer, however, is comparatively rigid in bending. It will be seen from Fig. 3.1 that the inner dynamometer unit which incorporates the torsion and thrust measuring systems is attached to the drive shaft by a flexible tube which locates the end of the inner dynamometer unit both axially and laterally. The lateral location of the other end of the inner dynamometer unit is provided by a very close

Fig. 3.1 Cut-away view showing construction of inner dynamometer unit.

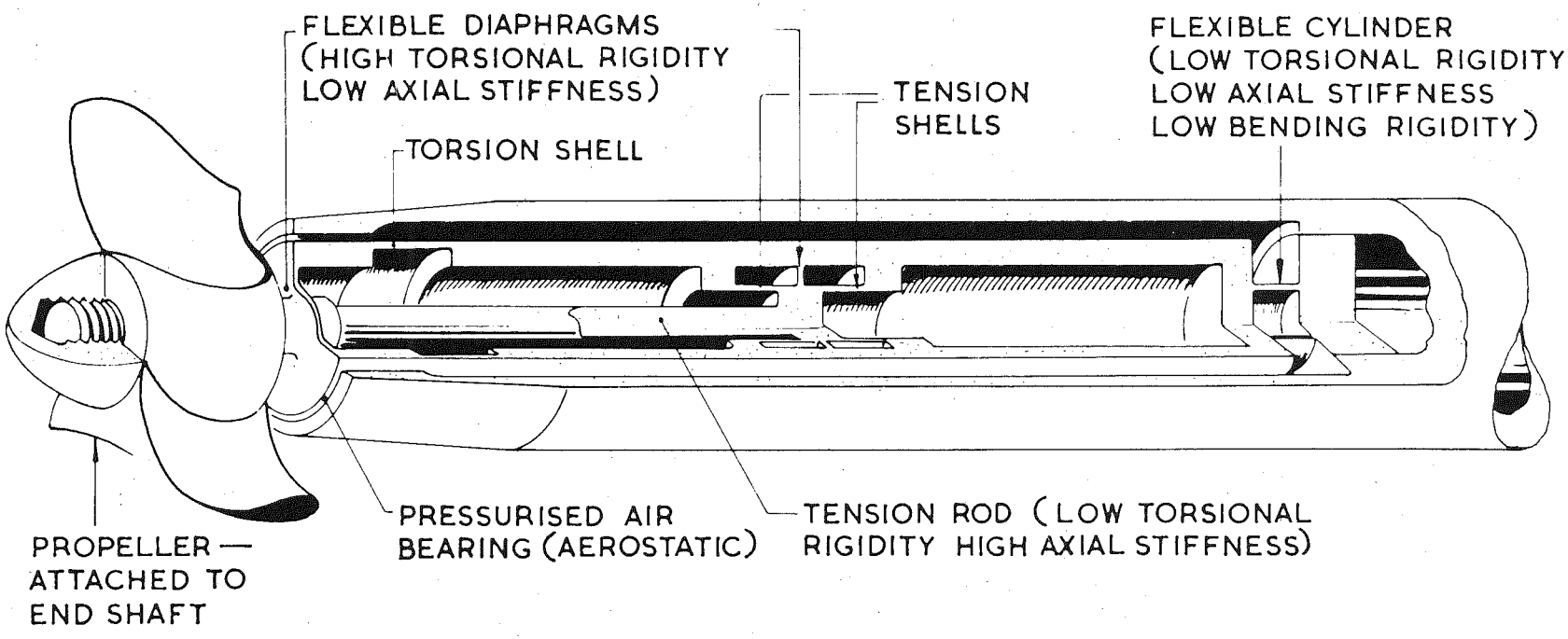
FLEXIBLE DIAPHRAGMS
(HIGH TORSIONAL RIGIDITY
LOW AXIAL STIFFNESS)
TORSION SHELL
TENSION
SHELLS
FLEXIBLE CYLINDER
(LOW TORSIONAL RIGIDITY
LOW AXIAL STIFFNESS
LOW BENDING RIGIDITY)
PROPELLER —
ATTACHED TO
END SHAFT
PRESSURISED AIR
BEARING (AEROSTATIC)
TENSION ROD (LOW TORSIONAL
RIGIDITY HIGH AXIAL STIFFNESS)

clearance (0.0005" diametral) pressurised aerostatic bearing. The flexible tube is a separate component, and may be removed and replaced by alternative tubes of different torsional and axial stiffnesses. In this way the torsional and axial natural frequencies of the dynamometer system can be altered, since this tube provides the largest portion of the torsional and axial flexibilities between propeller and fly-wheel. Although other modes of vibration are possible, the only significant mode of vibration of the propeller is the first mode in which the propeller is at the anti-node and the fly-wheel is at the nodal position.

3.2.2. The Torsion and Thrust Cells

The torsion cell consists of a thin aluminium shell (0.004" thick) on which is cemented eight strain gauges at angles of 45^{o} and 135^{o} to the dynamometer axis. The gauges are wired in the bridge arrangement shown in Fig. 3.2 which ensures that signals due to side force, end thrust, or bending moment on the cell will be cancelled out within the fully-active bridge.

The thrust measuring unit consists of two thrust cells which are pretensioned during the assembly of the dynamometer unit. A thrust force on the propeller is transmitted to the centre of the thrust unit, causing the tension stress in one cell to increase, and in the other cell to decrease. Each cell consists of a thin aluminium shell (0.002" wall thickness) on which is cemented four strain gauges parallel to the axis of the dynamometer. The eight gauges are wired in a fully-active bridge as shown in Fig. 3.2 in such a way that signals due to side thrust, torque and moment on the thrust unit are cancelled within the bridge.

Fig. 3.2 Strain gauge arrangement on torsion and thrust shells

(a) Gauge layout on the shells

(b) Bridging arrangement of gauges

A.

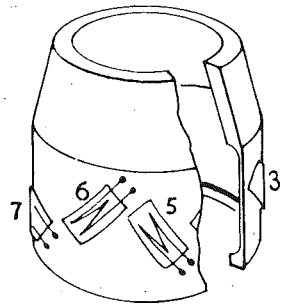

TORSION SHELL

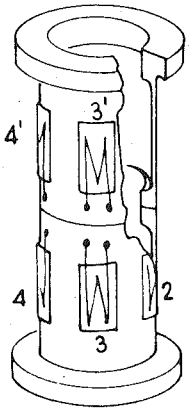

THRUST CELLS

B.

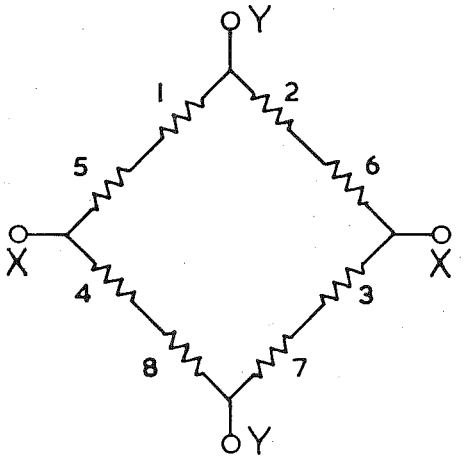

TORSION BRIDGE

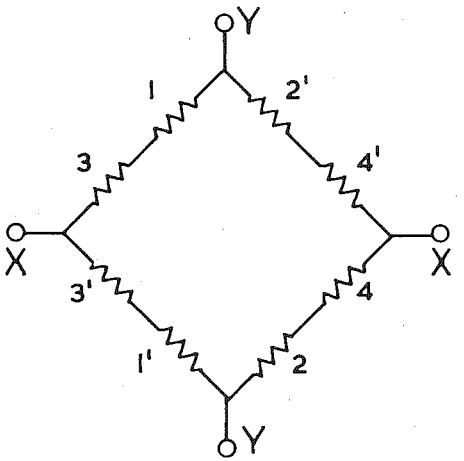

THRUST BRIDGE

3.2.3. The Electrical System

Because of simplicity, a direct-current strain-gauge system is used. A constant-voltage supply is transmitted via slip-rings and internal wiring to the strain-gauge bridges on the measuring elements. The output from the bridges is taken to the fly-wheel pre-amplifiers by electrically-shielded cables. Shielding was found necessary to prevent stray induction effects. The fly-wheel pre-amplifiers have a gain of approximately 1000, and use matched transistor pairs in push-pull stages to reduce zero drift.

In a transistor amplifier, the major cause of zero drift is the variation of transistor characteristics with changes in temperature. Drift will be reduced, therefore, if the amplifier is kept at constant temperature. The amplifiers are enclosed in recesses in the fly-wheel, sealed by a heavy cover plate to assist in reducing temperature variations.

The output from the fly-wheel pre-amplifiers is transmitted to the measuring and recording equipment through monel-metal slip-rings, fitted with silver-carbon brushes. The values of mean torque and thrust are displayed on millivolt-meters fitted in the control panel. Meters on an adjacent panel indicate the supply voltage to the dynamometer strain-gauge bridges, and also to the transistor pre-amplifiers. Fluctuating torque and thrust components are displayed on a cathode ray oscilloscope, and permanently recorded either by a camera attached to the oscilloscope or by means of a mirror-galvanometer sensitized paper recorder.

3.3. THE DYNAMOMETER CHARACTERISTICS

For accurate measurements it is essential that the characteristics of the dynamometer be linear, and also that cross-coupling between the torque and thrust measuring systems be negligible. Static calibration has shown that there is a linear relationship between applied thrust and output voltage, and similarly between applied torque and output voltage. No cross-coupling between torque and thrust could be detected during static calibration tests, the torque output being entirely independent of the applied thrust, and the thrust output being independent of the applied torque. The sensitivity of the dynamometer to bending-moments applied to the propeller was found to be negligible. When a dynamic calibration was carried out, however, by measuring the natural frequency with discs of various inertias replacing the propeller, it was found that the torsional stiffness varied slightly with amplitude of oscillation. The mean value of torsional stiffness was 7,000 lbf-in/radian, and the corresponding natural frequency in air when a variable-pitch model propeller was fitted, was 159 cycles per second. The maximum torque and thrust which can be measured on the dynamometer are 50 lbf-in and 50 lbf.

CHAPTER 4.

THE CHARACTERISTICS OF THE DYNAMOMETER

4.1 INTRODUCTION

The dynamometer as originally designed was to possess only two degrees of freedom of movement of the propeller. These were:-

(a) Movement along the axis of the dynamometer

(b) Angular movement about the axis of the dynamometer.

In both cases, movement could be in either direction from the equilibrium position, and was to be against an elastic system.

For the axial mode, the elastic system was to have a stiffness which was linear, and equal to the combination of the stiffnesses of the components (primarily the central rod, the thrust cells, the interchangeable stiffness element, and the drive shaft).

For the angular mode, the elastic system was to have an angular stiffness which was linear, and equal to the combination of the stiffnesses of the components (primarily the torsion cell, the interchangeable stiffness element, and the drive shaft).

Care was taken to reduce damping and hysteresis in the systems to a minimum. The thrust system was supported within the torque system by thin flexible diaphragms. The supports for the torque system were a thin flexible cylinder (at the end furtherest from the propeller) and a pressurised air bearing (aerostatic) at the propeller end.

The masses and inertias of the principal components of the systems were made small compared with the propeller mass and inertia. The dynamic behaviour of each system should therefore have closely approximated to the dynamic behaviour of an equivalent single-degree-of-freedom

system consisting of a mass on a linear spring with negligible damping

When constructed, the behaviour of the dynamometer appeared to approximate to that of the ideal system, as shown by simple tests, and was used for several projects on this basis. Before being used in the experimental work described in this thesis, however, it was taken apart, modified in several respects and reassembled. A simple check at this time indicated that its behaviour still approximated to the ideal. It was later found, during careful calibration, that its behaviour deviated slightly, but significantly, from the ideal. As is shown later, some of this deviation is due to contact at the air bearing between the torque system and the outer cover i.e. to a "bearing rub". This was caused by the alignment of the components not being perfect, after the final reassembly. It is quite possible, that before this time the "rub" did not occur.

The characteristics of the dynamometer (in its final form) are described in the following sections from the viewpoint of knowing why these depart from the ideal. The order in which they are discussed was not the chronological order in which the corresponding tests were carried out. It might be mentioned that although the dynamically non-linear behaviour of the dynamometer was ultimately found to have a comparatively simple physical explanation, it initially appeared that it would be impossible to deduce from the complex dynamic behaviour of the dynamometer, the reasons for the deviation from the ideal. It was only after various hypotheses were suggested, and tested by specifically designed experiments, that the physical phenomena occuring began to become apparent. In the following sections, many of these hypotheses and experiments are not

described. It should also be mentioned that the dynamic behaviour of thrust system was not investigated in detail, as this system was used only to obtain measurements of mean thrust. The dynamic behaviour of the torque system was, however, investigated in detail.

4.2. THE STATIC CHARACTERISTICS OF THE DYNAMOMETER

4.2.1 The Thrust Characteristics

A calibration rig was constructed which would apply pure thrust loads to the dynamometer without imposing at the same time torque or bending loads. The design of the rig was as follows. A special nut was manufactured which could be screwed to the propeller end shaft. When this nut was in the correct position, a slot midway along its length was in the vertical plane. At either end of the slot was fitted a small ball-bearing, halfway up the vertical end-faces of the slot. Each ball-bearing thus lay on the axis of the dynamometer. A thin flat bar fitted vertically through the slot, and was pivoted at its upper end on thin flexible strips. A terylene thread attached to the lower end of the bar passed over a nearby pulley, and was then attached to a weight pan. The position of the pulley was adjusted so that the section of thread between the pulley and the end of the bar was parallel to the axis of the dynamometer. Weights placed in the pan would then apply (via the ball-bearing in the propeller nut) a pure thrust load to the dynamometer.

Only one calibration was carried out for thrust. This was a

calibration of electrical output from the thrust cell (as measured in volts at the slip-rings) against thrust load applied to the dynamometer. The results of this calibration are shown in Fig: 4.1. It will be seen that the characteristic is a straight line, showing that the elastic system for thrust, in the static case is linear.

4.2.2 The Torsion Characteristics

A test rig was devised which would apply pure torsional loads to the dynamometer without applying at the same time thrust or bending loads. The construction of the rig was as follows. A special nut was attached to the propeller end shaft. To this was rigidly attached a thin flat metal bar 10 inches in length, the connection to the nut being at its mid point. Relative to the axis of the dynamometer the bar was at right angles. In relation to the earth's surface the bar was horizontal. To each end of the bar a terylene thread was attached, the thread at one end leading directly up over a nearby pulley and then vertically downward to a "balance" bar. The thread at the other end led vertically downwards to the other end of the "balance" bar. At the centre of the balance bar was attached by a terylene thread a weight pan. To reduce frictional errors the pulley was fitted with a precision ballrace. Weights placed in the pan caused loads of half this magnitude to be applied to opposite ends of the bar in opposite directions, thus applying a pure torsional load to the dynamometer.

Two calibration tests were carried out using this rig. The first test related electric output from the torsion cell (as

Fig. 4.1 Dynamometer calibration graph of voltage output (at slip-rings) versus applied thrust.

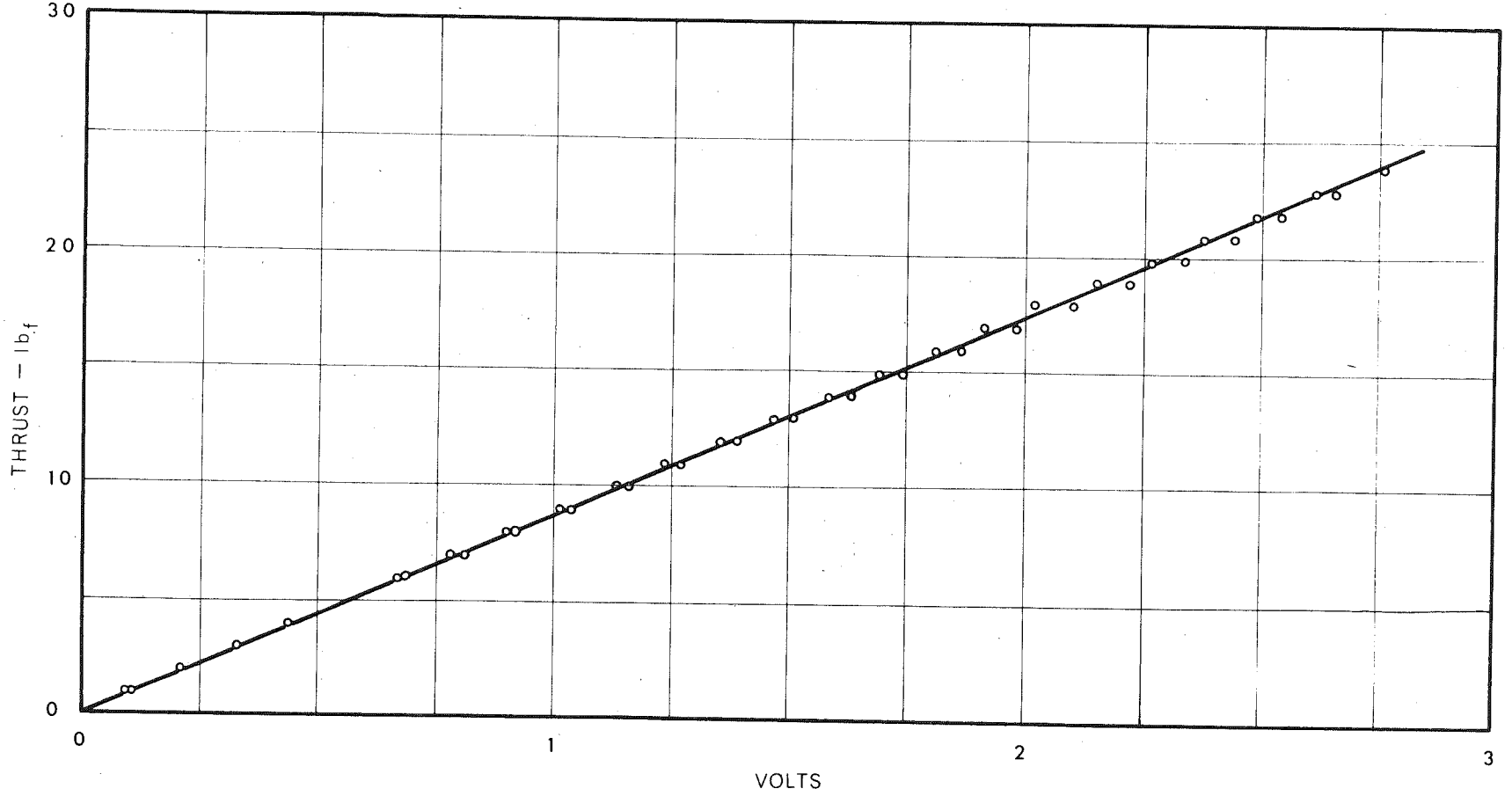
30
20
10
0
THRUST – lb.f
0
1
2
3
VOLTS

measured in volts at the slipring) to applied torque. The results of this calibration are shown in Fig: 4.2. It will be seen that the characteristic is a straight line showing that the torsional elastic system is linear, in the static case. It will be further noted that hysteresis effects are small.

The second test was carried out with an additional "indicator" bar(21 inches in length) attached to the propeller end-shaft at its mid-point. Sensitive dial gauges were fitted near each end of the indicator bar, so that the linear movement of each end of the bar could be measured to a high degree of accuracy. From the readings obtained on the two dial gauges, the change in slope of the indicator bar from its original position could be calculated, making allowance for any vertical movement of the centre of the bar which might have occurred due to slight movement of the propeller end-shaft laterally within the air bearing. From the change in slope, the angular rotation of the propeller end-shaft from the original position could be calculated. From the tests carried out in this way, a graph was prepared of angular deflection against applied torque, Fig: 4.3. It will be seen that the characteristic is a straight line, indicating that the elastic system for torsion is a linear one. It will again be noted that hysteresis effects are small.

Fig. 4.2 Dynamometer calibration graph of voltage output (at slip-rings) versus applied torque.

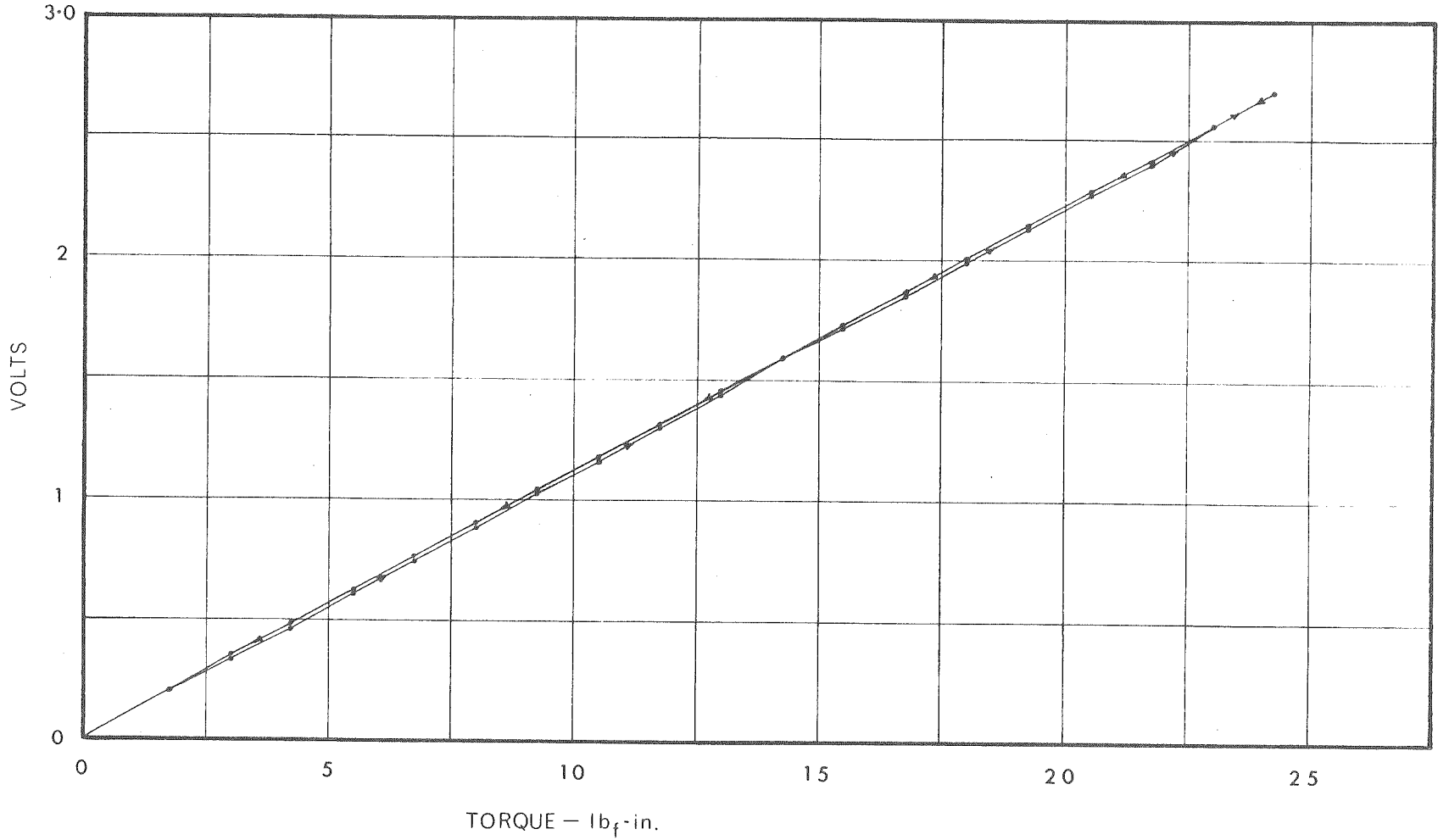
3·0
2
1
0
VOLTS
0
5
10
15
20
25
TORQUE — lb$_f$-in.

Fig. 4.3 Dynamometer calibration graph of angular deflection versus applied torque.

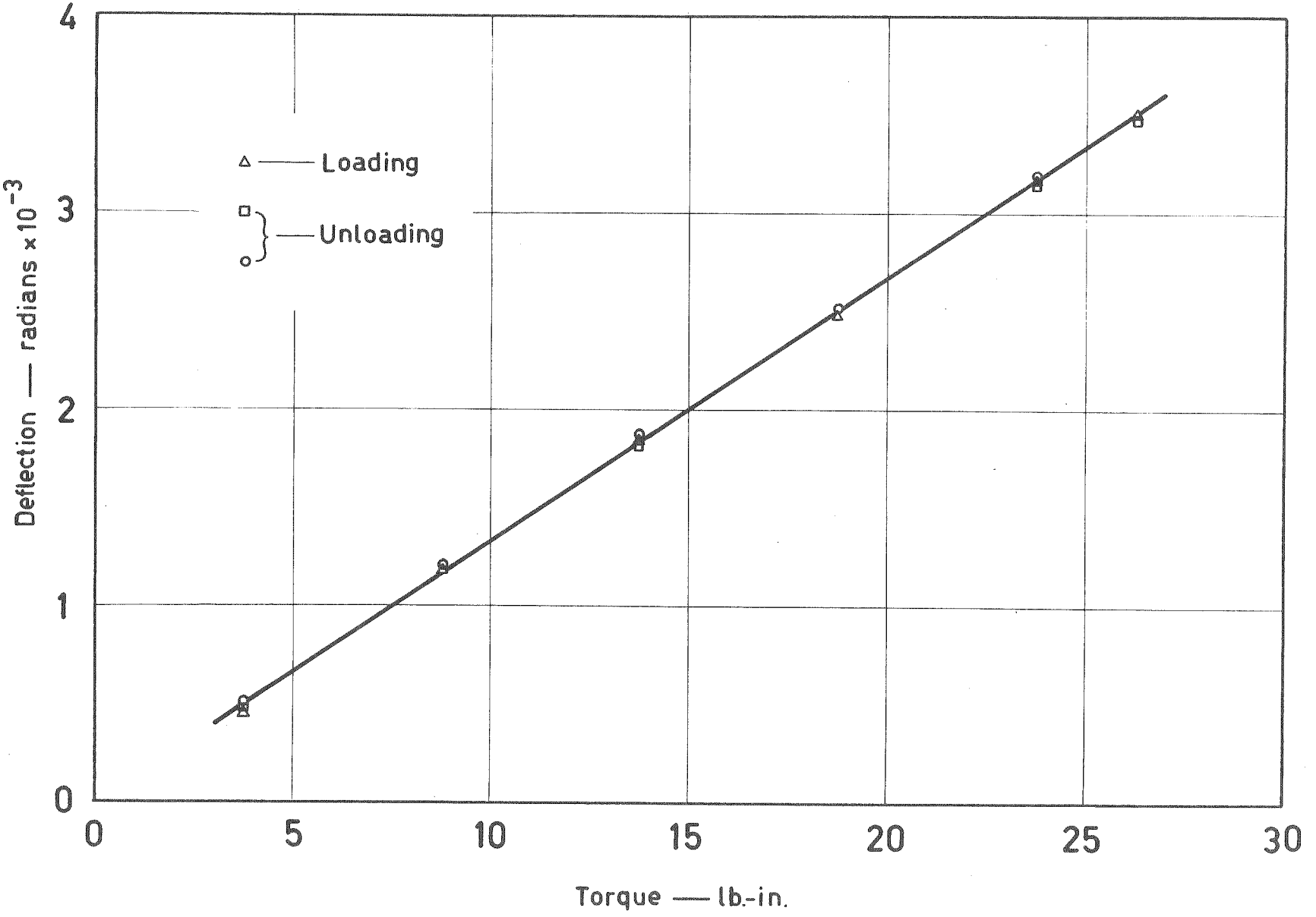
Deflection — radians x10⁻³
Torque — lb.-in.
Loading
Unloading
0
1
2
3
4
0
5
10
15
20
25
30

4.3. THE DYNAMIC CHARACTERISTICS OF THE DYNAMOMETER

4.3.1. The Dynamic Thrust Characteristics

It was intended to carry out dynamic calibrations of the thrust system, using attached masses on the propeller end-shaft. Since, however, the thrust system was only used to measure values of mean thrust, this calibration was not required for the experimental work described in this thesis, and due to shortage of time was not carried out.

4.3.2 The Dynamic Torsion Characteristics

The dynamic characteristics of the torsion system were carefully determined by a series of experiments in which "inertia discs" of various inertias but the same mass (equal to the mass of the propeller), were attached to the propeller end-shaft in turn. Each disc was fitted with a small projecting pin. When the dynamometer was rotated at a slow steady speed, this pin hit an adjustable rubber striker, causing free vibrations in the torsional mode to be set up. The electrical output from the dynamometer torsion cell was amplified by the fly wheel preamplifier, and the D.C. component removed by a negative bias voltage. The resulting wave form after further amplification was recorded on a ultra-violet galvanometer recorder. A high frequency voltage which served as a time reference was also recorded, using another channel of the recorder. Measurements were taken from the recorder paper of the amplitude and period of successive cycles of the oscillation. Several runs were made with each inertia disc, the level of impact being varied from run to run by varying the position of the striker.

The results of this calibration are shown in Fig. 4.4 in which the period of oscillation is plotted against the amplitude of the corresponding cycle, for the various constant values of inertia. It is immediately apparent from this figure, that the system is not behaving in an exactly linear fashion, since in a linear system the period of oscillation would be independent of amplitude. It will be noted that for each inertia there appears to be a lower value of amplitude below which the period appears to be independent of amplitude, and an upper value of amplitude above which the period again appears to be independent of amplitude. The periods are different, however, for the two regions. In between these two regions is a transition region in which there is a variation of period with amplitude.

On Fig. 4.5 values have been cross-plotted from Fig. 4.4, to present the variation of period with inertia, for constant values of amplitude. It will be seen that for a given value of amplitude the relationship between period squared and inertia is a straight line i.e the system behaves as a linear system with one degree of freedom.

The static calibration for torsion showed that the elastic system is a linear one in so far as the spring force is concerned. It might therefore be deduced that the nonlinearity in the dynamic case is due to nonlinearity in the damping. It is shown in standard texts on vibration that if the damping force is proportional to the velocity, constant, or proportional to amplitude, the period of oscillation will in each case be independent of

Fig. 4.4 Dynamometer calibration graph of amplitude versus period of oscillation, for various inertias.

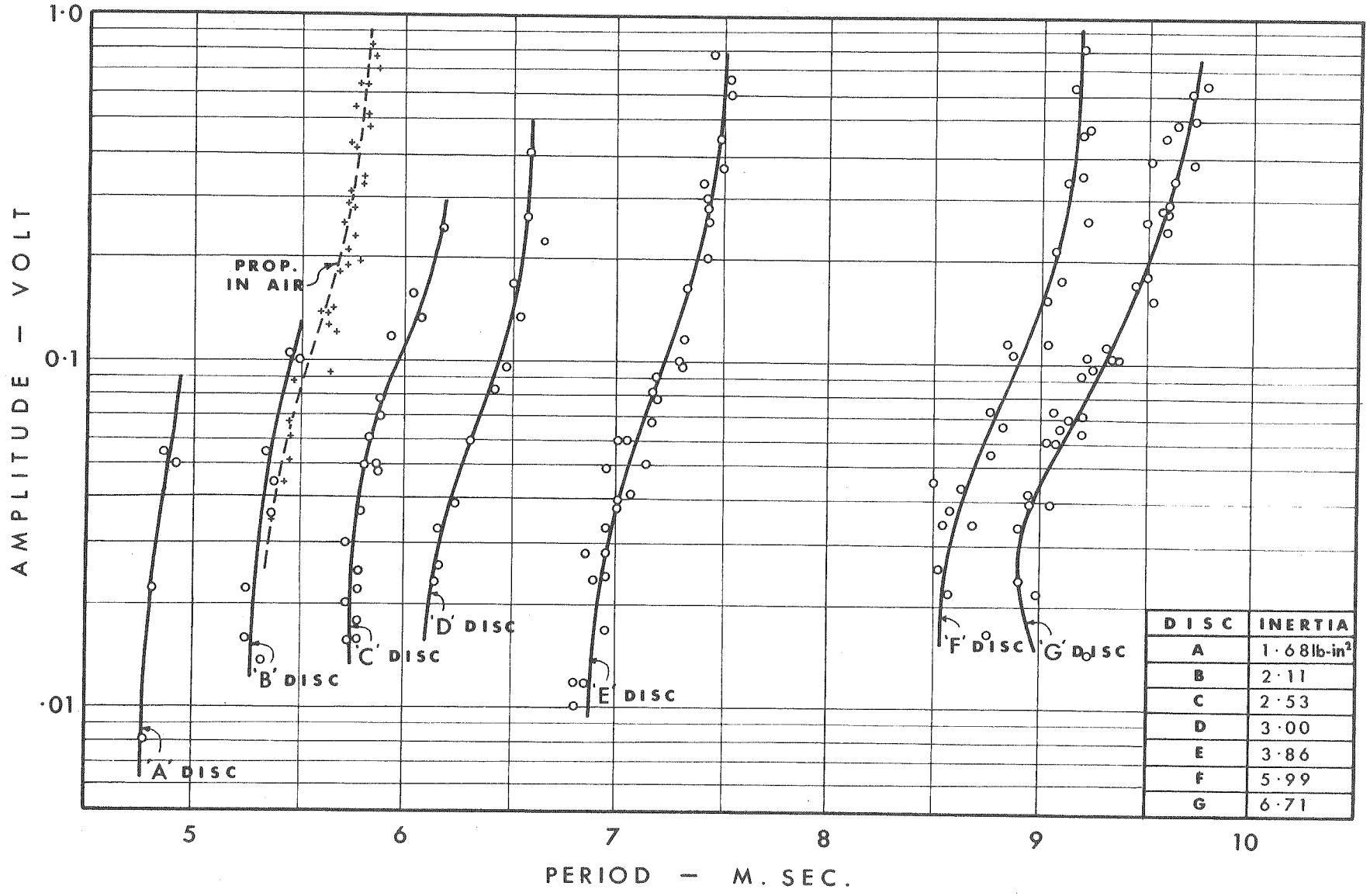
1·0
0·1
·01
AMPLITUDE — VOLT
PROP. IN AIR
'A' DISC
'B' DISC
'C' DISC
'D' DISC
'E' DISC
'F' DISC
'G' DISC
5
6
7
8
9
10
PERIOD — M. SEC.
DISC | INERTIA
A | 1·68 lb-in²
B | 2·11
C | 2·53
D | 3·00
E | 3·86
F | 5·99
G | 6·71

Fig. 4.5 Dynamometer calibration graph of period^2 versus moment of inertia, for various amplitudes of oscillation.

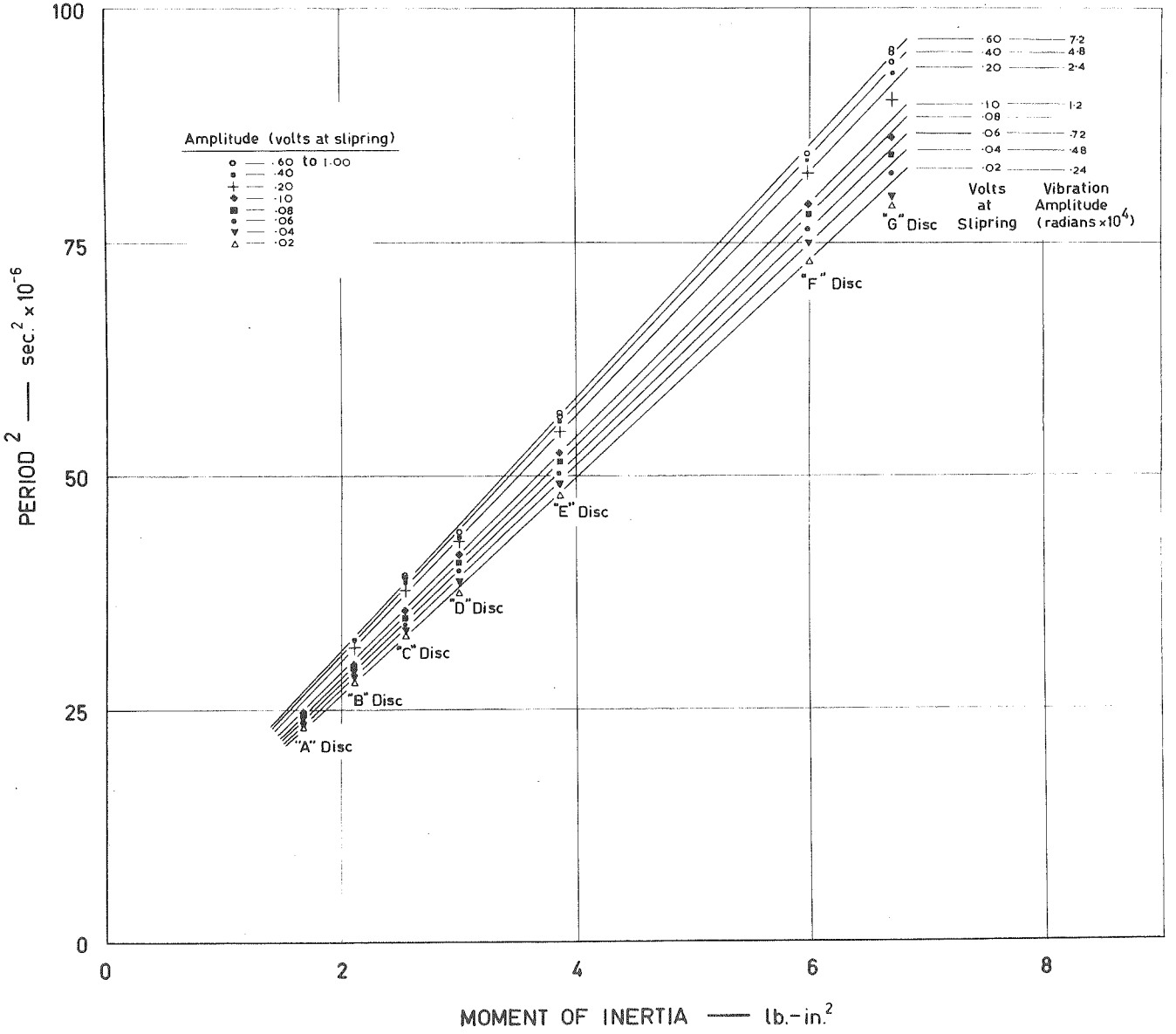
100
75
50
25
0
0
2
4
6
8
PERIOD 2 —— sec.2 x 10-6
MOMENT OF INERTIA —— lb.-in.2
Amplitude (volts at slipring)
.60 to 1.00
.40
.20
.10
.08
.06
.04
.02
"A" Disc
"B" Disc
"C" Disc
"D" Disc
"E" Disc
"F" Disc
"G" Disc
Volts at Slipring
Vibration Amplitude (radians x10-4)
.60 7.2
.40 4.8
.20 2.4
.10 1.2
.08
.06 .72
.04 .48
.02 .24

amplitude. The damping which is occurring in the dynamometer must therefore be of some other form than these.

After a careful analysis, it was decided that there were only three possible places in which damping could occur to any appreciable extent within the dynamometer. These were:

(1) Within the material of the components.

This damping would be of the "solid" type, in which the damping force is proportional to amplitude, and for which the period of vibration is independent of amplitude. If this form of damping is occurring it must therefore be of small magnitude.

(2) Damping due to a frictional rub within the air-bearing.

It was first thought that this damping would have to be of the type for which the damping force is independent of amplitude and velocity, i.e. is constant. This form of damping does not cause the period to vary with amplitude, however, and would therefore not have accounted for the observed effect. It was then realised that where relative motion occurs the coefficient of dry friction usually has the variation with velocity shown in Fig: 4.6, i.e. the coefficient is a non-linear function of velocity. As indicated below, it can be deduced that damping of this form would cause the frequency to vary with amplitude of oscillation. Thus a dry rub in the dynamometer could be a possible source of damping. Evidence that a dry rub was occurring was given by a later series of tests (described in the following section).

Fig. 4.6 Coefficient of friction versus relative velocity, for dry friction.

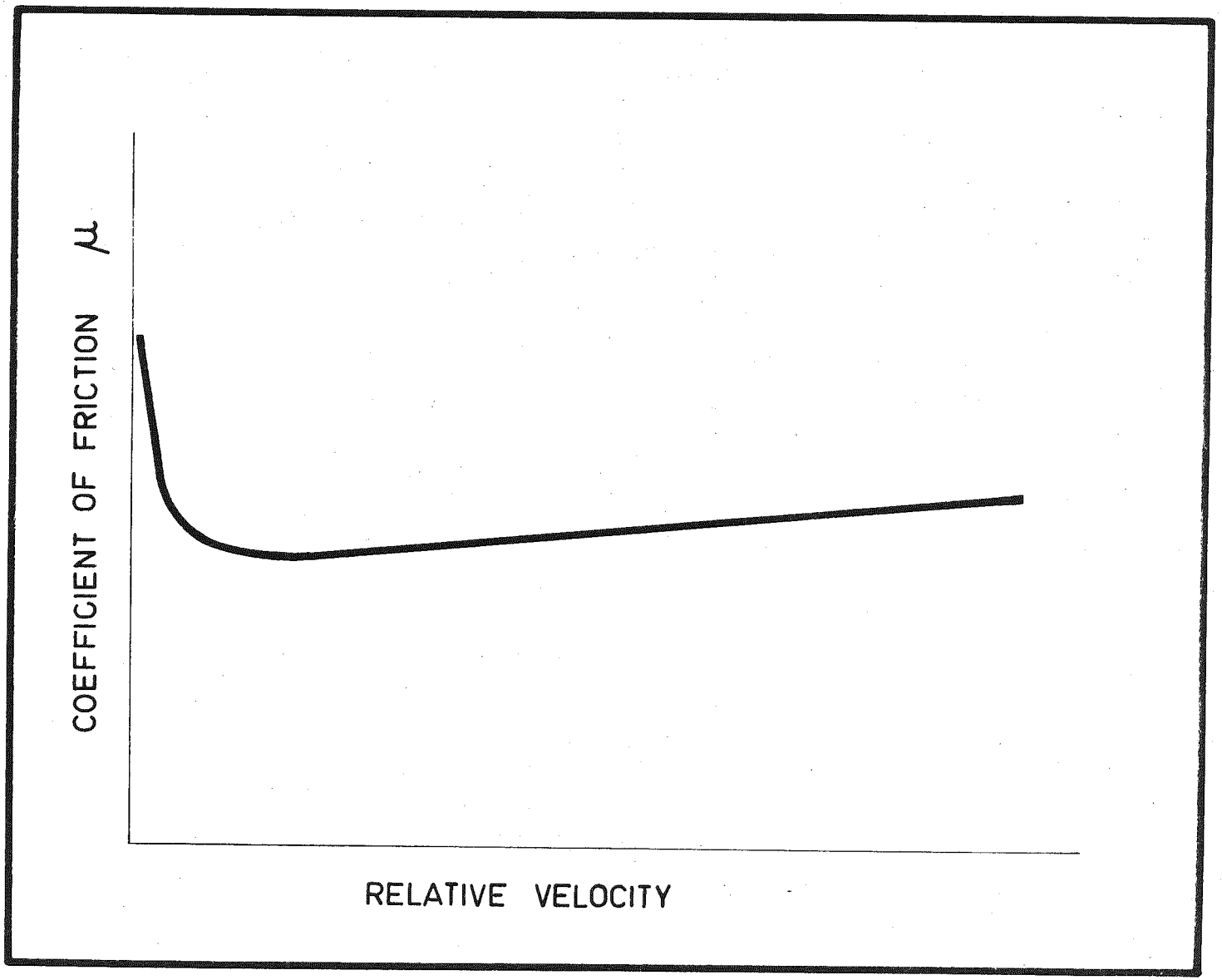
COEFFICIENT OF FRICTION μ
RELATIVE VELOCITY

(3) Damping within the wax layer over the strain-gauges in the torsion shell

The torsion shell is very thin being, only of 0.004 inches wall thickness. The thickness of the wax coating over the shell is at least as thick as the shell wall, and possibly several times thicker. The strains which occur in the metal of the shell are of a large magnitude, and the wax layer would therefore be subject to correspondingly large shear strains. It may be expected that the wax would behave as a super-cooled liquid i.e. to behave as a very viscous fluid. The damping force due to the wax would therefore be expected to be dependent on some function of velocity. The damping due to the dry rub ((2) above) is also dependent on a function of velocity. The total damping force would therefore also be a function of velocity. This function could be closely approximated by a polynomial in velocity.

As the form of this polynomial is not known, an analytic solution to the equations of motion is not possible in the present case. If the polynomial were known in general form, however, then an analysis could be carried out by the analytic methods given in standard texts on non-linear systems (such as Ref. 4.1) If the polynomial coefficients were known explicitly as numerical coefficients, a graphical solution by the method given in Ref.4.2 would have been the simplest way to solve the equations of motion. The general effect which the non-linear damping would have on the system, however, can be deduced in the present case.

From the physical nature of the damping in the dynamometer, it can be expected that the damping force would vary with velocity, in accordance with a curve (1) in Fig: 4.7, rather than curve (2). If a single cycle of the oscillation is considered, from one peak of the oscillation to the next (opposite) peak, the motion can be considered to closely approximate to an equivalent harmonic oscillation, if the damping is small as in the present case. For a harmonic system the velocity V at any given point in the oscillation is proportional to the maximum (half) amplitude a according to the equation

$$V = a\ \omega \cos \omega t$$

where ω is the angular frequency of the motion (4.1)

The horizontal axis in Fig: 4.7 may therefore have the velocity V replaced by the maximum amplitude a . Consider now a cycle of oscillation. If the amplitude of the oscillation is large the damping force near the extreme of amplitude will be comparatively large on both the outward stroke and the return stroke, and the velocities during these sections of the stroke will be reduced from what they otherwise would have been if damping had been linear. (i.e. damping force proportional to V). The times taken during these sections of the stroke will therefore be comparatively long. If the amplitude of oscillation is small, however, the damping force during the outward and return strokes, will also be small, and the velocities during these sections of the oscillation will

Fig. 4.7 Variation of damping force F_d with velocity V,
(and amplitude α)

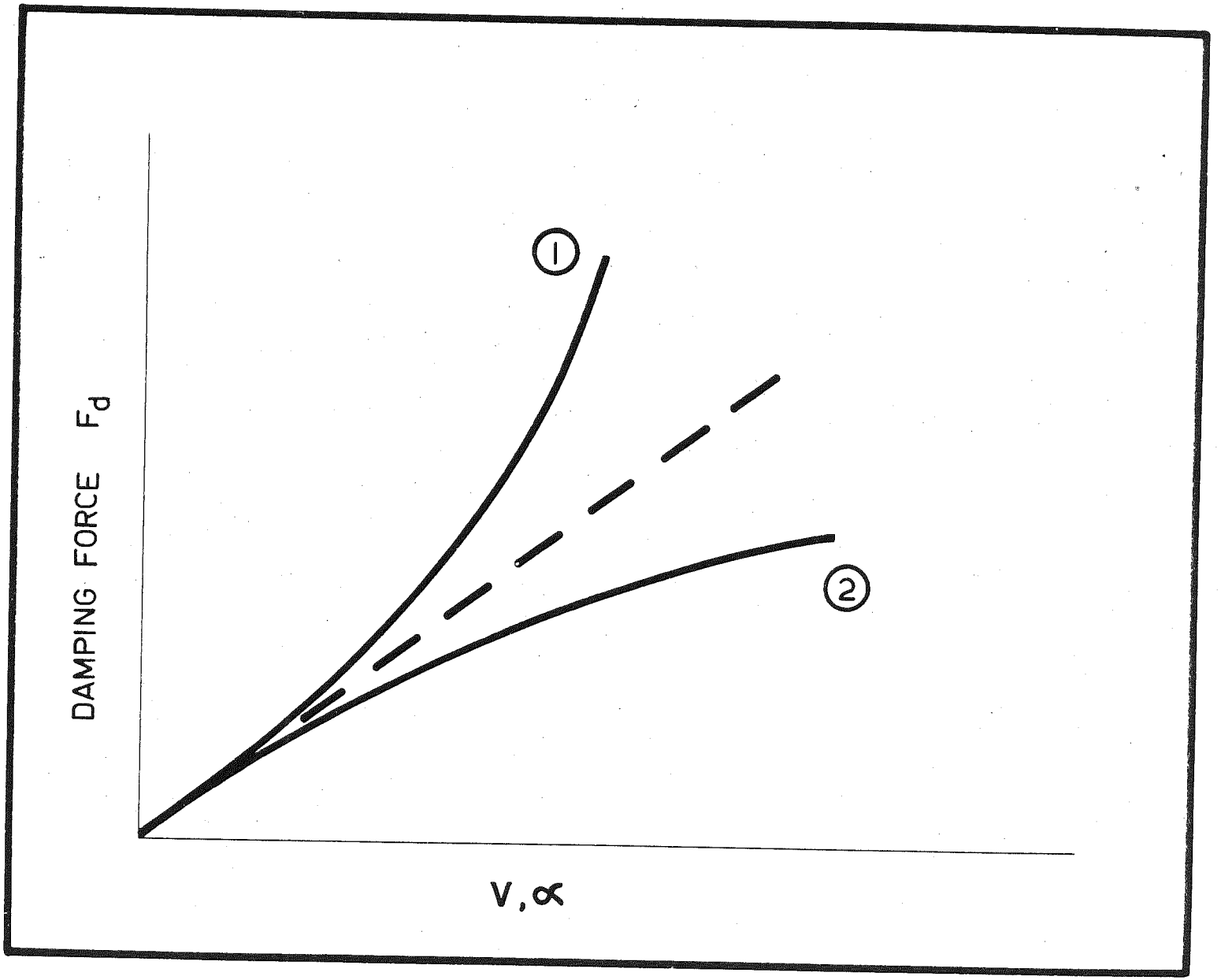
DAMPING FORCE F_d
1
2
V, ∝

be higher than in the previous case (at corresponding points in the cycle). It will therefore be seen that with non-linear damping of the type indicated by curve 1 in Fig. 4.7, the velocities will tend more nearly to those in the case of linear damping, and the period will decrease as the amplitude of oscillation decreases. As amplitude decreases therefore, the frequency of oscillation will increase. Reference to Fig. 4.4, indicates that this is the trend which has been observed in the present case.

Analytic confirmation that this trend of decrease of period with decrease of amplitude occurs with a particular case of this type of damping curve is given in Ref. 4.3. It is shown there, that where damping force is proportional to velocity squared, the following result is obtained for a single-degree-of-freedom system:-

$$\omega = \frac{p}{\sqrt{1 + \frac{a^2\alpha}{3}}} \qquad (4.2)$$

where ω = angular frequency of the oscillation

$p = \sqrt{\frac{k}{I}}$

k = spring torsional stiffness (torque /angular deflection)

I = inertia

a = half-amplitude of oscillation

α = damping coefficient as defined in the following equation (4.3)

$$\text{Damping force } F_d = \alpha I \dot{\theta}^2 \tag{4.3}$$

where θ is the angular displacement during the motion.

By substituting for p in (4.2) and rearranging, is obtained:-

$$\omega^2 = \frac{k}{I\left(1 + \frac{a^2\alpha}{3}\right)} \tag{4.4}$$

Since the period τ is given by $\tau = \frac{2\pi}{\omega}$, (4.4) may be written as:-

$$\tau^2 = \frac{4\pi^2 I\left(1 + \frac{a^2\alpha}{3}\right)}{k} \tag{4.5}$$

For a given system, in which α and k are fixed, it will be seen from (4.5) that a graph of τ^2 versus I, for constant values of amplitude a, will be a family of radiating straight lines. This is precisely the form of the characteristics obtained for the dynamometer (See Fig. 4.5) It will also be noted from (4.5) that the period decreases with decrease

in amplitude - again precisely the characteristic found in the dynamometer (See Fig. 4.4). It is not suggested that this proves the damping force in the dynamometer to be proportional to $(\text{velocity})^2$. The result does indicate, however, that the $(\text{velocity})^2$ type of damping is a possible form of damping which would explain the observed behaviour of the dynamometer.

To sum up, therefore, it would appear that the slightly non-linear behaviour of the dynamometer is due to non-linearity in the small amount of damping present. Most of this damping appears to have its origin in the wax layer over the gauges on the torsion shell. A damping characteristic in which damping force is proportional to $(\text{velocity})^2$ causes the period to vary with amplitude and inertia in the manner observed experimentally. A relatively minor amount of damping due to a very slight frictional rub in the air bearing also appears to be present (See Section 4.3.3)

4.3.3 The effect of mean load

To check the effect of mean load on the dynamic behaviour, the dynamometer was set up as for the static torsional calibration, and free oscillations were set up by knocking the projecting pin on the disc with a rubber striker. The rig used to apply the mean load was isolated from the dynamometer system as far as possible, by using very soft springs in each section of the terylene cord. This isolation was not as effective as it might have been, and the effect of the test rig was detectable in the results. Tests were made at various mean loads, with two of the inertia discs.

The curves plotted in Fig. 4.8 show the type of result which was obtained. It will be seen that there is a frequency modulation present, which is superimposed upon the frequency-versus-amplitude relationship previously observed (Fig. 4.4). It was deduced that thefrequency modulation was due to cross-coupling between the torsional mode of oscillation and the bending mode of oscillation of the dynamometer caused by the dry-rub in the air bearing. The bending mode of oscillation was excited by the sudden impact on the disc. During each cycle of the vibration in the bending mode, the pressure between the two surfaces in contact at the dry-rub varied. The damping force at this point, therefore varied cyclically at the a frequency equal to the frequency of the bending vibration. The modulation frequency was therefore equal to the bending frequency. If the effect of the superimposed frequency modulation is removed from Fig. 4.8 , by drawing in the mean line for each of the applied mean load conditions, it will be seen that the mean lines would coincide. The difference-graph plotted on the right hand side of Fig. 4.8 confirms this conclusion. It will be seen that the positive and negative areas in this graph, when taken over the whole length of the graph, are closely equal in area, thus indicating that the mean lines are almost coincident. This result indicates that mean load has no appreciable effect on the damping force, as would in fact be expected from the physical nature of the damping.

Fig. 4.8 Amplitude versus period of oscillation, for two applied mean torques (The curve on the right hand side is the difference-graph between curves (1) and (2))

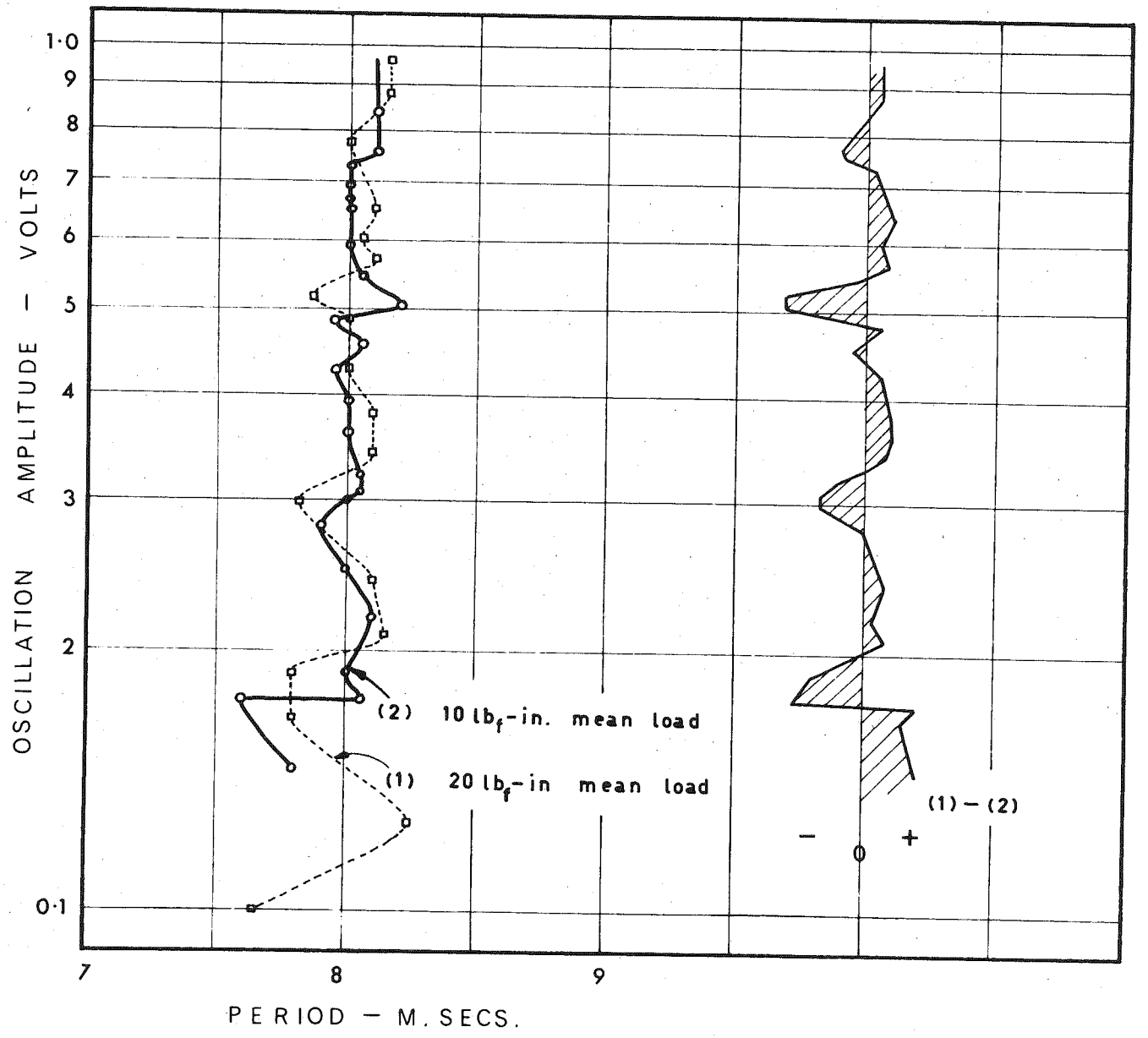
OSCILLATION AMPLITUDE – VOLTS
1·0
9
8
7
6
5
4
3
2
0·1
7
8
9
PERIOD – M. SECS.
(2) 10 lb$_f$-in. mean load
(1) 20 lb$_f$-in mean load
(1) – (2)
–
0
+

4.4. THE DYNAMOMETER AS A MEASURING INSTRUMENT

In the previous sections it has been seen that the behaviour of the dynamometer can be expressed by a set of characteristic curves such as those shown in Fig. 4.4 or 4.5. Since the behaviour of the dynamometer is consistent and does not alter with time, it is possible to use the dynamometer as a measuring instrument to determine unknown inertias from the frequency and amplitude of the corresponding free vibrations. Thus although the behaviour of the dynamometer deviates from the ideal, it can still be used as an accurate measuring instrument.

CHAPTER 5

THE ANALYSIS OF DYNAMIC RECORDS FROM THE DYNAMOMETER

5.1. INTRODUCTION

The procedure to be followed in analysing the dynamic records of the free vibration tests, presented some difficulties, since during each record the amplitude of vibration was diminishing. It was desired to deduce from these records the behaviour of the system for vibrations of constant amplitudes. The following analysis was derived, which showed that if the information on amplitude and frequency was taken off the record traces in the appropriate fashion, the required information for free vibrations at constant amplitude could be estimated to a reasonable degree of accuracy.

5.2. THE ASSUMPTION OF THE EQUIVALENT CONSTANT-AMPLITUDE VIBRATION

A typical record of the fluctuating torque in the dynamometer during a free vibration test in water as shown in Fig. 5.1. It will be seen that the decay of the oscillation is comparatively slow. If it is assumed that the damping is of the viscous type i.e. damping force proportional to instantaneous velocity, and if the system is assumed to be linear with one degree of freedom, then the damping factor (as deduced from the number of cycles for the amplitude to decay 50%) is found to be quite small. For example, for the record given in Fig. 5.1, the number of cycles, for 50% decay is approximately 2.0. From Ref. 5.1 the damping factor is

Fig. 5.1 Typical free vibration records from the dynamometer.

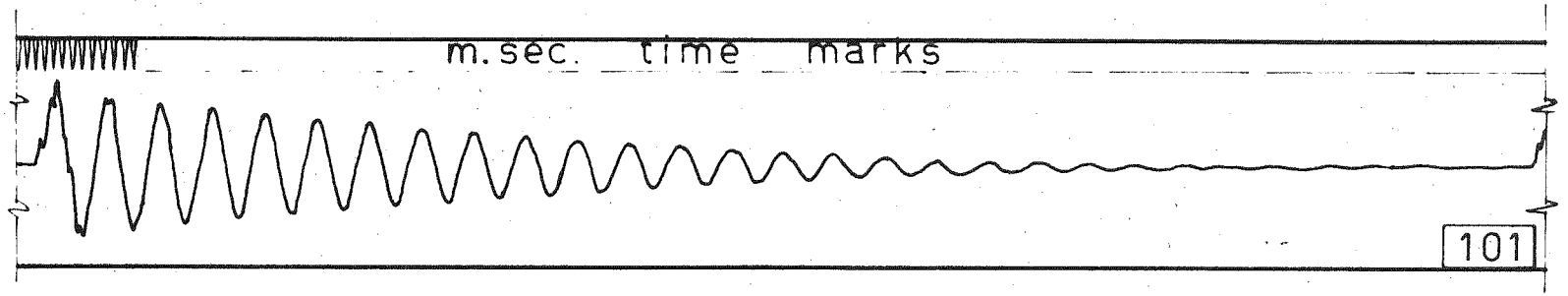

(a) PROPELLER IN AIR : blade setting −10°

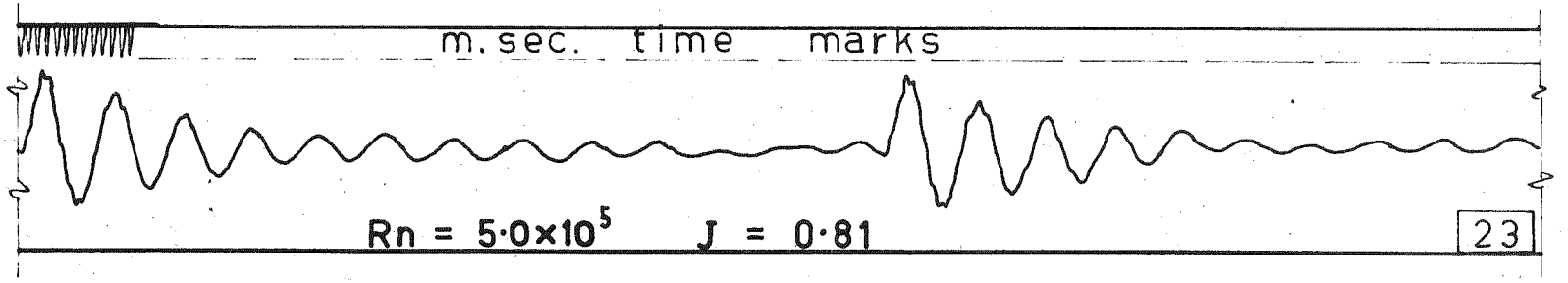

(b) PROPELLER IN WATER : blade setting 0°

estimated as 0.056. For torsional vibrations, the system is known to behave as a single-degree-of-freedom system, and it has been shown experimentally that the system is elastically linear. The damping force however, has been deduced from experiments to be dependent on a function of instantaneous velocity, not simply proportional to it. This difference in damping means that the behaviour of the system differs slightly from that of the idealised system above. The conclusion regarding the relative smallness of the damping, obtained by considering the idealised system, however, may be expected to apply also to the actual system.

It thus may be concluded from the decay rate of the oscillations, that the damping force is relatively small compared to the elastic and inertia forces operating. Thus the influence of the damping on the character of the oscillations may be expected to be small.

For the free vibration tests in air (carried out during calibration of the dynamometer) it will be seen from Fig. 5.1 that the damping factor is even smaller and would thus influence the vibration to an even lesser extent.

The damping being small and the decay of the oscillations being relatively slow, means that an analysis based on the "equivalent constant-amplitude oscillation" can be applied to the problem with little error being introduced. For this analysis it is assumed that over a period of the vibration, the factors which determine the hydrodynamic inertia (such as the instantaneous velocity field around the propeller) are on the average the same as they would be during a corresponding cycle in

an otherwise identical but undamped vibration whose amplitude (constant) is equal to the mean amplitude of the cycle of the damped vibration. This may be illustrated for a half-cycle by reference to Fig. 5.2. The value of hydrodynamic inertia (as determined from its effects over a cycle is assumed to be the same for the half-cycle of the damped vibration (Fig. 5.2a) as it is for the half-cycle of the undamped vibration (Fig.5.2b) whose amplitude is equal to the mean amplitude of the damped vibration half-cycle.

For this assumption to be valid each half cycle must be able to be considered as a separate entity, and the behaviour of the system during the half-cycle must be independent of the history of the system both previous to the half-cycle and also after it. It is shown in the next section that this is so.

5.3. THE INDEPENDENCE OF EACH CYCLE OF VIBRATION

Consider a free oscillation such as is shown in Fig. 5.2 (a) for the system shown in Fig. 5.3. At point A, which is a maxima of the curve, the rate of change of torque in the dynamometer is instantaneously zero.

$$\text{i.e.} \qquad \frac{dQ}{dt} = 0 \qquad (5.1)$$

(Point A is assumed to be both the maximum of the oscillation curve, and the point of tangency with the envelope curve, the difference which actually exists between these points being assumed negligible).

Fig. 5.2 (a) Varying amplitude oscillation

(b) Constant amplitude oscillation with the same mean amplitude as the varying amplitude oscillation shown in (a).

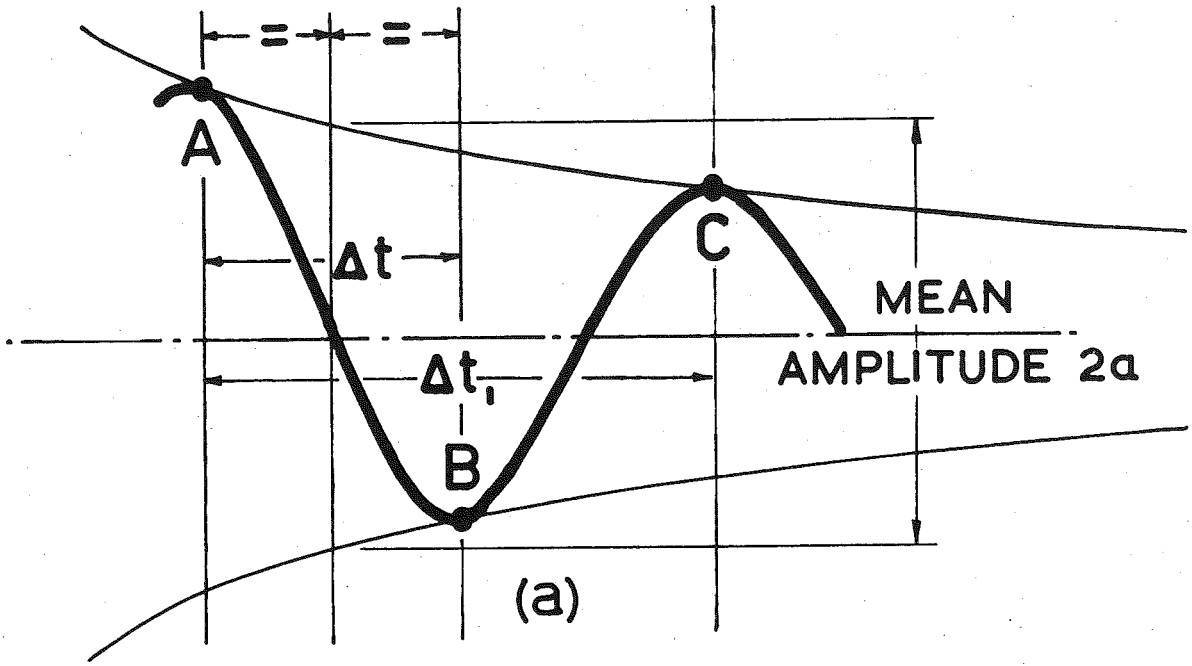
A
Δt
C
MEAN
AMPLITUDE 2a
Δt₁
B
(a)

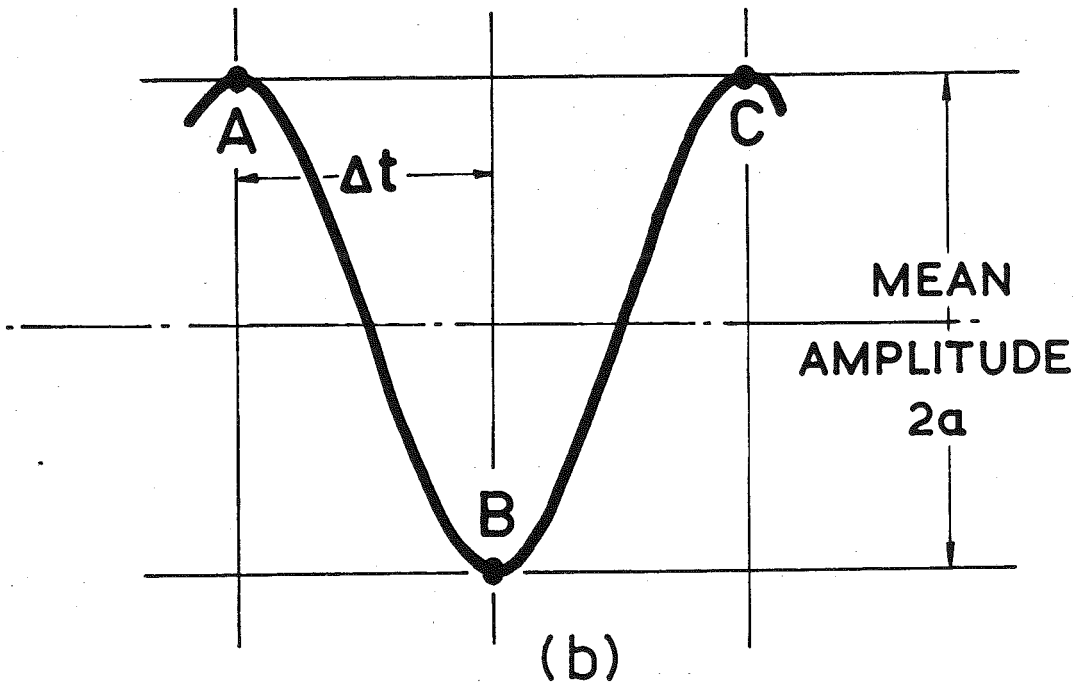
A
Δt
C
MEAN
AMPLITUDE
2a
B
(b)

Fig. 5.3 Diagrammatic representation of dynamometer torque system.

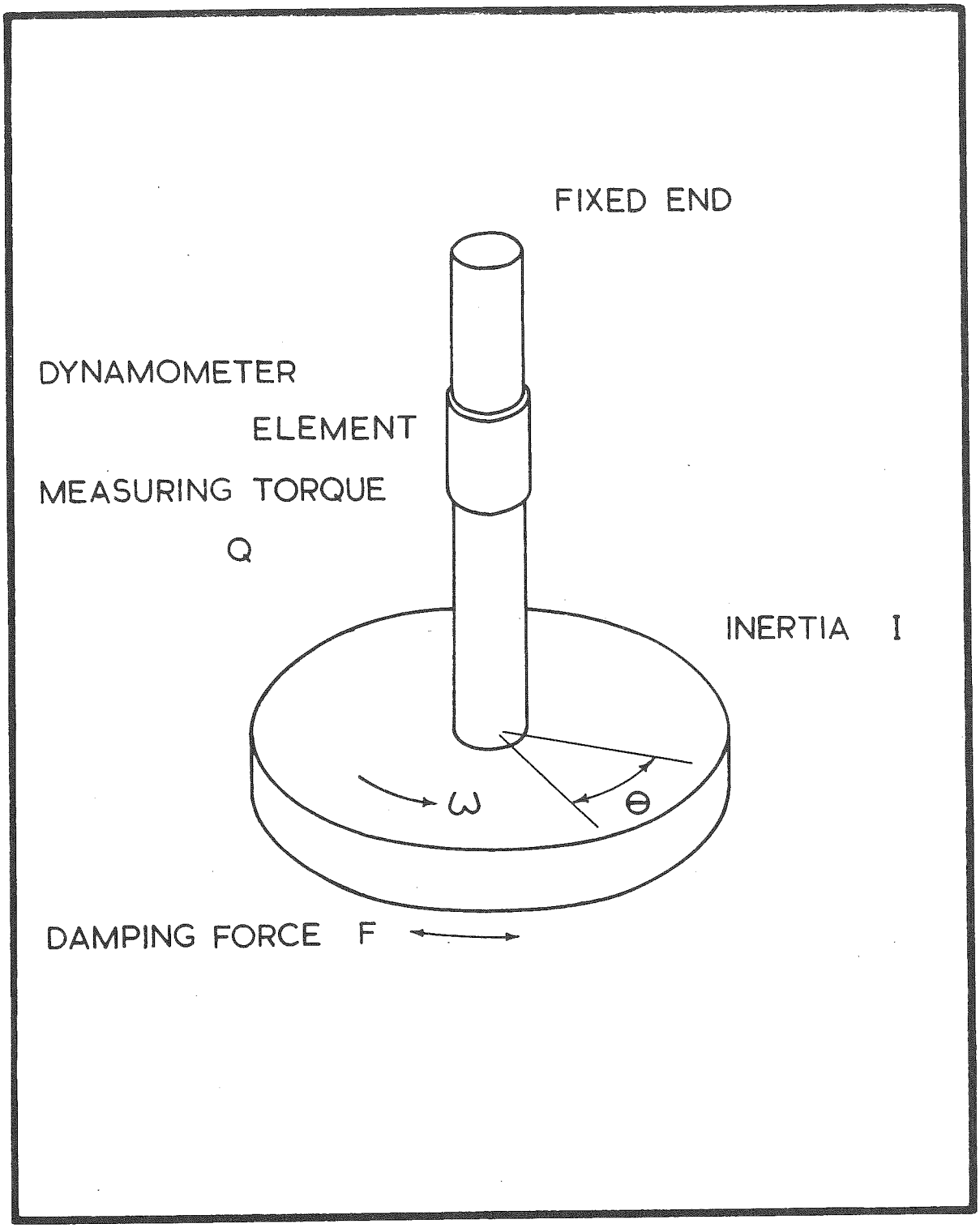
FIXED END
DYNAMOMETER
ELEMENT
MEASURING TORQUE
Q
INERTIA I
ω
Θ
DAMPING FORCE F

For a single-degree-of-freedom system in free vibration, each component reaches the condition of zero motion (at the extremes of its vibration amplitude) simultaneously. At the condition shown by point A, therefore, each component is instantaneously at rest.

$$\text{Thus} \qquad \frac{d\omega}{dt} = 0 \qquad (5.2)$$

where ω is the angular velocity of the component. (If this were not so, then equation (5.1) could not apply. But equation (5.1) is known to be applicable, hence equation (5.2) must also apply).

The previous history of the motion before point A will therefore have no effect on the motion after A, except in so far as it has determined the value of the amplitude at A. The behaviour of the system from A onwards is dependent only on the amplitude at A, and does not otherwise depend on the history previous to A. The manner in which the system was set to the amplitude corresponding to A is irrelevant. For example, it might have been statically set to that value by an externally-applied force (e.g. by hand), or it may have been carried to that position by inertia forces during a previous vibration cycle. A similar conclusion may be reached for the history of the system after point B. The converse will also be true and it may therefore be concluded that the behaviour of the system during the half-cycle AB is independent of the subsequent history after B.

Thus it may be concluded that the behaviour of the system during the half-cycle AB depends only on the initial amplitude at A, and the inherent

characteristics of the system, and not on the history prior to or subsequent to AB.

This conclusion will not be quite true if at A or B there is some portion of the system which still has velocity.

The "entrained mass" of fluid surrounding the propeller is coupled to the propeller by fluid forces. These forces are of two kinds; pressure and viscous i.e. normal and shear. In a fluid, a shear force is not directly related to amplitude (as in a solid) but instead is related to velocity. This means that amplitude of fluid motion is not directly related to the shear force applied. Thus if a body has been applying a viscous force to the fluid (by virtue of moving relatively to the fluid) and the body suddenly stops, the fluid motion will not stop at the same instant but continue for a time.

Only for a perfect (non-viscous and incompressible) fluid is a change in boundary motion instantaneously reflected in a change of fluid motion.

In the present case, therefore, it is to be expected that the previous history immediately prior to A will have some slight influence on the vibration in the half-cycle AB in Fig. 5.2(a), due to the fluid effects. However, since the previous history of the vibration immediately prior to A, closely approximates to the previous history prior to point A for the vibration shown in Fig. 5.2(b), it may be expected that the effect due to the fluid motion will be closely the same as would occur in the case of the vibration shown in Fig. 5.2(b).

This means that even allowing for the "fluid effect", the behaviour of the system during the half-cycle of the constant-amplitude vibration

shown in Fig. 5.2 (b), may be regarded as being closely equivalent to the behaviour of the system during the half-cycle of the varying-amplitude vibration shown in Fig. 5.2(a).

The "fluid effect" described above is only associated with viscous forces and may be expected to be small. It may thus be also assumed that the behaviour of the system during the half-cycle AB of the vibration shown in Fig. 5.2(a), is independent to a high degree, of the history prior to and subsequent to AB.

5.4. THE DYNAMIC CALIBRATION OF THE DYNAMOMETER

The method of dynamically calibrating the dynamometer is also discussed in section 4.3. The calibration was carried out by attaching (in succession) discs of various inertias to the dynamometer. Recordings were made of free vibrations of the system (in air). Excitation was by means of a transient impact. A typical record is very similar to the record for the propeller in air shown in Fig. 5.1 (a).

The conclusions derived in Section 5.3 above for propeller vibrations are valid for the calibration vibrations also. These conclusions were:-

(1) that each half-cycle of the oscillation may be regarded as being dependent only on the initial amplitude at the beginning of the half-cycle and on the inherent characteristics of the system.

(2) that the behaviour of the system during a half-cycle such as AB in Fig. 5.2(a), may be closely approximated by the half-cycle AB of the harmonic oscillation of constant-amplitude shown in Fig. 5.2(b).

A further conclusion, of some importance, may also be drawn regarding

the amplitude of the waveform. The behaviour of the system during a half-cycle such as AB in Fig. 5.2(a) includes the amplitude-time relationship during this period. Once the initial amplitude at A has been fixed, the amplitudes throughout the rest of the half-cycle are determined. In particular, the mean amplitude 2a is determined. Thus, there is a direct relationship between the mean amplitude and the initial amplitude for a given system. The mean amplitude can thus be taken as a parameter instead of the initial amplitude. Since it is in practice easier to determine the mean amplitude from the traces than it is to determine the initial amplitude (which requires the determination of the centre-line) the mean amplitude has been taken as the amplitude parameter for each half-cycle. Therefore, where ever amplitude is referred to in this context, it is the mean amplitude 2a which is meant. This mean amplitude is identical with the mean amplitude of the equivalent-harmonic-oscillation of constant amplitude (such as is shown in Fig. 5.2(b)).

It was found in practice that period Δt of the half-cycle (from which was determined the corresponding frequency) could be best determined by measuring the interval Δt_1 between successive peaks (such as A and C in Fig. 5.2a) and then halving this value. That any error introduced would be small was checked by comparing the values of Δt obtained by taking the interval between 2,3 and 5 peaks and dividing the values obtained by 2,3 and5 respectively. The values obtained from the three determinations were almost identical (especially for 2 and 3 peaks).

The method given above for obtaining the amplitude parameter 2a and the period Δt for a half-cycle, in the case of the dynamic calibrations,

was adopted also for the analysis of all the traces obtained during the experimental runs of the propeller in water.

The following method, based on the conclusions above and in Sections 5.2 and 5.3, was used to determine the value of hydrodynamic inertia during the propeller tests. The results of the dynamic calibration tests were plotted in the form of mean-amplitude versus half-period, for the various values of inertia (See Fig. 4.4). Actually, for convenience, the half-period values were doubled to give 2 Δt, and the graphs were plotted using 2 Δt as a parameter instead of Δt. On the graphs the value of $2\Delta t$ has been called the period. Cross plotting then gave curves (actually straight lines) of inertia versus (half-period)^2, for various values of amplitude (See Fig. 4.5). These calibration graphs were then used to determine the value of the unknown inertia (propeller and hydrodynamic inertia) in each of the hydrodynamic inertia test runs, for each half-cycle of oscillation of the run, from the mean amplitude and half-period of the cycle as determined from the record trace. The known inertia of the propeller was then subtracted from the total calue of inertia determined, to obtain the value of hydrodynamic inertia.

5.5. ERRORS IN THE ANALYSIS DUE TO FLUID DAMPING

It has been shown in Sections 5.2 - 5.4 that the method of determining hydrodynamic inertia from the dynamic calibration graphs, should yield results of a reasonable degree of accuracy. That this is actually so in practice is indicated by the data shown in Fig. 4.4 and Fig. 4.5. This data was taken from vibration tests on various inertia discs, excited by

various degrees of impact. It will be seen that in Fig. 4.4 the data points fall closely on unique lines. That these curves when cross-plotted on to Fig. 4.5 give straight lines for constant values of amplitude (except in the extreme upper range of period^2) is further confirmation of the validity and reliability of the method of analysis.

There is, however, a source of error, as yet undiscussed which is present during the propeller tests in water. This is the reduction of mean amplitude and period of a cycle of the oscillation due to the additional fluid damping present, and the consequent error which is introduced when determining the inertia from the dynamic calibration data (since these calibrations are strictly only valid for oscillations in which the fluid damping is absent).

Fig. 5.4 shows how the error is introduced. This figure shows a half-cycle of the free vibration for a total inertia I, for the two conditions i.e. with and without the additional fluid damping. In both cases, the half-cycle has the same initial amplitude. The decay for the fluid-damped oscillation $A'B'$ is more rapid than for the non-fluid-damped oscillation AB. From the record trace the mean-amplitude $2a'$ and the half-period $\Delta t'$ are determined. The mean-amplitude $2a'$ and half-period $\Delta t'$ are then taken across to a dynamic calibration graph and set equal to the mean-amplitude and half-period of a non-fluid-damped oscillation, which by reference to Fig. 5.4, is seen to be the oscillation A"B". The inertia I_2 corresponding to the oscillation A"B" is then taken as the inertia for the actual fluid-damped case.

The error introduced in the determination of the inertia will

Fig. 5.4 Diagram showing the relationship between the oscillations obtained with an inertia I_1 attached to the dynamometer (with and without fluid damping present), and the oscillations obtained with an inertia I_2 attached to the dynamometer (without fluid damping present)

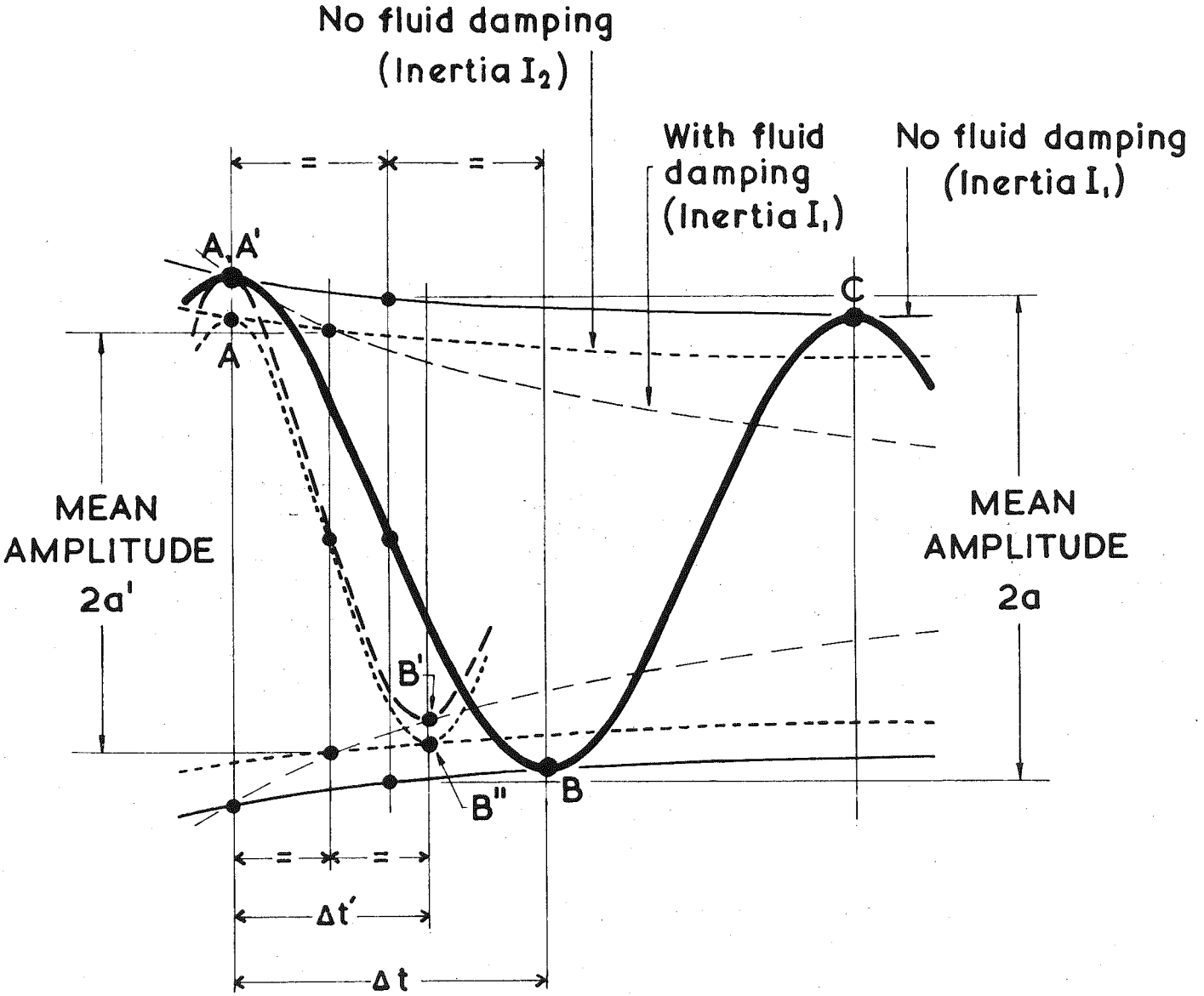
No fluid damping
(Inertia I_2)
With fluid damping
(Inertia I_1)
No fluid damping
(Inertia I_1)
A, A'
A
C
B'
B''
B
MEAN AMPLITUDE
2a'
MEAN AMPLITUDE
2a
$\Delta t'$
Δt

however be small due to the following reasons:-

(1) over a half-cycle, the decay envelopes for the oscillations A'B' and A"B" differ in practice by only a small amount.

(2) The effect of damping on the frequency of any free vibration is, in general, small (see for example Ref. 5.2). Hence the half-period of a slightly damped vibration such as A'B' for a system with a given inertia does in fact closely approximate to the half-period of an undamped vibration such as AB for which the inertia is the same.

(3) In general, damping shows its influence mainly in amplitude changes (see for example, Ref. 5.3). The error introduced in the above outlined method of determining inertia is mainly in amplitude, although even here the error is slight. As may be seen from the dynamic calibration graph Fig. 4.5, the calibration is in any case only slightly amplitude dependent.

It may thus be concluded that the technique of determining hydrodynamic inertia from the calibration data, in the manner outlined in the foregoing, should yield results of good accuracy.

PART III

MODEL RESEARCH -

THE VIRTUAL INERTIA

OF

PROPELLERS UNDER LOAD

CHAPTER 6

THE IMPORTANCE OF VIRTUAL INERTIA

A body in unsteady motion in a fluid has an apparent increase in mass. This is because the body causes movement of the fluid i.e. produces accelerations of fluid particles. The acceleration of each fluid particle requires the application of a force to the particle. To provide these particle forces, a net additional force must be applied to the body over and above that force required to accelerate its own mass. This additional force acting on the body may be conceived as causing the acceleration of an additional mass attached to the body, the magnitude of this mass being defined by the additional force divided by the acceleration, according to Newton's second law. This hypothetical additional mass is known as the hydrodynamic mass. The total apparent mass of the body (which is known as its "virtual mass") is thus equal to the sum of its mechanical mass plus the hydrodynamic mass.

If the motion of the body is rotational, then the hydrodynamic mass effect appears as an increase in inertia, which is known as the "hydrodynamic increase in inertia" or the "hydrodynamic inertia". For such motion therefore, the total apparent inertia, which is known as the "virtual inertia", is equal to the sum of the mechanical inertia plus the hydrodynamic inertia.

The phenomenon described above is sometime referred to as the entrained mass effect, as well as the hydrodynamic mass effect. It would appear that this phenomena was first recorded, by Bessel, in 1828.

A knowledge of the value of the hydrodynamic mass is especially important in oscillatory motion since the value of the virtual mass is one of the parameters which determine the value of frequency and amplitude.

In the field of naval architecture, problems associated with virtual mass arise in several connections. The two most important are in hull vibration, and in propeller vibration. The research described in this part of the thesis is concerned with virtual mass in the latter field.

A marine propeller can vibrate in various modes. The most important modes of vibration are (see also Ref. 6.1)

(1) Torsional

(2) Longitudinal

(3) Diametral rotation

(4) Vibration of the blades (as distinct from the vibration of the propeller as a whole)

In each case, since the mode of oscillation is different, there will be a different value of hydrodynamic mass which applies. The research project described in this Part of the Thesis is concerned only with the mode of vibration (1), i.e is only concerned with torsional virtual inertia. (Previous work by other investigators in this field is described in Refs. 6.2 - 6.9). The determination of torsional virtual inertia is particularly important in the problem of determining the natural frequency of propeller shaft systems, and the associated applitudes and stresses.

CHAPTER 7

THE IDEAL HYDRODYNAMIC MASS AND INERTIA

When a body is vibrating in a fluid, the oscillatory motion of the body causes a corresponding motion of the fluid. In the case of the ideal fluid, this motion can be calculated by potential flow methods. In the case of simple shapes the calculation is comparatively simple, but in the case of complex shapes such as propellers, the calculation is difficult and has only been attempted in a few such cases. The hydrodynamic mass (or inertia if the motion is rotational) which obtains under the ideal fluid condition is known as the ideal hydrodynamic mass (or inertia). In this case, the fluid velocities are those predicted by potential flow and the relationship of these particle velocities to the hydrodynamic mass of the body may be considered in the following two ways:

(1) Force Transfer

Because the motion is unsteady, the velocity of fluid particle near the body at any instant will be changing i.e the particle will be undergoing an acceleration. This acceleration requires an applied force. The nett sum of these applied forces must ultimately be provided by the body acting through the medium of pressure forces on its surface (By Newton's Third Law of Motion; "Action and reaction are equal and opposite"). The nett sum of the applied forces on the particles is thus an additional force (sometimes called the liquid accelerating force) which must be provided by the body. This force if divided by the

acceleration of the body, defines a hypothetical mass. This mass is called the hydrodynamic mass. If this mass were attached rigidly to the body, a force equal in magnitude to the liquid accelerating force would be required to accelerate the mass at the same rate as the body itself. In the rotational motion case there is a liquid accelerating torque which may be used to define the hydrodynamic inertia I_h in a similar way.

(2) Energy Transfer

Each fluid particle in the neighbourhood of the body has a finite velocity, and hence an associated kinetic energy. The kinetic energy of each particle must ultimately have been supplied by the body. The total kinetic energy of the fluid is equal (by the Law of Conservation of Energy) to the energy supplied externally to the body minus that necessary to accelerate the body's own mass up to the condition considered. The kinetic energy of the fluid divided by the square of the body's velocity, defines a hypothetical mass, which is called the hydrodynamic mass. In the rotational motion case the hydrodynamic inertia is defined in a similar way.

That the hydrodynamic masses as defined by the alternative methods (1) and (2) above are identical is shown in the following paragraphs.

The total kinetic energy E of the fluid at an instant when the body velocity is U, may be expressed in terms of the sum of the kinetic energies of the particles. If a typical particle mass is m and its velocity u, this relationship may be written

$$E = \sum \frac{1}{2} mu^2 \qquad (7.1)$$

It should be noted that the fluid velocities u are the particle velocities relative to earth axes i.e are the absolute velocities. At one or more points in the fluid touching the body surface, the particle velocity will be U i.e equal to the body velocity. Such a point will be taken as a reference point, and the velocity U at this point will be taken as a characteristic velocity for the fluid motion.

For an ideal fluid, the ratio k of the particle velocity u (at a given point relative to the body) to the characteristic velocity U is dependent only on the body shape and is thus independent of the value of the body velocity. (This may be easily shown by Dimensional Analysis for the general case).

That is

$$\frac{u}{U} = k \quad \text{or} \quad u = kU \tag{7.2}$$

where k is a numerical constant dependent only on the position of the point considered (relative to the body), for a given body shape.

Thus (7.1) can be rewritten as

$$E = \sum \left(\tfrac{1}{2}mk^2U^2\right)$$

$$= \tfrac{1}{2}U^2 \sum (mk^2) \tag{7.3}$$

Since $\sum (mk^2)$ has the dimensions of a mass, it may be written as

$$M_h = \sum (mk^2) \tag{7.4}$$

Thus

$$E = \frac{1}{2}M_h U^2 \qquad (7.5)$$

M_h is thus seen to be the hydrodynamic mass as defined in section (2) above.

The liquid accelerating force F, moving at the body velocity U, is doing work at a rate given by F.U. In an interval of time dt, the work done on the fluid will thus be F.U.dt. This must equal the increase dE in kinetic energy of the fluid particles.

Thus

$$dE = F.U.dt \qquad (7.6)$$

or

$$\frac{dE}{dt} = F.U \qquad (7.7)$$

Substituting from (7.1) for E gives

$$\frac{d}{dt}\left(\sum \frac{1}{2}mu^2\right) = F.U$$

i.e

$$\sum\left(mu\,\frac{du}{dt}\right) = F.U$$

and substituting from (7.2) for u

$$\sum\left(mkU.k\,\frac{dU}{dt}\right) = F.U.$$

or $$U. \frac{dU}{dt} . \sum (mk^2) = F.U$$

Rearranging gives

$$\sum (mk^2) = F \Big/ \frac{du}{dt} \qquad (7.8)$$

The right-hand-side of equation (7.8) is the hydrodynamic mass M_h as defined in section (1) above

Thus $$\sum (mk^2) = M_h \qquad (7.9)$$

This expression (7.9) is identical to (7.4), thus showing that hydrodynamic masses as defined in sections (1) and (2) respectively, are identical.

The constant k at a given point (relative to the body) is dependent only on the body shape. Thus the hydrodynamic inertia

$$M_h = \sum mk^2$$

is dependent only on the body shape, and independent of the velocity or acceleration of the body. For oscillatory motion, therefore, the ideal hydrodynamic mass is independent of the frequency and amplitude of the oscillation.

For the real fluid case, it can be easily seen by considering the force transfers or the energy transfers, that any factor which causes the velocities (and hence accelerations) of the fluid particles around

the body to depart from the ideal fluid values, will cause the value of the hydrodynamic mass or inertia to depart from the ideal value. In the case of oscillatory motion in a viscous fluid for example, the amplitude and frequency of the oscillation will therefore be parameters on which the hydrodynamic mass will depend, in addition to parameters defining the body shape. This is because the shear velocity on which the viscous effects will be dependent, are functions of amplitude and frequency (See also Section 8.2)

CHAPTER 8

FACTORS INFLUENCING THE ACTUAL HYDRODYNAMIC INERTIA OF PROPELLERS

8.1 THE EFFECT OF SHAPE

The configuration of the propeller and neighbouring surfaces will be the major factors which determine the value of the hydrodynamic inertia in the real fluid case, since in the ideal fluid they are (with the fluid density) sufficient to uniquely determine the value of hydrodynamic inertia. The effects associated with the real fluid may be expected to be secondary influences on the hydrodynamic inertia, compared with the shape parameters. That this is so in reality may be seen from previous work in this field (Refs. 6.1-6.9). However, the variations in hydrodynamic inertia for a given shape due to real fluid effects, could be significant under some conditions.

Unless other surfaces, such as the hull and the water-air interface are very close, the effect on the velocity pattern and hence on the hydrodynamic inertia will probably be small. If the free-surface is very close however, gravity waves will be caused on the surface and these will affect the hydrodynamic inertia separately, and in addition to the distortion of the velocity field caused by the presence of the free-surface boundary. To produce the gravity waves, additional pressure force transfers will have to be provided by the surface of the propeller, andthese will require an additional nett force F_g to be exerted by the body over and above that force F_h which would be required if the gravity waves did not occur. Corresponding to this additional force an

additional hydrodynamic inertia component can be defined if desired.

Actually there is no necessity to define a hypothetical inertia corresponding to the additional force F_g. In an experimental determination of hydrodynamic inertia, however, a correction for F_g would not usually be made, and the value of hydrodynamic inertia deduced from the test would therefore include a component due to the gravity wave effect. It would seem logical and convenient to describe this component as the "gravity hydrodynamic inertia" (component).

8.2 THE EFFECT OF VISCOSITY

In the real fluid case, where the body is surrounded by a fluid possessing viscosity as well as mass, the effects of the viscous forces on the hydrodynamic inertia must be considered.

In the case of an oscillatory body in a real fluid the definition of the hydrodynamic mass itself presents some difficulties because of the forces on the body surface associated with viscous effects. In the ideal fluid, the only forces on the body surface are pressure forces. These integrate to give a zero nett force in the case of steady motion. For unsteady motion, however, the nett force is finite - the "liquid accelerating force".

In the real fluid, the total force F' (in the direction of motion) applied by the body to the fluid (at an instant when the body velocity is U) does work at a rate equal to $F'.U$. In time dt the work done is $F'.Udt$. This energy provides both an increase dE in the kinetic energy of the fluid and an increase dQ in the heat energy of the fluid.

$$\text{Thus} \quad F'.U.dt = dE + dQ \qquad (8.1)$$

The increase dE in the kinetic energy is associated with an increase in fluid particle velocities. To produce the increases in fluid particle velocities, forces must be applied to the particles. These forces are of two kinds, pressure and viscous i.e normal and tangential forces. The nett sum of these forces throughout the fluid must be provided by a force applied to the fluid by the body. This force will be applied to the fluid by pressure and viscous forces on the surface of the body. Let the component of this force in the direction of movement be F_E. The work done in time dt by F_E will be $F_E.U.dt$, and this must be equal to the increase in kinetic energy dE.

$$\text{i.e} \quad dE = F_E.\ U.\ dt \qquad (8.2)$$

The increase dQ in heat energy results from viscous dissipation. The shear forces which are associated with this dissipation must ultimately be provided in nett sum by the body. This force which the body provides is transmitted to the fluid by both pressure and viscous forces on the body surface, as was the force F_E. The component of this force on the body in the direction of motion, is the damping force F_d. The work done by the damping force can be equated to the dissipation.

$$\text{Thus} \quad dQ = F_d.\ U.\ dt \qquad (8.3)$$

From equation (8.1), (8.2) and (8.3) may be obtained the relation:-

$$F' = F_E + F_d \qquad (8.4)$$

From the force F_E, an hypothetical hydrodynamic mass M_h' can be defined by dividing F_E by the acceleration $\frac{d^2x}{dt^2}$ of the body:-

Thus, $$M_h' = F_E \frac{d^2x}{dt^2} \qquad (8.5)$$

This definition is not particularly useful, since because of viscous effects the value of M_h' will be dependent on the body shape and size, its velocity (and possibly acceleration), and the fluid density and viscosity. It will not, as in the ideal fluid case, be only dependent on the body shape. Thus throughout a cycle of the oscillation the value of M_h' will change. In any case, the determination of F_E, in practice, would be very difficult. It might be thought that it could be found by subtracting F_d from F', but the difficulty is that the damping force F_d can only be calculated for very simple configurations (such as the flat plate) for which the dependence of F_d on the various factors (such as velocity) is known.

It is suggested, therefore, that the hydrodynamic mass be defined in terms of its effect on a cycle of the oscillation. This is the approach which has been applied by previous investigators for the case of the damping force F_d. In this case the assumption which has been made is that the actual damping force can be replaced by an equivalent linear resistive force $k \frac{dx}{dt}$ which over a cycle dissipates the same amount of

energy as the true damping force (Ref. 6.2, 8.1).

The corresponding definition for hydrodynamic mass M_h would then be as follows:- "The hydrodynamic mass M_h for an oscillating body in a real fluid is that constant mass which assumed attached to the oscillating body would give a period of oscillation the same as is found for the actual vibration, at the same amplitude". Since the instantaneous hydrodynamic mass M_h' probably does not vary greatly during the oscillation, this assumption should yield a reasonable approximation to the actual behaviour of the oscillating system.

These two assumptions above (dealing respectively with the damping and the mass) allow the actual vibration to be replaced by an equivalent damped vibration, in which the mass is constant and in which the damping is given by a simple linear relationship. The solution of the differential equation in such a case is then possible. In an actual case, by measurement of the frequency and the damping of the oscillation, and by substitution in the appropriate equations, the hydrodynamic mass M_h and the damping constant can be calculated.

The assumption of an equivalent (constant) hydrodynamic mass M_h, as defined above, has been often made, in investigations into virtual mass (see for example, Ref. 6.2)but the author has never seen this assumption explicitly stated. It can be seen that the hydrodynamic mass M_h as defined above corresponds to the equivalent effect of the kinetic energy of the fluid over a whole cycle, instead of instantaneously as in the ideal fluid case.

For the real fluid, M_h (like M_h') will be dependent on the body shape and size, its velocity and possibly acceleration, and on the fluid

density and viscosity. Since the amplitude and frequency of the oscillation determine the velocity and the acceleration of the motion, they may be used as parameters on which M_h is dependent in place of velocity and acceleration.

Whether M_h will be larger or smaller in the real fluid case than in the ideal fluid, is a question difficult to answer. It has been suggested by Brahmig (Ref. 6.2) that in the real fluid case the fluid kinetic energy is always less than in the ideal case, and thus

$$M_{h_{actual}} < M_{h_{ideal}} \tag{8.6}$$

This would appear reasonable on two counts, if only the velocities (and kinetic energies) associated with pressure forces are considered. In the first place, if one considers the ideal case and suppose that viscosity suddenly becomes a property of the fluid, it is easily seen that the velocities will decrease (due to the introduction of viscous forces) resulting in a decrease of kinetic energy and thus of M_h. Secondly, if the body is bluff, separation will tend to occur in the real fluid. As a separation region is a relatively low-energy zone, the total kinetic energy and hence hydrodynamic mass of the fluid will tend to decrease. In this connection, it is significant that Brahmig's results, which show a decrease in M_h for the real fluid, were obtained with a very bluff body viz a circular disc.

If one also considers the kinetic energy associated with the velocities caused by viscous forces, however, it is apparent that the contribution of this kinetic energy to M_h (which will be called the

viscous component of M_h)will be larger in the real fluid case than in the ideal fluid (when its value will be zero). In general, this component will be small, and may be expected to be swamped by the general tendency for decrease of M_h described above. In special cases, however, such as a thin streamlined body oscillating along its chord, the viscous contribution to M_h may be significant. For such cases M_h may remain approximately constant, or even increase slightly. For bodies with rotational motion, the conclusions in the above discussion regarding M_h may be applied to the hydrodynamic inertia I_h.

The trends which the various parameters such as frequency and amplitude might be expected to have on the hydrodynamic mass, or in the case of rotational motion on the hydrodynamic inertia, are discussed in the following sections.

8.3 THE EFFECT OF AMPLITUDE

In the ideal fluid case there is no change of hydrodynamic inertia with amplitude.

In the real fluid case at amplitudes approaching zero, there will be no separation around the body and the velocity pattern (and value of M_h) will tend to the ideal. As the amplitude of oscillation increases, separation will tend to occur, with low-energy separation regions appearing. This together with viscous reduction of the potential flow velocities, would be expected to cause an increasing deviation from the ideal value of M_h. Thus as amplitude increases, M_h would be expected to decrease.

For a thin circular disc, Brahmig (Ref. 6.2) has demonstrated

such a decrease in M_h, with increase in amplitude.

The effect of the viscous component of M_h on this trend is likely to be negligible, except for streamlined bodies moving along their major axes. In such cases, M_h may tend to remain constant or possibly slightly increase.

8.4 THE EFFECT OF FREQUENCY

For the ideal fluid, there is no change in the hydrodynamic mass or inertia with frequency. For the real fluid, a trend with frequency can be postulated, by considering the physical nature of the shear stresses which occur within the fluid. Shear stress is related to the rate of transfer of the momentum which has its direction parallel to the shear plane, in the direction normal to the shear plane i.e. across the shear plane. For laminar flow the transfer is by molecular motion, and for turbulent flow the transfer is by both molecular movement and eddy convection (See Ref. 8.2)

Consider now the shear stresses and momentum transfers in the fluid layers adjacent to the body. As motion of the body commences in one direction, the surface layer of fluid attached to the body will begin to exert a shear stress on the adjacent layer and will begin to accelerate it. In terms of momentum transfer, the nett additional momentum parallel to the shear plane which has been transferred across the plane in one direction over and above that transferred in the opposite direction, has increased the total momentum of the adjacent outer layer. Since the mass in this layer is constant, this corresponds to an increase in its velocity. This layer then begins to accelerate

the next layer and so on.

If the acceleration of the body during the oscillatory motion is infinitely small then equilibrium will exist at all times throughout the boundary layer, and the boundary layer will correspond to the steady-state boundary layer. If the acceleration is high, the boundary layer will be thinner at any given point in the cycle than it would have been if the acceleration were small. Thus, as the frequency, and hence acceleration (for a given amplitude) increases, the region around the body in which viscous effects predominate (i.e the boundary layer) decreases in size.

The tendency for separation to occur around a body increases as boundary layer thickness increases. Thus increase in frequency will decrease the tendency for separation. It has been previously seen that separation is associated with a decrease in the hydrodynamic mass. Thus, as the frequency tends to very high values, the hydrodynamic mass will tend to the ideal value. Conversely, decrease in frequency will be associated with decrease in M_h or I_h. This effect has been shown experimentally for a thin circular disc by Brahmig (Ref. 6.2).

8.5 THE EFFECT OF PROPELLER LOADING

If the propeller is rotating steadily under load in an ideal fluid then the steady flow pattern associated with this motion will be superimposed upon the unsteady flow pattern due to the torsional oscillation.

For the ideal fluid, by the principle of superposition of potential flows, the composite flow pattern will be given by the superposition of the two separate potential-flow patterns. It is also true that in this

case, the two component flows and the forces they produce on the body, can be considered separately. Thus the oscillating forces on the body are associated with the oscillatory flow pattern and are quite independent of the steady rotational flow pattern. For the ideal fluid therefore, the hydrodynamic mass or inertia is independent of propeller rotation or load.

For the real fluid, however, the flow pattern around a propeller which is rotating and also oscillating, cannot be broken down into two independent flow patterns. This means that the oscillatory flow pattern will be to some extent dependent on the flow pattern of the steady rotational motion. Thus, the hydrodynamic mass or inertia of a propeller will depend upon the propeller loading, in the real fluid case.

In the oscillating but non-rotating case, if the oscillation amplitude is small, the flow in the boundary layer will probably be laminar. In the oscillating and rotating case, the steady relative flow may cause turbulent conditions and separation regions. It might therefore be expected that under these conditions the effect of propeller loading would be considerable. It may be postulated, however, that the effect of propeller loading on hydrodynamic inertia will be small, if the oscillation amplitude is relatively small, for the following reason. If the relative magnitudes of the flow velocities due to the steady movement of the propeller and due to the oscillatory movement of the propeller are considered, it may be easily shown that unless the propeller speed is extremely high, the steady flow velocities are small compared to the oscillatory peak velocities.

Thus, the effect on the oscillatory flow pattern of an increase or

decrease in the small steady velocities associated with the rotation, should be small. Change of propeller loading should thus have a small effect on hydrodynamic mass and inertia.

If the propeller loading causes separation to occur when it would not otherwise have resulted from the oscillatory motion, however, significant changes in the hydrodynamic mass or inertia might occur.

8.6 THE EFFECT OF ROUGHNESS

The effect of roughness on hydrodynamic mass may be postulated as being small for low frequencies and small amplitudes, if it is assumed that the oscillatory boundary layer is turbulent, since under these conditions the oscillatory boundary-layer profile would probably not be steep enough to expose the roughness peaks above the laminar sub-layer. However, under these conditions of low frequency and small amplitude, the oscillatory boundary layer is most likely to be laminar. It is known that roughness has a negligible effect on such flows (cf. pipe and flat-plate friction data), and the effect of roughness on the hydrodynamic mass or inertia in these cases would almost certainly be small. If, however, the amplitude of the oscillation is large, the frequency is high, or the scale of the roughness is large, the effect of roughness may need to be taken into account when considering the value of hydrodynamic inertia.

8.7 THE EFFECT OF TURBULENCE

The shear stress across a plane in a fluid increases if turbulence is introduced, as there is now momentum transfer by eddy convection as well as by molecular diffusion. There will thus tend to be a decrease

in the oscillatory velocities around an oscillating body as the intensity of turbulence increases. Thus, the hydrodynamic mass or inertia will tend to decrease as turbulence increases. This effect, will probably be relatively small.

Increase of turbulence, however, increases the tendency for separation in a boundary layer. It has been seen previously that separation is associated with a decrease in hydrodynamic inertia. If the increase in turbulence, therefore, is sufficient to cause separation a significant decrease in hydrodynamid inertia could occur.

CHAPTER 9

DIMENSIONAL ANALYSIS OF THE PROPELLER VIRTUAL INERTIA PROBLEM

A dimensional analysis of the propeller virtual inertia problem has been given previously by Brahmig (Ref. 6.2). The following dimensional analysis, although generally similar, differs in certain important respects from Brahmig's analysis.

For a propeller in torsional oscillation in a fluid, the hydrodynamic inertia I_h will depend upon the shape of the propeller and the neighbouring boundaries, the blade surface roughness, the propeller forward speed, the amplitude and frequency of the vibration, the fluid properties, and the gravitational constant.

Thus

$$I_h = f(a,b, \text{ -- } P,D,\delta,h,\rho,\mu,V,n,\theta,f,g) \qquad (9.1)$$

where

I_h = Hydrodynamic inertia

a,b- = Dimensions specifying the blade shape and its relationship to neighbouring boundaries

P = Blade pitch

D = Outside diameter of the propeller

δ = Average roughness

h = Depth of immersion

ρ = Fluid mass density

μ = Fluid viscosity

V = Propeller forward speed

n = Propeller rotational speed

θ = Angular amplitude of vibration

f = Frequency of vibration

g = Acceleration due to gravity

Thus

$$f_1 (I_h, a, b, -- P, D, h, \delta, \rho, \mu, V, n, \theta, f, g) = 0 \qquad (9.2)$$

By dimensional analysis, a set of dimensionless groups or π terms involving the variables in equation (9.2), can be obtained which will satisfy the equation

$$f (\pi_1, \pi_2 \text{ ---------- } \pi_n) = 0 \qquad (9.3)$$

In the present case these π terms are

$\pi_1 = \dfrac{I_h}{\rho D^5}$ = N A form of Newton's Number

$\pi_2 = \dfrac{\rho D^2 f}{\mu}$ = S The frequency parameter (a form of oscillatory Reynold's Number)

$\pi_3 = \dfrac{g}{Dn^2}$ = F A form of Froude Number

$\pi_4 = \dfrac{V}{nD}$ = J The Advance ratio

$\pi_5 = \dfrac{\rho n D^2}{\mu}$ = R The propeller Reynolds Number

$\pi_6 = \theta$ The amplitude parameter

$\pi_7 = \frac{P}{D}$ The pitch parameter

$\pi_8 = \frac{h}{D}$ The immersion parameter

$\pi_9 = \frac{\delta}{D}$ The roughness parameter

$\pi_{10} = \frac{a}{D}$, $\pi_{11} = \frac{b}{D}$, $\pi_{12} = \frac{c}{D}$, etc Shape parameters.

Thus

$$F\left(N,S,F,J,R,\theta, \frac{P}{D}, \frac{h}{D}, \frac{\delta}{D}, \frac{a}{D}, \frac{b}{D}, \frac{c}{D} \text{---}\right) = 0 \qquad (9.4)$$

For propellers of geometrically similar shape π_{10}, π_{11}, --- are constant. If the propellers have fixed blades, then $\pi_7 = \frac{P}{D}$ is also constant. If the propeller is of the variable-pitch type, however, π_7 will still be a parameter. The effect of $\pi_8 = \frac{h}{D}$ and $\pi_9 = \frac{\delta}{D}$ should be small under most practical conditions and they can therefore be neglected. If however, h is very small, or δ is very large, the effect of these parameters may be significant. Similarly, the effect of $\pi_5 = \frac{\rho n D^2}{\mu}$, in most cases should be small. If h is small, gravity waves associated with the oscillation should be small, and

therefore the effect of g should be negligible. In this case $\pi_3 = F$ can be dropped from the analysis.

Thus, for variable-pitch propellers with geometrically similar blades, where h is large and δ is small

$$f\left(N,S,J,R,\theta,\frac{P}{D} \right) = 0 \qquad (9.5)$$

or

$$N = f(S,J,R,\theta,\frac{P}{D}) \qquad (9.6)$$

If the conditions are such that the effects of S,J,R,θ are small then for a fixed-bladed propeller :-

$$N = \text{a constant } k \qquad (9.7)$$

and

$$I_h = k\rho D^5 \qquad (9.8)$$

An alternative presentation of the results of the dimensional analysis may be made as follows:-

From equation (7.4)

$$\frac{I_h}{\rho D^5} = f\left(S,J,R,\theta, \frac{P}{D}, \frac{h}{D}, \frac{\delta}{D}, \frac{a}{D}, \frac{b}{D}, \frac{c}{D} \text{-------} \right) \qquad (9.9)$$

In equation (9.9) the left-hand-term is multiplied, in numerator and denominator, by I_w, where I_w is the inertia of the equivalent water propeller. The equivalent water propeller is a hypothetical rigid propeller assumed to replace the metal propeller. It is identical in every way with the metal propeller except that it is made from material whose specific gravity is that of water. Its inertia can easily be shown to be equal to the inertia of the metal propeller, divided by the ratio of the densities of the propeller material and water.

From equation (9.9) is then obtained the relation

$$\frac{I_h}{I_w} \cdot \frac{I_w}{\rho D^5} = f(S,J,R,\theta, \frac{P}{D}, \frac{h}{D}, \frac{\delta}{D}, \frac{a}{D}, \frac{b}{D}, \frac{c}{D} \text{---}) \qquad (9.10)$$

Rearranging (9.10) gives

$$\frac{I_h}{I_w} = \frac{\rho D^5}{I_w} \quad f(S,J,R,\theta, \frac{P}{D}, \frac{h}{D}, \frac{\delta}{D}, \frac{a}{D}, \frac{b}{D}, \frac{c}{D} \text{---}) \qquad (9.11)$$

i.e

$$\frac{I_h}{I_w} = f_1 \left(\frac{I_w}{\rho D^5}, S,J,R,\theta, \frac{P}{D}, \frac{h}{D}, \frac{\delta}{D}, \frac{a}{D}, \frac{b}{D}, \frac{c}{D} \text{--}\right) \qquad (9.12)$$

The water inertia I_w is dependent upon the shape parameters, a,b,c--- P,D of the propeller, and upon the density ρ of the fluid (assumed to be water).

By dimensional analysis, it may be simply shown that

$$\frac{I_w}{\rho D^5} = f_2\left(\frac{a}{D}, \frac{b}{D}, \text{---} \frac{P}{D}\right) \tag{9.13}$$

By substitution of (9.13) in (9.12) is obtained the relationship

$$\frac{I_h}{I_w} = f_3\left(S,J,R,\theta, \frac{P}{D}, \frac{h}{D}, \frac{\delta}{D}, \frac{a}{D}, \frac{b}{D}, \frac{c}{D} \text{---}\right) \tag{9.14}$$

If geometrically similar propellers, of the variable-pitch type are considered, then equation (9.14) reduces to

$$\frac{I_h}{I_w} = f_4\left(S,J,R,\theta, \frac{P}{D}\right) \tag{9.15}$$

when h is large and δ small

For fixed-bladed propellers under the same conditions

$$\frac{I_h}{I_w} = f_5\left(S,J,R,\theta\right) \tag{9.16}$$

If the effects of S,J,R,θ are small then (9.16) reduces to

$$\frac{I_h}{I_w} = \text{constant } k'$$

and

$$I_h = k' I_w \qquad (9.17)$$

The ratio $\frac{I_h}{I_w}$ when expressed as a percentage is known as " the percentage increase in inertia due to the entrained mass".

When comparing propellers of different shapes, by means of equations (9.4) or (9.14), it may not be necessary to retain all the shape variables, $\frac{a}{D}$, $\frac{b}{D}$, ------. For propellers of a given general type (e.g.for cargo vessels), the demands of other factors may be such that blades with the same value of pitch diameter ratio P/D and the same value of blade-area-ratio BAR (or some similar specifying parameter) are approximately the same general shape. This is especially likely in the case of a standard series of propellers. Thus a correlation may well be possible for propellers of different shape on the basis of pitch diameter ratio and BAR (or some similar parameter). This can only be determined to be the case or otherwise by experiment. It is therefore possible that in equation (9.4) the terms $\frac{a}{D}$, $\frac{b}{D}$ --- can be replaced by a single parameter such as BAR.

It has in fact been shown (Ref. 6.8, 6.8) that for a standard series a correlation is possible using as shape parameters only pitch diameter ratio and BAR. For a standard series therefore equation (9.4) may be written as

$$f\left(N,S,F,J,R,\theta, \frac{P}{D}, \frac{h}{D}, \frac{\delta}{D}, \text{BAR} \right) = 0 \qquad (9.18)$$

It should be noted that a correlation obtained for a standard series, using P/D and BAR, is not valid for any other series. If the series considered do not differ greatly in their shapes, a correlation obtained from one series may give reasonable results, for another series. If they differ widely in shape, then there may be considerable error introduced by using a correlation derived from one series for another series. How significant this error will be can only be found by experiment. It is suggested that the deviations between the correlations presented in Refs. 6.7, 6.8, and 6.9 may be due to the fact that they are based on different series.

CHAPTER 10

EXPERIMENTAL METHODS FOR DETERMINING THE VIRTUAL INERTIA

There are two main methods for obtaining experimentally the value of hydrodynamic mass or inertia of an oscillating body. These methods are described in detail in the following sections.

10.1 THE FREE VIBRATION METHOD

In this method, the body is attached to a very large mass (usually the earth) by means of flexible supports. The body is then given an initial deflection by external movement or by impact, and is then allowed to execute a vibratory motion at the natural frequency of the system. By comparing the frequency of vibration in the fluid and in air, the increase in the virtual mass (i.e the hydrodynamic mass) can be determined.

The equation of motion if the oscillation of the body is along a straight line is

$$M_h = \frac{k}{4\pi^2} (t_f - t_a) \qquad (10.1)$$

where M_h = Hydrodynamic mass

k = Spring rate (deflection force / distance moved)

t_f = Period of vibration in fluid

t_a = Period of vibration in air

For angular motion of the body the corresponding equation is

$$I_h = \frac{K}{4\pi^2} (t_f - t_a) \qquad (10.2)$$

where I_h = Hydrodynamic inertia

K = Torsional stiffness (deflecting torque/angular movement)

t_f = Period of vibration in fluid

t_a = Period of vibration in air

The fluid damping can also be obtained, from the rate of decay of the oscillation. A disadvantage of the method is that it may be difficult in a given case to adjust the mechanical mass and spring rate sufficiently to cover the desired range of frequencies and amplitudes of oscillation of the body.

10.2 THE FORCED VIBRATION METHOD

In this method, the body is attached to a very large mass (usually the earth) by means of flexible supports. A forcing frequency is then applied to the body, causing it to execute forced vibratory motion. By relative adjustment of the spring rate, the mechanical mass and the amplitude of the applied force, it is possible to carry out a series of tests for a given body, in which the amplitude and frequency of the oscillation of the body are the same, but in which the spring rate, mechanical mass, and amplitude of applied force vary from test to test. From the results of any two such tests the hydrodynamic mass or inertia can be calculated (See Ref. 6.2) for an excellent discussion of the theory of this method)

The advantage of this method is that any desired range of frequency and amplitude of oscillation of the body may be usually obtained by

adjusting the dynamic parameters, without extreme values of these parameters being required. Another advantage is that during the test, the frequency and amplitude of oscillation of the body remain constant, whereas in the free vibration method the amplitude varies during the test.

This method should allow more precise determination of hydrodynamic mass than the free vibration method, since the effects of damping and entrained mass can be separated. In the free vibration method, complete separation of the effects of damping and entrained mass is almost impossible. It is possible, however, with the free vibration method, to achieve sufficient separation to allow results of reasonable accuracy to be obtained. Where the entrained mass investigation concerns a rotating propeller, the forced vibration method involves considerable practical difficulties, and for this reason in the present investigation, the free vibration technique was used.

It should be noted that in either method, if there is another degree of freedom in the equipment, in which oscillation can take place, in addition to the degree of freedom in which the measured oscillation is taking place, then cross-coupling between the two modes of oscillation can occur through the hydrodynamic interaction at the propeller. If the ratio of the natural frequencies of the two modes is large, however, it can be deduced by simple physical reasoning that cross-coupling will be small and may be neglected. In the dynamometer used in the present investigation there are only two modes of oscillation possible in which oscillations of significant energy can take place; torsional and axial. It is shown in Ref. 6.7 that if the ratio of axial natural frequency to the torsional natural frequency for a system of this type is 2:1 or greater,

cross-coupling will be negligible for such a system. Since the natural frequencies (in water) in the present investigation were of the order of 130 c.p.s for the torsional and 470 c.p.s for the axial frequency, cross coupling should be negligible.

CHAPTER 11

THE EXPERIMENTAL EQUIPMENT AND PROCEDURE

11.1 THE WATER TUNNEL AND DYNAMOMETER

The research water tunnel, and the propeller dynamometer developed for these tests, have been described in Chapters 2,3,4 and 5 (See also Refs. 11.1, 11.2, 11.3). The following brief description is included, however, for completion.

The water tunnel was originally of open-circuit configuration but has been converted to closed-circuit operation. In this configuration water is circulated around the circuit by two 125 H.P.pumps. The working-section is 18" diameter, and the maximum velocity attainable in the working-section is 31.0 ft per second.

For the simultaneous measurement of torque and thrust on a model propeller in the research water tunnel, a strain-gauge dynamometer has been developed.

Provision was made in the design of the dynamometer for varying the torsional stiffness, by having a removable torsionally-weak element, which could be interchanged with an element of any desired stiffness. In the present series of tests, however, the original element was used, and the tests were therefore carried out over a very narrow range of frequency.

The dynamometer incorporates a mechanical system using thin diaphragms and a slender rod to separate the torque and thrust forces. Strain-gauges cemented to thin strain shells are then used to measure the forces. The electrical signals from the strain-gauges are carried through shielded wires to transistor pre-amplifiers rotating with the shaft. (The reason for the pre-amplifiers is that the strain-gauge

signals are small, and would be seriously interfered with by brush noise at the slip-rings, unless amplified to a sufficient level). The amplified signals from the pre-amplifiers are then transmitted through slip-rings to the measuring and recording equipment.

During the tests described in this thesis the torque and thrust signals from the slip-rings were recorded in two ways:-

(1) Each signal was transmitted to a high-impedance voltmeter (heavily damped), and the mean value of torque (or thrust) read from the meter scale.

(2) Each signal was reverse-biased with a D.C.voltage to reduce the D.C. component of the signal to a small value. Further amplification then enabled the voltage fluctuations corresponding to the torque or thrust fluctuations to be recorded on an ultra-violet galvanometer recorder at a sufficiently large scale to enable the waveform to be measured with adequate accuracy during subsequent analysis of the traces.

A block diagram of the layout of the instrumentation is given in Fig. 11.1.

11.2 THE PROPELLER

The propeller used for the investigation did not conform to a standard series, having been originally designed to check a propeller design-method (Ref. 11.4). The original propeller was first replicated by a precision-casting technique (with hand finishing), The blades were then cut from the replica and fitted to a new hub to form a variable-

Fig. 11.1 Block diagram of instrumentation

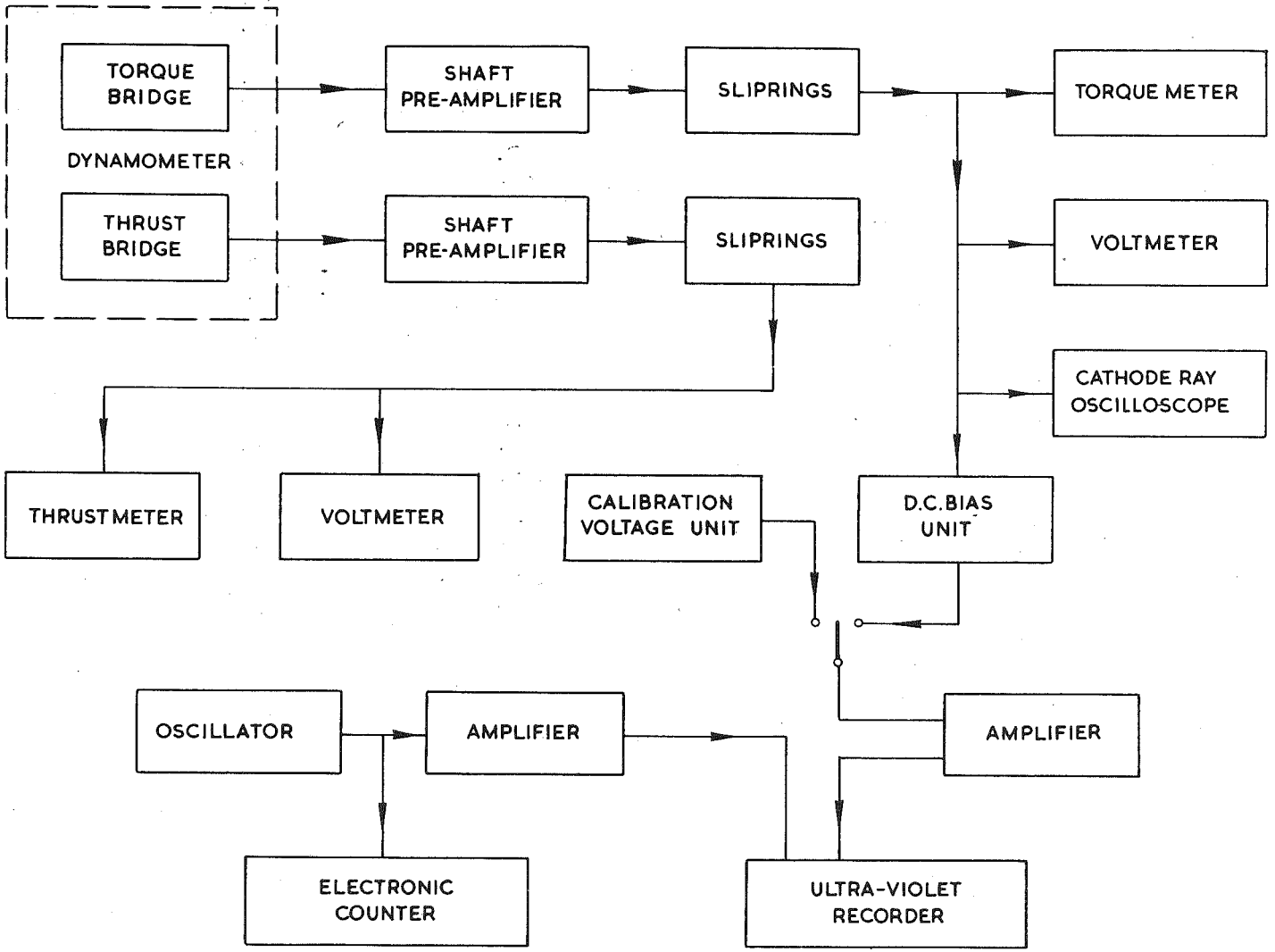
TORQUE BRIDGE
DYNAMOMETER
THRUST BRIDGE
SHAFT PRE-AMPLIFIER
SHAFT PRE-AMPLIFIER
SLIPRINGS
SLIPRINGS
TORQUE METER
VOLTMETER
CATHODE RAY OSCILLOSCOPE
THRUSTMETER
VOLTMETER
CALIBRATION VOLTAGE UNIT
D.C.BIAS UNIT
OSCILLATOR
AMPLIFIER
AMPLIFIER
ELECTRONIC COUNTER
ULTRA-VIOLET RECORDER

pitch propeller. The root attachments of this propeller were carefully designed to obtain maximum rigidity. The pitch setting corresponding to the original design has been taken arbitrarily as 0°, and pitch angles are specified relative to this setting. The design of the original fixed-blade propeller is shown in Fig. 11.2. It will be seen that there is no rake or skewback. The blade sections have been made appropriate combinations of the NACA a = 1 mean line and NACA 66 series basic thickness form. Except for the root fixings, the variable-pitch propeller in the 0° setting is identical with this propeller. The main particulars of the propeller in 0° setting are given in Table 11.1. The performance of the propeller under steady conditions is given in Appendix I.

TABLE 11.1

Variable-Pitch Propeller Design

Hand	R.H.
Number of Blades	3
Outside Diameter	8"
Design Thrust	14 lb
Design RPM	960 rpm
Design forward velocity	8 ft/s
Material	Aluminum alloy
Pitch diameter ratio for various blade settings:-	
-10°	1.58
-5°	1.20
0°	0.96
$+5^{\circ}$	0.74
$+10^{\circ}$	0.53

Fig. 11.2 Design of fixed-blade propeller

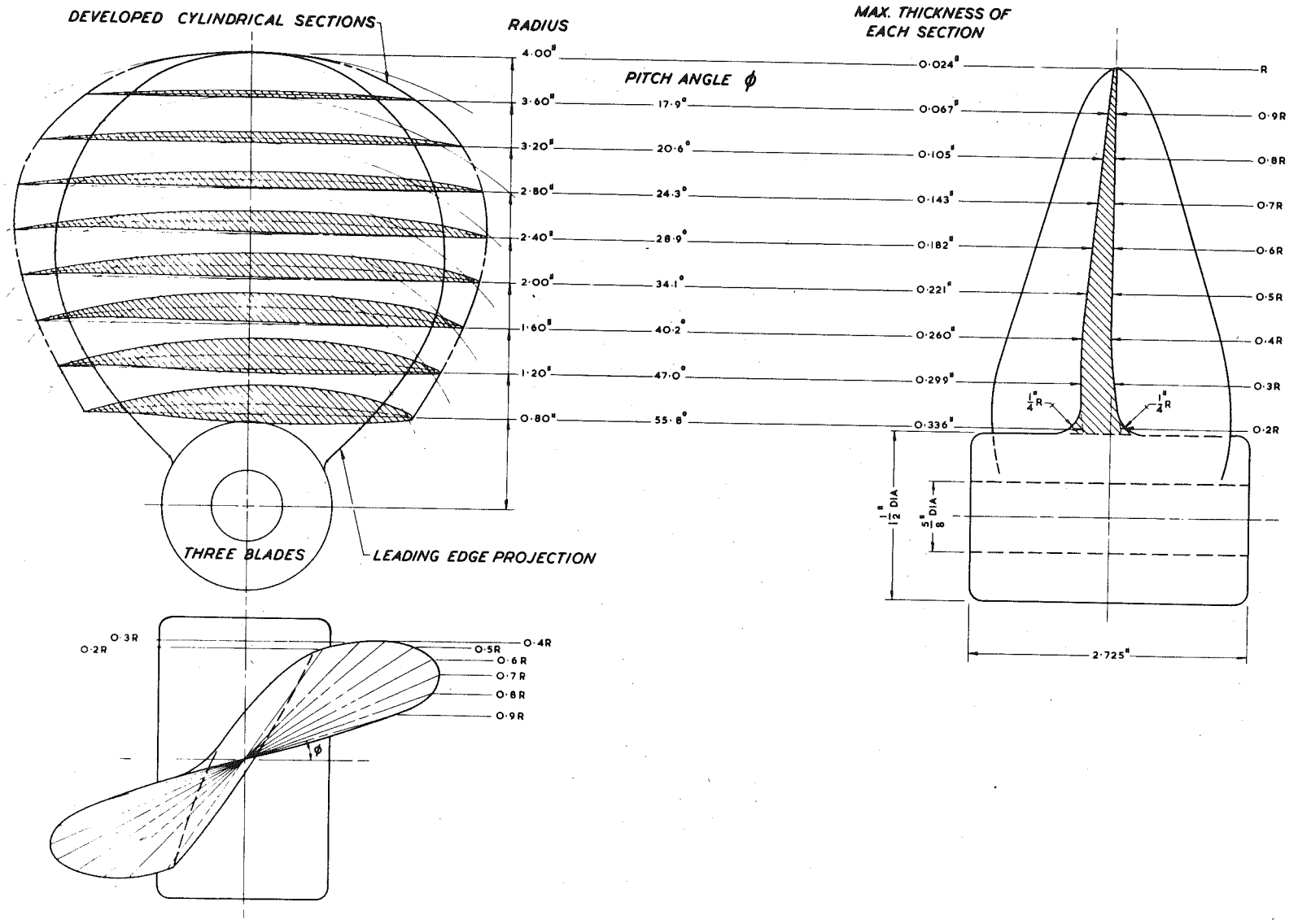
DEVELOPED CYLINDRICAL SECTIONS
RADIUS
PITCH ANGLE φ
MAX. THICKNESS OF EACH SECTION
4·00"
3·60"
3·20"
2·80"
2·40"
2·00"
1·60"
1·20"
0·80"
17·9°
20·6°
24·3°
28·9°
34·1°
40·2°
47·0°
55·8°
0·024"
0·067"
0·105"
0·143"
0·182"
0·221"
0·260"
0·299"
0·336"
R
0·9R
0·8R
0·7R
0·6R
0·5R
0·4R
0·3R
0·2R
1/4"R
1/4"R
1/2" DIA
5/8" DIA
2·725"
THREE BLADES
LEADING EDGE PROJECTION
0·3R
0·2R
0·4R
0·5R
0·6R
0·7R
0·8R
0·9R
φ

11.3 CALIBRATION OF THE EQUIPMENT

The calibrations described in the following sections were carried out at appropriate intervals during the test series.

11.3.1 System Gain Calibration

This calibration was carried out on both the torque and thrust channels.

A high-stability calibrating resistor was switched into one leg of the strain-gauge bridge to give an output signal from the system corresponding to a simulated value of applied stress. Any variation in the system gain would be indicated by a change in the output voltage under calibration conditions.

11.3.2 Static Calibration of Dynamometer Torsion and Thrust Cells

A specially-developed rig allowed a thrust load to be applied to the dynamometer without simultaneous torsion or bending loads. A similar rig allowed a pure torsional load to be applied without introducing axial or bending loads. Using these rigs, calibrations were carried out to obtain graphs of static thrust versus electrical output, and static torque versus electrical output. These graphs showed a linear relationship to exist between applied load and electrical output in both cases. It may therefore be deduced that the torsion and thrust cells are linear elements within the dynamometer.

The torque calibration rig incorporated two sensitive dial-gauges to measure the movement of the ends of loading moment-bar. From these measurements the angular deflection of the dynamometer for a given applied torque could be calculated.

A linear relationship was found to exist between torque and deflection, over the range from zero torque to the maximum safe torque. This showed that the dynamometer to be elastically linear in the torsional mode, as would be expected.

Although a similar calibration was not carried out for the thrust mode, it may be assumed that the system would be elastically linear in this mode also.

11.3.3 Dynamic Calibration of the Dynamometer

A dynamic calibration to determine the dynamic behaviour of the whole of the mechanical system of the dynamometer was only carried out for torque, although a similar calibration could have been carried out also for thrust if required. A series of inertia discs were manufactured, each with the same weight, but varying in diameter and thickness, and hence in inertia. These were in turn attached to the dynamometer. The dynamometer was slowly rotated, and the natural torsional frequency of the system excited by the impact of a projecting pin on the disc against a stationary rubber striker. A record of the torsional oscillation was recorded on the ultra violet galvonometer recorder (Ref. Fig. 11.1). Analysis of the traces from the recorder gave values of frequency and amplitude for the various inertias. From the results, a plot of (period of oscillation)^2 versus disc inertia was made (Fig. 4.5). This shows that for a given amplitude of oscillation, a straight line results, as would be expected. For each amplitude, however, the straight line has a slightly different slope, indicating a non-linearity of the system

under dynamic conditions. Since the system was shown (by static calibration) to be elastically linear, the slight non-linearity in the dynamic characteristics must be associated with non-linearity in the dynamometer damping. Tests indicated that the small amount of damping in the dynamometer was due to two causes; a slight rub in the air-bearing, and damping-forces in the wax protective layer covering the gauges on the strain cells. These tests also indicated that both forms of damping were non-linear.

The behaviour of the system was found to be consistent and repeatable results could be obtained. The dynamic calibration graph was therefore used to deduce the added inertia of a body (or body plus hydrodynamic inertia) attached to the dynamometer, from measurements of both the frequency and the amplitude of the oscillation.

11.3.4 Propeller Dynamic Inertia Calibration

The propeller was fitted to the dynamometer and using the method described in (3) above, its inertia was determined for various amplitudes of oscillation in air. The results when plotted showed the value of mechanical inertia to vary slightly with amplitude. This is possibly due to the effect of blade flexibility.As the variation is slight, the assumption was made that this calibration graph was valid not only for the case of the propeller oscillating in the air but also for the case of the propeller oscillating in water. Even if this assumption is not completely valid, the error resulting will be small as the variation in mechanical inertia with amplitude is in any case almost negligible.

11.3.5 Propeller and Disc Static Inertia Determination

The inertia of the propeller, and of the various inertia discs was determined under "static" conditions, by means of a single-wire torsional pendulum method, to a high degree of accuracy. In the case of the discs, the inertias were also calculated (as a check) from the dimension of the disc. The variation of propeller inertia with blade angle was found to be negligible over the range of angles used.

11.3.6 Amplifier and Recorder Calibration

A gain calibration of the amplifier-recorder section of the system was obtained by injecting a known voltage into the input of the external (driver) amplifier (See Fig. 11.1). A relationship between spot-deflection on the recorder paper, and slipring voltage could thus be obtained, for use when later analysing the traces on the recorder paper.

11.3.7 Time Calibration

A known sinusoidal frequency from an oscillator, checked by an electronic counter, was fed on to one of the recorder galvanometers so that a time marking was recorded simultaneously on the paper with the torque or thrust records.

11.4 THE ANALYSIS OF RESULTS

Tests on the variable-pitch propeller at various pitch-settings were carried out over a range of tunnel velocities and shaft rotational speeds, for a range of oscillation amplitudes. The excitation of the

free vibration in the torsional mode was by the impact method described in section 11.3.3. The various test series were planned so that each group of tests was carried out under conditions of almost constant propeller Reynolds Number R_n and almost constant advance ratio J. To facilitate computation of R_n and J, the graphical construction given in Appendix II was derived (by E.H.Watkins).

The values of R_n at which tests were carried out were 4.0, 5.0, and 6.0 x 10^5, these values being chosen to be above the critical R_n for the propeller. This critical R_n has been variously quoted at values ranging from 2.0 x 10^5 to 4.0 x 10^5.

Dr. H.W.Lerbs has presented evidence (Ref. 11.5) indicating that transition from turbulent to laminar turbulent flow occurs on model propellers at a critical Reynolds number (at 0.7 radius) of 4.0 x 10^5. Murray, Korvin-Kroukovsky and Lewis (Ref. 11.6), from an analysis of self-propulsion tests with small models have concluded that the critical Reynolds number can be as low as 0.5 x 10^5, the hypothesis being advanced " that the vibration associated with a rapidly rotating model propeller is probably effective in stimulating turbulence". Leaper (Ref. 11.7) suggests (for a ducted propeller) that "unless the Reynolds number based on blade chord is greater than 2.0 x 10^5 the results are likely to be very unreliable". O'Brien (Ref. 11.8) quotes a typical Reynolds number for model propeller testing as 5.0 x 10^5.

In view of the above somewhat contradictory views, the value for the critical R_n which was chosen as the minimum value for any tests in the present series was the conservative one of 4.0 x 10^5.

A typical record from a test run is shown in Fig. 5.1. It will be seen that the trace exhibits the typical characteristics of a damped free vibration. Due to tunnel background noise, the peaks of the oscillation were often "knocked off", and the estimated true position of such peaks (without noise) was obtained in such cases by sketching in the envelope of the vibration record.

The mean amplitude of each cycle of the oscillation and also the corresponding period for the cycle was measured manually from the recorder chart. Each record thus yielded a series of corresponding amplitude and frequency values for the oscillations. From the frequency values and the appropriate dynamometer calibration graphs (Section 4.3) the corresponding hydrodynamic inertia values were obtained. The justification for this method of analysis of a damped free vibration is given in Chapter 5.

The conversion of the amplitude values recorded on the paper to the corresponding angular amplitudes of the propeller motion was carried out in the following manner. The values of deflection taken from the recorder paper in terms of millimeters were converted to the corresponding voltages at the slip-ring, using the amplifier-recorder calibration described under heading (6) of Section 11.3.6. These voltages were then converted to the corresponding angular deflections of the propeller using the static calibration graph of slipring-voltage versus angular deflection described in Section 11.3.2.

For each test-run, values of mean torque and thrust, shaft rotational speed, and the tunnel velocity were calculated from the experimental data. The values of tunnel velocity were corrected to the open-water condition, by using the tunnel wall interference correction given in Ref. 11.9.

The corresponding values of advance ratio J, thrust coefficient k_T, and torque coefficient k_Q were then calculated.

A supplementary set of tests was later carried out to obtain the values of hydrodynamic inertia for the "still water" condition. Strictly, these should have been carried out with the propeller stationary in still water. It was difficult, however, to consistently excite the torsional vibrations under these conditions. The tests were therefore carried out with the propeller rotating very slowly and with the tunnel velocity set to a very small value.

The recorder traces from the "still water" tests were analysed in a similar way to those of the main test series. Instead of measuring the amplitude and period of each cycle of the oscillation, however, the analysis was carried out on groups of three cycles. For each group the mean amplitude and mean period was then calculated by dividing by three. Since the first nine cycles were analysed on each trace, this meant that three sets of values of amplitude and period were obtained from each trace.

CHAPTER 12

HYDRODYNAMIC INERTIA RESULTS

12.1 RESULTS

The main test series were divided into five basic groups corresponding to the pitch angles settings + 10°, + 5°, 0°, -5°, -10°. For each pitch there were three sub-groups corresponding to propeller Reynolds number R_n values of 4.0×10^5, 5.0×10^5, 6.0×10^5. Each sub-group

TABLE 12.1

NOMENCLATURE OF TEST SERIES

Reynolds No. R_n	Pitch Setting.				
	- 10°	-5°	0°	+5°	+10°
4.0×10^5	A1	B1	C1	D1	E1
5.0×10^5	A2	B2	C2	D2	E2
6.0×10^5	A3	B3	C3	D3	E3

was identified by the nomenclature shown in Table 12.1 within each sub-group (such as A1,B2 etc) individual tests were carried out at a range of values of advance ratio J. Each individual test yielded a series of corresponding values of hydrodynamic inertia I_h and amplitude of oscillation θ .

The initial plotting of the results was as follows. Several sub-groups were selected and for each of these, graphs were plotted of I_h/I_w

versus amplitude θ for constant values of advance ratio J. Since there were only a comparatively small number (6-10) of data points for each value of J the points corresponding to three adjacent values of J were grouped together. The mean line drawn through these points was assumed to correspond, to a value of J equal to the mean value of the three J's.

For each of these sub-groups, by crossplotting, graphs were prepared of I_h/I_w versus J, for various constant values of amplitude. Two of these graphs (for $R_n = 4.0 \times 10^5$ and $R_n = 6.0 \times 10^5$ at pitch setting 0°) are shown in Figs. 12.1 and 12.2. The following features may be observed from the graphs of which Figs. 12.1 and 12.2 are representative:-

(1) There is a greater scatter of results in the case of $R_n = 6.0 \times 10^5$ than for $R_n = 4.0 \times 10^5$. The scatter for $R_n = 5.0 \times 10^5$ was found to be intermediate between that for these two Reynolds numbers. This trend was traced back to the original data, where it was found that the scatter in the data increased with increase of Reynolds number. An increase of Reynolds number corresponds to an increase in both tunnel velocity and rotational speed. It is known that for this tunnel both the scale and intensity of turbulence increase with increased velocity. It would appear reasonable to conclude that the increase in scatter is associated with the increase in tunnel turbulence.

(2) There is no clearly observable trend due to amplitude. If there is a variation in I_h / I_w due to amplitude, the effect is small and below the discrimation level of the present tests. It was therefore decided to adopt the following approach in the

Fig. 12.1 Graph of I_h/I_w versus J for constant values of amplitude.

Pitch setting 0^o. $R_n = 4.0 \times 10^5$

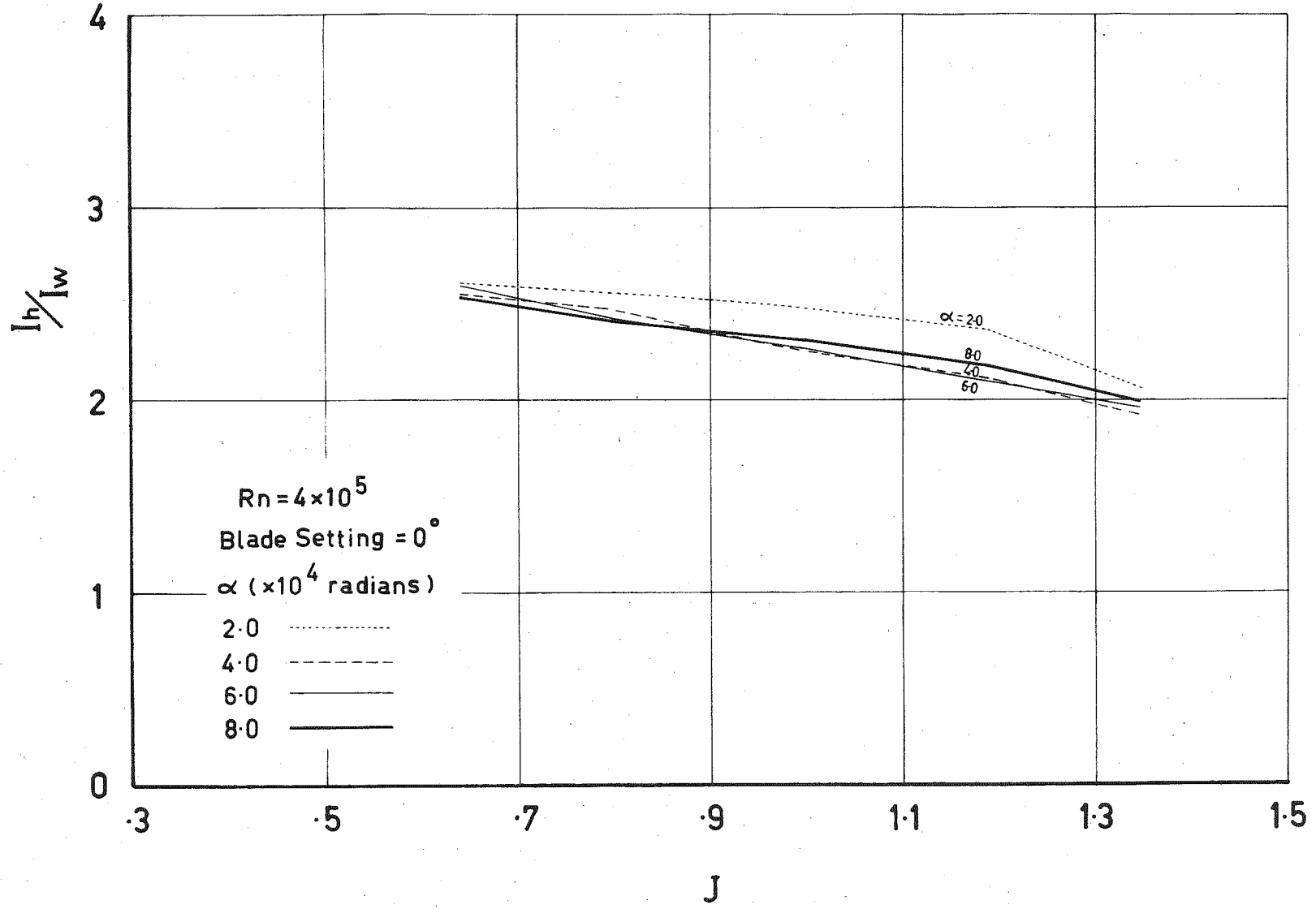
4
3
2
1
0
I_h/I_w
·3
·5
·7
·9
1·1
1·3
1·5
J
α=2·0
8·0
4·0
6·0
Rn = 4×10^5
Blade Setting = 0°
α (×10^4 radians)
2·0
4·0
6·0
8·0

Fig. 12.2 Graph of I_h/I_w versus J for constant values of amplitude.

Pitch setting 0^o. $R_n = 6.0 \times 10^5$

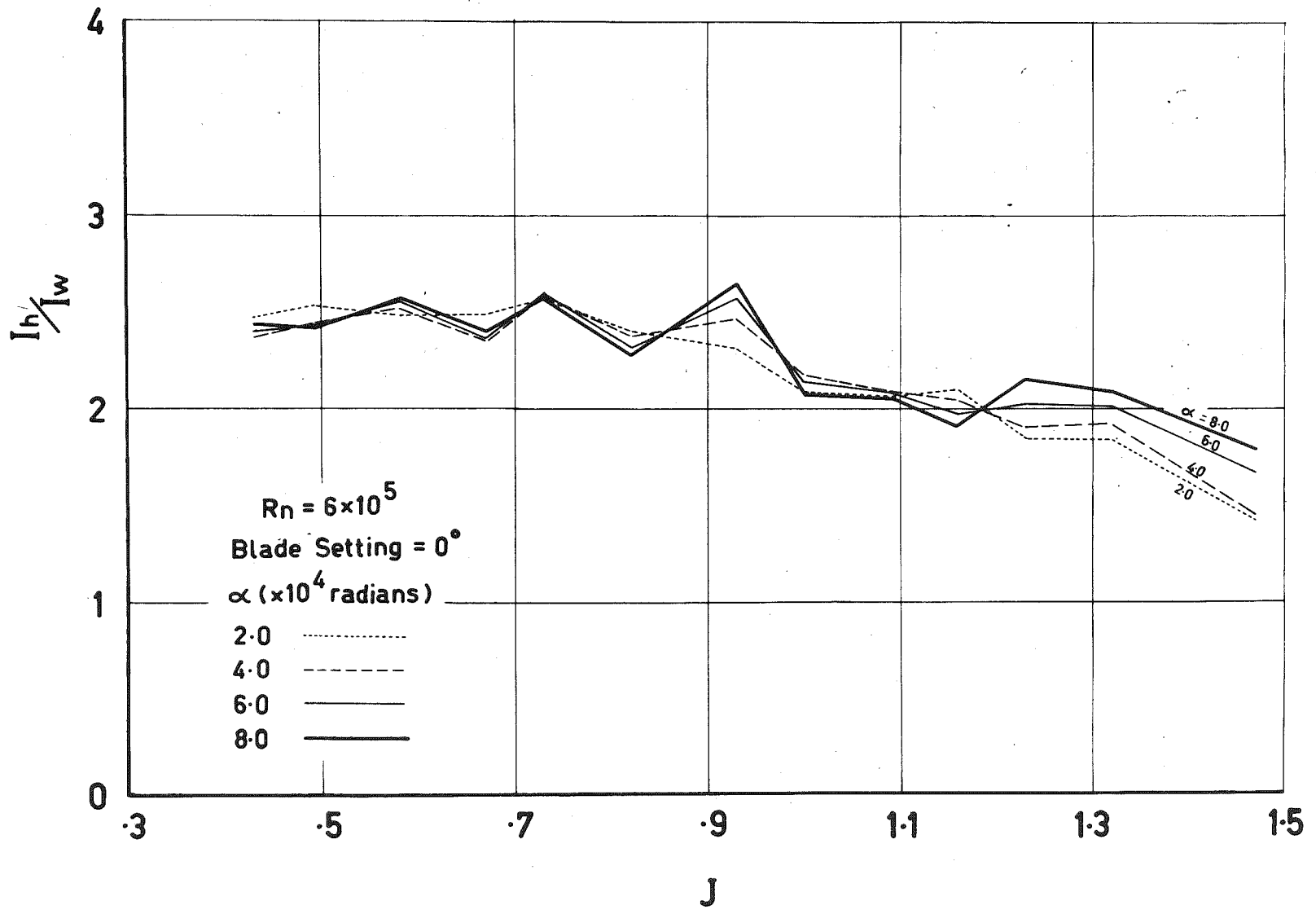
4
3
2
1
0
I_h/I_w
·3
·5
·7
·9
1·1
1·3
1·5
J
Rn = 6×10^5
Blade Setting = 0°
∝ (×10^4 radians)
2·0
4·0
6·0
8·0
∝ = 8·0
6·0
4·0
2·0

plotting of the test data. The data points for all amplitudes within each sub-group were plotted in the form of I_h / I_w versus J. Two of these graphs (for $R_n = 4.0 \times 10^5$ and $R_n = 6.0 \times 10^5$ for a pitch setting of 0^o) are shown in Figs. 12.3 and 12.4. The previously mentioned increase in scatter with increase in R_n will be noted.

On each of these graphs, a best-fit line was drawn, and these lines were then collected together on a single graph. This graph is shown in Fig. 12.5. It will be seen from this figure, that there is no clear trend evident with variation in Reynolds number, and furthermore, that the effect of Reynolds number would appear to be small, if the occasional "wild" swings of the $R_n = 6.0 \times 10^5$ lines are disregarded (since these are probably associated with drawing a mean line through an insufficient number of points scattered due to turbulence).

Fig. 12.6 was prepared from Fig. 12.5 by replacing the various constant-Reynolds-number lines at each pitch setting by a mean line (weighted heavily in favour of the lower Reynolds number data). Fig.12.7 was then prepared from Fig. to show the primary trends, by smoothing out what might be regarded as "secondary variations."

The values of hydrodynamic inertia I_h and amplitude θ obtained in the still water tests are given in Table 12.2. The mean value of hydrodynamic inertia and the corresponding mean amplitude have been calculated for each blade setting and are also given in Table 12.2.

Fig. 12.3 Graph of I_h/I_w versus J

(R_n = 4.0 x 10^5, Pitch setting 0°)

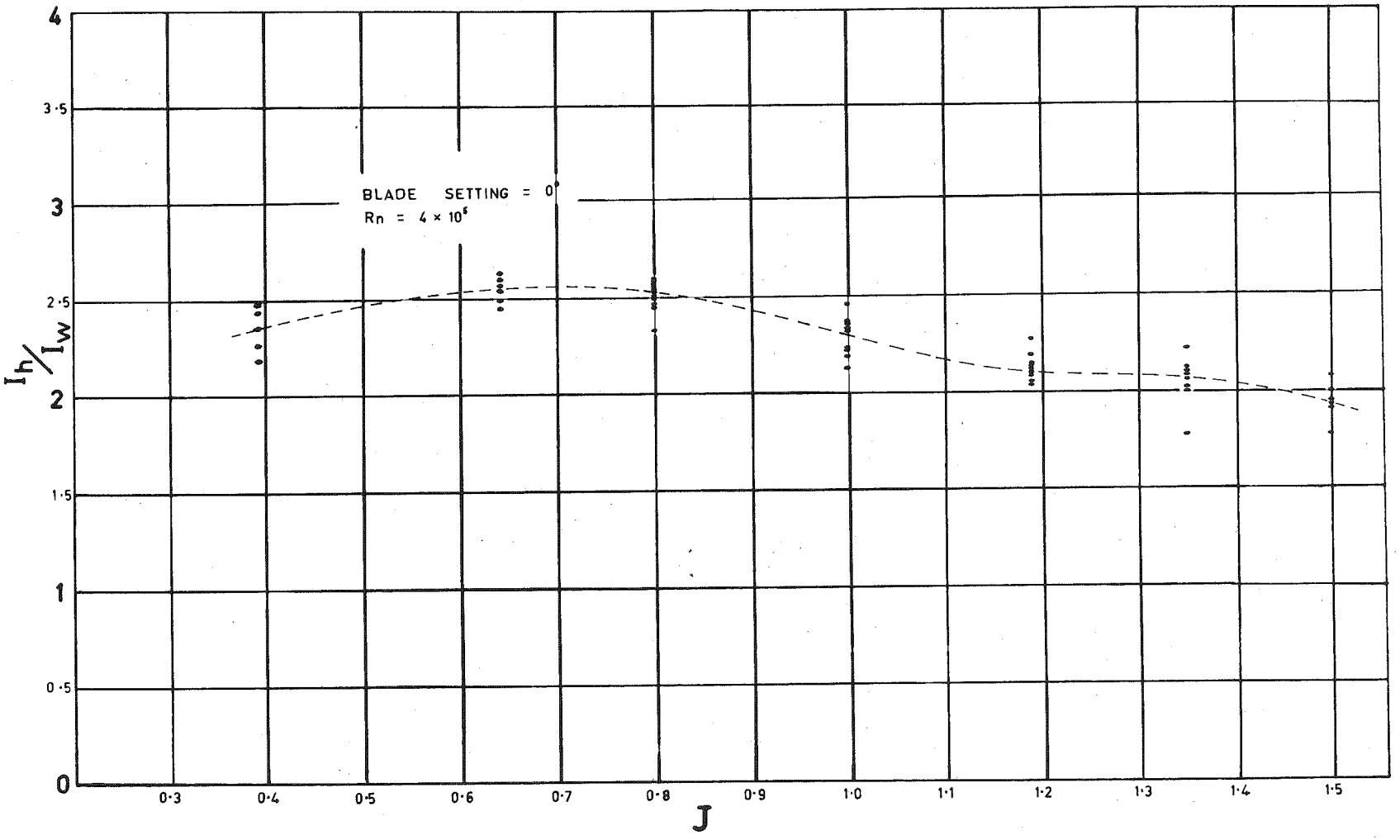
BLADE SETTING = 0°
Rn = 4 × 10⁶
I_h/I_w
J
4
3·5
3
2·5
2
1·5
1
0·5
0
0·3
0·4
0·5
0·6
0·7
0·8
0·9
1·0
1·1
1·2
1·3
1·4
1·5

Fig. 12.4 Graph of I_h/I_w versus J

($R_n = 6.0 \times 10^5$, Pitch setting 0°)

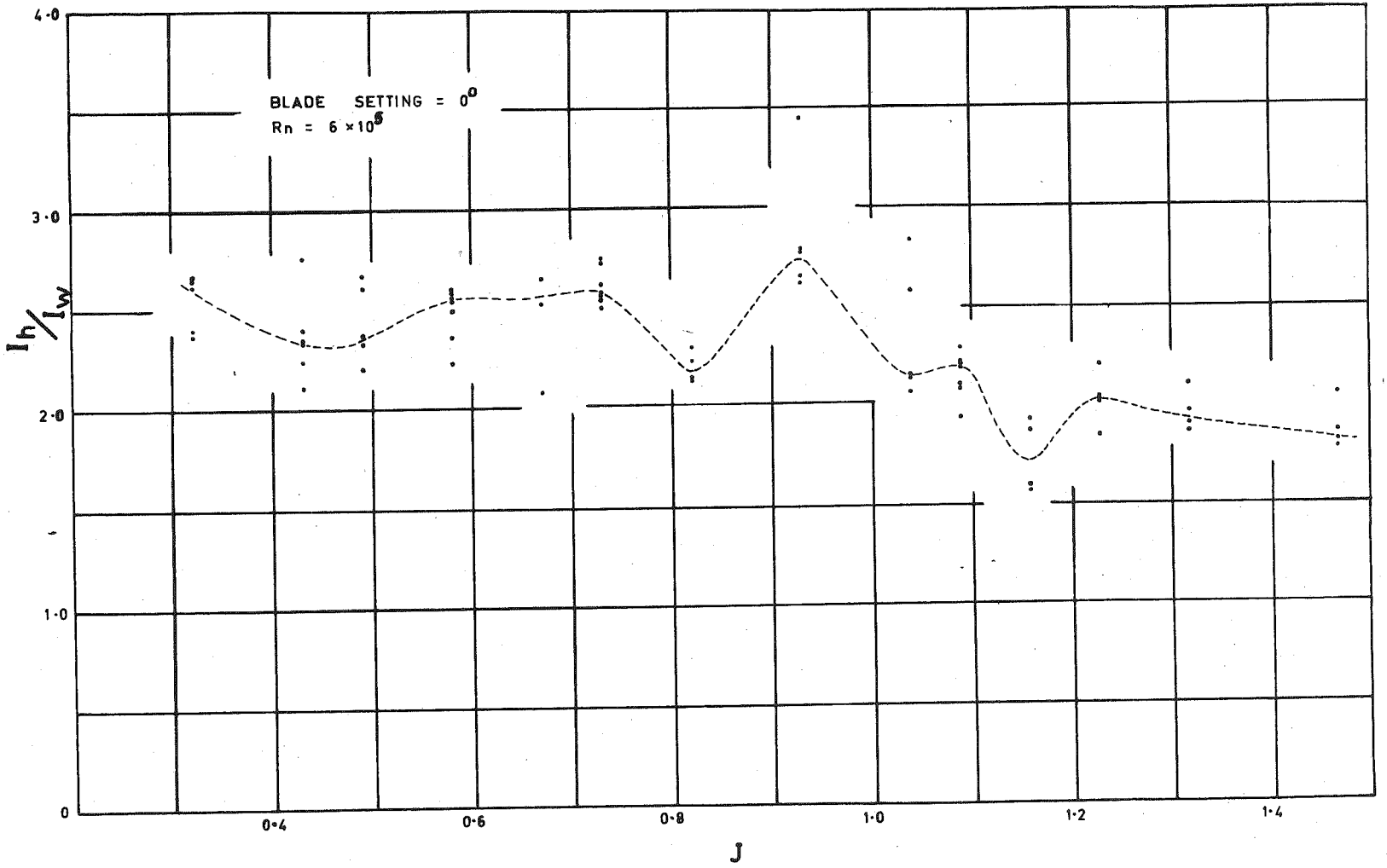
BLADE SETTING = 0°
Rn = 6 × 10⁶
4·0
3·0
2·0
1·0
0
l_h/l_w
0·4
0·6
0·8
1·0
1·2
1·4
J

Fig. 12.5 Graph of I_h/I_w versus J, for constant pitch settings and for constant Reynolds numbers.

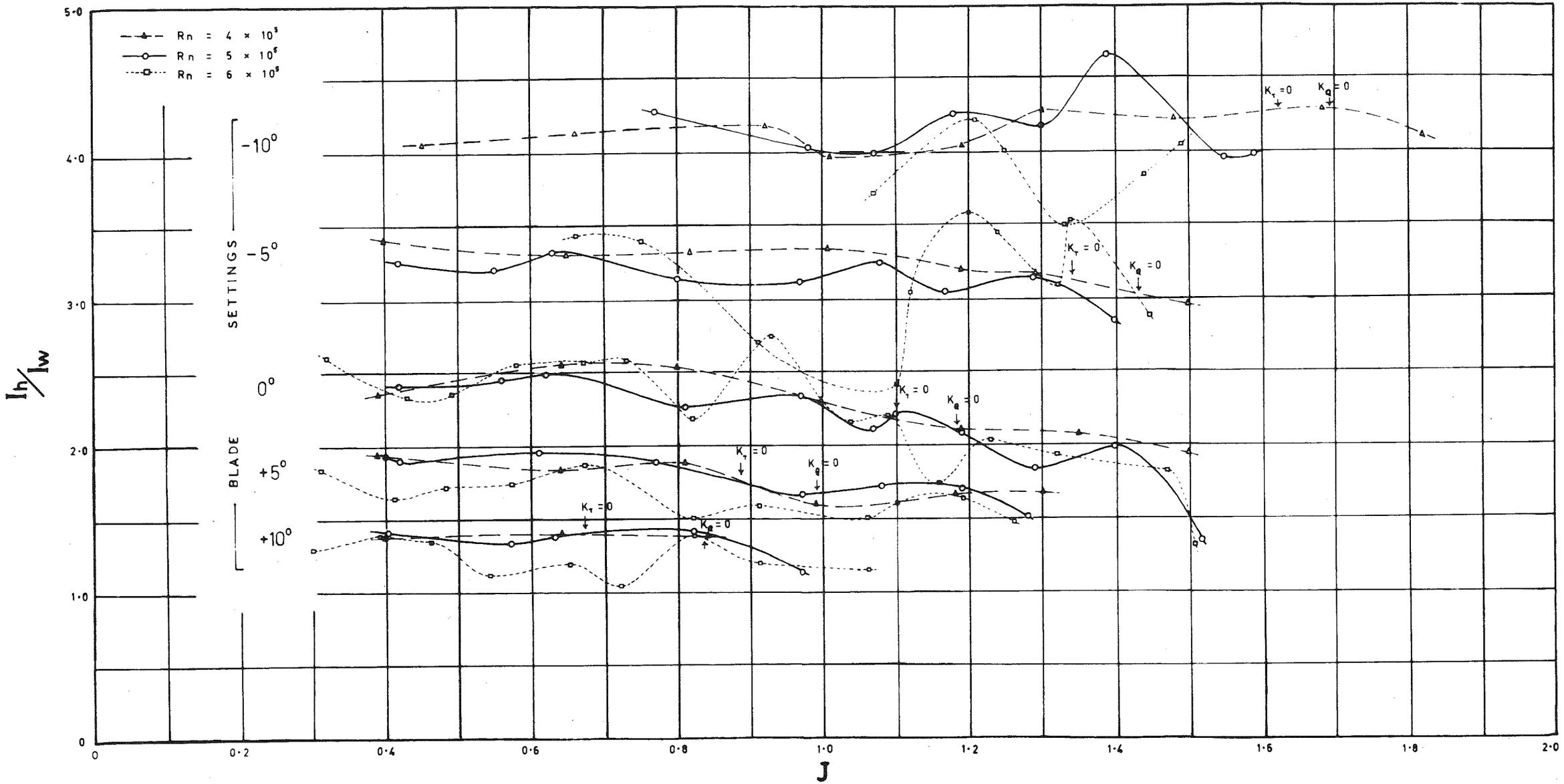
Rn = 4 × 10⁵
Rn = 5 × 10⁵
Rn = 6 × 10⁵
BLADE SETTINGS
-10°
-5°
0°
+5°
+10°
$K_T = 0$
$K_Q = 0$
I_h/I_w
J
5·0
4·0
3·0
2·0
1·0
0
0·2
0·4
0·6
0·8
1·0
1·2
1·4
1·6
1·8
2·0

Fig. 12.6 Graph of I_h/I_w versus J, for constant pitch settings.

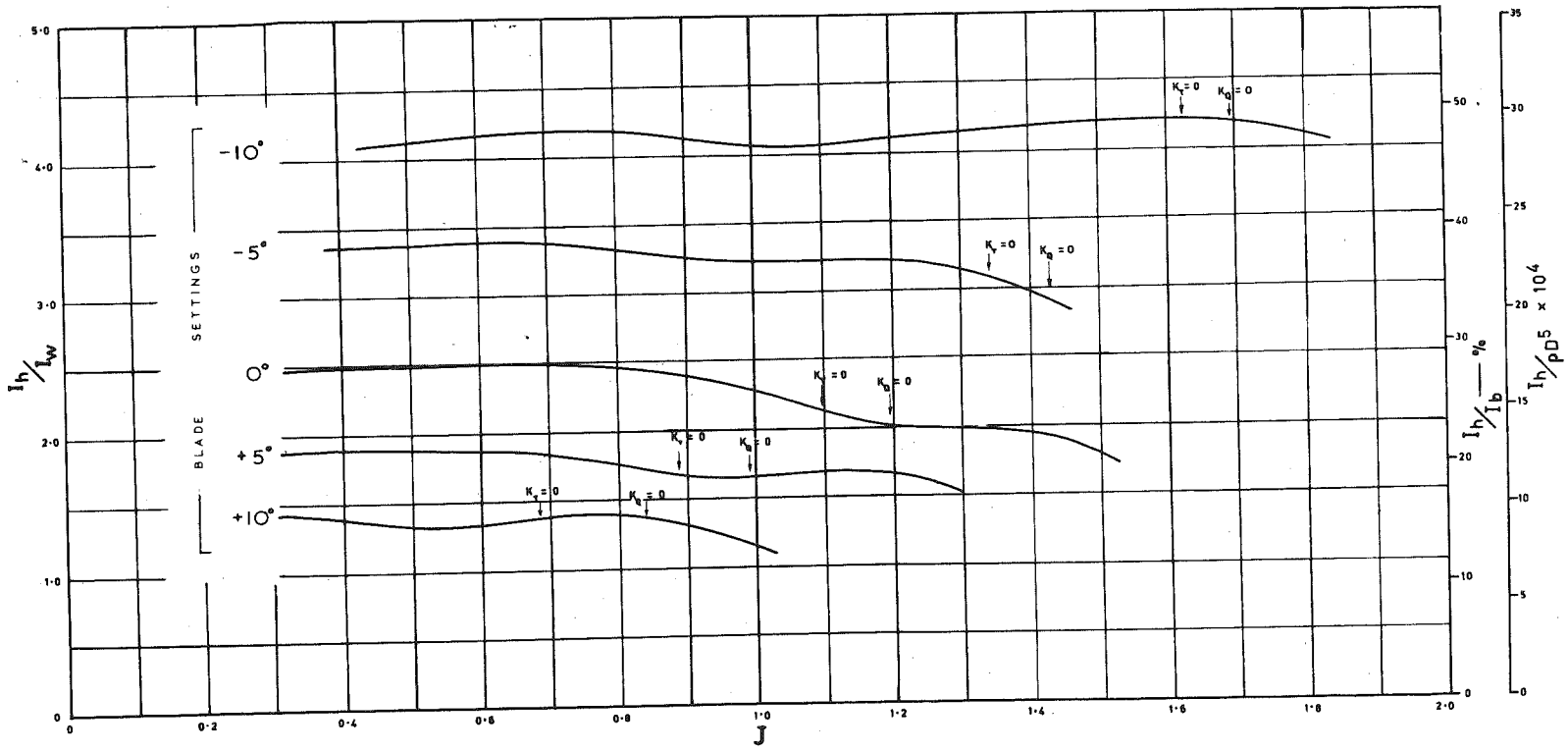
BLADE SETTINGS
-10°
-5°
0°
+5°
+10°
$K_T = 0$
$K_Q = 0$
I_h/I_W
I_h/I_b — %
$I_h/\rho D^5 \times 10^4$
J
0
0·2
0·4
0·6
0·8
1·0
1·2
1·4
1·6
1·8
2·0
1·0
2·0
3·0
4·0
5·0
10
20
30
40
50
5
15
25
35

Fig. 12.7 Smoothed graph of I_h/I_w versus J, for constant pitch settings.

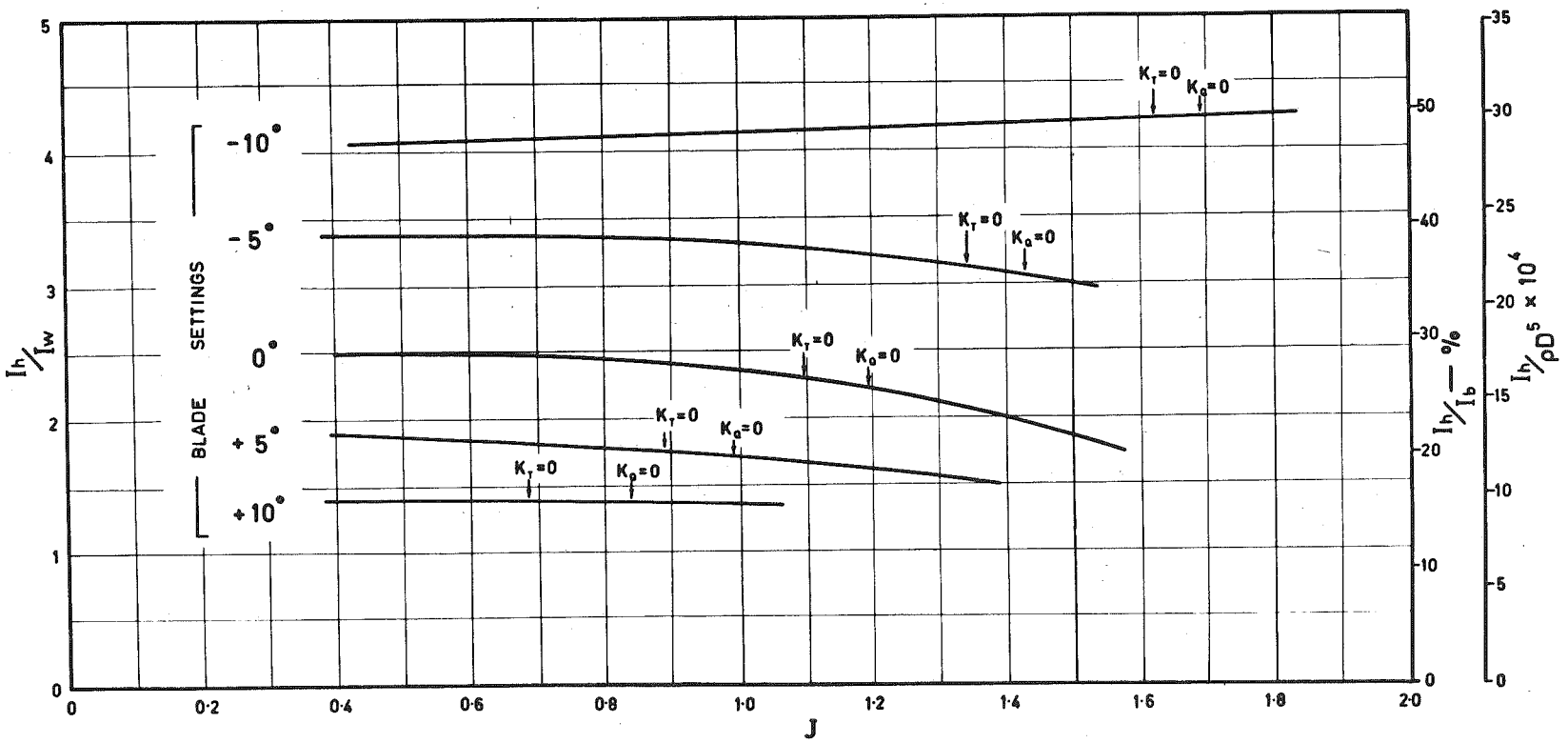
I_h/I_w
I_h/I_b — %
$I_h/\rho D^5 \times 10^4$
J
BLADE SETTINGS
-10°
-5°
0°
+5°
+10°
$K_T=0$
$K_Q=0$
0
0·2
0·4
0·6
0·8
1·0
1·2
1·4
1·6
1·8
2·0
1
2
3
4
5
10
15
20
25
30
35
40
50

TABLE 12.2

RESULTS OF STILL-WATER TESTS

P/D	1.58		1.20		0.96		0.74		0.53	
Pitch Setting	-10^0		-5^0		0^0		$+5^0$		$+10^0$	
	I_h/I_w	$\theta \times 10^4$ (radians)	I_h/I_w	$\theta \times 10^4$ (radians)	I_h/I_w	$\theta \times 10^4$ (radians)	I_h/I_w	$\theta \times 10^4$ (radians)	I_h/I_w	$\theta \times 10^4$ (radians)
	4.10	9.7	3.42	11.3	2.55	9.2	1.93	11.2	1.37	9.5
	4.24	5.4	3.42	7.9	2.57	6.0	1.87	8.8	1.24	7.2
	4.42	4.6	3.62	4.9	2.65	3.5	1.93	7.3	1.25	5.4
Mean Values	4.25	6.6	3.49	8.0	2.59	6.2	1.91	9.1	1.29	7.4

12.2 DISCUSSION OF RESULTS

12.2.1 Effect of Amplitude

It has been shown in Section 12.1 that the effect of amplitude on the hydrodynamic inertia is small within the range of amplitude covered by the main test series. The maximum amplitude varied slightly depending on the individual test. An average value for maximum amplitude would be 1.0×10^{-3} radians, and for minimum amplitude 2.0×10^{-4} radians.

In the results of the still-water tests (Table 12.2),however, there is evidence of the following trends with amplitude. At high values of P/D, the hydrodynamic inertia I_h decreases as the amplitude θ increases. This trend becomes less marked as the P/D becomes smaller, and finally reverses at the lowest value of P/D. In every case, however, the variation with amplitude is small.

In Ref. 6.5 (as reported in Ref. 6.1) McGoldrick stated that "the effect on polar moment of inertia increases with frequency and amplitude". This would appear to mean that I_h was found to increase with amplitude. In the discussion in Ref. 6.9, Calderwood mentions that when " I was concerned with torsional vibration at Swan Hunter's I tried from measured frequencies on various (ship) trial trips to establish some figures on inertia addition due to entrained water -----. My impression from very limited information was ----- that entrained inertia increased with increasing amplitude and decreased with increasing frequency". Brahmig (Ref. 6.2),however, has demonstrated experimentally that

for a thin circular disc the hydrodynamic mass M_h decreases as amplitude increases.

The author has postulated (Ref. Sections 8.3 and 8.4) that M_h and I_h decrease with increasing amplitude and increase with increasing frequency, tending to their ideal values at small amplitudes and high frequencies.

It is the conclusion of Fottinger (Ref. 12.1, 12.2) that for a body in translational oscillatory motion, the flow around the body approaches potential flow (and thus M_h and I_h approaches the ideal value) at oscillations of small amplitude and high frequency. It is also the conclusion of Brahmig (Ref. 6.2) that M_h and I_h tend to the ideal value at small amplitudes and high frequencies.

The consensus of opinion would appear to be that M_h and I_h tend to their ideal value at small amplitude and high frequency. Whether M_h and I_h increase or decrease with an increase in amplitude is still an unresolved question. Experimental evidence is contradictory on this point. This may indicate that the trend with amplitude depends on the shape of the body. In section 8.3, the author has tentatively suggested that the "viscous component" could cause an increase of M_h and I_h above the ideal value. It is significant that in those cases in which I_h was found to increase with amplitude (McGoldrick, Calderwood), the bodies (which were propeller blades) approximated to flat plates having a significant component of oscillation along their chords. For such blades the "viscous component" could be significant and could be responsible for the observed effect.

12.2.2 Effect of Reynolds Number

It has been shown in Section 12.1 that the effect of Reynolds number is small over the range (4.0 - 6.0 x 10^5) covered by the main test series. It is of interest to compare the values from these tests with those of the still-water tests, which were carried out at very low Reynolds number. Mean values of I_h/I_w over the positive thrust range have therefore been taken from Fig. 12.6 for the five values of P/D, and are given in Table 12.3, together with the mean values of I_h/I_w from the still-water tests.

TABLE 12.3

EFFECT OF R_n ON I_h/I_w

Pitch setting	P/D	I_h/I_w (R_n = 4.0-6.0 x 10^5)	I_h/I_w "Still-water"
-10°	1.58	4.2	4.25
-5°	1.20	3.3	3.49
0°	0.96	2.4	2.59
$+5^\circ$	0.74	1.8	1.91
$+10^\circ$	0.53	1.4	1.29

It will be seen that except at the lowest value of P/D, the still-water values of hydrodynamic inertia are slightly higher than the values obtained under load at high Reynolds numbers.

The deviations are small however, and reinforce the previous conclusion that the effect of R_n on hydrodynamic inertia is not significant.

12.2.3 Effect of Frequency

Since the tests were carried out over a narrow range of frequencies, and since the frequency effect on I_h may be reasonably assumed to be small, it may be assumed as a reasonable approximation that the values of I_h obtained are those corresponding to a constant value of frequency equal to the mean frequency for the tests. The comparatively small range of frequencies over which the tests were carried out is indicated by the following. If the highest and lowest values of I_h/I_w are taken from Fig. 12.6, and the corresponding frequencies are calculated, the highest frequency is only 1/3 greater than the least i.e the variation of frequency over the whole of Fig. 12.6 is only 34% , or $\pm$ 17%. For a single value of P/D ratio, the variation is even smaller. Consider for example, the curve for P/D = 0.96 in Fig. 12.6. The variation of frequency from one end of the curve to the other is only 9% i.e $\pm 4\frac{1}{2}$ % on the mean. Thus the effect of frequency on the data for any P/D curve should be negligible. The effect of frequency on the data for the whole of Fig.12.6 should also be negligible, especially in comparison with the effect due to variation of P/D ratio. The mean values of frequencies and frequency parameter for each value of P/D and for the whole of tests, are tabulated in Table 12.4.

TABLE 12.4

VALUES OF FREQUENCY AND FREQUENCY PARAMETERS FOR THE TESTS

Pitch Setting	P/D	Mean Frequency f c.p.s	Mean Frequency Parameter $S = \frac{\rho D^2 f}{\mu}$
-10°	1.58	110	4.44×10^6
-5°	1.20	119	4.80 "
0°	0.96	128	5.16 "
$+5^\circ$	0.74	136	5.48 "
$+10^\circ$	0.53	142	5.73 "

Since the tests were at almost constant frequency, no conclusions regarding the effect of frequency on I_h can be drawn.

Other investigators are generally in accord with the conclusions that :-

(a) The effect of frequency on M_h or I_h is small

(b) M_h and I_h tend to the ideal value at high frequencies.

There is disagreement, however, on whether M_h and I_h increase or decrease with increased frequency.

Burrill and Boggis (Ref. 12.3) noted during initial model tests on propeller virtual inertia that "when the frequency was doubled the entrained moment of inertia was slightly decreased, the effect being to increase the frequency in water by about 1.2 % " (Quotation taken from reply to discussion in Ref. 6.9). Calderwood (see Section 12.2) also noted a decrease in I_h with increase of frequency, from ship trial data.

McGoldrick (see Section 12.2) however, apparently noted the opposite trend during model tests. Brahmig (Ref. 6.2) also found that for a thin circular disc, there was a definite trend of increase in M_h with increase in frequency. The author (Section 8.4 was also in agreement that M_h and I_h should increase with increase in frequency.

Fottinger (Ref. 12.1, 12.2,) Brahmig (Ref. 6.2) and the author (Section 8.4) agree that M_h and I_h tend to the ideal value at high frequencies.

It may be that M_h and I_h increase or decrease with increased frequency, depending on the importance of the "viscous component" as suggested in Sections 8.4 and 12.2.1. This may be the explanation for the apparently contradictory experimental results.

To sum up therefore, it is suggested that conclusions (a) and (b) above be accepted as valid, but that the question of whether M_h and I_h increase or decrease with increase of frequency be regarded as unresolved.

12.2.4 Effect of P/D and J

From Figures 12.6 and 12.7, it will be seen that the primary parameter affecting hydrodynamic inertia is the pitch setting. This is only as would be expected since the discussion in Section 8.1 indicated the primary parameter for hydrodynamic inertia in a real fluid as well as an ideal fluid to be the shape of the body.

The variation of I_h with J, shown in Figs. 12.6 and 12.7, may not be in practice as significant as it first might appear from a study of these figures. The range of J shown covers a variation from almost as low as the static thrust condition of the propeller

($J \rightarrow 0$) up through the zero thrust ($k_T = 0$) and zero torque ($k_Q = 0$) conditions into the negative thrust (windmilling) region of operation. Over the normal positive thrust range of operation, the variation of I_h with J is comparatively small and could be for most practical purposes neglected. It should be noted, however, that under certain conditions torsional resonance in the propulsion system can occur with the propeller windmilling. An experimental record of such a resonance is given in Ref. 12.4. In this case, the variation of I_h with J would cause the resonance frequency in the windmilling condition to be different from that for normal operation. The variation, however, would not usually be significant, in practice.

As regards the shape of the I_h versus J curves, there are two features which may be distinguished :-

(1) There is a "saddle" evident in the curves, for all P/D ratios. The position of the saddle varies with J, being at $J = 0.5$ for the lowest P/D and moving across to higher J's as the P/D is increased up to $P/D \simeq 1.0$, after which it drops back to about $J = 0$ with further increase of P/D. It could be argued that the "saddles" as shown in Fig. 12.6 are associated with the higher R_n data in Fig. 12.5, and that since this data shows considerable scatter less reliance should be placed upon it. If the $R_n = 4.0 \times 10^5$ curves in Fig. 12.5 are studied, it will be seen that although there are hollows in the curves, it is only in the case of the highest P/D that there is a pronounced saddle. The $R_n = 4.0 \times 10^5$

test data showed comparatively little scatter (See.Fig.12.3). For the highest P/D curve, there is good reason therefore to assume that there is a definite saddle present (at about $J = 1.1$) in the curve. The work of Price (Ref. 12.5) on the virtual inertia of a loaded propeller also showed a saddle in the curves of I_h versus J, although in this case it was a clearly pronounced minimum in the vicinity of the usual operating point, and was evident in curves for P/D values from 0.78 to 1.4. The frequency at which these tests were carried out differed though from the present case. There is evidence therefore, that depending on the shape of the propeller and the experimental conditions, the I_h versus J curves may show "saddles" or hollows.

(2) If the smoothed curves in Fig. 12.7 (based mainly on the $R_n = 4.0 \times 10^5$ data) are studied it will be seen that for the medium values of P/D there is a decrease of I_h with increase of J, whereas with the lowest and highest values of P/D, I_h remains practically constant. Over the normal operating range of J (below $k_T = 0$) the values of I_h are almost constant with J for all P/D ratios.

The values of I_h for various P/D's obtained from the still-water tests are very close to the average values (over the positive thrust range) obtained from the main test series (See Table 12.3). With the exception of the value of the lowest P/D, the still-water values are slightly higher.

12.2.5 Comparison with Data from Other Sources

Various relationships for I_h have been put forward in the literature, and it is of interest to compare the values obtained in the present tests with those calculated by these methods. The principal relationships are given below:-

(1) I_h = 25-30 % of the inertia of the propeller (Ref. 6.6)

(2) I_h = 25 % of the inertia of the propeller (Ref. 12.6)

(3) $$I_h = \frac{0.0042\ \rho P^2 D^3\ (MWR)^2 n}{[\{1 + (\frac{P}{D})^2\}\{0.3 + MWR\}]}$$

i.e

$$I_h = \frac{0.0042\rho\ (\frac{P}{D})^2\ D^5\ (MWR)^2 n}{[\{1 + (\frac{P}{D})^2\}\{0.3 + MWR\}]} \qquad (12.1)$$

These equations are obtained by rearrangement of those given by Lewis and Auslander in Ref. 6.7

I_h = hydrodynamic inertia (lb ft^2)

ρ = mass density of fluid (lb ft^{-3})

$\frac{P}{D}$ = pitch diameter ratio

D = diameter (ft)

MWR = mean width ratio

n = number of blades

(4) In Ref. 6.9 it is assumed by Burrill and Robson that the entrained body of fluid around each blade is given by a solid-of-revolution lying along the axis of the blade. The diameter of this solid-of-revolution, at any blade radius is given by the projection of the chord on to the plane containing the propeller axis and the blade axis. The inertia of the fluid within this body-of-revolution is referred to as the calculated value of hydrodynamic inertia. The actual value of hydrodynamic inertia is obtained by multiplying the calculated value by a constant K_I. A graph of K_I plotted as a function of $\left(\frac{BAR}{n}\right)$, determined from a number of tests, is given in the reference, and allows the actual value of hydrodynamic inertia to be calculated for any propeller. Values calculated in this way will be referred to as "Burrill integration values" of hydrodynamic inertia.

(5) In Ref. 6.9 the following empirical formulae derived from model tests are given :-

(a) <u>3 - blade</u>

$$I_h = 0.00385\rho D^5 \left[1.37 \left(BAR \times \frac{P}{D}\right) - 0.30\right] \text{ for } \left(BAR \times \frac{P}{D}\right) > 0.4 \quad (12.2)$$

$$I_h = 0.00493\rho D^5 \left(BAR \times \frac{P}{D}\right)^{1.80} \text{ for } \left(BAR \times \frac{P}{D}\right) < 0.4 \quad (12.3)$$

(b) <u>4 - blades</u>

$$I_h = 0.00385\rho D^5 \left[1.09 \left(BAR \times \frac{P}{D}\right) - 0.23\right] \text{ for } \left(BAR \times \frac{P}{D}\right) > 0.4 \quad (12.4)$$

$$I_h = 0.00412\rho D^5 \left(BAR \times \frac{P}{D}\right)^{1.8} \text{ for } \left(BAR \times \frac{P}{D}\right) < 0.4 \quad (12.5)$$

(c) 5 - blades

$$I_h = 0.00385\rho D^5 \left[0.98 \left(BAR \times \frac{P}{D}\right) - 0.21\right] \text{ for } \left(BAR \times \frac{P}{D}\right) > 0.4 \quad (12.6)$$

$$I_h = 0.00358\rho D^5 \left(BAR \times \frac{P}{D}\right)^{1.8} \text{ for } \left(BAR \times \frac{P}{D}\right) < 0.4 \quad (12.7)$$

(d) 6 - blades

$$I_h = 0.00385\rho D^5 \left[0.90 \left(BAR \times \frac{P}{D}\right) - 0.20\right] \text{ for } \left(BAR \times \frac{P}{D}\right) > 0.4 \quad (12.8)$$

$$I_h = 0.00323\rho D^5 \left(BAR \times \frac{P}{D}\right)^{1.8} \text{ for } \left(BAR \times \frac{P}{D}\right) < 0.4 \quad (12.9)$$

The symbol BAR represents Blade Area Ratio. The other symbols and units are as in (3) above

(6) In Ref. 6.8, a method of calculating hydrodynamic inertia similar to that described in (4) above, is deduced by Thomsen from theoretical considerations. The value of hydrodynamic inertia calculated from the fluid body-of-revolution is multiplied by a correction factor K to obtain the actual value of hydrodynamic inertia. This factor K is given by the equation

$$K = \frac{1}{1.05 + 9.6\left(\frac{BAR}{n}\right)^2} \quad (12.10)$$

To compare the results obtained in the present tests with those calculated from the above relationships, mean values of I_h / I_w over the positive thrust range were taken from Fig.12.6 for the five values of P/D ratio. The corresponding values of I_h / I_b were then calculated. These values, together with those calculated from the relationships given in sub-sections(1) to

(6) above, are given in Table 12.5. The values from the still-water tests are also included in Table 12.5. I_b is the mechanical inertia of the model propeller, assuming it to be made of manganese bronze. A density for manganese bronze of 0.31 lb $-in^{-3}$ has been assumed. A mean value for I_w of 0.840 lb $-in^2$ taken from the experimental data has been used for all P/D ratios. The corresponding value of I_b is 7.16 lb $-in^2$. The value of $\frac{BAR}{n}$ for the propeller is 0.225.

It will be seen from Table 12.5 that the first two methods of calculating I_h give reasonable agreement with the experimental values only at P/D ratios close to unity. Over the whole range of P/D ratios, methods (1) and (2) are clearly inadequate, giving too high a value at the lower P/D ratios and too low a value at the higher P/D ratios. The Lewis method gives values about 18 % on the low side over the whole range. The Burrill integration method, the Burrill formulae, and the Thomsen method give values close to the experimental values at the lowest P/D ratios, but all give values which are too high at the higher P/D ratios. Of these three, the Burrill integration method shows the least deviation from the experimental values.

12.2.6 Effect of Depth in the Full-Scale Case

The influence of depth of immersion is probably slight in the full-scale case for fully-laden vessels. In Ref. 6.9, no change in I_h was observed below a depth of immersion of 12 inches, for 16 inch propellers oscillating about a vertical axis. If in these tests the propellers were oscillating about a horizontal axis,

TABLE 12.5

COMPARISON OF MEASURED AND CALCULATED VALUES OF I_h / I_b

Pitch setting	P/D	Main Test Series (R_n = 4.0- 6.0x10^5)		Supplementary Tests (Still-water)		I_h/I_b as calculated from the relationships given in sub-sections:-					
		I_h/I_w	I_h/I_b	I_h/I_w	I_h/I_b	1 Kane	2 Garibaldi	3 Lewis	4 Burrill (Integration)	5 Burrill (Formulae)	6 Thomsen
-10°	1.58	4.2	0.49	4.3	0.50	0.25-0.30	0.25	0.39	0.59	0.73	0.65
- 5°	1.20	3.3	0.39	3.5	0.41	0.25-0.30	0.25	0.32	0.45	0.51	0.50
0°	0.96	2.4	0.28	2.6	0.30	0.25-0.30	0.25	0.26	0.33	0.37	0.37
+ 5°	0.74	1.8	0.21	1.9	0.22	0.25-0.30	0.25	0.19	0.23	0.24	0.26
+10°	0.53	1.4	0.16	1.3	0.15	0.25-0.30	0.25	0.12	0.14	0.13	0.16

little effect on I_h would therefore be expected below a depth of immersion (axis to surface) of say, 16". At this condition the blade tips would be no closer than D/2 to the surface. Most fully laden vessels have depths of immersion of this order. At light load, however, the depth of immersion would be much less and the influence of depth on I_h could be considerable.

The results from Ref. 6.9 quoted above also indicate that the influence of neighbouring boundaries on the I_h of a full-scale propeller is probably small, since aperture clearances around the propeller are fairly generous these days.

To summarise therefore, it would appear that as a reasonable approximation for propellers with boundaries not too close, equation 9.9 may be rewritten as

$$\frac{I_h}{\rho D^5} = f\,(\text{shape}) \qquad (12.11)$$

For a given propeller series, it is suggested that 12.11 can be written with sufficient accuracy as

$$\frac{I_h}{D^5} = f\left(\frac{P}{D}, \text{BAR}\right) \qquad (12.12)$$

It would appear to be a worthwhile project to determine the form of the function in equation (12.12) for the commonly used propeller series.

CHAPTER 13

CONCLUSIONS AND RECOMMENDATIONS

13.1 CONCLUSIONS

For the propeller configuration tested, it can be concluded that :-

(1) The influence of amplitude of oscillation and of propeller Reynold's number on the hydrodynamic inertia I_h is small.

(2) The influence of propeller loading as expressed by the advance ratio J, on I_h is small within the positive thrust region. In the negative thrust region, however, there is an appreciable decrease in I_h for medium values of P/D (around 1.0). At high and low values of P/D there is little variation of I_h in the negative thrust region.

(3) The value of I_h determined in "still-water" is only very slightly different to the average value of I_h for the loaded propeller (in the positive thrust region). It would thus appear that the hydrodynamic inertia of a propeller can be determined to a reasonable degree of accuracy by tests on a non-rotating propeller in still water.

(4) The Burrill integration method of determining I_h gives the closest approximation to the experimental values of any published method. The Burrill method, however, gives values which are higher, in the higher range of P/D ratios. The Lewis method gives the next closest approximation to the experimental values. In this case, the calculated values are about 18 % lower than those determined experimentally.

13.2 RECOMMENDATIONS FOR FURTHER WORK

In the light of the information obtained from the present investigation, it is recommended that the following lines of research should be considered:-

(1) An investigation into the effect of frequency and amplitude of oscillation, propeller Reynolds Number and loading, and changes in shape on the hydrodynamic mass for axial oscillations M_h of a propeller. This could be carried out using the existing equipment with very little modification.

(2) An investigation into the effect of frequency and amplitude on the hydrodynamic mass M_h and hydrodynamic inertia I_h of bodies of both simple and complex shapes. Where possible the values of M_h should be compared with the ideal values, obtained by calculation.

(3) An investigation of the effect of pitch distribution on the values of I_h and M_h of propellers, as this has not yet been thoroughly investigated.

(4) The determination of I_h and M_h values for propellers of standard series, using the present equipment.

(5) The determination of the effect of depth of immersion on I_h and M_h of propellers.

(6) The improvement of methods of calculating I_h and M_h for complex shapes (particularly propellers) following the leads, perhaps, of Burrill (Ref. 6.9 and Thomsen (Ref. 6.8)

(7) An attempt to develop a mathematical analysis for the determination of I_h and M_h, for simple shapes, in a real fluid.

This would show the trends due to viscous effects, for the simple shapes, at least, and also indicate their magnitude.

PART IV

FULL SCALE RESEARCH - EXPERIMENTAL EQUIPMENT AND TECHNIQUES

CHAPTER 14

STRAIN-GAUGE INSTRUMENTATION FOR SIMULTANEOUS MEASUREMENT OF TORQUE AND THRUST

14.1 INTRODUCTION

The measurement of torque or thrust by strain-gauge methods is a problem of common engineering occurrence. The techniques used are, in general, well known and comparatively simple. However, difficulties arise in the simultaneous measurement of torque and thrust if any of the following conditions are present:-

1. A low value of stress associated with either torque or thrust.
2. A large ratio of thrust-caused stress to torque-caused stress, or vice-versa.
3. A large ambient temperature variation.
4. A high-accuracy requirement, for both mean and fluctuating components of torque and thrust.

All of these conditions occur in the measurement of torque and thrust in a ship tailshaft.

This chapter describes some of the measures found necessary to overcome the resulting difficulties, in tests carried out on ship tailshafts during this research project. In field tests such as this, the stressed measuring element must be the shaft itself, as it is not practical to incorporate an element of especially-designed section into the shaft system. In applications where a specially constructed dynamometer can be used, some of the difficulties listed above (for example, low stress) are easily

overcome by appropriate design of the dynamometer. Some of the other problems (for example, those due to variation of temperature), still remain, however. Some of the features which were adopted in the design of such a dynamometer are described in earlier chapters.

14.2 THE MEASUREMENT OF TORQUE AND THRUST

14.2.1 The Principle of Strain-Gauge Measurement

The basic principle in force or moment measurement by means of strain gauges, is the use of these gauges to measure the appropriate surface stresses in the load-carrying component. These gauges will measure tensile or compressive strain, but not shear strain, and therefore are usually placed along the axes of the principal tensile or compressive strsees. In the case of a shaft therefore, torque is measured by gauges at 45° and 135° to the shaft axis, and thrust by gauges at 0° and 90° to the shaft axis. In both cases, the tension and compression gauges are connected in a fully-active bridge in such a way that signals from both types of gauges are additive. Since such a bridge has four resistance legs, it is usual to use four (or multiples of four) gauges in the bridge. If more than four gauges are used they are arranged in four groups, the gauges in each group being wired in series to comprise one leg of the bridge.

14.2.2 Types of Strain-Gauge System

The stress in the component to which the strain-gauge is attached causes a proportional strain in the material. Since each gauge is firmly cemented to the surface, the strain in the gauge is

equal to that in the surface of the material. This strain, in the resistance wires comprising the gauge, causes a proportional change in the total resistance of the gauge. It is by the measurement of this change in the gauge resistance that the surface stress is deduced. There are many ways in which the gauge resistance change may be measured, each method with its own particular advantages depending on the application. These methods may be grouped according to the current-flow in the measuring system, into the following types:-

1. The Zero Current or Null Method

   In this method, the voltage difference across the gauge-bridge is matched against an equal but opposite voltage difference from an external source, so that no current flows from the measuring system into the bridge, this being indicated by some form of measuring instrument. The voltage difference in the external source is then measured. Since this voltage is commonly generated by a potentiometric method, estimation of the voltage is simply made in this case. The null method can clearly only be used for the measurement of a steady mean stress.

2. The Direct Current Method

   In this method, the gauges are supplied from a constant voltage supply, and the resulting voltage-variation across the bridge due to strain is measured or recorded. This voltage-variation is proportional to the stress. This system,

which has the advantage of simplicity, can be used for the measurement of both mean stress and fluctuating stress. If only the fluctuating component of stress is to be measured this system has many advantages. However, if the mean component of stress is to be measured with any accuracy, then the problems of drift in the gauges and measuring system become considerable.

3. Alternating current methods

These methods use an alternating current waveform supplied to the bridge at a frequency above that of any frequency to be measured. Changes in the bridge resistance due to stress, modulate the waveform. After appropriate amplification, the original carrier-frequency is removed from the output signal, leaving a voltage-variation proportional to the stress-variation. Although the equipment required is more complex than in the other two methods, this method has many advantages where the measurement of a steady mean-component is required. The most commonly-used waveform is sinusoidal, but in certain applications other forms such as the rectangular may be advantageous (Ref. 14.1).

14.2.3 Strain-Gauge Problems

Errors in measurement caused by the strain-gauges themselves may be divided into two classes; errors due to gauge position, and errors due to gauge variation, These two types of error are discussed in further detail below:-

1. Gauge Alignment Errors

If only torque or thrust is being transmitted (and measured) in a shaft, errors caused by gauge misalignment will depend upon the ratio of the stress along the gauge-axis, to the stress along the principal axis parallel to which the gauge is supposedly placed. It may be simply shown that this ratio does not vary rapidly in the neighbourhood of the principal axis, and the error is thus not great for small angular misalignment. If, however, both torque and thrust are being transmitted (and measured) simultaneously, and if the ratio of the principal stress due to torque, to the principal stress due to thrust (or vice versa) is large, then it can be appreciated that unless the gauges measuring the lowest stress are placed precisely in the direction of their principal stress, they will measure a component of the other (higher) principal stress. (The principal tensile stresses caused by torque and thrust in a shaft are at 45° to each other, and similarly for the principal compressive stress). In such a case, the tolerance on gauge position must be less than in the previous case. For ship tail-shaft tests, where during normal operation, the ratio of the principal compressive stress due to torque to the compressive stress due to thrust is of the order of 12 to 1, it was necessary for the gauges to be aligned to an accuracy of the order of $1/8^{\circ}$, for the required accuracy to be obtained. Since the gauge-grid was not aligned with the lines drawn on the strain-gauge surface by the manufacturer, to this degree

of accuracy, it was necessary to trim the side-edges of each gauge in a guillotine-jig mounted on a microscope, parallel to the mean axis of the gauge-grid as located visually in the eyepiece. The ends of the gauges were then trimmed at right-angles to the sides. Location of the gauges on the shaft during cementing was by means of a polytetrafluoroethylene jig, held on the shaft by a clamping ring.

2. Gauge Variation Errors

The gauge characteristics in which there may be variations are; gauge resistance, gauge-factor, and temperature coefficient.

Errors due to variation of gauge-factor and temperature coefficient, in gauges in the same bridge, may be reduced by selecting the gauges from the same manufacturing batch. Errors due to gauge resistance variations are of two types; those due to variations at the same temperature, and those due to variations caused by different temperatures. Errors of the first type may be reduced by resistance-matching the gauges under constant-temperature conditions. It is now standard practice in the Department of Mechanical Engineering at the University of Adelaide to match gauges to the fifth figure of resistance. Errors of the second type, caused by gauges being at different local temperatures, may be reduced in the following ways:

(a) By the use of gauges with a low temperature coefficient

(b) By the adoption of means to reduce the temperature difference between gauges (e.g. by wrapping the shaft in the neighbourhood of the gauge-location, with a

thermally-insulating layer of foam plastic).

14.2.4 Amplifier Problems in D.C.Systems

The main difficulty in amplifiers for a d.c. strain-gauge system is that of reducing drift to an acceptable level, i.e. the problem of achieving a sufficiently high stability. This becomes of increasing importance as the stresses to be measured (and the bridge output voltage) become smaller. As the bridge output voltages decrease in magnitude, the problem of achieving an acceptable signal-to-noise ratio in the amplifier also assumes increasing importance. The methods which have been developed in the Department of Mechanical Engineering at the University of Adelaide during the course of this research project to overcome these difficulties are described below.

For reasons of size and stability, amplifiers and preamplifiers of the transistor type are used. Drift in these amplifiers may result from a change in either the temperature or the supply voltage. It is a simple matter to hold supply voltage constant, but it is not practical, in most cases, to keep the ambient temperature constant. The main reason for temperature drift is that transistors have their performance greatly affected by temperature changes. Careful selection, however, makes it possible to obtain pairs which behave almost identically over a limited range of operating conditions, including temperature. If these matched pairs are used for push-pull stages, any drift that occurs in one will also occur in the other, provided that they are held at the same temperature by a suitable heat sink. In an ideal push-pull pair, drift voltages would have equal magnitude and the same phase, and

hence would not cause any change in output voltage. In practice, there is always some residual drift.

Other methods to reduce zero drift are also adopted. In the amplifier first stage, resistors in the emitter circuits cause a large reduction in both zero drift and gain. A low-valued resistor between the two emitters restores the gain to the desired level, but leaves the drift stabilization substantially unaffected. Over the whole amplifier, negative feed-back is used to control the gain further, and to improve the stability of the second and thrid stages and the linearity of all stages. As far as drift is concerned, however, the first stage does not benefit from the negative feed-back. High-stability resistors are used throughout the circuit and the first-stage resistors are carefully balanced to avoid drift due to resistance changes. In rotating amplifiers (i.e. pre-amplifiers attached to shafts) a wiring layout which is symmetrical is an advantage, because the voltages generated by the cutting of stray magnetic fields will cancel within the circuit, and such an arrangement is used where possible.

14.3 FIELD MEASUREMENT OF TORQUE AND THRUST

On several occasions during the research project described in this thesis, measurements of torque and thrust have been made in the field on ship tail-shafts. The instrumentation briefly described below (which was that used in the most recent investigation)illustrates the principles described in the preceding sections.(A detailed description of this equipment is

given in Chapter 15).

Measurements of the instantaneous torque and thrust in the tail-shaft were made by using electrical resistance strain-gauges cemented to the shaft surface, with suitable equipment to amplify, transmit, and record the electrical output from the gauges. The output from the gauges was amplified by transistorized pre-amplifiers attached to the rotating shaft. The pre-amplifier output was then transmitted through slip-rings to the recording equipment.

To measure the thrust in the tail-shaft, eight strain-gauges were used, in four pairs, two pairs being placed parallel to the shaft axis and two pairs at right angles to it. The four pairs of gauges were arranged at 90° from each other around the shaft, this arrangement ensuring that signals due to bending stresses would be cancelled out within the bridge.

For the measurement of torque, four strain-gauges were placed at angles of 45° and 135° to the shaft axis, i.e along the lines of the principal tensile and compressive stresses. The gauges were arranged symmetrically around the shaft, and connected in a fully-active bridge in such a way that signals due to bending stresses would be cancelled out within the bridge.

The stresses due to torque under normal operating conditions, although small, were within the range for which strain-gauges are commonly used without undue difficulty being experienced with temperature errors. The stresses associated with the thrust, however, were much smaller, and special precautions against drift caused by temperature had to be adopted.

The more important of these measures were:-

(a) Gauges were selected from the same manufacturing batch to reduce variations in gauge-factor and temperature-coefficient, and were resistance-matched under constant-temperature conditions, to the fifth figure.

(b) To reduce local temperature variations, the shaft in the neighbourhood of the gauge locations was covered with a thermally-insulating layer of foam plastic.

(c) The transistorised amplifiers on the shaft were designed to have very low drift.

The slip-rings were constructed of brass imbedded in an epoxy-fibreglass annulus retained on the shaft by a clamping ring. To enable the slip-ring assembly to be attached to the shaft, it was constructed in two sections, split on a diametral plane. Two sets of silver-carbon brushes were used, in perspex brush-boxes at approximately 120° apart, to eliminate effects due to the slip-ring end gaps.

The torque and thrust outputs from the slip-rings were recorded in two forms. The mean values were measured by a high impedance meter, heavily damped. The fluctuating components were separated from the mean values, further amplified, and recorded.

CHAPTER 15

THE DEVELOPMENT OF A D.C. STRAIN-GAUGE SYSTEM FOR SHIP TAIL - SHAFT MEASUREMENTS

15.1 INTRODUCTION

During the research project described in this thesis, a number of full-scale investigations on propeller-shaft vibrations in ships have been carried out. All of these tests have been based on the electrical resistance strain-gauge measurement of surface stresses in the tail-shaft. The techniques and instrumentation used in these tests have progressively become more complex, due to the demand to obtain a wider range of data with a higher degree of accuracy. The corresponding development in the equipment has resulted in an increase in both accuracy and reliability. The description given in this chapter is of the equipment used in the last of the recent series of tests on a 19,000 ton turbine-powered ore-carrier.

In the ore-carrier investigation, measurements of the instantaneous torque and thrust in the tail-shaft were made by using electrical resistance strain-gauges cemented to the tail-shaft surface. The output from these gauges was amplified by transistorised pre-amplifiers attached to the rotating shaft. The amplified output was then transmitted through slip-rings to the recording equipment.

15.2 THE STRAIN-GAUGES

The strain-gauges which were used were 600 ohm wrap-around type wire gauges, attached to the metal surface by epoxy cement. For the measurement

of torque stresses, strain-gauges were cemented to the tail shaft surface at angles of 45° and 135° to the shaft axis, so that the principal tension and compression stresses, respectively, would be measured. A fully-active bridge circuit, with a symmetric arrangement of four gauges, was used, to ensure that signals due to axial and bending stresses would be cancelled within the bridge. Eight strain-gauges were used for the thrust measurement, in pairs, at angles of 0° and 90° to the shaft axis. A fully-active bridge circuit, with a symmetric arrangement of gauges, was also used, so that signals due to bending stresses would be internally cancelled.

The methods of measuring torque and thrust in a shaft, by strain-gauges, are well known (See Chapter 14). In the present application, however, there were a number of difficulties which required considerable development before they were overcome. Some of the most serious of these difficulties were associated with the strain-gauges. Errors in measurement due to this cause, may be grouped into two classes; errors due to gauge position, and errors due to gauge variation.

Gauge misalignment errors were minimised by trimming the edges of each gauge in a guillotine-jig mounted on a microscope, with reference to the mean axis of the gauge-grid, as located by a scribed reference line on the perspex stage. Back-lighting was used through the transparent stage to make visible both the reference line and the wires of the gauge-grid. During cementing, the gauges were located on the shaft by means of a polytetrafluorethylene jig.

Errors due to gauge variation in resistance, gauge factor, and temperature coefficient were minimised by careful matching. Thermal

insulation to reduce the temperature differential between gauges was also adopted. (Some of these measures are also discussed in Chapter 14).

It was then found that the most important residual error was associated with temperature differences between gauges. This error could have been further reduced if either temperature-compensating gauges or gauges with a lower temperature coefficient had been used. Due to difficulties of supply it was not possible to make use of these, at the time. In tests of this kind where the stresses to be measured are very small and where high accuracy is required, it is strongly recommended by the author that such special gauges should be used, if possible.

15.3 THE ROTATING PRE-AMPLIFIERS

In a D.C. strain-gauge system such as was used in the present application, errors due to temperature drift in the pre-amplifiers can be considerable. To obtain reasonable stability from a transistor pre-amplifier is in most cases not difficult, as there are now a variety of circuits available which will ensure low drift (Ref. 15.1). It is, however, rather more difficult to obtain low drift with a simple reliable circuit suitable for a miniature pre-amplifier mounted on a rotating shaft. The pre-amplifier described below was developed in order to obtain a satisfactory compromise between stability and complexity.

The circuit used was based on the conventional differential type of transistor pre-amplifier, and is shown in Fig. 15.1. The transistors used were carefully matched for both gain and leakage at room temperature. It was initially proposed to further match within these groups, for

Fig. 15.1 Circuit diagram of transistor pre-amplifier

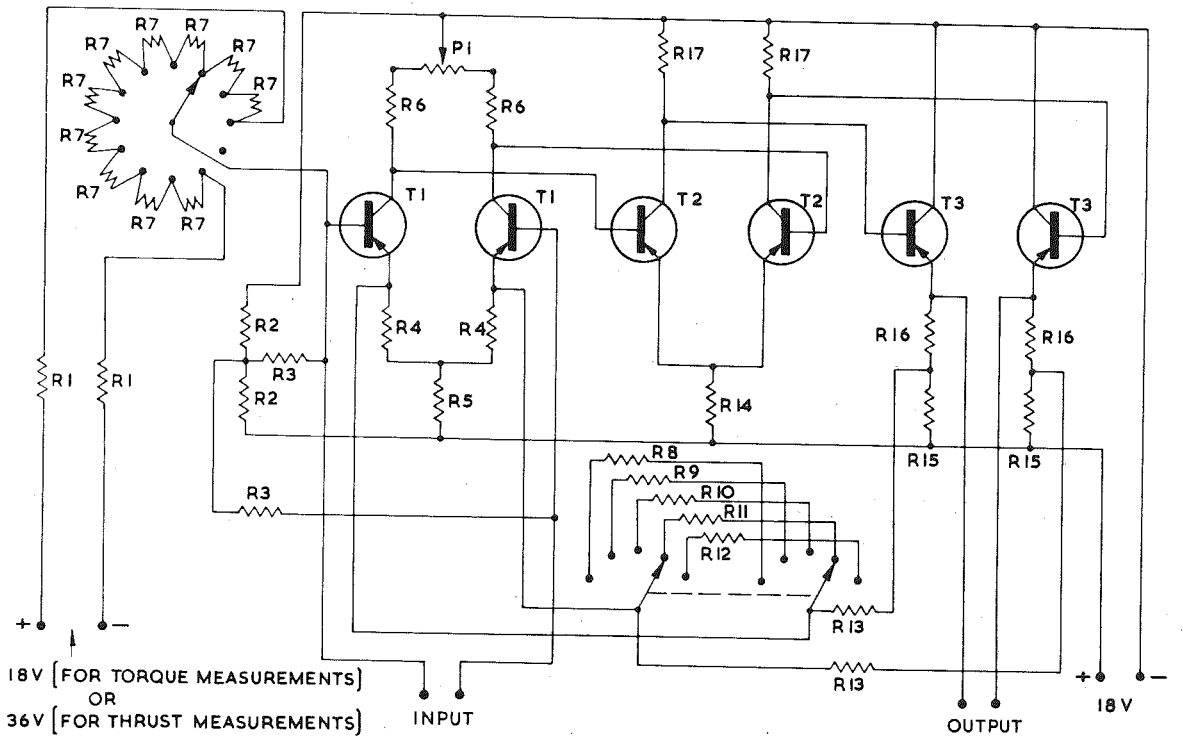

TRANSISTORS		
T1	TYPE	BCZ 10 SILICON
T2	TYPE	OC 44 GERMANIUM
T3	TYPE	OC 44 "
RESISTORS		
R1	100kΩ	METALLIC OXIDE
R2	40kΩ	" "
R3	40kΩ	" "
R4	4·7 kΩ	" "
R5	6 kΩ	" "
R6	30 kΩ	" "
R7	100 Ω	" "
R8	70 Ω	" "
R9	150 Ω	" "
R10	240 Ω	" "
R11	470 Ω	" "
R12	1 kΩ	" "
R13	100 kΩ	" "
R14	5·6 kΩ	CARBON
R15	5·6 kΩ	"
R16	3·9 kΩ	"
R17	10 kΩ	"
POTENTIOMETERS		
P1	1 kΩ	WIREWOUND

temperature-variation, but this would have required larger transistor stocks, and was in any event not found to be necessary. It appears that temperature-variation effects within the groups as selected, were of second order. Initially, low-leakage germanium transistors (Type OC44) were used. It was found, however, that an improvement in drift over the specified temperature range of the order of 2 times was obtained by replacing these in the first stage with audio-frequency silicon transistors (Type BCZ 10), and these were used in the final design.

To reduce temperature variations between transistors, they were mounted symmetrically within a circular aluminium block, whose function was to act as a heat sink of uniform temperature.

Initially, cracked-carbon high-stability resistors were used. It was later found that an improvement in drift of the order of 5 times could be obtained by replacing these in the first stage, with metallic-oxide-film high-stability resistors. Although the temperature coefficient of the metallic-oxide resistors is not greatly different from that of the carbon resistors, their consistency in this regard is better, and appears to account for the improvement obtained.

The drift characteristic of the pre-amplifier is shown in Fig. 15.2 which shows that the drift voltage after rising to a maximum at 88° decreases with further increase in temperature. The magnitude of the drift voltage over the working range 60° - 100°F is, however small.

The gain of the amplifier was 2150. The input and output impedances were 9000 ohm and 800 ohm respectively.

Because the pre-amplifiers had to be mounted on a rotating shaft,

Fig. 15.2 Drift characteristics of transistor pre-amplifier.

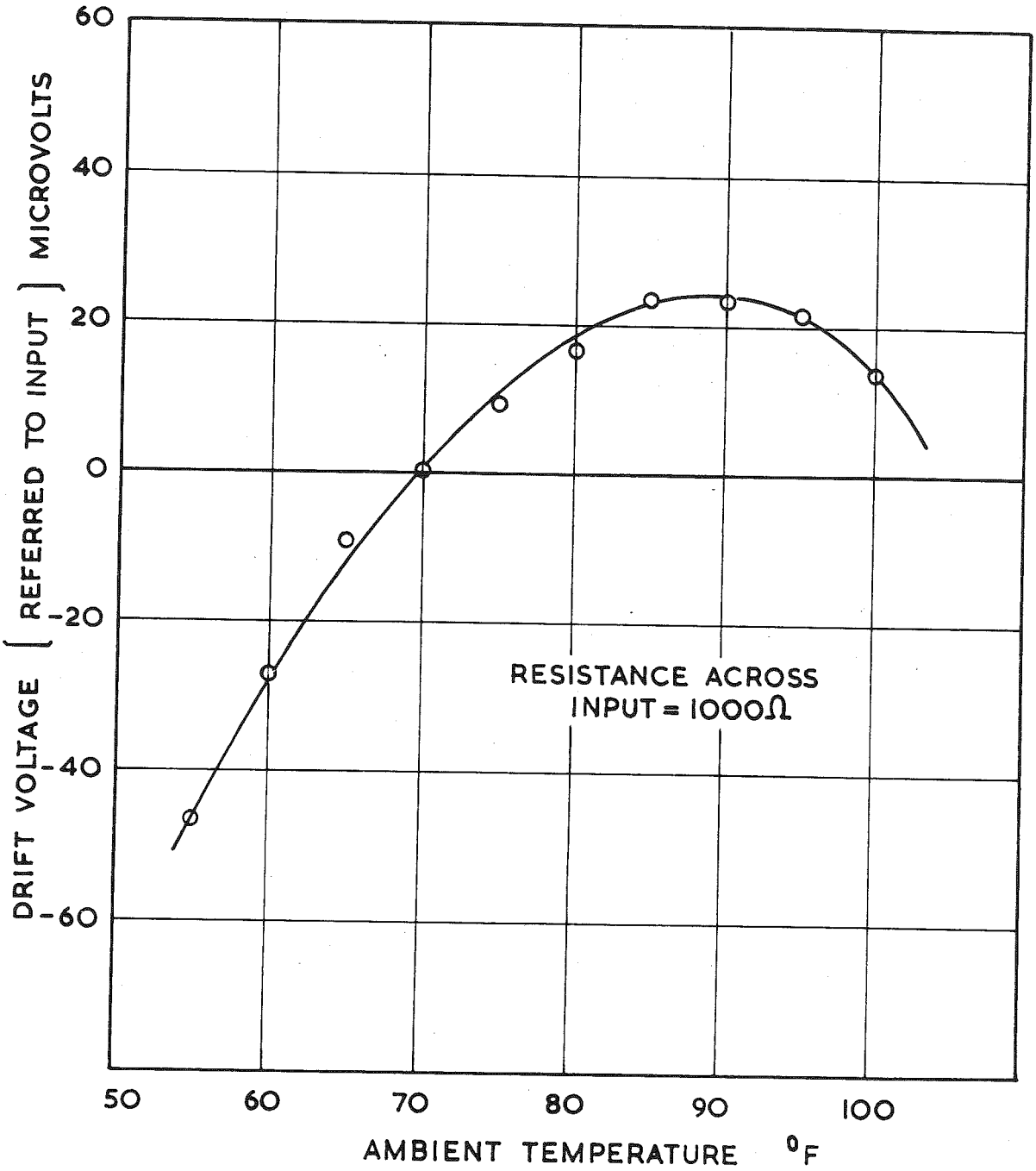
60
40
20
0
-20
-40
-60
DRIFT VOLTAGE [REFERRED TO INPUT] MICROVOLTS
RESISTANCE ACROSS
INPUT = 1000Ω
50
60
70
80
90
100
AMBIENT TEMPERATURE °F

it was important for size and weight to be kept small. The components were assembled on a section of matrix-board, and enclosed in an aluminium case of over-all dimensions 7" x 4" x $1\frac{1}{4}$".

15.4 THE SLIP-RING ASSEMBLY

In the earlier investigations, both cylindrical- and disc-type slip rings were used. In the first type of slip-ring, each individual ring is a short length of cylinder mounted co-axially around the shaft, with the brushes mounted radially. In the second type, each "ring" consists of an annular disc mounted normal to the axis of the shaft with the outer and inner peripheries of the disc concentric with the shaft. The brushes are mounted parallel to the axis of the shaft and bear on the faces of the disc. The principal advantage of the disc-type slip-ring is that it is very easy to construct, the sheet-metal discs and insulating segments being fixed together with bolts, and attached to the shaft with a split clamping-ring. The disadvantages of the disc-type are, in the first place, the length of shaft required for a large number of rings (since sufficient space must be provided between the discs for the axially located brushes), and in the second place, the relatively high susceptibility to damage of the thin discs during transportation and assembly. Because of these disadvantages the cylindrical type of slip-ring was used in all the later investigations.

With both types of slip-ring assembly, care must be taken to ensure correct alighment on the shaft. Misalignment is not desirable, as it causes a varying pressure between the brush and slip-ring, resulting

in variation of brush noise. In extreme cases of misalignment brush bounce may occur with the brush losing contact with the slip-ring surface intermittently.

In the most recent investigation, an assembly of 16 slip-rings (of the cylindrical type) were used, the rings being embedded in an epoxy-fibreglass annulus fitted to a duralumin clamping ring. The slip-rings were of square-section brass, and were curved to the appropriate radius by rolling. The rolled rings were cut in half and the resulting half slip-rings were cemented with epoxy cement into grooves turned in the epoxy-fibreglass annulus. The rubbing surfaces of the slip-rings were then turned to size and polished. To enable the slip-ring assembly to be attached to the shaft it was constructed in two half sections (split on a diametral plane) and bolted together in position. The slip-rings were wired internally to a connecting strip mounted on the side of the duralumin clamping ring. Silver-carbon brushes were used to reduce brush noise. Two sets of brushes were used at positions approximately 120° apart around the shaft. Each half-slip-ring was wired electrically to the complementary half-ring to also help reduce end-gap effects. An exception was the slip-ring used to measure angular position. In this case, the half-slip-ring was insulated from its complementary half-ring. This half-ring was supplied with an electrical voltage from an adjacent slip-ring. A single brush was then used to contact this half-slip-ring, so that a rectangular wave-form was obtained which indicated the position of the slip-ring end-gap. Since the relative angular positions of the end-gap and the propeller blades were known, the angular position

of any blade at a given instant during rotation, could be determined.

Although brass was used for the slip-rings, because of its relatively low cost, previous experience had indicated that rather better results could be obtained by using monel-metal. One of the disadvantages of brass is that a thin oxide-film tends to form relatively rapidly and causes excessive brush noise, unless the slip-rings are regularly cleaned at intervals with 600-grit emery, followed by cleaning with a carbon tetrachloride impregnated cloth. Work carried out elsewhere indicates however, that the oxide trouble would have been prevented, had the brass slip-rings been plated with a precious metal.

15.5 THE DRIVER AMPLIFIERS AND THE RECORDER

The driver amplifiers were of the push-pull transistor type, using matched germanium transistors. These amplifiers were developed commercially (to the author's specification) for this work, and were designed to operate from a standard 12 volt lead-acid accumulator. The specification called for input voltages up to $\pm$ 50 millivolts with corresponding maximum output voltages of $\pm$ 6 volts. (These values correspond to full-scale deflection of the recorder pens). The maximum amplifier gain was 120. Coarse and fine attenuation was available in 2 db. steps up to 40 db. The input impedance of the amplifiers was 10,000 ohms.

The output from the amplifiers was used to drive 30 ohm centre-tapped recorder pens. The recorder was of the ink-on-paper type, and was supplied commercially to the author's specification. Eight recording

pens were used, each with a maximum travel of $\pm$ 2 centimetres. Nine marker pens were also incorporated in the instrument. A range of paper speeds from 0.0125 centimetres per second to 50 centimetres per second was available. The frequency response of the pens was flat, up to 50 cycles per second.

15.6 THE IMPEDANCE CONVERTER

Bothe the torque and thrust output from the slip-rings after amplification were recorded in two forms. The total output for either torque or thrust can be regarded as the sum of two components; a mean D.C. value (corresponding to the mean torque or thrust), and an A.C. component (corresponding to the fluctuating torque or thrust) superimposed upon the mean. The output from the slip-rings was, for both torque and thrust, recorded in three separate forms, the three recording systems operating in parallel ;

(a) The total output was amplified by a driver-amplifier and recorded as an ink-on-paper trace.

(b) The mean value was recorded by a high-impedance voltmeter, which was heavily damped.

(c) The A.C. component was separated from the mean value by means of a specially designed impedance converter, then further amplified, and recorded as an ink-on-paper trace.

The design of the impedance converter posed the following problem. The A.C. component of the total output was comparatively small (of the order of 1 to 2 %) of the mean D.C. component, under many operating

conditions. To enable the A.C. component to be amplified and recorded, the large D.C. signal had to be completely blocked. The A.C. component, however, had to be transmitted through the impedance converter with negligible phase change, and at a gain, preferably near 1, which was constant with both frequency and time. The use of a blocking condenser in each leg of the system was the obvious method of accomplishing the above requirement. However, the phase shift θ for such a circuit is given by

$$\tan \theta = \frac{1}{2\pi f R C} \qquad (15.1)$$

where f = frequency, R = circuit resistance, C = $\frac{1}{2}$ the capacitance of each condenser. The resistance R for the case being considered is the input impedance of the driver amplifiers to which the circuit is connected. The input impedance of these amplifiers was low, of the order of 10,000 ohms. The frequencies of the A.C. component were comparatively low. For example, the fundamental frequency in the torque or thrust wave-form at half of the maximum shaft speed was about 4 cycles per second. Equation (15.1) shows that for θ to be kept small under these conditions would require extremely large values of C. In the present case, the values of C required were impractically large. Hence, between the capacitor and the driver input, a cathode follower circuit was inserted, as shown in Fig. 15.3. The resistance R in equation (15.1) now became the input impedance of the cathode follower. This was a very high value, of the order of several megohms. Thus the value of C required was very much smaller than previously. It was found that θ could be kept below 1^{o} at

Fig. 15.3 Circuit diagram of impedance converter

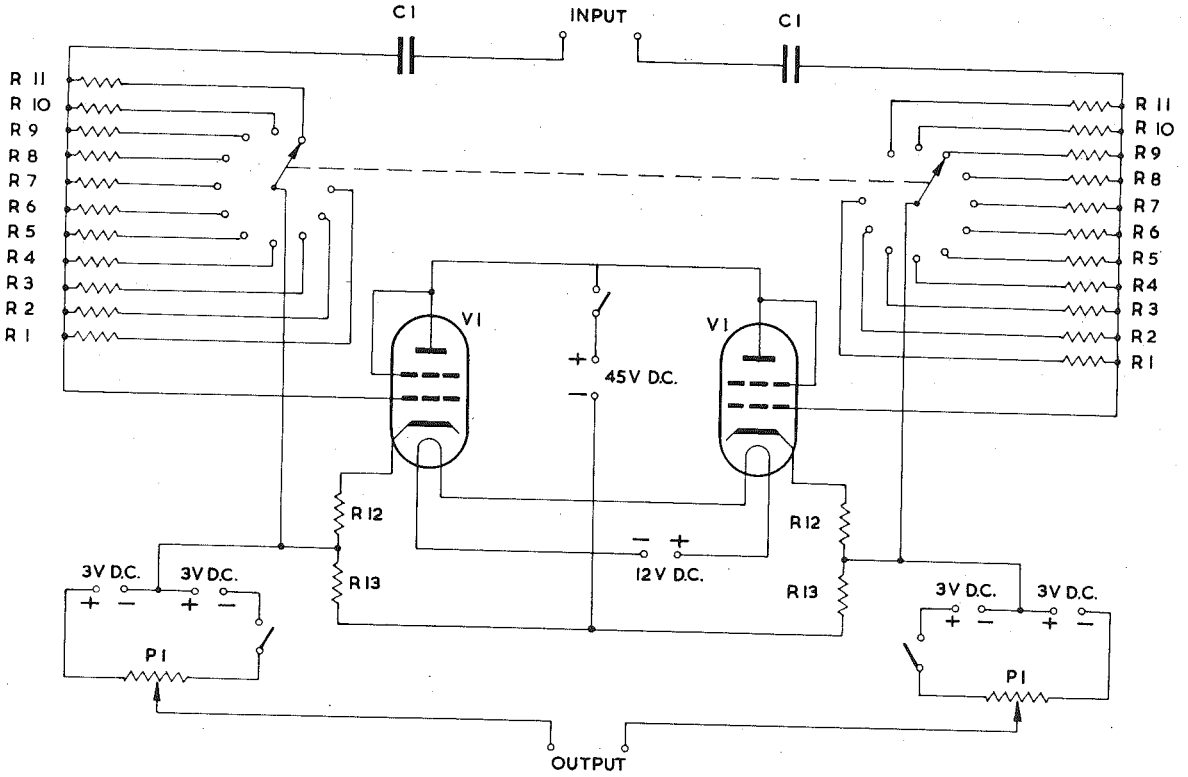

VALVES	
V1	TYPE E80F
CAPACITORS	
C1	1 μF
POTENTIOMETERS	
P1	1 kΩ
RESISTORS	
R1	180 kΩ
R2	220 kΩ
R3	270 kΩ
R4	390 kΩ
R5	560 kΩ
R6	1·2 mΩ
R7	1·5 mΩ
R8	2·2 mΩ
R9	3·3 mΩ
R10	4·7 mΩ
R11	6·8 mΩ
R12	1·8 kΩ
R13	33 kΩ

4 cycles per second with the use of quite small values of C. To cover a range of operation, it was arranged that R could be varied, as shown in Fig. 15.3 by switching in an additional resistance into the circuit.

A disadvantage of the above circuit was that the time constants were comparatively large. Hence, during sudden changes of engine speed the variation of output voltage from the cathode follower circuit while the condensers were discharging, was found to be too great to be accommodated by the driver amplifier. A manually-operated bias voltage was therefore applied to the output of the cathode follower to enable the signals during such sudden changes to be kept within recording limits.

The input impedance of the impedance converter, when connected to the driver amplifier was 34.8 megohms maximum. The gain of the impedance converter was 0.85, constant over the range of frequencies encountered.

15.7 CALIBRATIONS

Despite the measures taken in the design of the pre-amplifier and driver-amplifiers, it was to be expected that there would still be residual drift in these amplifiers due to temperature. By periodically switching off the power to the strain-gauges and measuring the amplifier outputs, it was possible to obtain a continuous record of amplifier drifts. These drift values were then used to correct the recorded data where necessary.

Although it was not expected that the over-all gain of the whole measuring system would vary appreciably with time, it was considered desirable to have a continuous record of the gain during the tests. To

calibrate the overall gain of the system, a high-stability calibrating resistor could be switched into either strain-gauge bridge. The switching was carried out on the shaft by a relay operated by an external voltage transmitted through a pair of slip-rings.

In order to estimate drift due to local temperature variations of the strain-gauges, a log was kept of output voltages at the zero-stress condition, i.e. when the shaft was under no load, usually with the ship at the dock.

15.8 ASSOCIATED EQUIPMENT

The power for the strain-gauges and the rotating pre-amplifiers was supplied from dry cells. In the case of the strain-gauge power, the voltage across the strain-gauge bridge was kept constant by rheostat control and manual monitoring. The power for the rotating pre-amplifiers was also transmitted through the slip-rings. It was found that temperature variations of the strain-gauges caused by the strain-gauges being supplied with power at intermittent intervals (i.e. only when measurements were required), was an appreciable source of error. To conserve the dry cells during a long voyage, alternating current of the equivalent voltage was passed through the strain-gauges during periods between readings, to maintain the same level of power dissipation, to prevent the undesirable heating and cooling effects. This alternating current was obtained by breaking down the ship's 32 volt A.C. with resistances.

It was essential that a time standard be recorded on the recorder paper, in case there was any variation of the paper speed. A clockwork-operated contactor was used for this purpose, to provide a rectangular wave-form of known period (a half-second per period). A check on the contactor could be made by means of electronic counter.

Event marks were made on the recording paper by operating marker pens in various sequences, using a previously worked-out code.

During the investigation, much of the equipment was located in one of the noisiest sections of the ship's engine room. Other sections of the equipment were located at a considerable distance away. Communication between the three persons operating the equipment, was found to be impossible, without artificial aid. An intercommunication system was therefore built up, based on throat-microphones and ear-muffed headphones, incorporating a transistorised amplifier. This equipment was portable and worked well under conditions of very high ambient noise level.

CHAPTER 16

AN AUTOMATIC DIGITAL CURVE READER

16.1 INTRODUCTION

From the most recent (and comprehensive) of the full-scale ship tests, a considerable quantity of information in the form of analogue recordings from an eight-channel recorder was obtained. During the analysis of this data, harmonic analyses of many sections of the records were required. This necessitated these sections being converted into corresponding tables of digital values of curve ordinates. As there were some 35,000 ordinates to be measured, much thought was given to the method by which these ordinate values would be obtained. It appeared that there were five possible methods which might be used. The analogue to digital conversion could be obtained by :-

(1) Measuring the ordinates manually with dividers and accurately-graduated rule.

(2) Using a travelling microscope with graduated eye-piece.

(3) Using a manually-operated curve-reader of the projection type, in which the operator sets the position of two cross-wires to the desired point on the curve. Operation of a foot-switch then causes the digital value of the ordinate to be printed out on paper tape.

(4) Using a curve-reader of the conducting-ink type, in which a servo-controlled conducting stylus tracks along the curve (previously traced over with conducting ink).

Digital read-out is commercially available with this equipment.

(5) Designing and developing some form of automatic curve-reader based on an optical reading system.

A careful investigation of the merits of these methods showed the advantage to lie overwhelmingly with the automatic curve-reader. As at the time, there were no commercial curve-readers of this type available, a curve reader was designed and developed for the purpose. The general concept, and the mechanical design of the curve-reader, was by the author. The electronic design, development and manufacture was carried out by the firm of Electronics, Instrument and Lighting Co.Pty., Ltd. The mechanical section of the machine was built, and developed, within the Department of Mechanical Engineering. This chapter describes the design, and operational features, of the curve-reader. This instrument has been in satisfactory operation since mid-1963. An improved version of this equipment is now available commercially from the above firm.

16.2 GENERAL DESCRIPTION

The automatic digital curve-reader has been designed to convert analogue records in the form of visible traces into corresponding digital ordinates, the trace being sampled at fixed sequential intervals along the abscissa.

During operation of the curve-reader a photo-electric reading head scans the recording paper, and as the "eye" passes over the ink trace the change in photocell output is used to trigger a circuit which interrogates a digitiser coupled to the scanning-mechanism. The output from the digitiser, which is a measure of the value of the ordinate at

the instant of interrogation, is recorded in an electronic memory. The memory is subsequently interrogated and the memory signals after conversion from digital to decimal form used to operate a printer.

The curve-reader can be preset to read a given number of ordinates up to 999, with a given spacing between each ordinate. A sequential serial number corresponding to each ordinate is also generated.

The output from the machine is, therefore, a strip of paper tape on which is printed the serial numbers of the successive ordinates and their corresponding numerical ordinate values.

The operation of the machine is shown schematically in Fig. 16.1.

16.3 THE MECHANICAL MOVEMENT

For the machine to read successive ordinates of a curve, the optical reading-head must have two modes of motion relative to the analogue records:-

(1) The "eye" of the head must move across the paper with the same motion which the tip of the recorder-pen had. For example, if the pen-tip moved in an arc around the pen-pivot, then the "eye" must move in an arc in exactly the same way.

(2) After each scan of the "eye" across the paper, the paper must move along its longitudinal axis by an amount equal to the required interval between ordinates.

In the curve-reader, the two modes of relative motion are obtained by two separate mechanisms.

The correct scanning motion is obtained by movement of the optical

Fig. 16.1 Simplified block diagram of automatic digital curve reader.

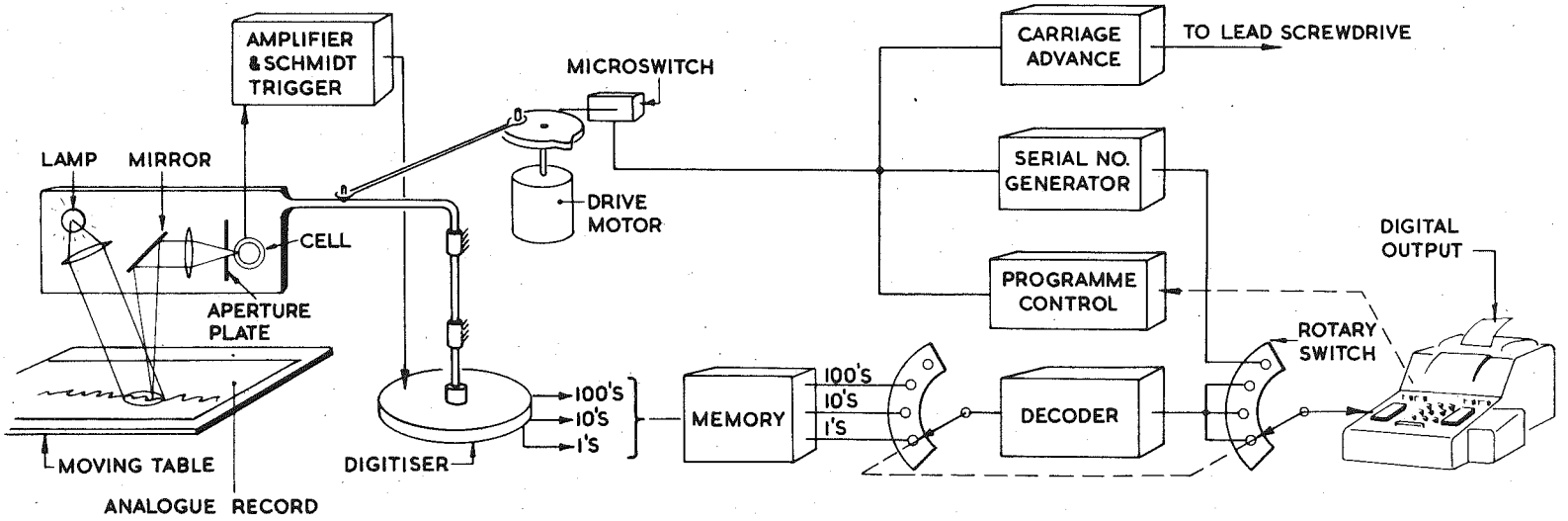
AMPLIFIER & SCHMIDT TRIGGER
MICROSWITCH
CARRIAGE ADVANCE
TO LEAD SCREWDRIVE
LAMP
MIRROR
CELL
DRIVE MOTOR
SERIAL NO. GENERATOR
DIGITAL OUTPUT
PROGRAMME CONTROL
APERTURE PLATE
ROTARY SWITCH
100'S
10'S
1'S
MEMORY
100'S
10'S
1'S
DECODER
MOVING TABLE
DIGITISER
ANALOGUE RECORD

reading-head across a stationary table. In the machine as originally constructed, the reading-head swings backwards and forth along a circular arc, whose radius can be varied as required. The head oscillates through an arc of 25 degrees, at a speed adjustable from 0 to 10 cycles per minute. The swinging arm on which the head is mounted, is driven by an adjustable link from an eccentric pin, the eccentricity of which can be varied. The pin shaft is driven by a geared electric motor. Attached to the swinging-arm shaft is a drum of 11.25 inches diameter. Phosphor-bronze strips 0.005 inch thick, transmit the angular motion of the drum, to a smaller drum of diameter 1.50 inches. Attached to the shaft of the small drum is the digitiser. The angular motion of the swinging arm is thus amplified by the ratio 11.25/1.50 i.e 7.5 to 1 in transmission to the digitiser. The angle of rotation of the digitiser is thus 188 degrees for a full scan of the reading head.

It should be noted that the setting of the reading-head arc at 25 degrees corresponds to the nominal setting. By altering the eccentricity of the eccentric-pin, it is possible to increase or decrease this arc. The angle of rotation of the digitiser will then correspondingly increase or decrease.

For records which were generated by a pen-tip or light beam moving rectilinearly to-and-fro across the paper, an alternative drive motion for the optical head is being constructed. The head is to be mounted on a carriage which will move to-and-fro across the paper on guide runners. Phosphor-bronze strips will connect the carriage to a small drive pulley mounted below the present large drum. The rectilineal

motion of the carriage will therefore be linked in a linear manner with the digitiser angular motion, a mechanical advantage will still be obtained.

Between scans, the relative movement of the reading-head in the longitudinal direction along the paper is obtained by movement of the table in this direction. The focal distance between the reading head and the paper is quite critical and hence it is necessary that the table movement takes place in the horizontal plane only. The table must therefore be mounted on slides which are parallel to the longitudinal axis of the paper, and which are also parallel to the plane of the paper. In the prototype, a lathe bed was used for the frame of the machine, the table being mounted on the saddle of the lathe. Movement of the table in the required ordinate steps was obtained by making use of the lead-screw mechanism of the lathe. A spur gear with an appropriate number of teeth was fitted to the lead-screw, and a stepping mechanism to operate on the gear was mounted adjacent. This mechanism when actuated by an electrical solenoid, rotates the gear through a distance of one tooth. This movement through the lead-screw, moves the carriage and table a distance of 0.005 inches.

Tyere are two distinct devices within the ordinate stepping mechanism, which performs successively the following functions:-

(1) The drive stroke of the solenoid first removes a lock from the gear, and then moves a ratchet-pawl to rotate the gear a distance of approximately one tooth.

(2) At the end of the drive stroke, the solenoid returns the lock into the gear to prevent any further major motion. On the

return stroke the solenoid rams a shaped-plunger into the space between two gear teeth, causing the gear to be moved precisely to the correct indexed position. On the control console, the number of solenoid operations to be carried out at the end of a given scan can be set at any number from 0 to 11. Since each solenoid operation corresponds to one ratchet step, and hence to a 0.005 inch movement of the table, it is possible to preset the interval between ordinates to be read from the curve, at any value from 0 to 0.055 inches, (in steps of 0.005 inches). This range could be further extended if required.

16.4 THE OPTICAL READING HEAD

The optical reading head is a standard scanning-head assembly from a MUIRHEAD type D901 picture transmitter. The unit as bought was completely assembled and adjusted, and had characteristics enabling its use without any modifications.

The head carries a light source which is projected as a small spot on to the chart paper. An image of a small circular area on the chart paper is, after reflection, focussed onto a diaphragm, behind which is a nine-stage photo-multiplier tube. The intensity of light falling on the photo-tube varies as the head moves across regions of different reflectivity on the paper, and causes fluctuations in the electrical output from the photo-cell. For example, as the image of a dark line on the paper passes over the diaphragm aperture, the output voltage shows a reduction in the otherwise steady output.

The electrical output from the photocell is connected to a Schmidt trigger circuit which determines the photocell illumination required to initiate the reading impulse. This reading pulse is fed through the digitiser to the memory. The trigger level can therefore be adjusted so that the reading impulse is generated at any given point as the "eye" crosses the ink line.

The resolution of the optical head is of the order of 200 lines per inch i.e. an effective resolution of 0.005 inches.

Because of the masking effect of the printed graph-background on the chart recording, a suitable coloured filter has been interposed in the optical path. The filter, of similar colour to the graph background, has resulted in an improvement in signal-to-background-noise ratio in the photo cell output. This ratio is now approximately 7 : 1.

16.5 THE DIGITISER

A mechanical digitiser (Type FD8) manufactured by Hilger and Watts Ltd., has been used. In this digitiser, the code disk has segmented areas of electrically conductive material (set into a matrix of insulating material), contact with which is established by metallic brushes.

The pattern of closed or open circuit established for the several contact paths through the digitiser, indicates the angular position of the code disk. Since the impulse applied to the memory via the digitiser is of short duration (20 m S), the state of the memory will effectively describe the position of the digitiser disk at the time of

the reading impulse.

The code used is the Watts reflected decimal code (Ref. 16.1) which produces minimum of complication in decoding to a decimal form, and furthermore has the advantage that only one element in the code changes for each digit change in the output numeral.

The digitiser has an output of 1000 equi-spaced coded numbers for 360° of disc rotation. For the nominal setting of the reading-head swinging-arm the relationship between digitiser numerals and scanning-head travel is 280 numerals for 30 mm movement of the "eye" over the recording paper (when the optical head is moving in on a 5 inch radius arc).

As the "eye" passes over the chart line a code pattern is established in the memory corresponding to the digitiser code pattern at the instant of interrogation. This pattern is then converted by a simple relay decoder to a decimal number code suitable for the printer.

Other forms of digitiser, for example, optical types using lamp sources and photo cells, were not considered for this application because of their higher cost.

16.6 THE MEMORY

The digitiser has twelve contact tracks arranged in three groups of four tracks. These groups of tracks correspond to the hundreds, the tens, and units of the number representing the digitiser position (Fig.16.2).

The electrical signals from the three groups of tracks at the instant of interrogation are fed directly to the memory. This consists of twelve (one for each track) solid-state bistable binary circuits, which, prior to the application of the read pulse are all set to the

Fig. 16.2 Contact scheme - Watts Reflected Decimal Code.

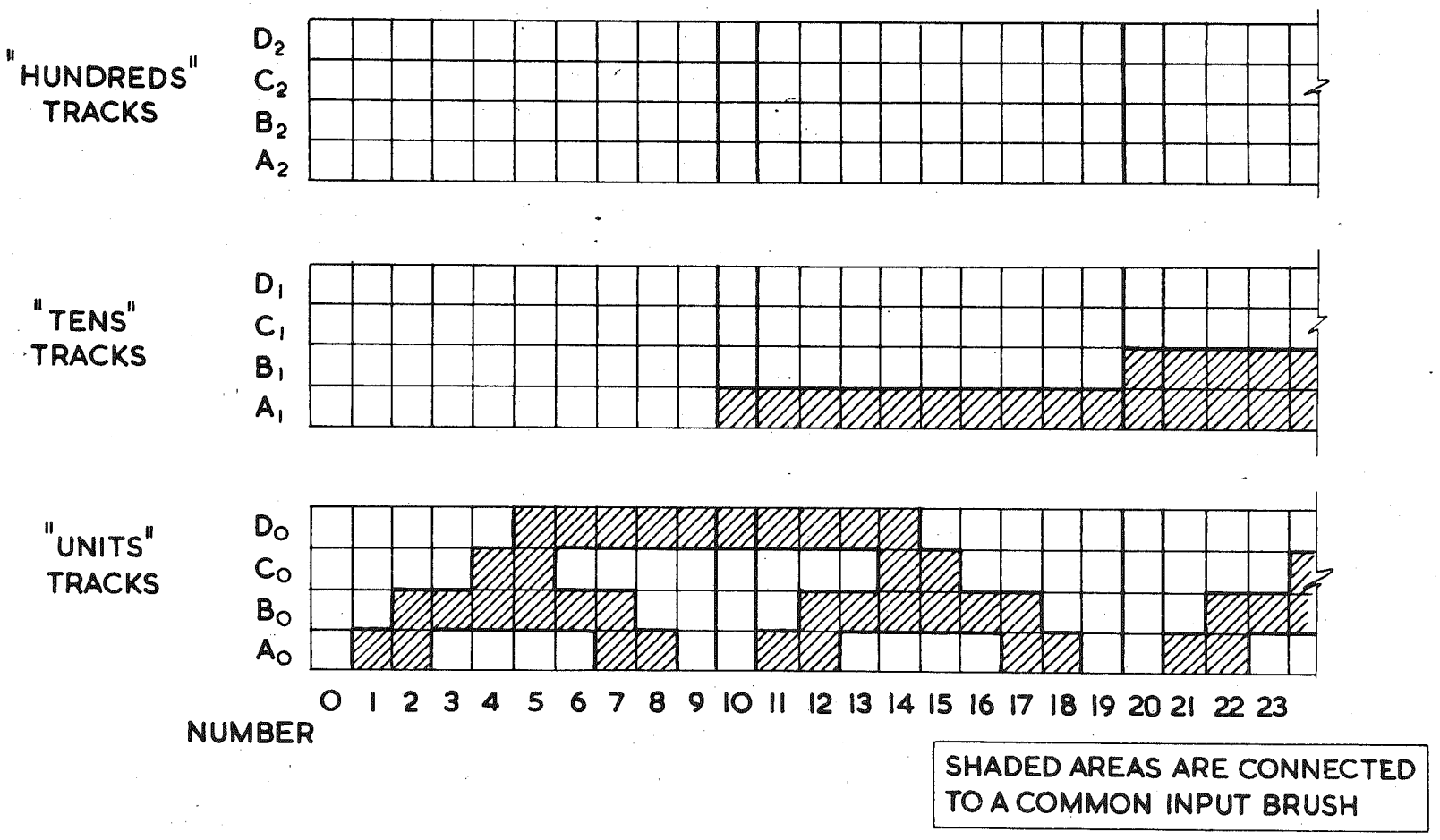
"HUNDREDS" TRACKS
D2
C2
B2
A2
"TENS" TRACKS
D1
C1
B1
A1
"UNITS" TRACKS
DO
CO
BO
AO
0 1 2 3 4 5 6 7 8 9 10 11 12 13 14 15 16 17 18 19 20 21 22 23
NUMBER
SHADED AREAS ARE CONNECTED TO A COMMON INPUT BRUSH

same state, e.g. left-hand side conducting.

The circuit diagram for each binary stage in the memory is shown in Fig. 16.3. Direct current at -12v is applied to a common bus "A" and also fed via a current-sensitive stage to a common bus "B". Thus, after reset, the current flowing into bus B will indicate whether any of the twelve memories have failed to take up their reset state; in this case the machine will be stopped automatically because faulty reset may result in the wrong value of an ordinate being obtained.

After the digitiser position has been read into the memory in a parallel fashion, the state of each binary is sampled by the decoder. The output from the decoder is then fed to the printer serially, and after the appropriate digit magnets have been set up in the printer, the programmer causes all the memory binary stages to be reset to their original state.

16.7 THE DECODER

It might appear that three decoders would be required to translate the signals from the three groups of digitiser tracks (Each group of four tracks represents a decade). It has been possible, however, to use a single decoder in this equipment, since the decades can be interrogated sequentially. Thus, after the decoder has interrogated the memory for the "hundreds" information and translated this to a decimal number and fed it to the printer, the decoder is reconnected to the remaining two groups of four stages in the memory successively, carrying out the same decoding function for the "tens" digit and again for the

Fig. 16.3 Circuit diagram of one element of the memory.

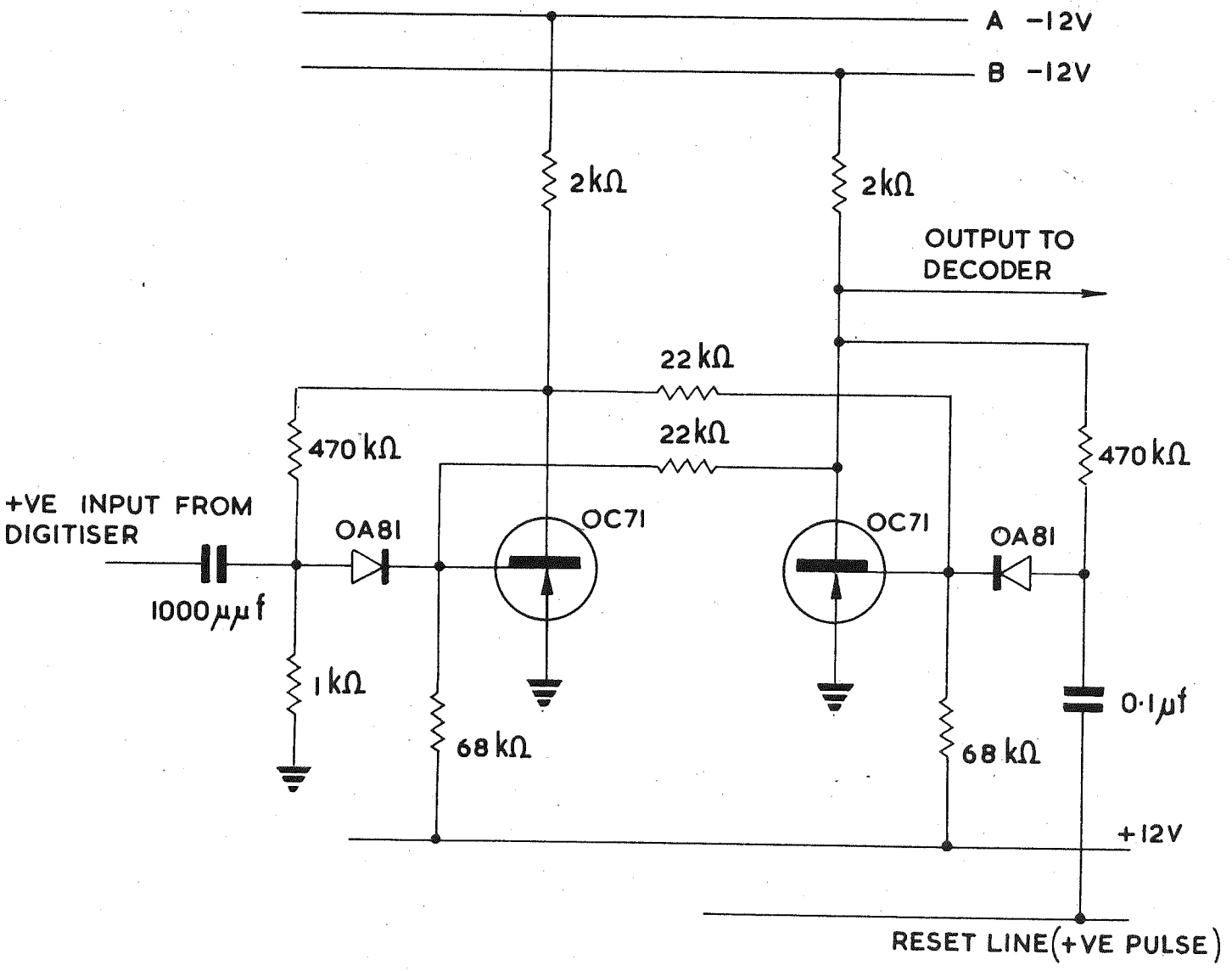
A -12V
B -12V
2kΩ
2kΩ
OUTPUT TO DECODER
22 kΩ
22kΩ
470 kΩ
470 kΩ
+VE INPUT FROM DIGITISER
OA81
OC71
OC71
OA81
1000μμf
1 kΩ
68 kΩ
68 kΩ
0·1μf
+12V
RESET LINE(+VE PULSE)

"units" digit. Carry-circuits are also provided, since to correctly decode the "tens" digit, information must be present to indicate whether the "hundreds" digit was an odd or an even number, and similarly for the "units" digit. This requirement derives from the character of the digitiser code. For example, reference to Fig. 16.2 shows that the "units" track arrangement for the numeral "6" is indistinguishable from "13" unless it is known whether the "tens" are even (when the number is 6) or odd (when it is 13).

The connection of the decoder to the appropriate memory binaries (and also the reading of serial-number generator), is performed by the programme control which uses a multibank post-office pattern stepping-switch ("uniselector").

The decoder arrangement is based on a "relay tree", the circuit for which is given in Fig. 16.4. In this figure, the small numbers against the decoding relay contacts represent the possible numbers which may form the output when the relay is in the position being considered. The "odd-function" output operates the inter-decade carry-relays G/1 and H/1 which determine whether a given number or its "reflexion" is to be recorded.

It can be shown that if the information contained in the "D" track is inverted, then instead of the number x being obtained, the number (9-x) is obtained instead. This inversion may be obtained by causing $\frac{E}{5}$ to operate when the $\frac{D}{1}$ relay does not, and vice versa. A switch is incorporated in the circuit so that the desired operating condition can be selected. This enables the instrument to be set to read numbers

Fig. 16.4 Memory decoding arrangement.

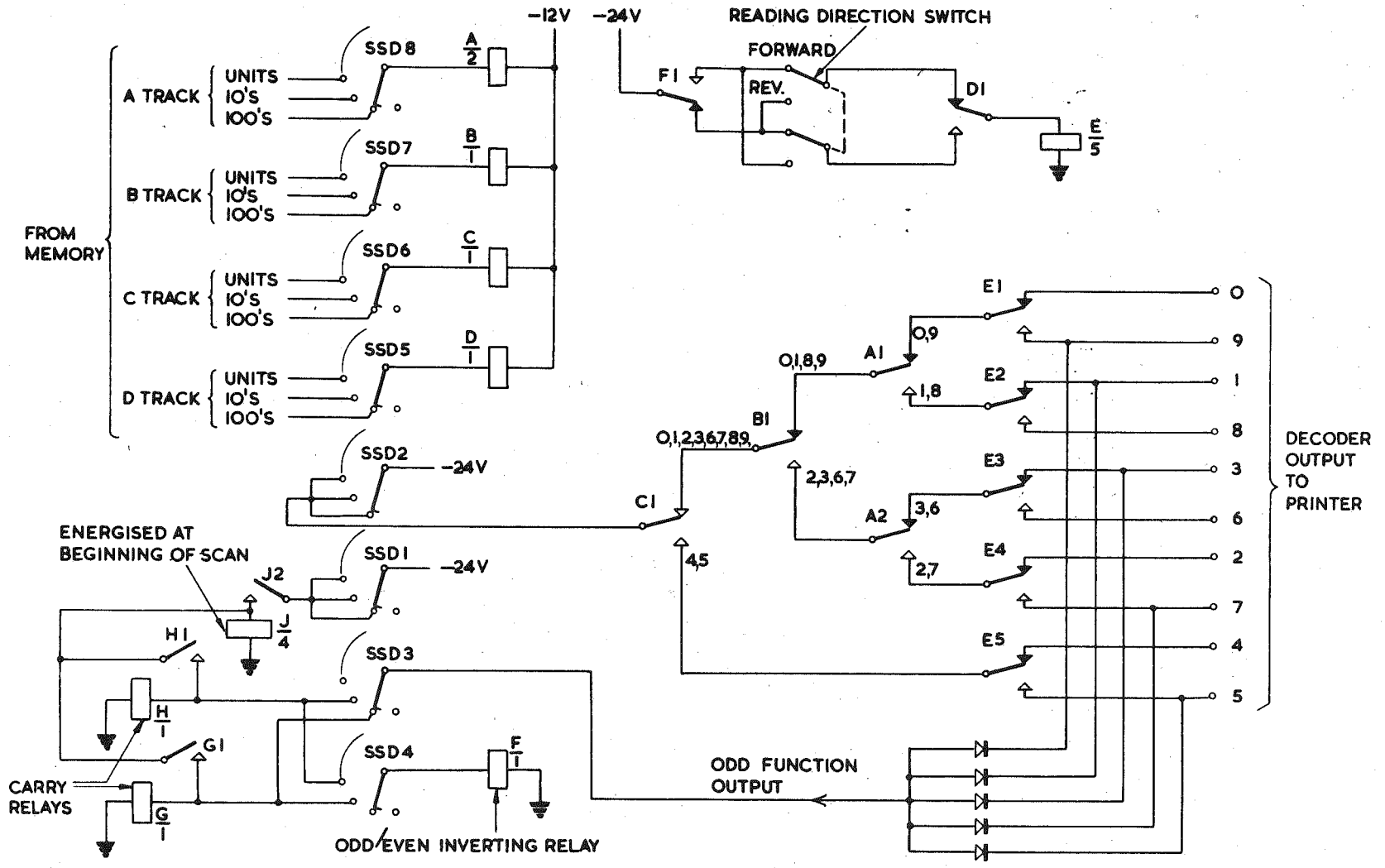
FROM MEMORY
A TRACK
B TRACK
C TRACK
D TRACK
UNITS
10'S
100'S
SSD8
SSD7
SSD6
SSD5
SSD2
SSD1
SSD3
SSD4
A/2
B/1
C/1
D/1
-12V
-24V
READING DIRECTION SWITCH
FORWARD
REV.
F1
D1
E/5
E1
E2
E3
E4
E5
0,9
1,8
2,3,6,7
3,6
2,7
4,5
0,1,8,9
0,1,2,3,6,7,8,9
A1
A2
B1
C1
DECODER OUTPUT TO PRINTER
0
9
1
8
3
6
2
7
4
5
ENERGISED AT BEGINNING OF SCAN
J2
J/4
H1
H/1
G1
G/1
CARRY RELAYS
F/1
ODD/EVEN INVERTING RELAY
ODD FUNCTION OUTPUT

increasing from 0 to 999 from a given chart datum, or alternatively, numbers decreasing from 999 to 0 from the same chart datum, i.e the apparent direction of rotation of the digitiser may be reversed at will, electrically. (see also Section 16.10).

16.8 THE SERIAL NUMBER GENERATOR

The sequential three-digit serial numbers for the ordinates are generated by three interconnected stepping switches, the first of these being actuated by a microswitch (Fig. 16.1) which is closed by a cam at the end of each scan of the reading head. The first stepping-switch moves one step with each scan. At the end of the tenth scan it thus moves into the tenth position, which transfers the supply voltage via the contacts of a slow-to-operate relay to the drive magnet of the second stepping switch, causing the latter to advance one step. (Fig.16.5).

The stepping switches advance in the manner described, with each successive scan until each stepping switch has reached the contact marked by the corresponding "preset" console switch. At this point, the configuration of the circuit is such that motion of the switches ceases. The "preset" switches thus determine the number of scans which will be made before the machine is automatically switched off. Further banks of stepping switches are connected to the printer digit-solenoids by the programme control switch to enable the serial number to be fed into the printer.

The microswitch (Fig. 16.1) is also used in the present installation to initiate the beginning of the memory-read, the memory reset, and the printing functions.

Fig. 16.5 Simplified circuit of serial number generator and preset stop.

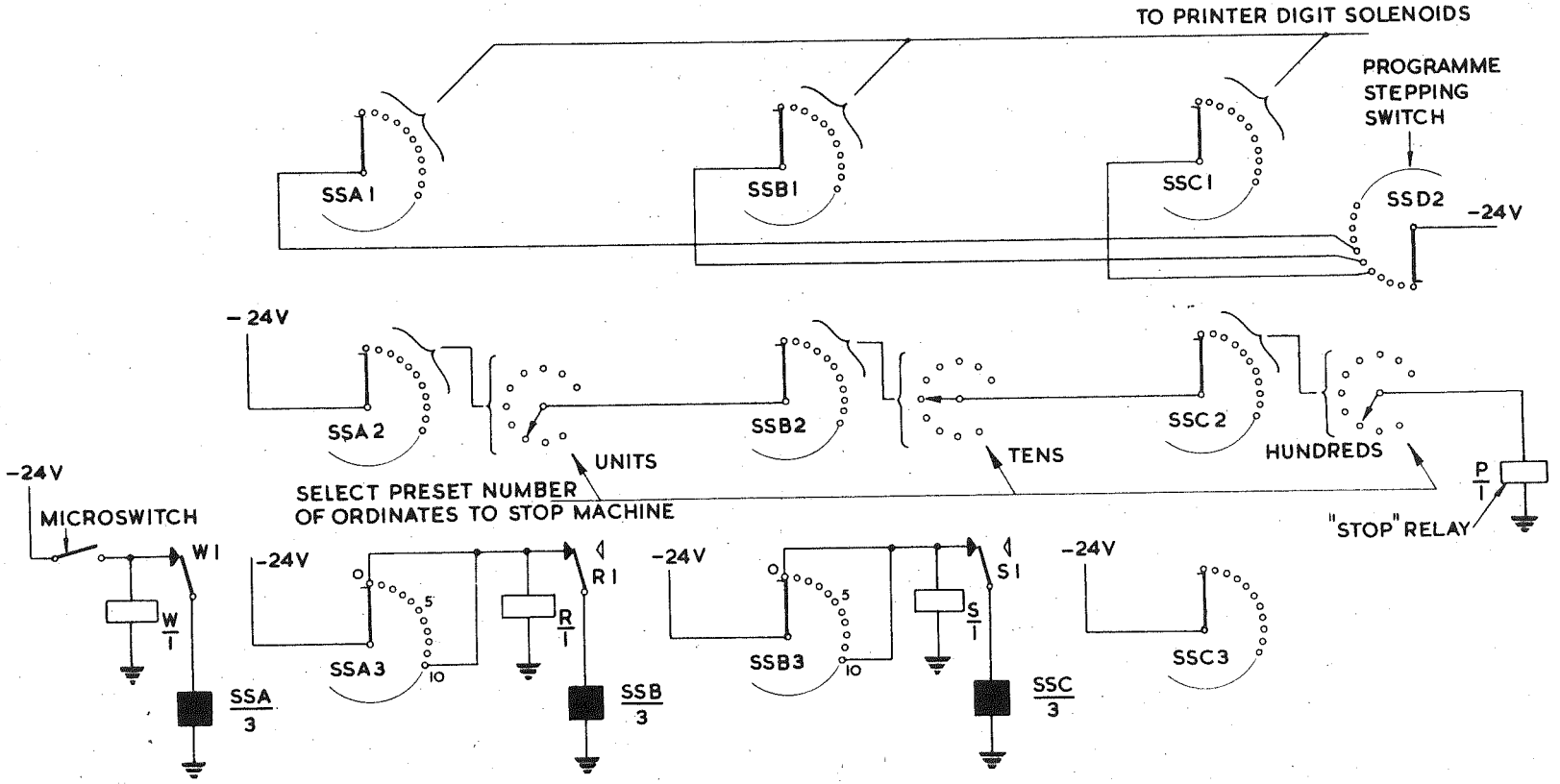
TO PRINTER DIGIT SOLENOIDS
PROGRAMME STEPPING SWITCH
SSA1
SSB1
SSC1
SSD2
-24V
-24V
SSA2
SSB2
SSC2
UNITS
TENS
HUNDREDS
SELECT PRESET NUMBER OF ORDINATES TO STOP MACHINE
P/1
"STOP" RELAY
-24V
MICROSWITCH
W1
W/1
SSA/3
-24V
SSA3
5
10
R1
R/1
SSB/3
-24V
SSB3
5
10
S1
S/1
SSC/3
-24V
SSC3

16.9 THE PRINTER

The printer is a standard model 41E-S-502 Addo-X machine which is used as a solenoid-driven listing machine. It can also be used as a manually-operated listing or adding-machine.

Provision is made on the printer for the attachment of a perforated paper-tape punch. It is intended to add this facility in the near future so that output from the machine in the form of perforated tape can be fed directly to the input of a digital computer without the present manual transcription from printer tape to punched cards.

The printer is used in a feedback circuit in conjunction with the programme stepping switch SSD (Fig. 16.6). This provides a convenient arrangement for sequencing the programme switch, and ensures that each digit is properly read into the machine, for, until the appropriate digit solenoid has reached the end of its travel, the feedback contact does not close initiating the transfer to the next digit.

At the end of scan, when the microswitch contact closes, relay $\frac{J}{4}$ is energised, and latches via X1 and J2, J1 closes, applying 24 volts D.C. to the drive magnet $\frac{SSD}{8}$ via the drive-magnet interrupter dmi, and the programme switch steps on one position. $\frac{M}{1}$ is now de-energised and M1 closes applying 24 volts D.C. via SSD2 and the decoder to one of the printer digit-solenoids. When the solenoid has reached the end of its travel the digit-feedback-contact in the printer closes, applying 24 volts D.C. to $\frac{SSD}{8}$ and to $\frac{M}{1}$ via X2. The drive-magnet attracts the armature of the stepping switch which, however, does not yet advance. M1 then opens removing 24 volts from the printer digit-solenoid resulting

Fig. 16.6 Simplified circuit of programme control.

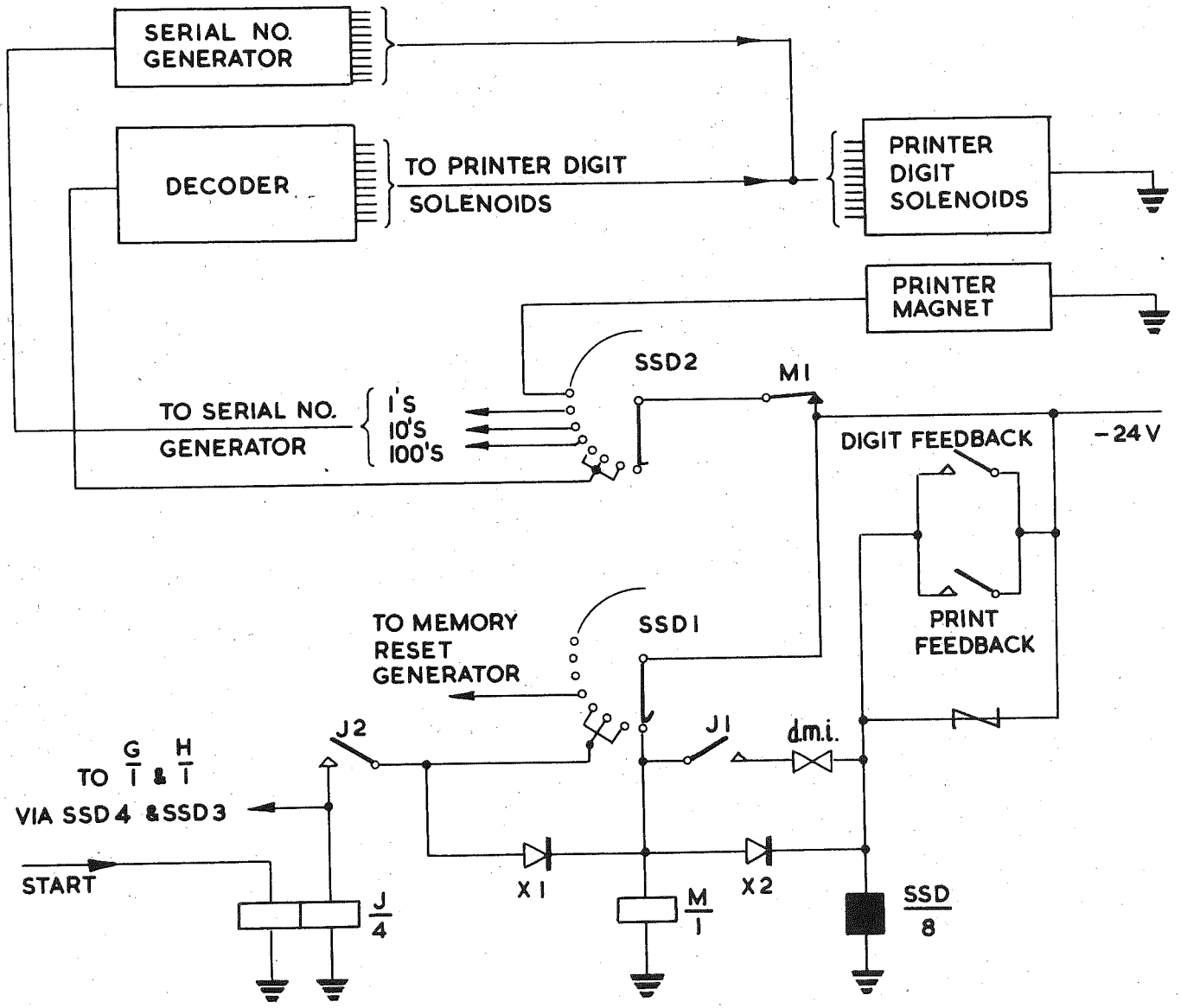
SERIAL NO. GENERATOR
DECODER
TO PRINTER DIGIT SOLENOIDS
PRINTER DIGIT SOLENOIDS
PRINTER MAGNET
SSD2
M1
TO SERIAL NO. GENERATOR
1'S
10'S
100'S
DIGIT FEEDBACK
-24 V
PRINT FEEDBACK
TO MEMORY RESET GENERATOR
SSD1
J2
J1
d.m.i.
TO G/1 & H/1
VIA SSD4 &SSD3
START
X1
X2
J/4
M/1
SSD/8

in the opening of the digit-feedback-contact, and hence de-energisation of the stepping switch drive-magnet. The stepping switch now advances one position, and the sequence repeats, until the print function is called for. After the print function is completed the stepping switch moves to the home position ready for the next operation.

16.10 THE CHARACTERISTICS OF THE CURVE READER

The curve-reader will read ordinate-values at a nominal rate of 10 per minute, the interval between ordinates being adjustable from 0.005 to 0.055 inches, in steps of 0.005 inch. The number of ordinates to be read can be preset at any number from 0 to 999. Because the digitiser code is of the reflected type, the inversion of one of the relays in the decoder tree by means of an inverting switch on the console causes the decoder to transmit the "reflexion" of the decimal number which would otherwise have been transmitted to the printer. This has the effect of reflecting the datum from which the curve ordinates are read, from one side of the curve to the other. The reader incorporates a multiple curve reading facility, so that where several lines are traced on the recorder paper the reader can be set to successively "read" these lines and print the ordinate value of each as the optical head scans across the paper.

The original specification of the curve-reader required the reading accuracy and reading speed to be at least equal to that which could be obtained manually using dividers and a ruler.

In its present configuration, the curve reader will read an ink trace with an accuracy of $\pm$ 0.007 inch (on a 45° line) at the rate of 10 ordinates per minute. With further development, the reading rate could be doubled or even trebled. Its performance is thus well within the original specification.

CHAPTER 17

THE DIGITAL COMPUTER PROGRAMMES FOR THE ANALYSIS OF RESULTS- (FORCED VIBRATION)

17.1 INTRODUCTION

The data obtained from the full-scale tests on the ore-carriers during both sea trials and the voyage was obtained primarily in analogue form as ink-on-paper traces from an eight-channel recorder. In addition, a considerable amount of supplementary data was recorded manually, in numerical form. The relevant calibrations which had been carried out both in the laboratory and in the field were recorded in the form of tabulated data as well as in the form of graphs. Since it was desired to have harmonic analyses made of the torque and thrust fluctuations recorded on chart paper by the eight-channel recorder, it was necessary that these records (or sections of them) to be converted into digital form. It was desirable that as much of the available data as possible be processed, since it was expected that considerable scatter would be obtained in the results due to unsteady ship motion and other factors which were outside the control of the experiment. (There was, however, a large amount of data available - almost 3 miles of eight-channel paper records !). If sufficient data was analysed, it could be expected (on a statistical basis) that reasonably reliable information could be obtained from the results of the harmonic analysis. It was obvious that to process this large amount of information, a digital computer programme (or series of programmes) would be required.

It also became apparent that in order to obtain the digital ordinates from the analogue records some automatic form of curve reader would need to be developed.

The automatic digital curve reader (described in Chapter 16) was developed and manufactured. This machine was used to obtain some 35,000 digital ordinates from sections of the analogue records. These digital values were then processed by the various computer programmes as indicated in Fig. 17.1. This figure shows the flow sheet for the analyses. Further details on the various analyses are given in the following sections.

As a matter of interest, the following figures are given, which show that the analysis of the data involved considerable effort, even with the aid of digital computers:-

Computers used	:-	IBM 1620 and IBM 7090
Total operating time on IBM 1620	:-	40 hours
Total operating time on IBM 7090	:-	15 minutes
IBM punched cards used	:-	20,000

(The total number of calculations involved can be gauged from the following. When using floating-point numbers the 1620 can perform approximately 40 multiplications or 50 additions per second, whereas the 7090 can carry out approximately 30,000 multiplications or 60,000 additions per second.

During the preliminary analysis of the trials data before the curve reader had been developed to a satisfactory stage, and before the digital computer programmes were ready, values of peak-to-peak fluctuations of torque and thrust were taken from the analogue records manually. These values were tabulated and then plotted graphically in various forms.

Fig. 17.1 Flow sheet for analysis of data
(forced vibrations)

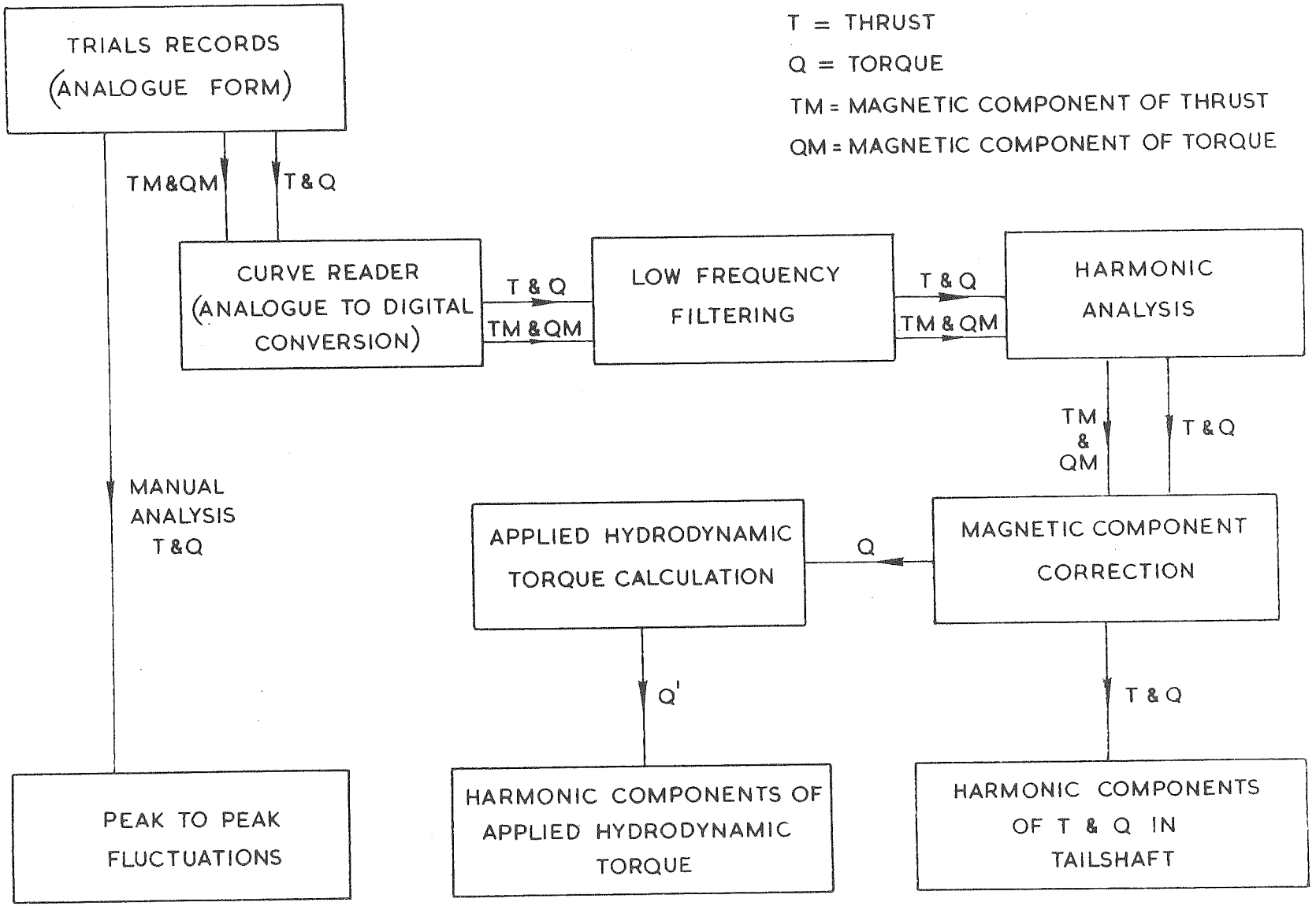
T = THRUST
Q = TORQUE
TM = MAGNETIC COMPONENT OF THRUST
QM = MAGNETIC COMPONENT OF TORQUE
TRIALS RECORDS (ANALOGUE FORM)
TM&QM
T&Q
CURVE READER (ANALOGUE TO DIGITAL CONVERSION)
T & Q
TM & QM
LOW FREQUENCY FILTERING
T & Q
TM & QM
HARMONIC ANALYSIS
TM & QM
T & Q
MANUAL ANALYSIS T&Q
APPLIED HYDRODYNAMIC TORQUE CALCULATION
Q
MAGNETIC COMPONENT CORRECTION
Q'
T & Q
PEAK TO PEAK FLUCTUATIONS
HARMONIC COMPONENTS OF APPLIED HYDRODYNAMIC TORQUE
HARMONIC COMPONENTS OF T & Q IN TAILSHAFT

17.2 THE ANALOGUE TO DIGITAL CONVERSION

The automatic digital curve reader (See Chapter 16) was manufactured and developed to rapidly convert an analogue record to a corresponding series of digital ordinates (at given spacing between the ordinates). Under normal conditions the rate of conversion was found to be 10 digital ordinates per minute. Setting up time, however, reduced this output somewhat. The output from the curve reader consisted of a paper tape on which the digital values of the successive ordinates was successively printed, together with the ordinate numbers. The number of digital ordinate values obtained from each section of record analysed varied between 200 and 700. These values were punched directly onto IBM computer cards from the curve reader output tapes. A header card, punched for each set of data, gave information such as run number, ship velocity, water depth, rpm, data intervals per shaft revolution, mean thrust, mean torque, The scaling factors relating digital-values to corresponding torque or thrust values (in ton-ft or tons) were also given on these header cards.

17.3 THE LOW-FREQUENCY FILTERING AND DATA PRECONDITIONING

Before any Fourier harmonic analysis (of the infinite harmonic series type) can be made, the Dirichlet conditions must be first satisfied. These conditions are as follows:-

(1) The function $f(x)$ to be analysed must be periodic. This means that the function must satisfy the following equation:-

$$f(x) = f(x + p) \qquad (17.1)$$

where p is the period. This condition implies that not only is the function established as periodic, but further that the period is known for the particular set of data being considered.

(2) There must be a finite number of maxima and minima.

(3) There must exist only ordinary bounded discontinuities and the number of these must be finite. Further, the function must be sectionally continuous.

The second and third Dirichlet conditions are usually satisfied in engineering problems. The first Dirichlet condition, that the function must be periodic, is often not perfectly satisfied, because of some random effect outside the control of the experiment. In the present case, the data (torque and thrust records from the ship tests) was not perfectly periodic. Therefore, before a harmonic analysis could be carried out the data had to be adjusted so as to be periodic over a given section of the record.

The data as obtained from the tests showed the following very important features:

(1) A high periodic correlation was evident. It was also evident that the periodicity was marred by the ship's motion not being perfectly steady and by the sea not being perfectly smooth. It may be deduced that under the theoretical condition of steady ship motion and perfectly smooth water, records of torque and thrust variation would be perfectly periodic. Any variation from these ideal conditions would be reflected by some degree of non-periodicity in the torque and thrust records. Since the smooth-sea, steady-motion conditions were taken as reference

conditions, it was regarded as legitimate to remove those components in the records which were associated with unsteady ship motion and random sea conditions.

(2) The records show evidence of very-low-frequency components relative to the significant components (See Fig. 17.2). These low-frequency components have the effect of swinging the "smooth-water steady-motion" record from side to side along the graph without significantly modulating the amplitudes of the significant components. It will be noted that these very-low-frequency components have frequencies which are several orders lower than any significant component associated with the reference condition. It was noted during the ship tests that the very-low-frequency components were due to the unsteady motion of the ship, in conjunction with wave motion. The peaks in the "swings" of the record were observed to coincide with the extreme positions of the vertical motion of the stern of the ship. If the very-low-frequency components are to be removed from the records, it is clear that a technique which is equivalent to a low frequency filtering must be used. (The technique which was developed to carry out this function is described in detail in the following sections)

(3) The records show evidence of very-high-frequency components associated with intermittent transient conditions. These also have the effect of making the wave-form slightly non-periodic. These components are again associated with unsteady ship motion and varying seaway conditions. To remove these components,

Fig. 17.2(a) Typical section of 8 - channel recorder chart from ship tests (The marker pens A,B,C, between the channels were used for coded event marks).

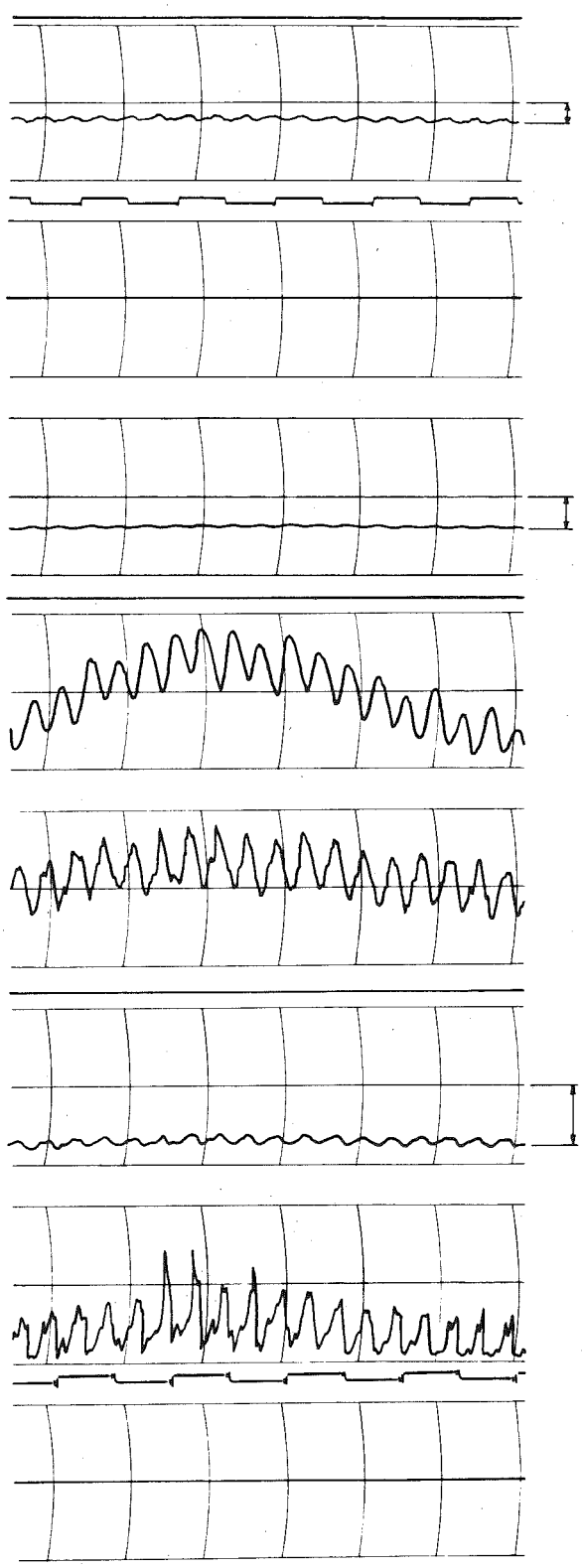

RUN 0103

102·5 R.P.M.

Fig. 17.2(b) Sections of torque and thrust waveforms from the 8 - channel recorder charts, showing the effect of shaft speed on the shape of the waveforms for Test Series B1. (The rpm shown are nominal values).

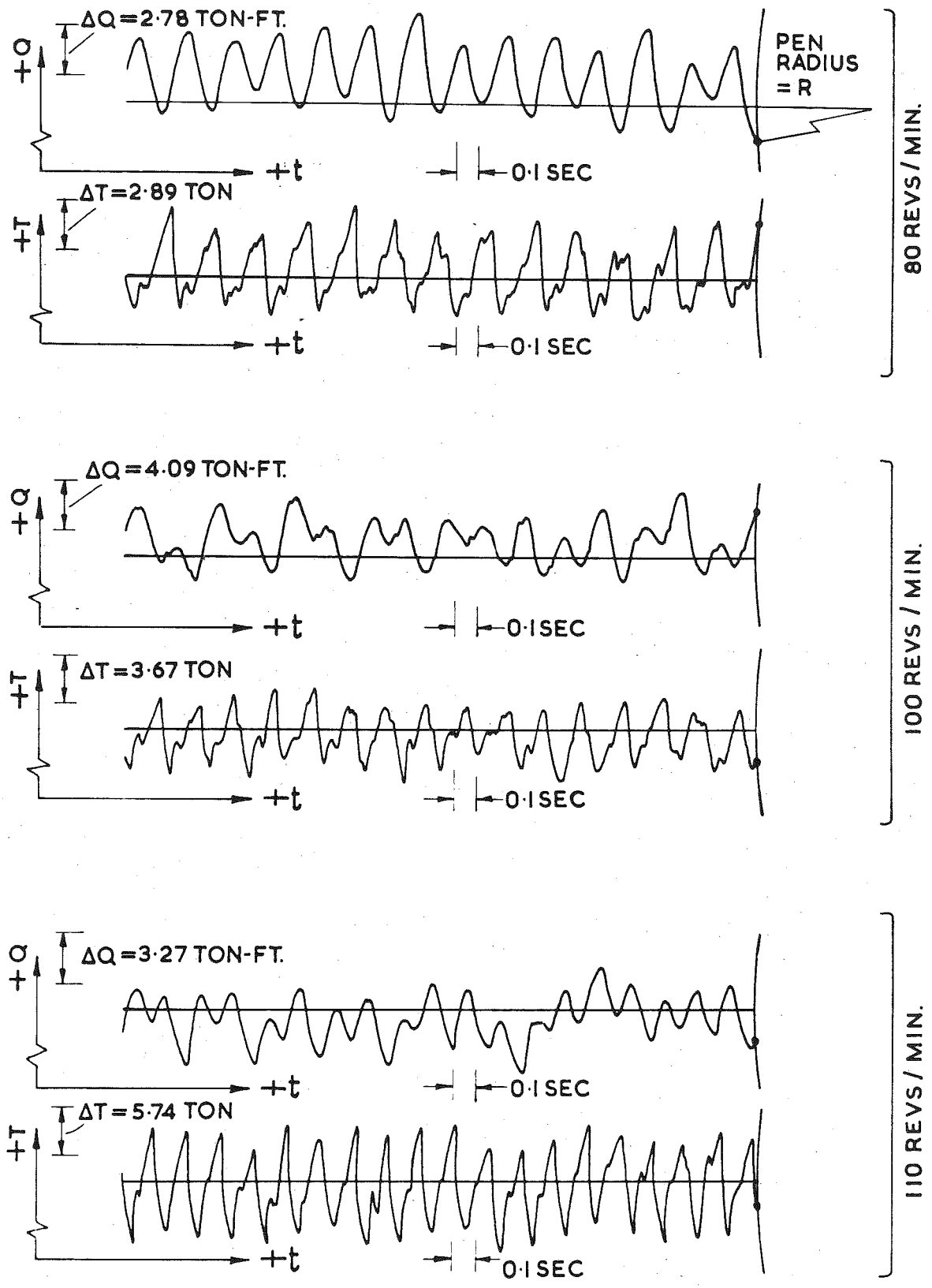
ΔQ=2·78 TON-FT.
+Q
PEN RADIUS = R
+t
0·1 SEC
ΔT=2·89 TON
+T
+t
0·1 SEC
80 REVS / MIN.
ΔQ=4·09 TON-FT.
+Q
+t
0·1 SEC
ΔT=3·67 TON
+T
+t
0·1 SEC
100 REVS / MIN.
ΔQ=3·27 TON-FT.
+Q
+t
0·1 SEC
ΔT=5·74 TON
+T
+t
0·1 SEC
110 REVS / MIN.

some form of high frequency filtering would appear to be required. It was not in fact necessary, however, to carry out such a filtering, since the frequencies of these components were mainly above the frequency of the highest harmonic for which the harmonic analysis was carried out. In effect, the harmonic analysis acted as its own high-frequency filter.

(4) The records show four cycles of the most significant component within each basic period. The basic period, under ideal conditions would be equal to the time taken for the shaft to rotate once. That the most significant component of the wave-form has a frequency equal to four times shaft rotation frequency is only to be expected, since the propeller is four-bladed. It is well known that the most significant component of such a wave-form has a frequency equal to blade frequency (defined as number of blades times frequency of shaft rotation). The basic frequency for the wave-form in the present case, however, must be taken as equal to the frequency of the shaft rotation, as components of this order may be present due to the fact that each blade may not be hydrodynamically identical, or to some other cause.

In the electronic field, the very-low-frequency components evident in the present records would be described as "low-frequency drift" or as "experimental drift". For convenience, this terminology is used in the following sections. The process by which the very-low-frequency components are removed is described therefore as "low-frequency filtering". This process formed part of the "data pre-conditioning"

stage of the analysis.

17.4 THE DATA PRECONDITIONING PROGRAMME

In the data preconditioning programme (See Fig. 17.1) two distinct processes are carried out:

(1) A new set of ordinates are established by interpolation such that the period"p" is divided into an even number of data intervals. This is to allow subsequent integration by Simpson's rule.

(2) The very low-frequency drift is established as a "drift function" represented by a polynomial over the section of the data being considered, and is subtracted from the data to obtain a closer approximation to the "steady-ship smooth-sea" conditions. The establishing of the drift function and its subtraction is carried out in such a way that the corrected wave-form satisfies the Dirichlet conditions.

The mathematical analysis used in the programme is based on the following two assumptions:

(1) The "drift" can be represented sectionally by a second-order polynomial function of the form

$$f(x) = a + bx + cx^2 \qquad (17.2)$$

(2) It is much more important that the final function derived by subtracting the drift function from the source function should satisfy the Dirichlet conditions, than it is that the

drift function should satisfy a least-square-fit to the source function. This means that the drift function is established as a mean line by integration under the source curve rather than by a least-square method (See Fig.17.3)

The criteria which were chosen to establish the drift function were therefore:

(1) That the drift function should be of the form

$$f(x) = a + bx + cx^2 \tag{17.3}$$

(2) That the ordinates of the source function F(x) relative to the ordinates of the drift function f(x) should be such that

$$[F(x) - f(x)]_B \equiv [F(x) - f(x)]_C \tag{17.4}$$

This condition was chosen so that the first Dirichlet condition would be satisfied.

(3) That the following two integral conditions which define the drift function as a mean line, should be satisfied

$$\int_A^D F(x).dx = \int_A^D f(x).dx \tag{17.5}$$

$$\int_B^C F(x).dx = \int_B^C f(x).dx \tag{17.6}$$

Fig. 17.3 The relationship of the drift function to the source waveform.

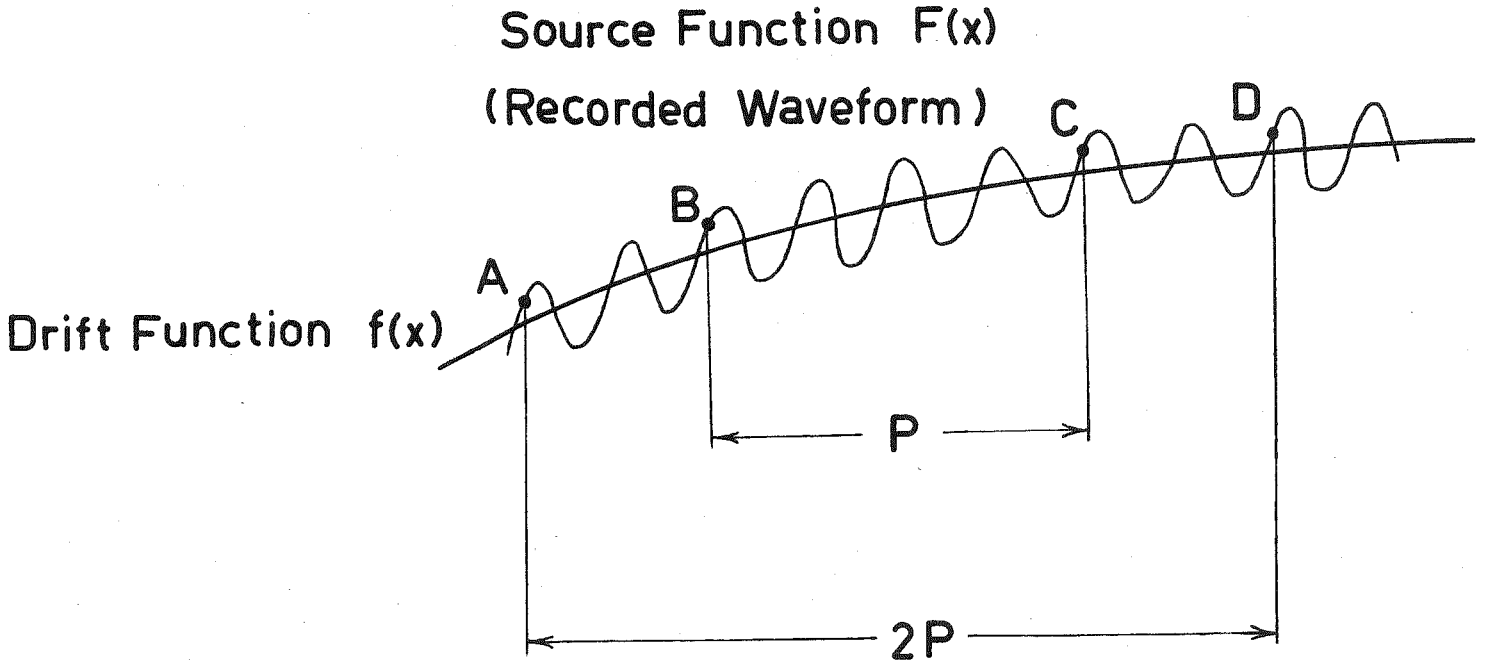
Source Function F(x)
(Recorded Waveform)
A
B
C
D
Drift Function f(x)
P
2P

It will be noted that the integration defined by equation 17.5 is over a length equal to twice the period. (Also refer to Fig.17.3). In the subsequent harmonic analysis only the data within the inner period BC is used. The reason for using in the data preconditioning an additional half-period at each end of the inner period, is that the establishment of a mean line by an integration condition can under certain conditions be in error at the extreme ends of the length over which the integration has been taken. Over the middle region of the integrational length, however, the mean line is always correctly established. By considering a double period over which the mean line is established and then by only using the middle period within this length, any erroneous sections at the extreme ends of the double period length become discarded and not used in the subsequent analysis.

The reason why the integration conditions in equations 17.5 and 17.6 are taken over a double period and a single period, respectively, instead of over fractional sections of a period is as follows. In a complex periodic waveform, the period is the only length over which each component of the waveform (including the fundamental component) has at the end points of the length the same ordinate values. For each component, therefore, the areas above and below the mid-amplitude line are equal, over the length of the period. (The mid-amplitude line is the line mid-way between the peaks of the curve). Thus for the complex waveform formed by the summation of components in such a way that their mid-amplitude lines are coincident, the areas above and below the mid-amplitude line must be equal, over the length of a period. The mean line as determined by integration will therefore be identical with this

mid-amplitude line. The same property also holds ,if lengths equal to integer multiples of the period are considered. If a feactional length of a period, however, is considered, the mean line obtained by integration will lie on one side of the mid-amplitude line, its exact position depending on the length chosen.

The criteria above are sufficient to establish the drift line exactly if :

(1) The drift is actually of the form of a second-order polynomial function

(2) If the corrected waveform (equal to the source function F(x) minus the drift function f(x))is exactly periodic.

If the drift function is not exactly a second-order polynomial and/or if the corrected waveform is not exactly periodic, then some error will be introduced. In the present case, it was considered that a second-order polynomial would be a close approximation to the drift function over the length considered,in the later stages of the analysis (a single period). The corrected waveform would only vary from being exactly periodic because of the transient very-high-frequency components which occur intermittently. Over the single period being considered, however, the corrected waveform could nevertheless be assumed to be sectionally periodic. Thus, in the present case the error introduced in the determination of the drift line would be of a small order. Outweighing the disadvantage of this small introduced error is the advantage that the corrected waveform will now satisfy the Dirichlet conditions, and can thus be validly harmonically analysed.

The computer programme is divided into the following stages:

(1) From the original equi-spaced curve ordinates, a new set of equi-spaced ordinates is established by interpolation (second order Bessel), such that the period p is divided into an even number of data intervals. A data interval is the distance between two successive ordinates. In the new set of ordinates, the first ordinate will therefore occur at the beginning of the period and the last ordinate will occur at the end of the period. The remainder of the ordinates will be equi-spaced along the period. Since there are an even number of data intervals, there will be an odd number (equal to the number of data intervals plus one) of ordinates within the period. The reason for establishing the period p as an even number of data intervals, is to obtain a data condition in which Simpson's integration rule may be validly and simply applied.

(2) The drift function coefficients a,b,c, are established by satisfying the three criteria discussed above. The integrations necessary to satisfy equations 17.5 and 17.6 are carried out by using Simpson's rule.

(3) The ordinates for the drift line are calculated and are subtracted from the ordinates for the source data. The resultant set of data points form the data set for the function $f'(x)$ defined by the relation

$$f'(x) = F(x) - f(x) \qquad (17.7)$$

This stage of the calculation, it will be seen, is equivalent to a filtering out of the very-low-frequency components from the data.

17.5 THE HARMONIC ANALYSIS PROGRAMME

The data set obtained for the corrected waveform $f'(x)$ is used as input for the programme which carries out the harmonic analysis. This analysis is of the Fourier infinite harmonic series type. The Fourier series is assumed to be of the form

$$f'(x) = \frac{1}{2}a_o + a_1 \cos\frac{2\pi x}{p} + a_2 \cos\frac{4\pi x}{p} + \text{----}$$

$$+ \frac{1}{2}b_o + b_1 \text{Sin}\frac{2\pi x}{p} + b_2 \text{Sin}\frac{4\pi x}{p} + \text{----} \qquad (17.8)$$

It is shown in standard texts on waveform analysis (See for example Ref.17.1) that the coefficients for such a series are given by the following equations:-

$$a_n = \frac{2}{p} \int_0^p f'(x).\cos\frac{2n\pi x}{p}.dx \qquad (17.9)$$

$$b_n = \frac{2}{p} \int_0^p f'(x).\text{Sin}\frac{2n\pi x}{p}.dx \qquad (17.10)$$

It should be noted that the coefficient b_0 is always 0.

From the data set for the function $f'(x)$ the coefficients for the above Fourier series are determined in the programme, the integrations being performed using an extended form of Simpson's rule. This is, in effect, a repeated application of the basic form of Simpson's rule which is

$$A = \frac{h}{3}\left(y_{n-1} + y_n + y_{n+1} \right) \qquad (17.11)$$

where A is the summation area and h is the distance between any two adjacent ordinates.

Simpson's rule was chosen for the integrations, for the following reasons:

(1) The accuracy obtainable in the present case with its use was more than sufficient

(2) It may be deduced from Ref. 17.2 using the table showing the relative accuracy of various processes, that Simpson's rule gives the highest accuracy yield per unit of computing effort of any integration process.

From the coefficients a_n and b_n are calculated at the last stage of the programme the coefficients of the alternative form of the Fourier series

$$f'(x) = \frac{1}{2}c_o + c_1\cos\left(\frac{2\pi x}{p} - \phi_1\right) + c_2\cos\left(\frac{4\pi x}{p} - \phi_2\right) + \cdots \qquad (17.12)$$

where $$c_n = \sqrt{a_n^2 + b_n^2} \qquad (17.13)$$

$$\cos^{-1}\phi_n = \frac{a_n}{\sqrt{a_n^2 + b_n^2}} \qquad (17.14)$$

$$\mathrm{Sin}^{-1}\phi_n = \frac{b_n}{\sqrt{a_n^2 + b_n^2}} \qquad (17.15)$$

The putput from this programme was in card form, in a format suitable for use as input to the next programme.

17.6 THE MAGNETIC COMPONENT CORRECTION PROGRAMME

At a certain stage of the voyage the ship passed through a magnetic field sufficiently intense to create a semi-permanent magnetic field within the engine room. This field caused induced voltages to be generated in the lead wires from the strain-gauges on the tail-shaft. The magnitude of these was large enough to cause appreciable error unless corrected for. Records of the induced voltage due to the magnetic effect were made at intervals during the voyage by switching off the power to the strain-gauges. Under these conditions the only alternating current output from the equipment on the tail shaft was that due to the magnetic effect. Following most of the test runs in this section of the voyage the strain-gauge power was switched off and the magnetic effect recorded. These analogue recordings of the magnetic effect were later onverted by the curve reader to corresponding digital values.

For each of the records taken from these test runs there was therefore a corresponding section of magnetic-effect record. Care

had been taken to ensure that the two sections of record were in the correct phase relationship to another. This was done by taking the first ordinate in each section at the top-dead-centre position of the reference propeller blade.

A digital computer programme was written which subtracted the Fourier coefficients of the magnetic-effect record from the Fourier coefficients of each corresponding test run (See Fig. 17.1). The output from this stage of the analysis was punched on cards in a format suitable for use as input to the next stage.

Those test runs in which there was no magnetic effect to be corrected for were not processed through this stage but bypassed it. This was carried out by writing the programme in such a way, that when the computer came to such a test set of data, it did not carry out a magnetic correction but simply punched a corresponding output set of data.

17.7 THE APPLIED HYDRODYNAMIC FORCE PROGRAMME

The corrected amplitudes and phase angles of the various frequency components of the complex waveform $f'(x)$ formed the output from the previous computing stage. Since the initial source data (see sections 17.1 and 17.2) was obtained from either torque or thrust waveform records, the subsequent processed data also refers to torque or thrust (in the tail shaft). It is shown later that although information on the torque and thrust waveform components in the tail shaft is of value, this data is only applicable to a particular ship tested. It is much more useful for test results to be presented in terms of the hydrodynamic forces applied to the propeller. If sufficient data is obtained in

this form for sufficient number of ships, a correlation between the applied hydrodynamic forces and the major shape parameters of the ship and propeller should become possible.

In the present case, therefore, the calculation of the applied hydrodynamic forces was attempted. In the case of torque, it was possible to compute with some confidence the applied hydrodynamic torque corresponding to the torque waveform in the tail-shaft, since the dynamic parameters of the system, including the damping, were either known or could be estimated to a reasonable degree of accuracy. In the thrust case, however, it was initially felt that some of the dynamic parameters were not known sufficiently accurately for a reasonable estimation of the applied hydrodynamic thrust to be made. Measurements were nevertheless made during the tests in an effort to determine some of these parameters particularly the thrust block flexibility. The stiffness of the thrust block was found from these tests to be about 14.1×10^7 lbf/ft. The total mass involved in axial vibration (including an allowance on the propeller mass of 50% for entrained water) was estimated as 43 ton. The frequency for the first mode of axial vibration (of the propulsion system on the thrust block) was calculated from these figures as just over 2,000 cycle/min. The frequency of axial vibration of the propeller against the stiffness of that section of shaft between the propeller and the gauge-location is estimated to be many times greater than 2000 cpm. Under these conditions, therefore, the instantaneous thrust force as measured in the shaft at the gauge-location will be equal to the instantaneous applied hydrodynamic thrust on the propeller, to a high degree of accuracy. Thus the measured

tailshaft thrust may be taken as equal to the applied hydrodynamic thrust, no further calculation being in fact necessary.

The propulsion system of the ore-carrier is shown diagrammatically in Fig. 17.4. It consists of a multiple-branch system having four branches with two inertias in each branch. Damping is assumed to be negligible except at the propeller. A discussion of the various types of damping which occur in a ship shaft-system of this type is given in Ref. 17.3. It may be seen from the discussion in this reference that in a typical turbine propulsion system, the propeller damping term is the only significant damping term in the system.

An analysis of this system was carried out for a forcing function $f''(x)$ representing the applied hydrodynamic torque function applied to the propeller. The analysis was derived using the mobility method for the solution of forced vibrations (Ref. 17.4). (The schematic diagram of the propulsion system for this analysis is shown in Fig.17.5) The corresponding computation in the programme was carried out for each harmonic component of the forcing function in turn. The form of each forcing component was assumed to be T'' sin ωt. The form of the corresponding torque variation in the tailshaft, caused by this forcing component, was assumed to be $T \sin(\omega t + \phi)$. T'' and T are thus the amplitudes of the harmonic torque components, for the applied hydrodynamic torque and the torque in the tail-shaft respectively. The angle ϕ is the phase angle between the forcing torque and the torque in the tail shaft. The programme first calculates the ratio $\frac{T''}{T}$ and the corresponding angle ϕ, at the appropriate frequency ω, for each of the components of the torque waveform in the tail-shaft

Fig. 17.4 Diagrammatic arrangement of ore-carrier propulsion system.

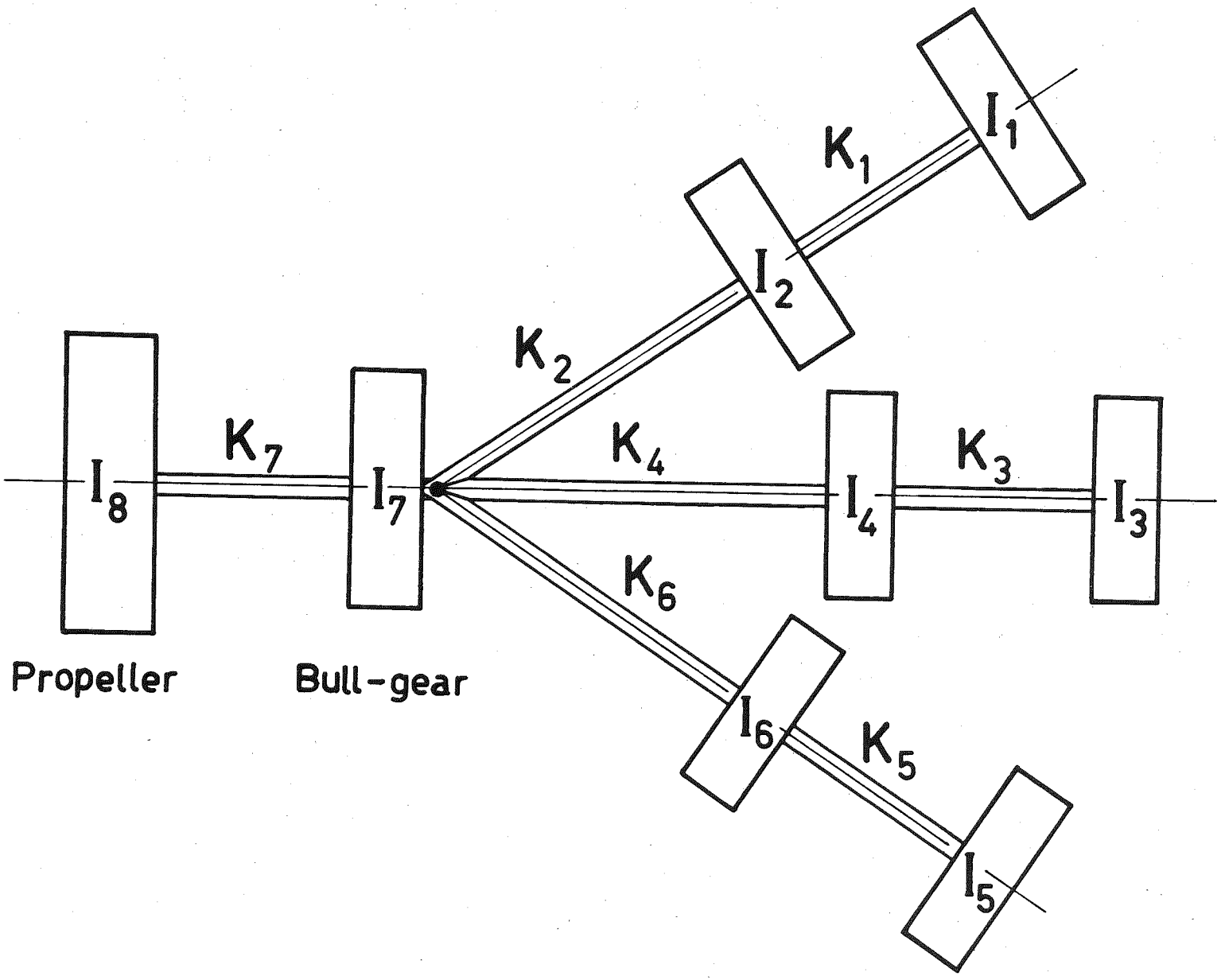
I1
K1
I2
K2
K7
I8
I7
K4
I4
K3
I3
K6
I6
K5
I5
Propeller
Bull-gear

Fig. 17.5 Schematic diagram of propulsion system for mobility analysis.

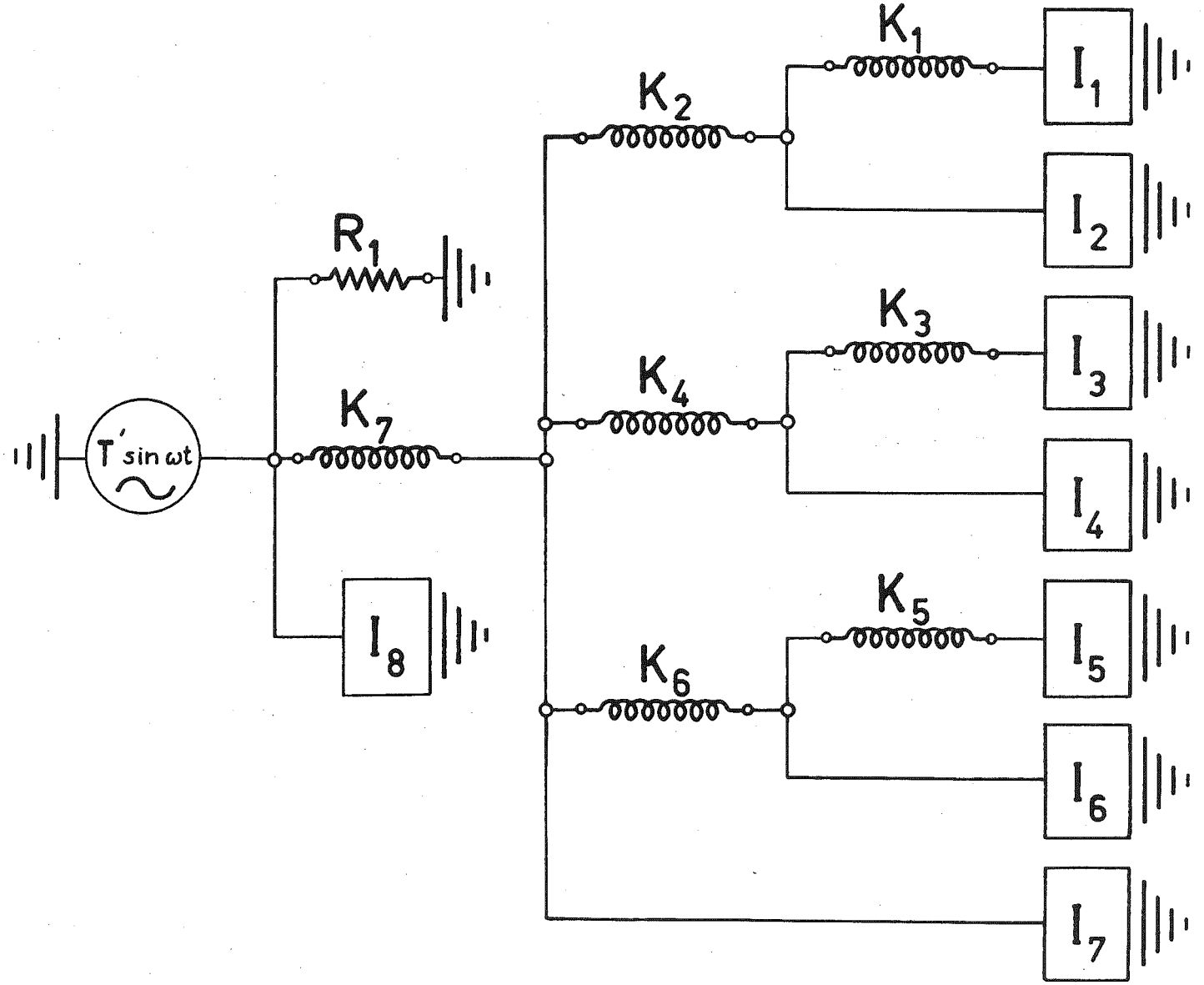
T'sin ωt
R1
K7
I8
K2
K1
I1
I2
K4
K3
I3
I4
K6
K5
I5
I6
I7

The values of T" for each component are then computed. The output from the programme is therefore the amplitude and phase angle of each of the harmonic components of the forcing torque. The amplitudes are also computed as percentages of the mean torque in the tail-shaft, and these values form part of the output from the programme.

The estimation of propeller damping was made in the following way. Provision had been made in the mobility analysis programme for the damping to be fed in as a variable, since there were one set of damping values relating to the sea trials tests and another set relating to the sea voyage. From the sea trials data of ship B a graph was prepared of shaft horsepower versus rpm under steady conditions. This data was replotted as torque versus shaft speed on a logarithmic basis when it was found that the equation

$$Q = 1344\, N^{2.19} \qquad (17.18)$$

where Q is in lbf-ft and N is in radians/second

represented the data to a high degree of approximation. The relationship between the torque Q and shaft speed N was thus a power relationship of the form

$$Q = K N^{n}$$

where K and n are constants. For the sea voyage of ship B a similar set of

graphs were prepared, and an equation of the same form, but with different constants, was obtained. In the sea voyage case the equation was

$$Q = 1006N^{2.25} \qquad (17.20)$$

for the test series B2-B

It is shown in Ref. 17.5 that the propeller damping constant B_p is given by

$$B_p = 2\frac{dQ}{dN} \qquad (17.21)$$

i.e by twice the slope of the propeller torque versus angular velocity curve.

Since the torque versus angular velocity relationship is a power law of the form given in equation (17.19), the propeller damping constant can be derived as

$$B_p = 2\frac{dQ}{dN} = 2Kn\,N^{n-1} \qquad (17.22)$$

The computer programme was arranged so that the constants K and n were input data. Depending on whether the data being analysed was from the sea trials or the sea voyage, the appropriate values of these constants were used.

CHAPTER 18

THE DIGITAL COMPUTER PROGRAMMES FOR THE ANALYSIS OF RESULTS - FREE AND RESONANCE VIBRATIONS

18.1 INTRODUCTION

During both the sea trials and the sea voyage, there occur a number of records of free vibration of the propeller. These were generally obtained when the ship was stationary or only moving slowly. They usually occurred at a condition where the propeller which had been rotating slowly in one direction was rotated slowly in the other direction, the reversal of direction giving a slight transient load to the system causing it to vibrate in the free mode. From these sections of record, the values of the frequency of the oscillation and the amplitude of the oscillation (as a torque in the tail-shaft) were determined. This data was used to obtain values of hydrodynamic inertia for the various amplitude conditions, as described in the following sections.

The various stages of computation are shown in Fig. 18.1. These stages and their corresponding digital computer programmes are discussed in detail in the following sections.

18.2 THE HOLZER ANALYSIS

A generalized Holzer-analysis programme was developed, which was capable of dealing with a multi-branched system having up to six branches (from a single point), each branch containing up to six inertias.

Fig. 18.1 Flow sheet for analysis of data

(free and resonance vibrations)

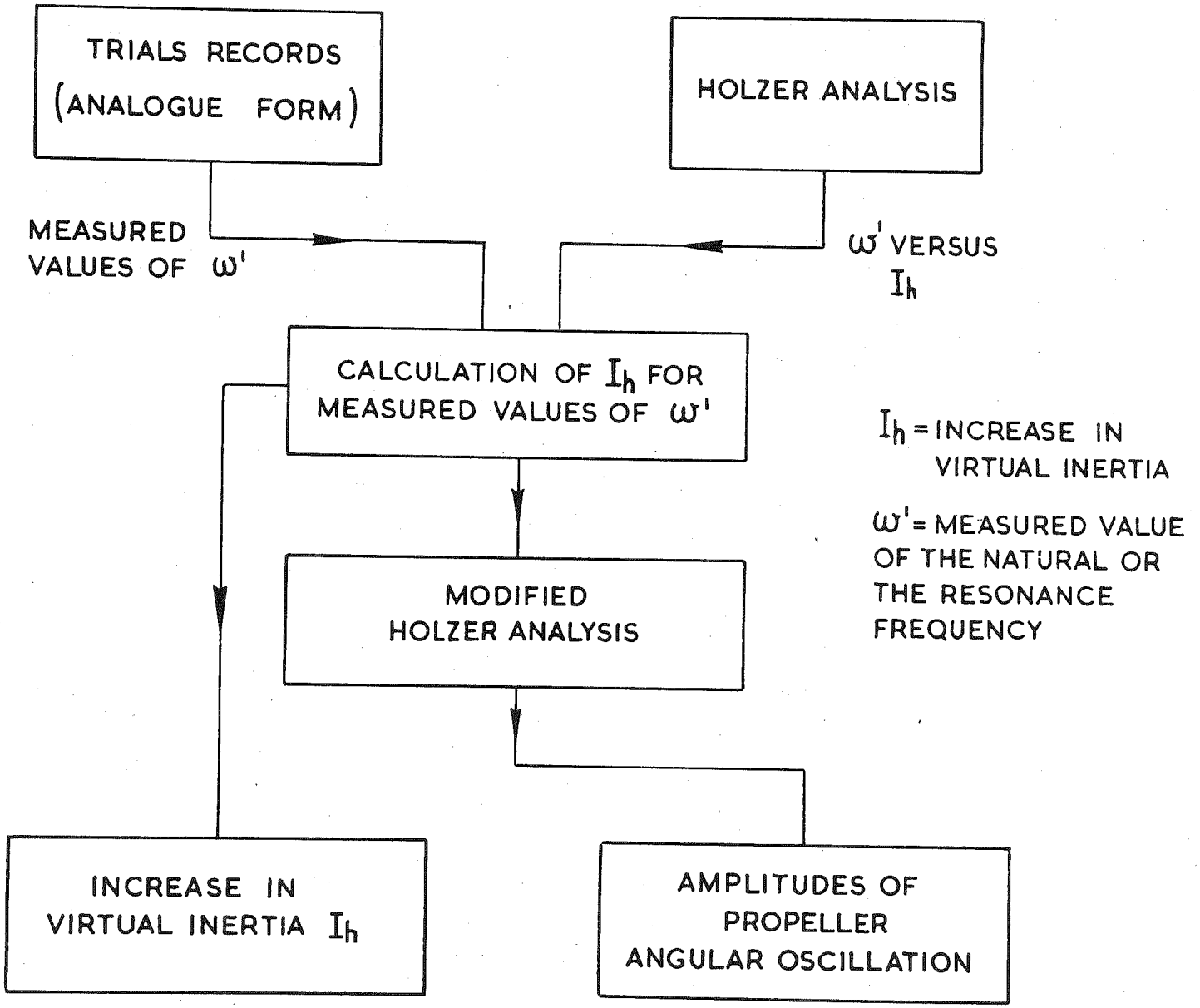
TRIALS RECORDS (ANALOGUE FORM)
HOLZER ANALYSIS
MEASURED VALUES OF ω'
ω' VERSUS Ih
CALCULATION OF Ih FOR MEASURED VALUES OF ω'
Ih = INCREASE IN VIRTUAL INERTIA
ω' = MEASURED VALUE OF THE NATURAL OR THE RESONANCE FREQUENCY
MODIFIED HOLZER ANALYSIS
INCREASE IN VIRTUAL INERTIA Ih
AMPLITUDES OF PROPELLER ANGULAR OSCILLATION

The method by which the Holzer calculation was carried out is as follows (Refer to Fig. 18.2). The branches were assumed to be initially uncoupled at O. Each branch was assumed to be harmonically oscillating in the torsional mode, at the same frequency. The amplitude of oscillation was assumed to be one radian at each of the ends A,B,C,--- of the branches. For each of these branches (by methods given in standard texts on vibration) the corresponding amplitudes at point O were calculated. One of the branches (A) was taken as the reference branch and its amplitude at O was taken as the standard amplitude. The vibrations in the other branches were adjusted so that the amplitudes at O were equal to the standard amplitude, by multiplying the amplitudes in each branch by the appropriate one of the following ratios:-

$$\frac{\text{Ampl}_A}{\text{Ampl}_B}\ ,\quad \frac{\text{Ampl}_A}{\text{Ampl}_C}\ ,\ \text{-----} \tag{18.1}$$

The torques in the branches were adjusted by the same ratios. In particular, the torques at O were adjusted by the same ratios. Although the amplitudes at O of the branches A,B,C,--- were now equal, the values of the torques at O were not necessarily the same. Since all branches had the same amplitude at O and since the oscillations were assumed to be in phase the branches could now be imagined as being coupled together at O. The torques due to the various branches at O were

Fig. 18.2 Diagrammatic arrangement of generalised propulsion system for Holzer analysis.

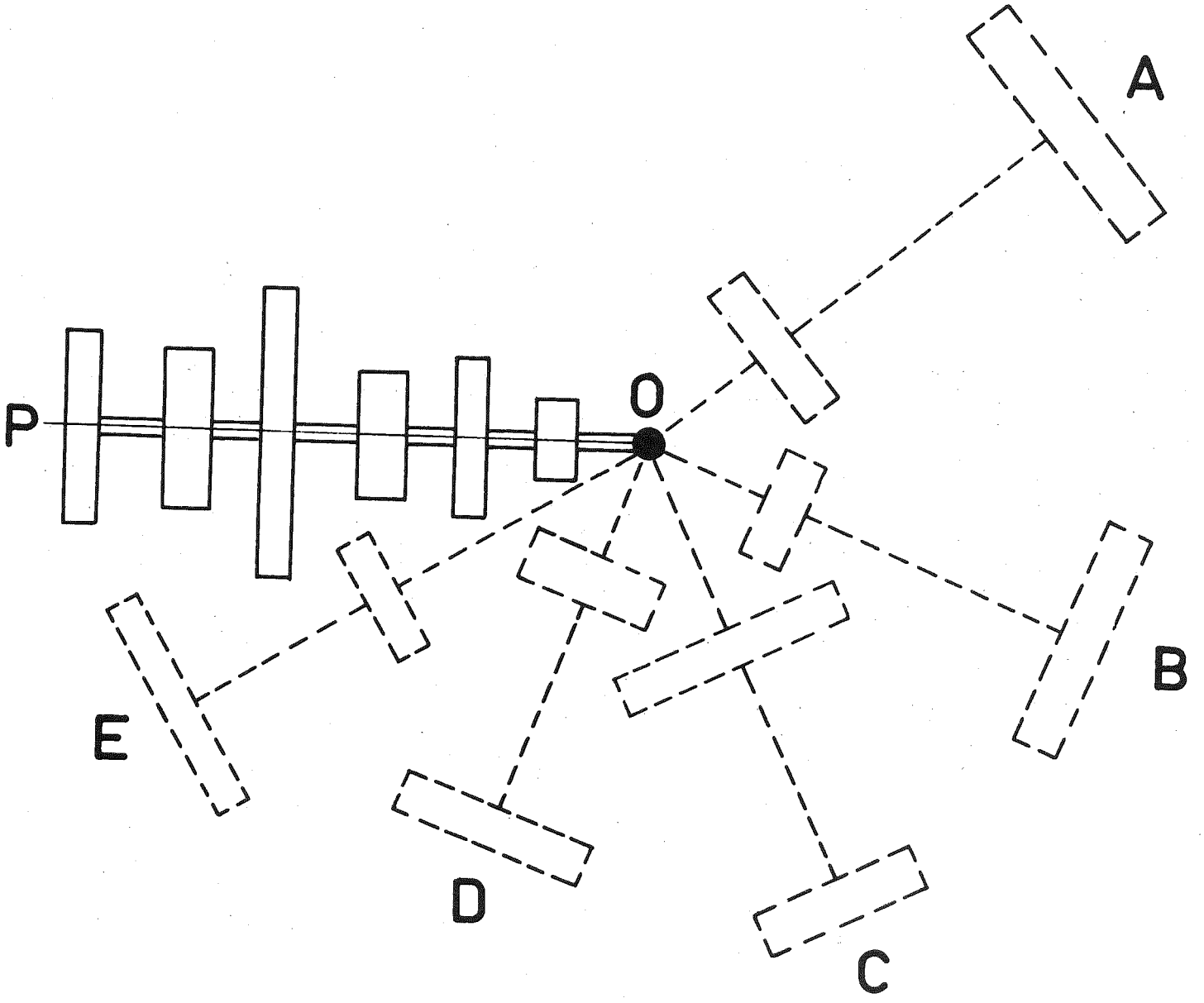
A
P
O
B
E
D
C

then added algebraically. If the algebraic sum of the torques was zero, then no external torque would need to be applied at O to maintain the vibrations in the various branches. Therefore, the branches could be assumed to be vibrating together in one of the natural frequency modes of the system. If however, the torques did not add to zero at O but gave a residual torque, then in order to maintain the vibration an external torque of this magnitude would have to be provided. The system would therefore be vibrating under forced vibrating conditions and would not be at one of the natural frequency modes of the system. In the programme the above calculations were repeated for a series of frequencies, known as the scan frequencies, each successive scan frequency being larger than the previous scan frequency by an amount Δf. The scan interval Δf was a variable in the programme and could be inserted in the input as any desired value. The programme was arranged to begin at zero frequency and to repeat the calculation for the successive values of scan frequency until the residual torque changed sign. At that point, by back-interpolation the frequency at which the residual torque was equal to zero was calculated and printed out as the natural frequency of the first mode of the system. The calculation process was then repeated until the next natural frequency was obtained, and so on until all the modes of the system had been obtained.

The propeller inertia used in the programme was equal to the sum of the propeller mechanical inertia plus the hydrodynamic inertia I_h. A series of values of I_h ranging from 5 % to 40 % of the propeller mechanical inertia, in steps of 5 % were chosen. For each of these

values of hydrodynamic inertia, the Holzer programme was run to determine the natural frequencies of all modes of the propulsion system, From these results the graphs given in Figs. 18.3a and 18.3b showing the variation of the natural frequencies with hydrodynamic inertia were prepared.

It will be noted that the frequencies for the 1st and 2nd modes of vibrations are very close together. From the values of natural frequency obtained from the test records for the free vibration cases, the values of the hydrodynamic inertia I_h were calculated using Figs. 18.3a and 18.3b. It was evident that the mode of vibration in every case was either the 1st or 2nd mode (or more probably a beating vibration betweenthe two modes since they are very close together). The values of the I_h were calculated first as if the vibration was occurring in the first mode and secondly as if the vibration was occurring in the second mode. These values, which did not differ greatly, were then averaged.

18.3 THE MODIFIED HOLZER ANALYSIS

A modified Holzer programme was developed, which was very similar to the Holzer analysis described above, except that the calculation procedure at any given frequency was as follows. (Refer to Fig.18.2). As in the case of the Holzer calculation the adjusted torques and amplitudes were calculated at O for each of the branches A,B,C,---, but not, however, for branch P. Branches A,B,C--P were then assumed to be coupled together at O and the torques added to obtain a residual

Fig. 18.3a Natural frequencies for the ore-carrier propulsion system versus percentage hydrodynamic inertia - Modes 1 and 2.

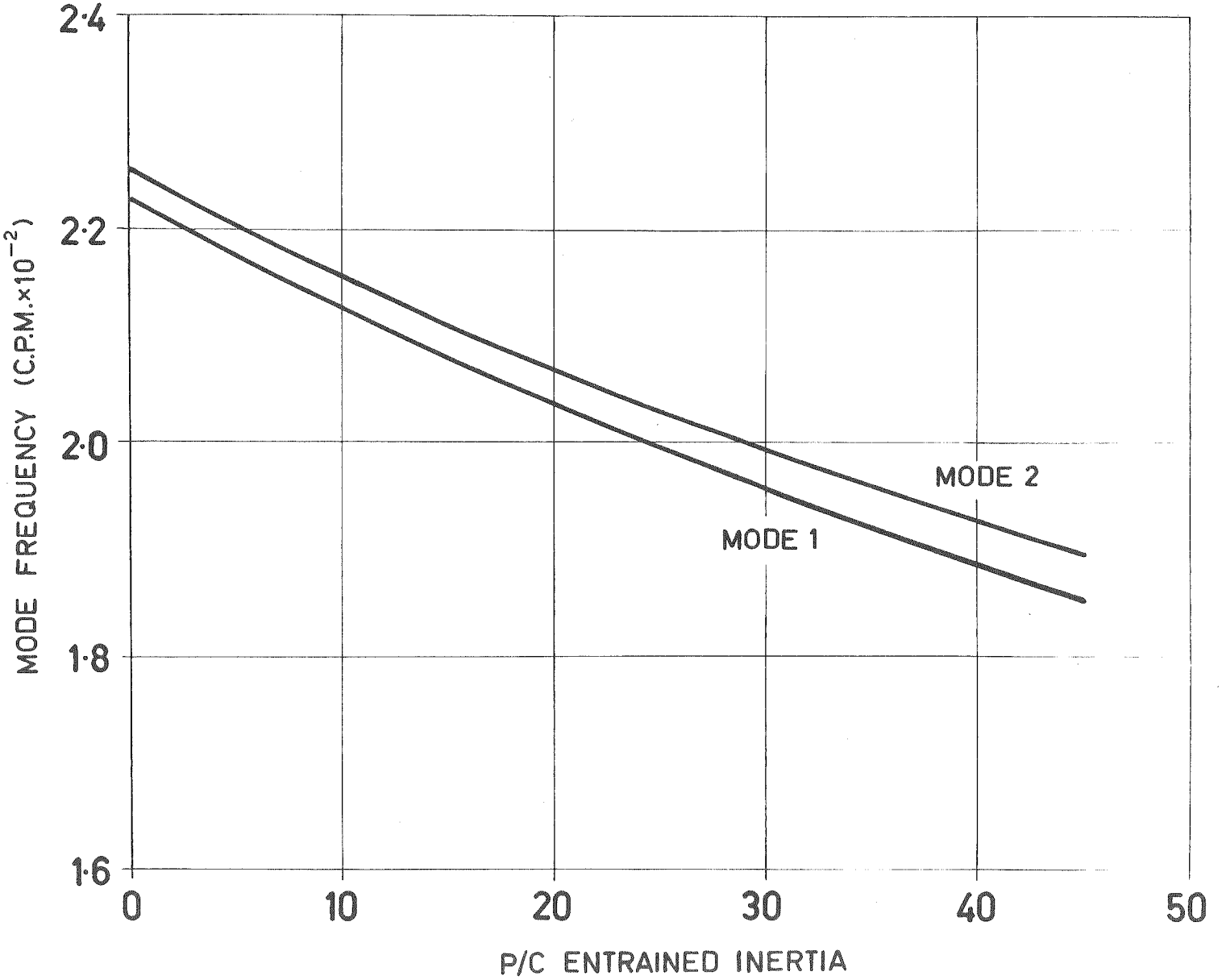
2·4
2·2
2·0
1·8
1·6
MODE FREQUENCY (C.P.M.×10⁻²)
0
10
20
30
40
50
P/C ENTRAINED INERTIA
MODE 2
MODE 1

Fig. 18.3(b) Natural frequencies for the ore-carrier propulsion system versus percentage hydrodynamic inertia - Modes 3 - 7.

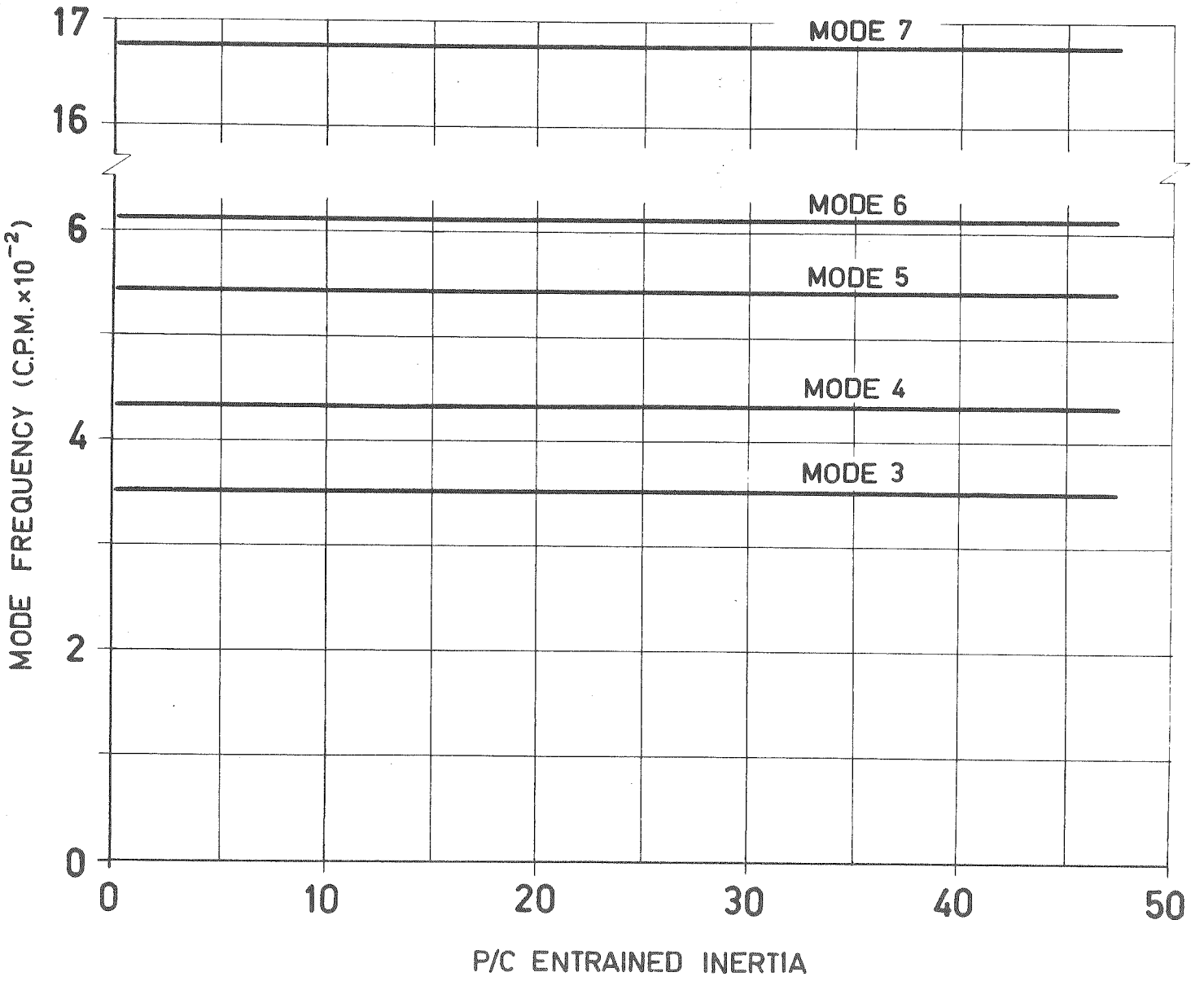
MODE 7
MODE 6
MODE 5
MODE 4
MODE 3
17
16
6
4
2
0
0
10
20
30
40
50
MODE FREQUENCY (C.P.M.×10⁻²)
P/C ENTRAINED INERTIA

torque at O. This torque was assumed to be applied to branch P at O, causing OP to be set into vibration. Calculation then proceeded along branch P, from O to P, to obtain the amplitude of oscillation at P. The torque in the tail-shaft section of branch P was also computed. Since the programme was only used for calculations at a frequency equal to one of the natural frequencies (previously determined from the Holzer analysis) there was no residual torque at P. The ratio of the torque in the tail-shaft section of branch OP to the (angular) amplitude of oscillation of the propeller at P was then calculated and printed out.

For each of the experimentally determined values of natural frequency obtained during the ship tests, the corresponding value of hydrodynamic inertia I_h was computed as described in Section 18.2 from the results of the Holzer calculation. Corresponding values of natural frequency and hydrodynamic inertia were tabulated (Assuming firstly a first-mode vibration and secondly a second-mode vibration) . Each test condition was referred to as a "run". For each "run" the value of hydrodynamic inertia I_h and a corresponding value of natural frequency was fed into the modified Holzer computer programme. The output from the programme gave the ratio of torque in the tail-shaft to the amplitude of the propeller oscillation, for each run. The measured value of torque in the tail-shaft was then divided by this ratio to obtain the angular amplitude of oscillation of the propeller for the particular run. There were of course, two values of amplitude determined in each case, corresponding to an assumed 1st mode vibration and an assumed 2nd mode vibration.

PART V

FULL SCALE RESEARCH -

MEASUREMENT OF FORCE FLUCTUATIONS

AND

VIRTUAL INERTIA OF PROPELLERS

CHAPTER 19

THE SCOPE OF THE FULL-SCALE SHIP TESTS

19.1 INTRODUCTION

This part of the thesis describes the most recent full-scale ship tests, which were carried out on two 19,000 ton ore carriers. The objects of these tests were :

(1) To further develop instrumentation for the measurement of fluctuating forces in ship tail-shafts.

(2) To obtain data on the tail-shaft fluctuating stresses under various conditions of operation.

(3) From the fluctuating stresses to calculate the applied hydrodynamic forces on the propeller, for various conditions of operation.

(4) From measurements taken of natural resonances of the shaft system when excited under various conditions, to obtain full-scale data on the virtual inertia of propellers.

(5) To obtain information on the thrust-block rigidity, and damping.

19.2 DESCRIPTION OF THE SHIPS

The vessels tested in these investigations were two sister ships. These were 19,000 ton turbine-powered ore-carriers, designed and built in Australia for coastal use. The major dimensions of these vessels are given in Table 19.1. The lines and after-body arrangement are shown in Fig. 19.1.

Fig. 19.1 Lines plan and afterbody arrangement of ore-carrier.

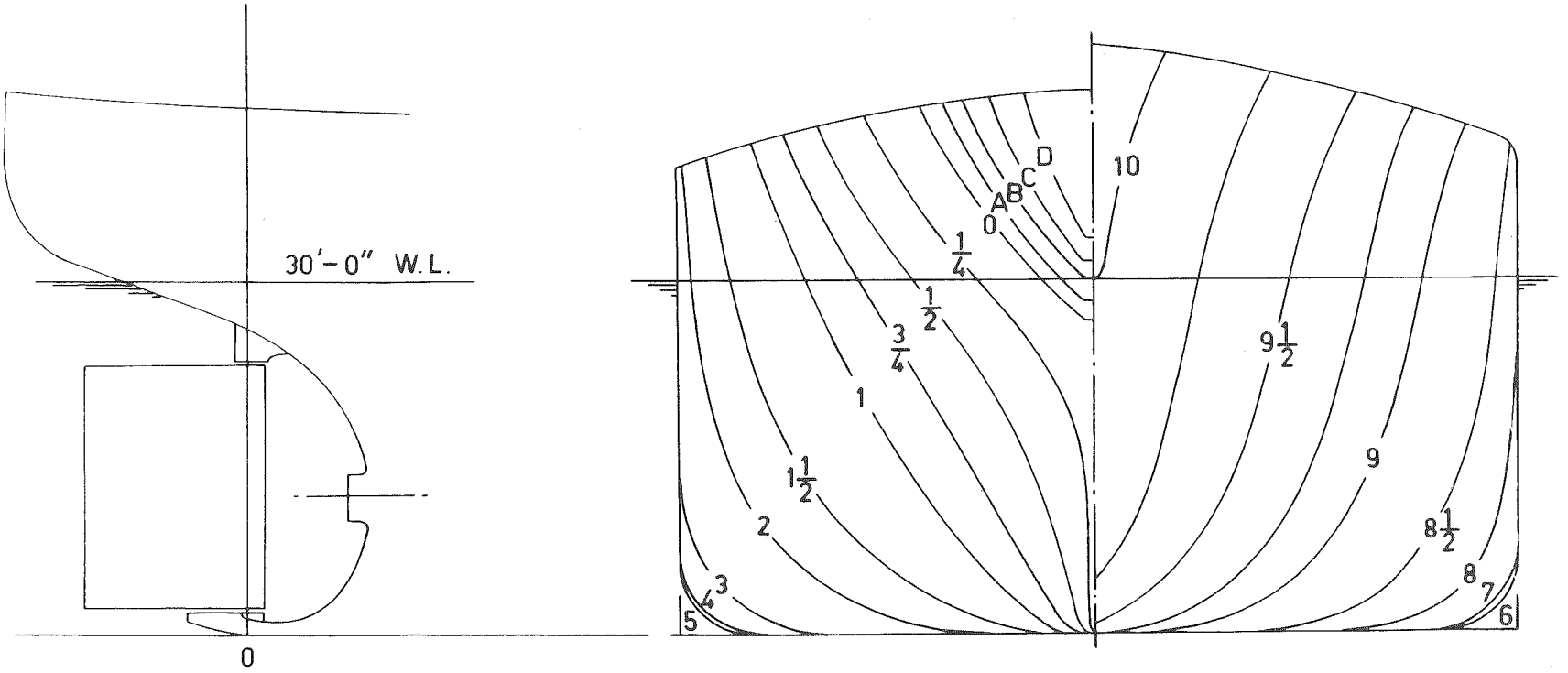
30'-0" W.L.
0
A
B
C
D
10
0
1/4
1/2
3/4
1
1 1/2
2
3
4
5
9 1/2
9
8 1/2
8
7
6

TABLE 19.1

Major Dimensions of the Ore-Carriers

Length between perpendiculars	550 ft
Moulded breadth	70 ft
Moulded draft	30 ft
Displacement (Loaded)	26,100 ton
Block coefficient	0.78

Details of the propeller which was designed from the Troost "B" series (See Ref. 19.1) are given in Table 19.2

TABLE 19.2

Particulars of Propeller

Diameter	17.5 ft
Number of blades	4
Rake	10°
Skewback	$10\frac{1}{4}^{\circ}$
Designed pitch - at tip	13.65 ft
Designed pitch - at root	10.92 ft
Pitch ratio (at 13.65 ft pitch)	0.78
Developed area (outside boss)	119.6 ft^2
Projected area (outside boss)	111.2 ft^2
Area ratio (developed)	0.496
Area ratio (projected)	0.462
Blade thickness ratio	0.056
Boss diameter to screw diameter (on rake line)	0.20

19.3 DESCRIPTION OF THE INSTRUMENTATION

For the ore carrier investigations described in this part of the thesis, measurements of the instantaneous torque and thrust stresses in the tail shaft were made using strain-gauges cemented to the tail-shaft surface. The output from the gauges was amplified by transistorised preamplifiers attached to the rotating shaft. The amplified output was then transmitted via sliprings to the recording equipment. A detailed description of the instrumentation is given in Chapters 14 and 15.

Simultaneous measurements were also made of thrust-block deflection, shaft rotational speed, shaft angular position, water depth under the keel, and shaft horsepower. Records were also made of wind strength and direction, seaway conditions, rudder position, and air and sea temperature.

19.4 OPERATING CONDITIONS DURING THE TESTS

Three series of tests were carried out on the 19,000 ton ore carriers as follows:

(1) Series A

These were carried out on ship A during the maker's sea trials.

(2) Series B1

These were carried out on ship B during the maker's sea trials.

(3) Series B2

These were carried out on ship B during the course of a

6,000 mile voyage around the coast of Australia. The outward voyage was made under ballast at an average draft of 22 ft and the return voyage fully loaded at an average draft of 30 ft. The tests carried out in this series can be subdivided into two groups:

B2-A

These were carried out at the nominally steady cruise speed of 115 rpm. The main variation in operating conditions was that the depth under the keel varied from 13 ft to 460 ft. There were also variations in the sea state, and wind strength and direction.

B2-B

These were speed trials carried out in deep water over a range of rpm.

The operating conditions during the various tests are summarised in Table 19.3

TABLE 19.3

OPERATING CONDITIONS DURING TESTS

Test Series	A	B1	B2-A	B2-B
Draft (ft)	23.0	22.5	22,30	30
Shaft speeds-nominal (rpm)	60-110	80-115	115	65-112
Depth under keel (ft)	40-50	40-50	13- 460	460
Sea state	Smooth	Slight	Smooth-Medium seas	Medium seas
Wind (Beaufort scale)	3-5	4	0-7	6-7

CHAPTER 20

THE RESULTS OF THE FULL-SCALE TESTS

20.1 THE ANALYSIS OF RESULTS

The analysis of the results may be conveniently discussed under the following headings:

(1) The tail-shaft torque and thrust fluctuations

(2) The applied hydrodynamic fluctuations

(3) The virtual inertia of the propeller

The analysis of the results is briefly discussed in this order in the following sections. For a detailed discussion of the analysis see Chapters 17 and 18.

20.1.1 The Tail-Shaft Thrust and Torque Fluctuations

The thrust and torque stresses were recorded during the tests in the following forms:-

(1) The torque and thrust were both recorded as ink-on-paper traces, using a 8 - channel pen-recorder. The fluctuations on the records were small in comparison with the mean values, and thus no attempt was made to use these records to obtain fluctuating values. These records however, were used to obtain mean values by drawing a mean line through the fluctuations on the traces

(2) The mean values of torque and thrust were blocked in the instrumentation by means of a specially developed impedance converter, which however, transmitted the fluctuations with negligible phase change. These fluctuations after further

amplification were recorded on the 8-channel recorder.

(3) The mean values of torque and thrust voltages were measured directly using a highly-damped moving-coil meter.

Movement of the thrust-block, propeller angular-position pulses, and a half-second timing pulse, were also recorded on the 8-channel paper. Marker pens in the recorder were used to identify records by means of a coded pattern of signals. Typical sections of chart record are shown in Fig.17.2.

From the chart records, values of mean torque and thrust were calculated and were checked against the values obtained from the moving-coil meter. Peak-to-peak amplitudes of fluctuations were also taken from the chart over selected portions corresponding to various operational conditions.

Harmonic analysis of the torque and thrust waveforms were carried out for selected sections of the records. This required that the wave-forms be first converted to tables of corresponding ordinate values. As some 35,000 ordinates were required, the task would have been a formidable one if carried out manually. An automatic digital curve reader (Chapter 16) was therefore designed, developed, and manufactured. In this instrument a photo-electric reading head coupled to a digitiser scans the ink traces on the recorder paper. Changes in photo-cell output as the "eye" of the head passes over the trace are used to trigger a pulse through the digitiser. The ditigiser output signal at that instant to be recorded in an electronic memory. The memory is then interrogated, and the memory output used to operate a digital printer. The machine can be preset to read a given number of ordinates, with

given spacing between the ordinates. A serial number for each ordinate is also sequentially generated within the machine, and printed on the output tape. The machine output is therefore a strip of paper tape on which is printed the serial numbers of successive ordinates and their corresponding digital ordinate values.

Using the automatic digital curve reader, the ordinates for selected sections of torque and thrust waveform were obtained in tabular form. These values were then used as input data for a digital computer programme (See Chapter 17) which carried out the harmonic analysis after first removing the superimposed low-frequency "swinging" of the traces which was associated with the ship motion in the seaway (See Fig. 17.2)

During the voyage, the ship passed through a highly magnetic region and became strongly magnetised. The intensity was sufficient to cause appreciable magnetic fields inside the ship. Lines of force passing approximately vertically through the engine-room caused the strain-gauge connecting leads to generate a once-per-revolution voltage sufficiently large to require correction for. By switching off the strain-gauge power supply the magnetically induced signal could be recorded on the 8-channel recorder. These records were later read by the automatic digital curve reader. The appropriate ordinate values were then fed into the digital computer programme and used to correct the results from the harmonic analysis of the torque and thrust waveforms (See Section 17.6).

Other data such as echo-sounder records, shaft torsion-meter readings, and pitotmeter readings were correlated as necessary with the information taken from the 8-channel recorder. Corrections for instrumentation calibrations were also carried out where necessary.

20.1.2 The Applied Hydrodynamic Fluctuations

From the data obtained in the manner described in Section 20.1.1, and from a knowledge of the dynamic parameters of the shaft system, the applied hydrodynamic torque on the propeller was calculated. The mobility method was used, a digital computer being employed for the detailed calculations (See Section 17.7) The virtual inertia used for the propeller was the value obtained during the tests (See Chapter 18). Values for propeller damping were calculated from the torque characteristic of the propeller according to the method given in Ref.17.5.

It is shown in Chapter 17 that it is not necessary to calculate the applied hydrodynamic thrust on the propeller, since the dynamic parameters of the shaft system for axial vibration are such that the applied hydrodynamic thrust is equal to the tail-shaft thrust to a high degree of accuracy.

20.1.3 The Virtual Inertia of the Propeller

Records of torsional natural vibration of the propeller in the first mode were made on several occasions during the tests. Using a generalised Holzer method (Chapter 18) the natural torsional frequencies for the shaft system were calculated by digital computer, for values of virtual inertia between 0 and

40 %. These values when plotted, allowed the determination of the virtual inertia from the various recorded values of natural torsional frequency. The corresponding angular amplitudes of propeller oscillation were calculated from the torque variations recorded in the tailshaft, using a modified Holzer analysis (See Chapter 18).

20.2 RESULTS

The results are presented in graphical and tabular form, and are considered in detail under various headings in the following sub-sections.

20.2.1 Peak-to-Peak Fluctuations

The torque and thrust fluctuations Δq and Δt are plotted against rotational speed N for conditions during the sea trials of ships A and B in Figs. 20.1 and 20.2, and for conditions during the voyage of ship B in Figs. 20.3 and 20.4. The sea trials data has been replotted in a dimensionless form in Figs. 20.5 and 20.6. The justification for this method of dimensionless plotting is given in Appendix III. For ship B the mean torque during the tests may be obtained from the relationships given in Section 17.7, and the mean thrust from the curves given in Appendix IV.

The following features may be observed from Figs. 20.1-20.6:-

(1) There is considerable scatter evident in the results from a given test series. This is a feature which has been noted in other full-scale tests (Ref. 20.1). This would appear to be due to slight variations in shaft speed (See Ref.20.1)

Fig. 20.1 Shaft torque fluctuations ΔQ (peak-to-peak) versus shaft speed N for ship A during Test Series A, and for ship B during Test Series B1

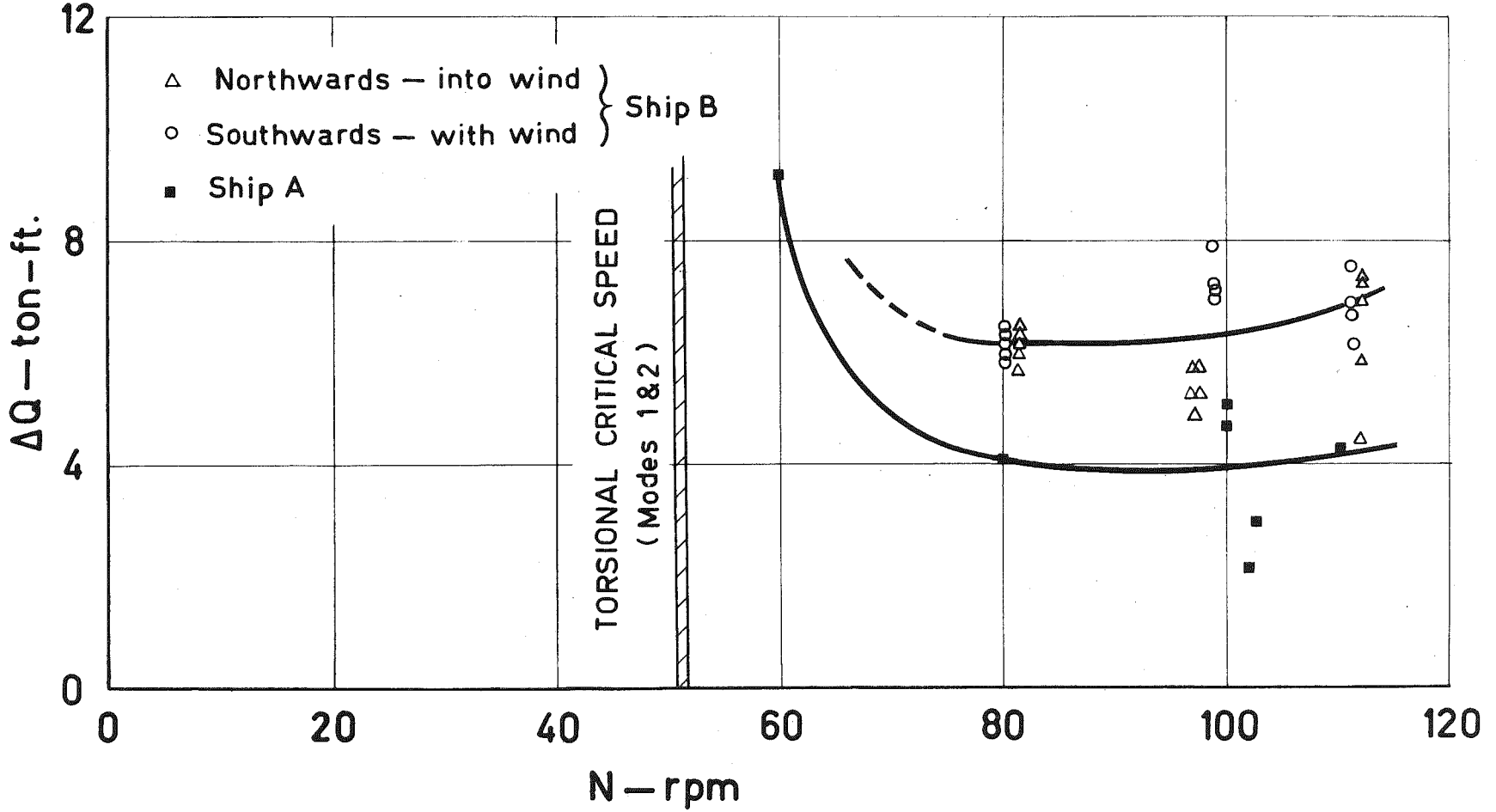
12
8
4
0
ΔQ — ton-ft.
△ Northwards — into wind
○ Southwards — with wind
Ship B
■ Ship A
TORSIONAL CRITICAL SPEED
(Modes 1&2)
0
20
40
60
80
100
120
N — rpm

Fig. 20.2 Shaft thrust fluctuations ΔT (peak-to-peak) versus shaft speed N for ship A during Test Series A, and for ship B during Test Series B1.

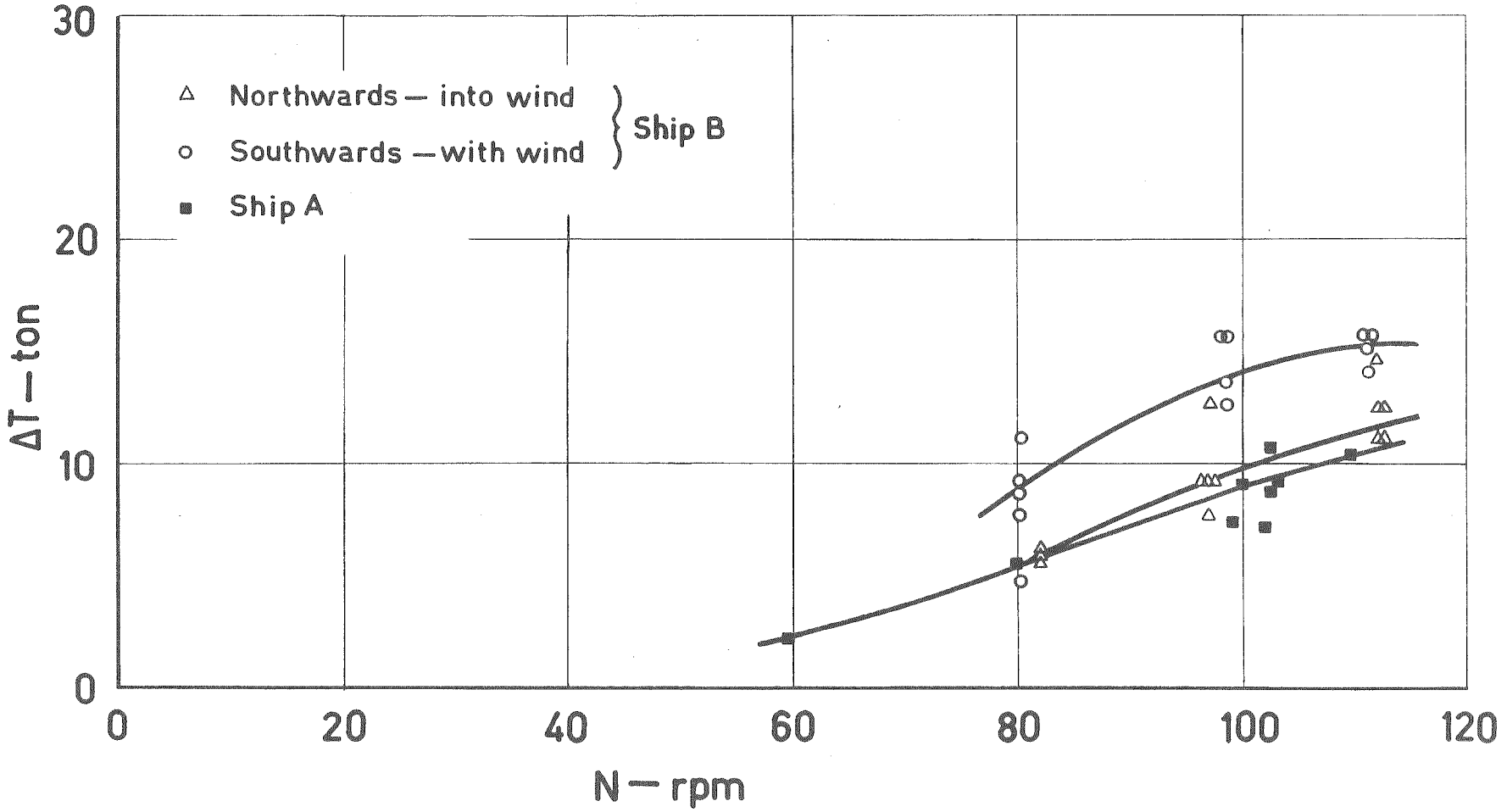
30
20
10
0
ΔT — ton
0
20
40
60
80
100
120
N — rpm
Northwards — into wind
Southwards — with wind
Ship B
Ship A

Fig. 20.3 Shaft torque fluctuations ΔQ (peak-to-peak) versus shaft speed N for ship B during Test Series B2-B.

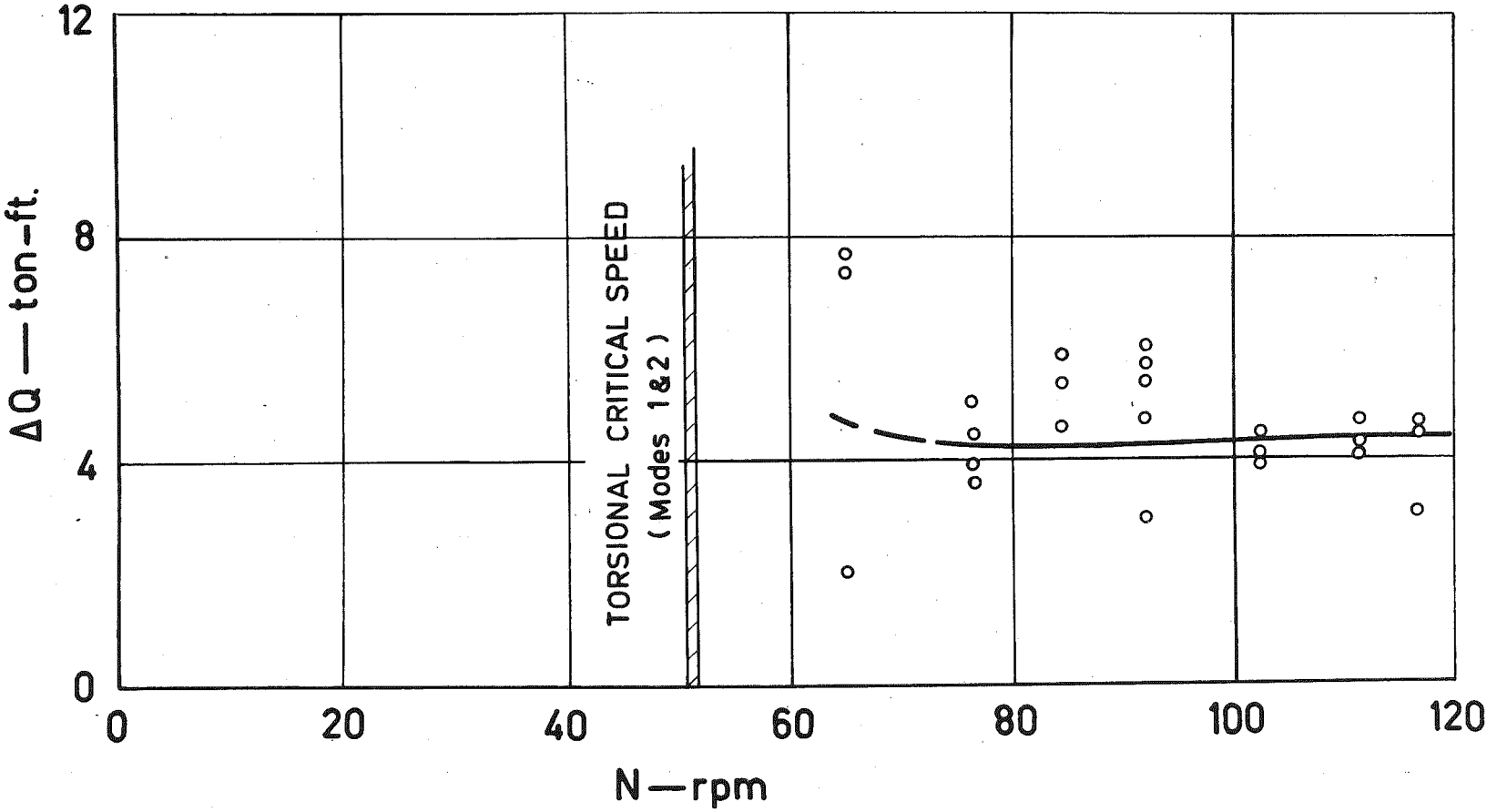
12
8
4
0
ΔQ — ton-ft.
0
20
40
60
80
100
120
N — rpm
TORSIONAL CRITICAL SPEED
(Modes 1&2)

Fig. 20.4 Shaft thrust fluctuations ΔT (peak-to-peak) versus shaft speed N for ship B during Test Series B2-B.

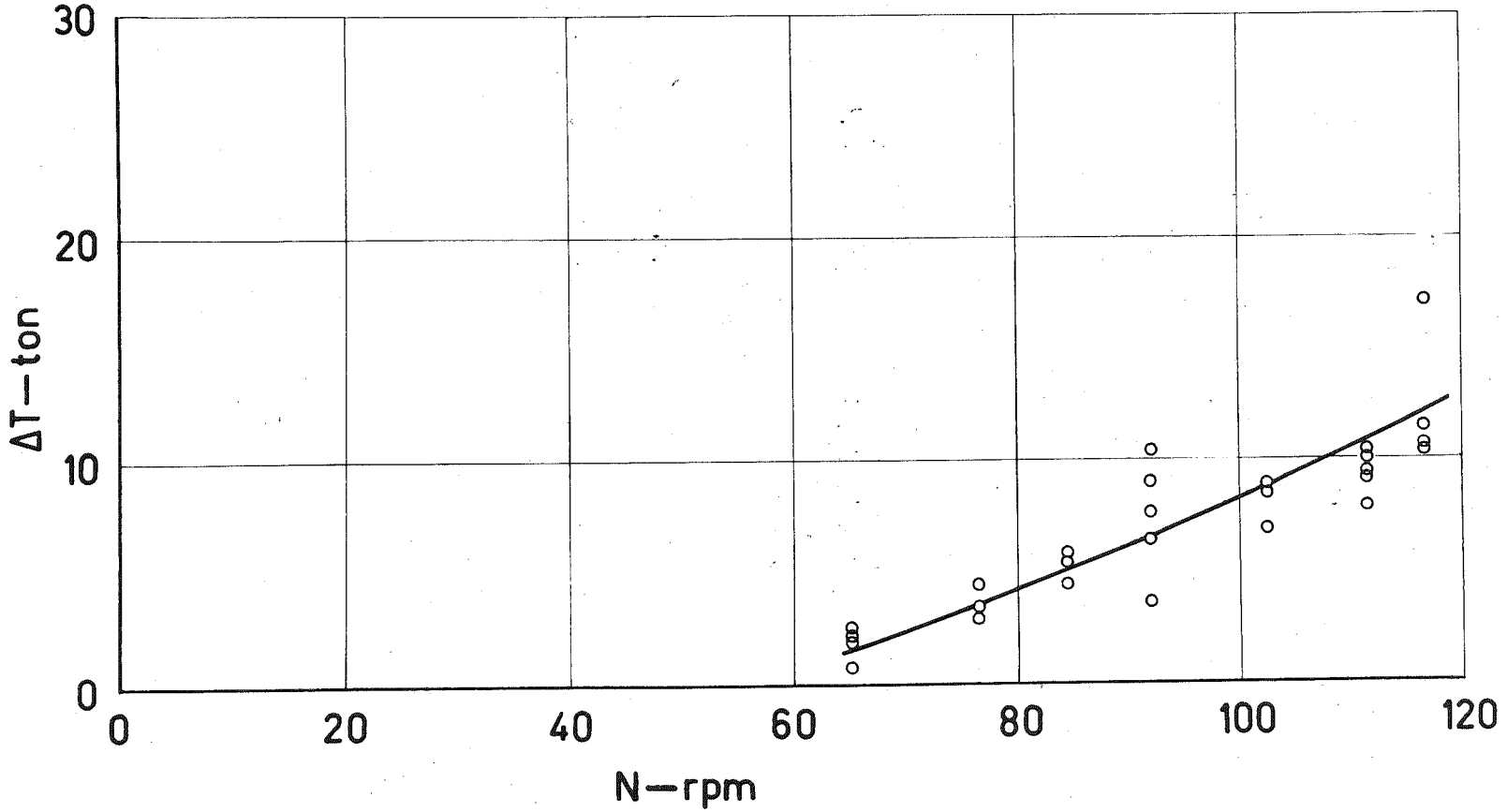
30
20
10
0
ΔT—ton
0
20
40
60
80
100
120
N—rpm

Fig. 20.5 Percentage shaft torque fluctuations $\frac{\Delta Q}{Q}$ versus thrust coefficient K_t for ship A during Test Series A, and for ship B during Test Series B1.

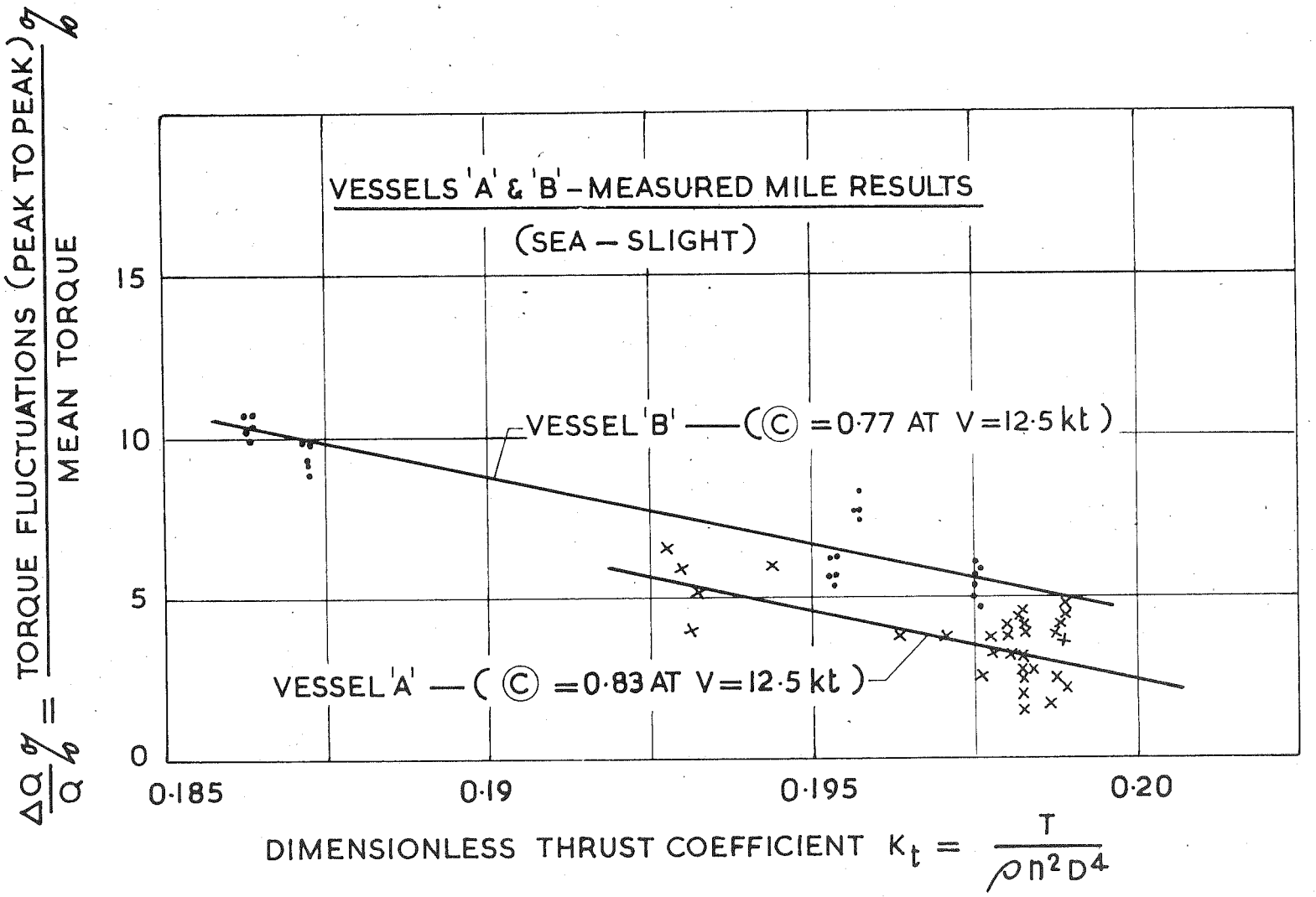
VESSELS 'A' & 'B' – MEASURED MILE RESULTS
(SEA – SLIGHT)
VESSEL 'B' — (Ⓒ = 0·77 AT V = 12·5 kt)
VESSEL 'A' — (Ⓒ = 0·83 AT V = 12·5 kt)
15
10
5
0
0·185
0·19
0·195
0·20
$\frac{\Delta Q}{Q}\% = \frac{\text{TORQUE FLUCTUATIONS (PEAK TO PEAK)}}{\text{MEAN TORQUE}}\%$
DIMENSIONLESS THRUST COEFFICIENT $K_t = \frac{T}{\rho n^2 D^4}$

Fig. 20.6 Percentage shaft thrust fluctuations $\frac{\Delta T}{T}$ versus thrust coefficient K_t for ship B during Test Series B1.

VESSEL 'B' — MEASURED MILE RESULTS

(SEA — SLIGHT)

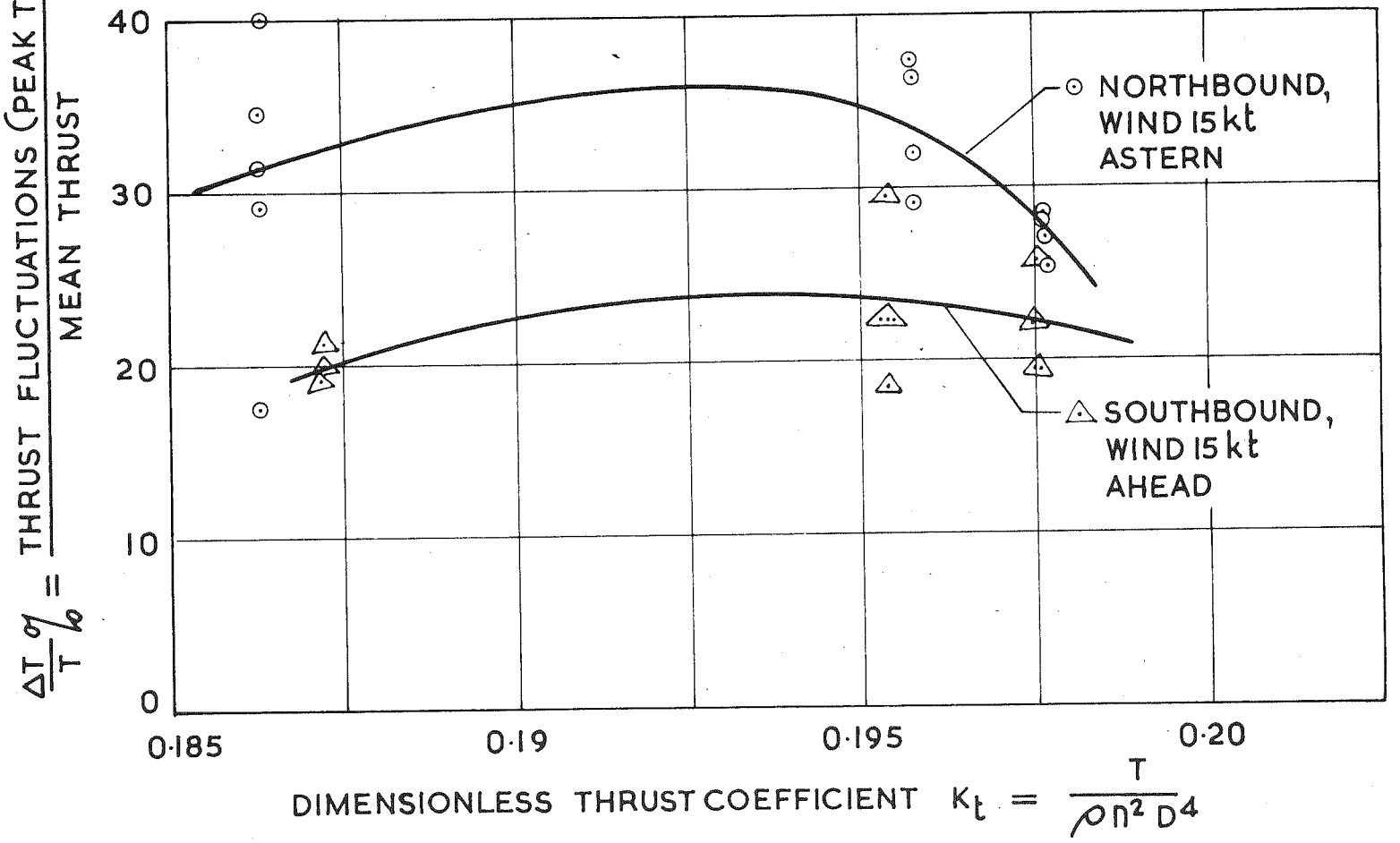

and variations in depth, wind, seaway, and motion of the ship.

(2) There is appreciable deviation between the results not only of the two sister ships, but also between the results of the same ship on two different occasions. This is probably only partly due to the factors given in (1) above. The main cause is probably the difference in hull fouling. This would cause not only differences in the velocity pattern of the fluid stream entering the propeller disc, but would also cause variations in hull resistance.

(3) Despite the deviations discussed in (1) and (2) above, the general trends in the corresponding curves are the same (see below)

(4) Except in the neighbourhood of a torsional resonance, the torque fluctuations ΔQ remain approximately constant with speed rising slightly, however, with increase in speed. The fluctuations expressed as a percentage of mean torque, decrease with increase of thrust coefficient K_t.

(5) The thrust fluctuations ΔT increase with increased speed. The fluctuations expressed as a percentage of mean thrust, remain approximately constant with thrust coefficient K_t, possibly decreasing slightly at the highest and lowest values of K_t.

(6) Whether a wind of as low a velocity as 15 knot is ahead or astern makes an appreciable difference to the values of ΔT and $\frac{\Delta T}{T}$, but little difference to ΔQ and $\frac{\Delta Q}{Q}$.

(7) The plotting of ΔT and ΔQ data in the dimensionless form used in Figs. 20.5 and 20.6 would appear to give some improvement in correlation, especially for the torque data.

The data in Figs. 20.4 - 20.6 has been taken from tests at approximately constant depths (see Table 19.3). However, none of this data refers to very shallow water tests. To determine the effect of shallow depth on ΔQ and ΔT, data from ship B during Test Series Be-A covering a wide range of depths at a constant nominal speed has been plotted in Figs. 20.7 - 20.10.

The torque and thrust fluctuations ΔQ and ΔT have been plotted against depth below the surface H, in Figs. 20.7 and 20.8. This data has been replotted in dimensionless form in Figs. 20.9 and 20.10.

The following features will be noted from Figs. 20.7 - 20.10:-

(1) There is little change in the torque fluctuations even at very shallow depths, ΔQ appears to increase very slightly at very shallow depths, whereas $\frac{\Delta Q}{Q}$ appears to decrease very slightly. (The decrease of $\frac{\Delta Q}{Q}$ may be due to an insufficient number of data points, as it is later shown that the harmonic components of ΔQ when plotted as percentages of mean torque, show a definite increase at very shallow depths). The effect of bottom depth first becomes perceptible when the depth under the keel is about 2 propeller diameters.

(2) The effect of depth on thrust fluctuations is quite marked. The trend for both ΔT and $\frac{\Delta T}{T}$ is for an increase, as depth decreases. There is no noticeable effect, however, until the

Fig. 20.7 Shaft torque fluctuations ΔQ (peak-to-peak) versus sea depth H, for ship B during Test Series B2 -A. (Draft 30 ft)

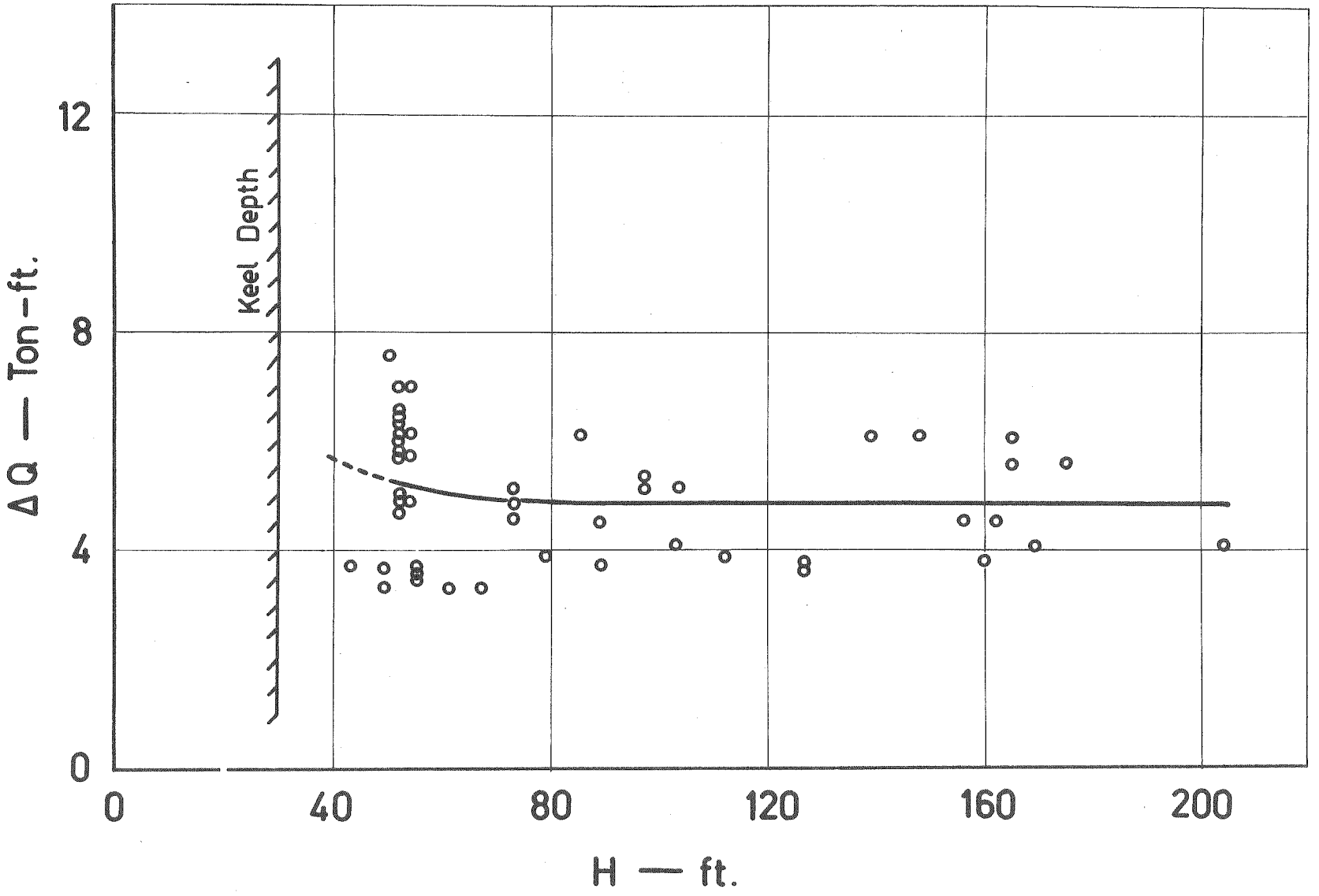
ΔQ — Ton-ft.
12
8
4
0
Keel Depth
0
40
80
120
160
200
H — ft.

Fig. 20.8 Shaft fluctuations ΔT (peak-to-peak) versus sea depth H, for ship B during Test Series B2-A (Draft 30 ft).

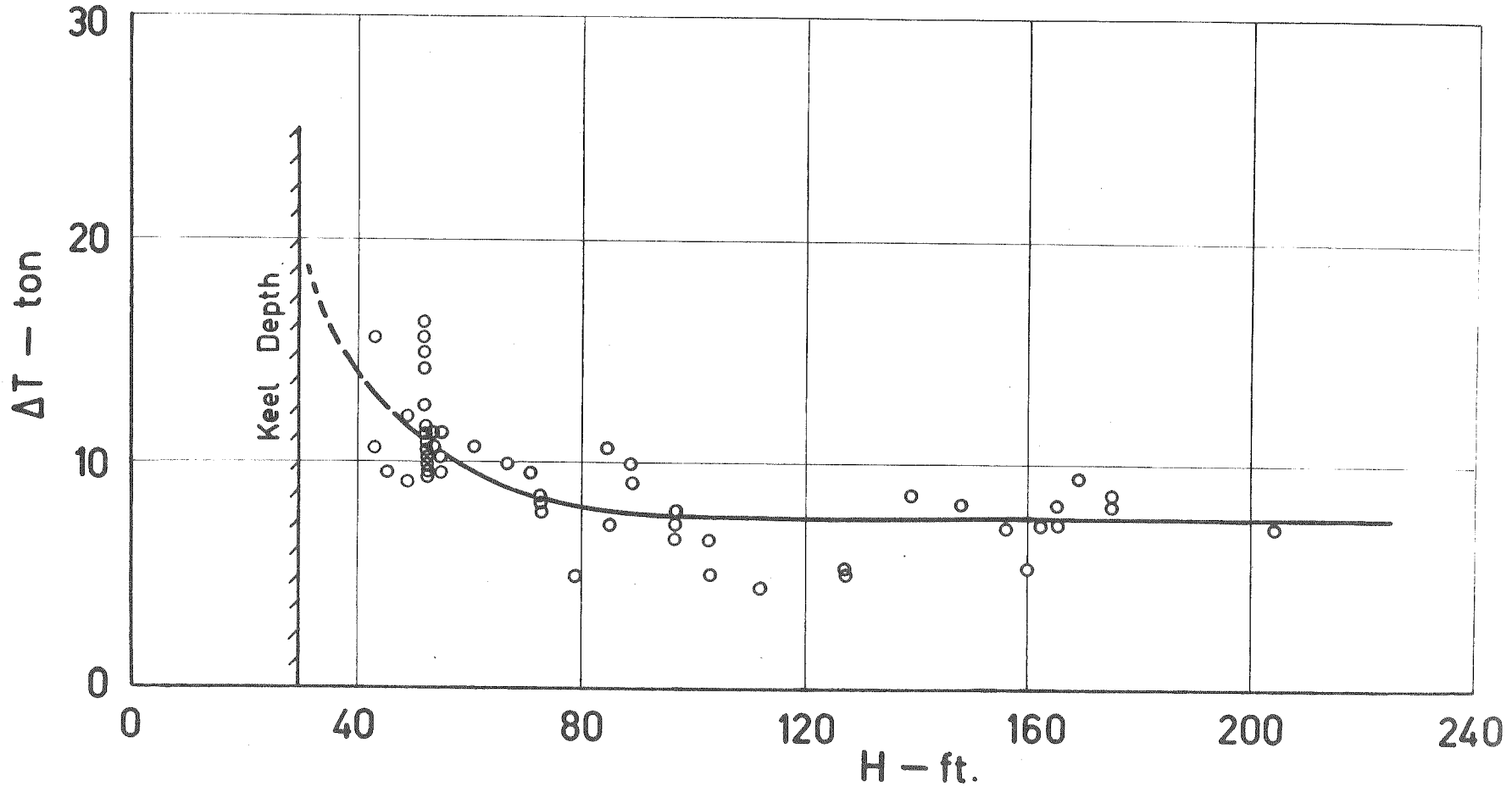
30
20
10
0
ΔT – ton
Keel Depth
0
40
80
120
160
200
240
H – ft.

Fig. 20.9 Percentage shaft torque fluctuations $\frac{\Delta Q}{Q}$ versus $\frac{\text{Depth below keel } H'}{\text{Propeller diameter } D}$ for ship B during Test Series B2 - A (Draft 30 ft)

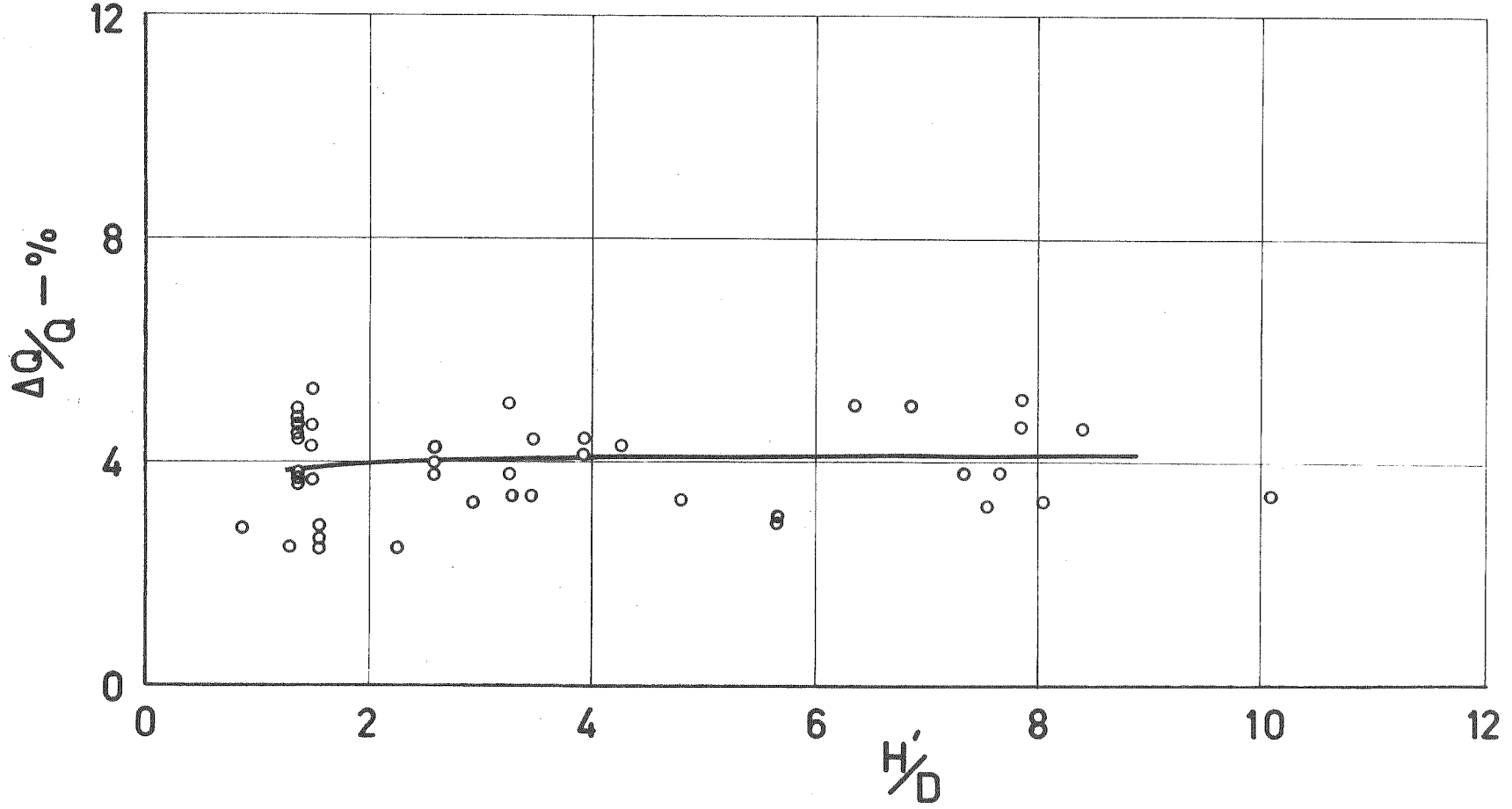
12
8
4
0
ΔQ/Q – %
0
2
4
6
8
10
12
H'/D

Fig. 20.10 Percentage shaft thrust fluctuations $\frac{\Delta T}{T}$ versus $\frac{\text{Depth below keel } H'}{\text{Propeller diameter } D}$ for ship B during Test Series B2-A (Draft 30 ft)

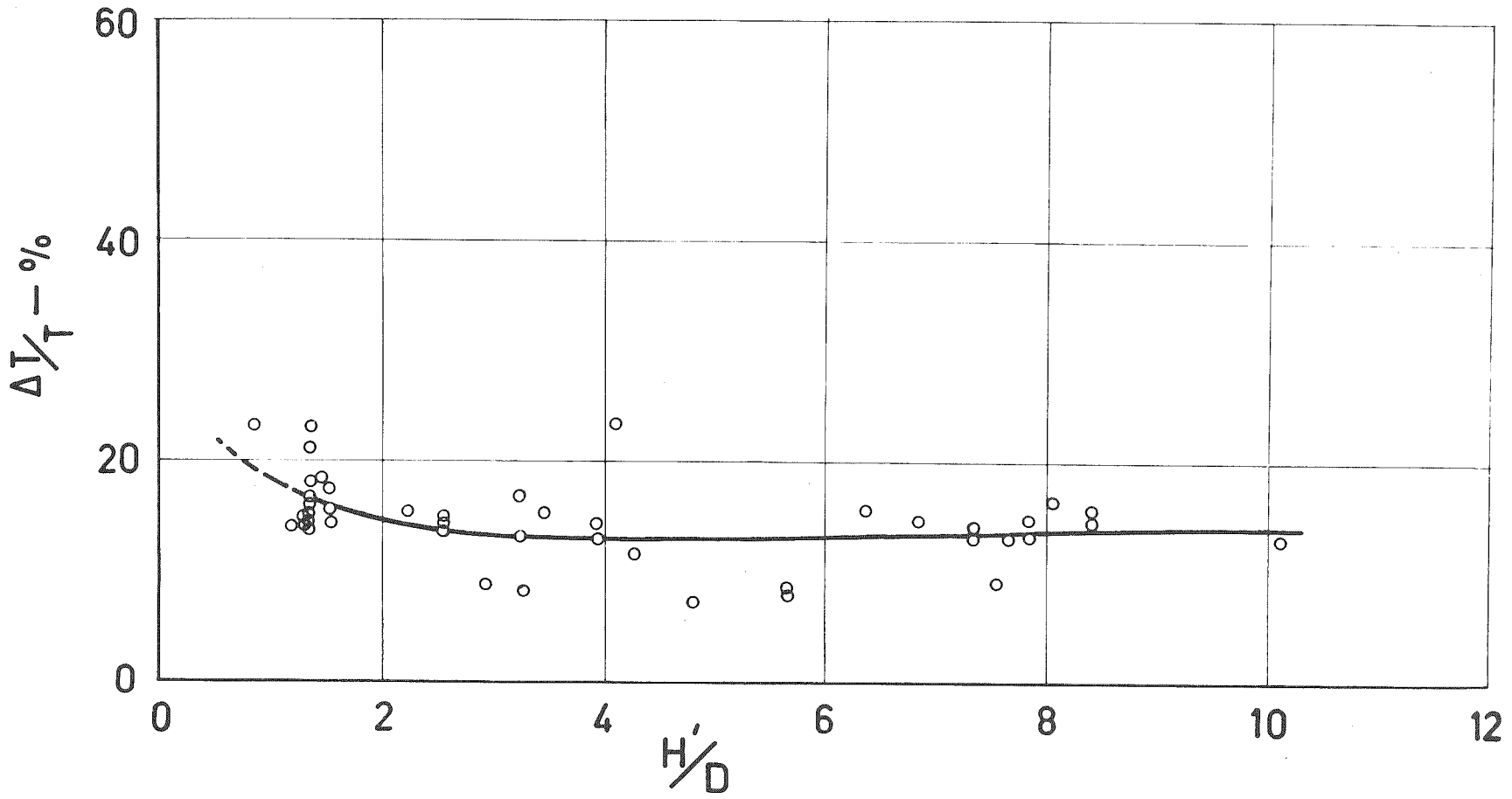
60
40
20
0
ΔT/T — %
0
2
4
6
8
10
12
H'/D

depth under the keel is below about 2 propeller diameters.

It is worth recording that the surface force fluctuations on the hull, as noted subjectively from the increased level of plate vibration increased very considerably at very shallow depths.

20.2.2 The Harmonic Components of the Tailshaft Torque and Thrust

The harmonic analysis of the tailshaft torque and thrust waveforms was carried out up to the 24th harmonic of shaft rotation. After the 12th harmonic, however, the amplitudes of the components were generally insignificant, and have not been included in the data presented in the following sections. Plots were made of the phase angle relationships under various conditions, but it was found impossible to obtain any valid correlations. For any given steady test condition it was found that the phase angles obtained from analyses of sections of record only a few hundred revolutions apart differed widely, although the amplitudes of the harmonic components for the same records showed reasonably good correlation. Even for successive revolutions the phase angles showed poor correlation, in contrast to the amplitudes of the components. The scatter in the amplitudes of the harmonic components at any given steady condition, varied from slight to considerable. For one particular run where conditions were apparently unusually steady, the variation in the amplitudes of the harmonic components for six analyses taken at intervals during a period of over 200 revolutions, was negligible. On other occasions, there

was appreciable scatter between the results taken over a similar period. For analyses taken from successive revolutions, however, the amplitudes of the harmonic components were almost identical in each case. This is in contrast to the results obtained by Silverleaf (Ref. 20.1), where data from successive revolutions did not show such a good correlation. The results obtained by the present author lead him to disagree with the conclusion expressed by Silverleaf, that "even when freedom from one set of (critical) vibration modes is achieved, interaction effects between different modes occur within the normal ship operational range of propeller speeds and this confuses the interpretation of measured shaft strain fluctuations". Interaction between the critical vibration modes of a multi-degree-of-freedom system does not usually occur. The dynamic coupling between modes is not significant unless the modal frequencies are close together, in which case a periodic interchange of energy is possible. In ship propulsion systems, the results of a harmonic analysis of torque or thrust will be suspect, very close to a critical mode, in any case. If two modes are close together, this will simply mean that the region in between as well as the adjacent regions on either side, are regions in which the results of a harmonic analysis will not be very trustworthy. It is the opinion of the author that the scatter observed in the experimental results is associated with slight variations in shaft speed (See also Ref. 20.1) together with variations in wind, seaway, and motion of the ship, rather

than with energy interchanges between modes of vibration. The possibility of coupling between the torsional and longitudinal modes of vibration via hydrodynamic effects at the propeller should not, however, be overlooked. This possibility has been investigated by Lewis who has shown (Ref.20.2) that provided the longitudinal frequency of vibration is at least twice the frequency of the lowest torsional mode, the coupling of the longitudinal and torsional motions by water inertia and damping will be weak. Except for very unusual designs, then, the likelihood of this coupling being significant is negligible.

The variation of the harmonic components of torque and thrust with shaft speed are summarised in Figs. 20.11 and 20.12, for conditions during the sea trials and voyage of ship B. The following features may be observed from these figures:-

(1) The fourth harmonic component(which is the first harmonic of blade frequency) is as would be expected, the dominant component. The eighth harmonic, which might also be expected to be prominent, is significant in the thrust case but not in the torque case.

(2) In the torque results, the prominence of the third harmonic in the voyage data (Series B2-B), and of the first,second and third harmonics in the sea trials data (Series B1), is unexpected. Since the major difference between the voyage and sea trials data is in the draft

Fig. 20.11 The semi-amplitudes ΔQ of the harmonic components of shaft torque (expressed as a percentage of mean torque Q), for various shaft speeds.
(The draft at which these results were taken was 22.5 ft for Test Series B1 and 30 ft for Test Series B2-B)

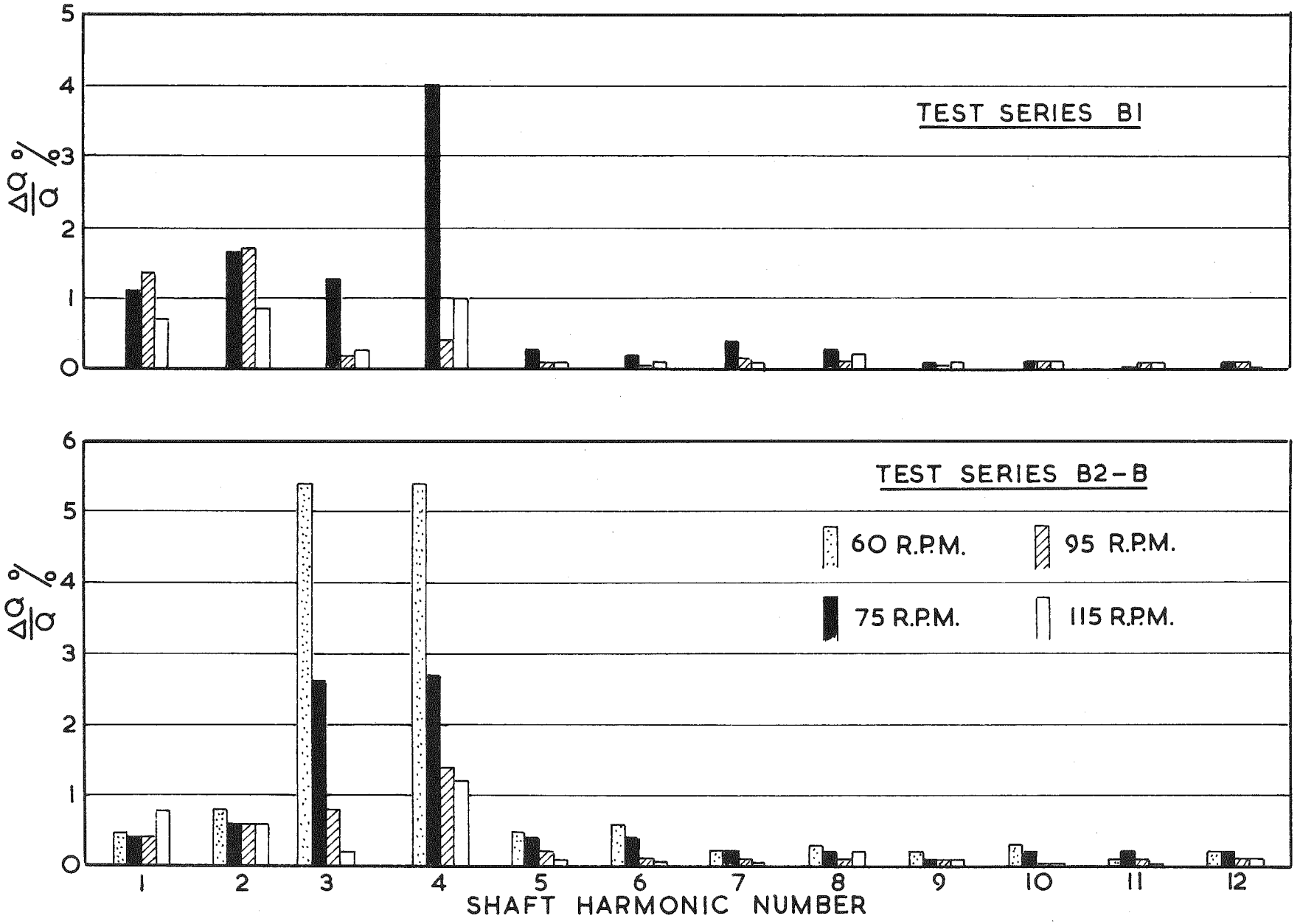
TEST SERIES B1
TEST SERIES B2-B
60 R.P.M.
95 R.P.M.
75 R.P.M.
115 R.P.M.
ΔQ/Q %
SHAFT HARMONIC NUMBER
0
1
2
3
4
5
6
7
8
9
10
11
12

Fig. 20.12 The semi-amplitudes ΔT of the harmonic components of shaft thrust (expressed as a percentage of mean thrust T), for various shaft speeds.
This figure also applies to the applied hydrodynamic thrust, since this is equal to shaft thrust.
(The draft at which these results were taken was 22.5 ft for Test Series B1 and 30 ft for Test Series B2-B)

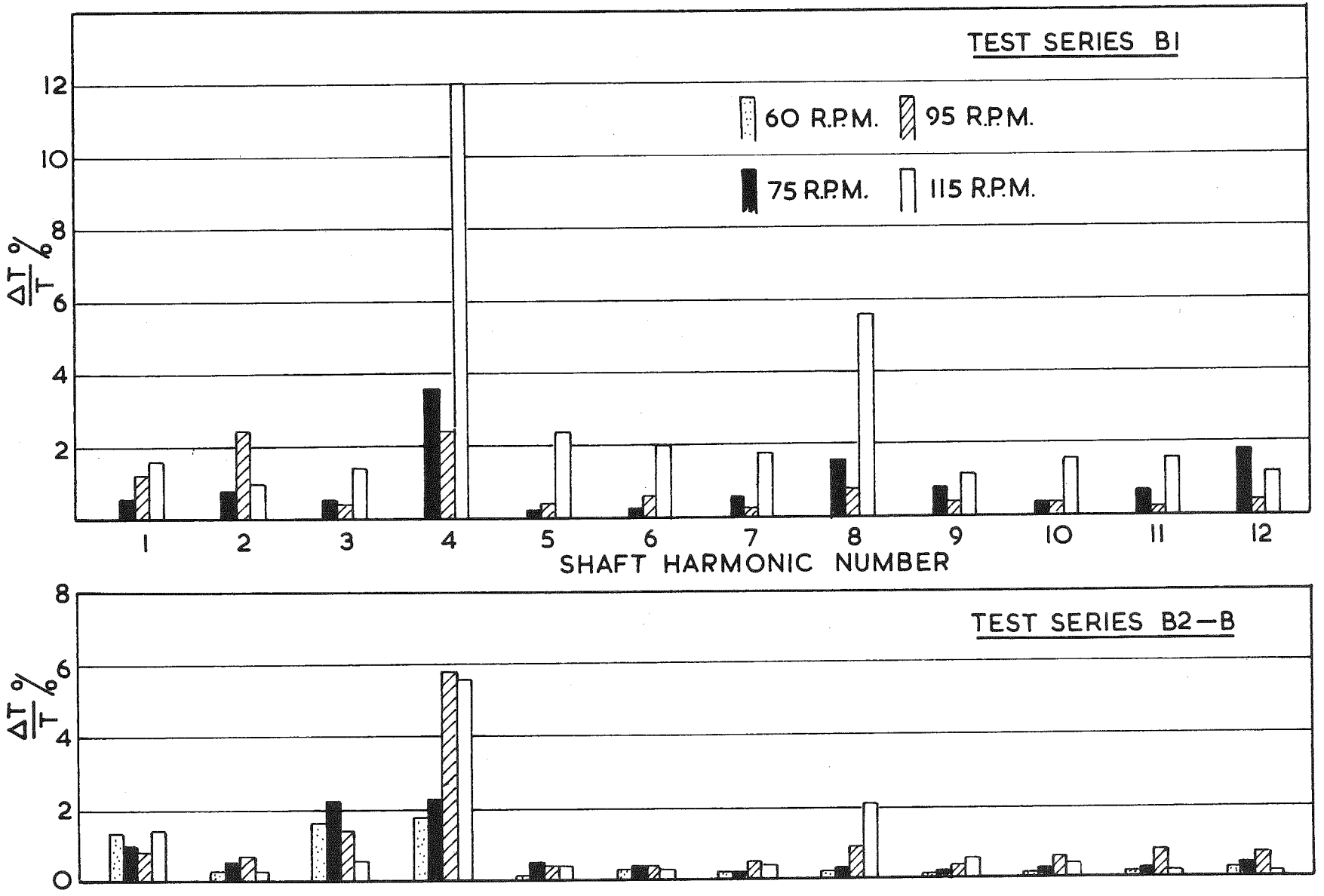
TEST SERIES B1
60 R.P.M.
95 R.P.M.
75 R.P.M.
115 R.P.M.
ΔT/T %
12
10
8
6
4
2
1
2
3
4
5
6
7
8
9
10
11
12
SHAFT HARMONIC NUMBER
TEST SERIES B2—B
ΔT/T %
8
6
4
2
0

(22.5 ft for sea trials, 30 ft for voyage) it might be postulated that this accounts for the difference in the two sets of results. It is possible, however, that the different states of fouling on the hull may have had some influence on the results. It is unlikely that variations in depth between the two test conditions was significant since the voyage results were taken in deep water, and the sea trials results were taken in water which although comparatively shallow was deep enough not to influence the results appreciably (See following sections for effect of depth)

(3) The torque results generally show an increase in the semi-amplitudes of the components as the shaft speed decreases down towards the first and second critical speeds which occur at approximately 50 rpm. At the higher speeds, the amplitudes either remain decrease or remain constant.

(4) In the thrust results, the prominence of the first, second and third harmonics is unexpected. As in the case of torque (see (3) above) the differences in character between the sea trials and voyage data may be tentatively ascribed to the effect of draft, possibly influenced to some extent also by fouling and sea depth effects.

(5) The thrust results generally show an increase in the semi-amplitudes of the components as the shaft speed increases. At the lowest shaft speeds, however, there is also an

increase in some components, at certain conditions. The effect of sea depth on the torque and thrust components is shown in Figs. 20.13 and 20.14. It will be seen that in almost every case, there is a marked increase in amplitude at the shallow depth. The curves from which Figs. 20.13 and 20.14 were abstracted showed a sharp bend upwards when the water depth under the keel had decreased to about two propeller diameters. There was little increase in the amplitudes until the water depth under the keel had decreased to about three propeller diameters, however. The curves were generally similar in shape to those shown in Fig. 20.17.

20.2.3 The Harmonic Components of the Applied Hydrodynamic Torque and Thrust

The harmonic components of the applied hydrodynamic torque and thrust were calculated, up to the 24th harmonic. As in the case of the components of shaft torque and thrust (Section 20.2.2) the components above the 12th were insignificant, and were neglected. The remarks given in Section 20.2.2 about the consistency (or otherwise) of phase angle and amplitude data under various conditions, also generally apply to the harmonic components of the applied hydrodynamic torque and thrust.

The variation of the harmonic components of torque and thrust with shaft speed are summarised in Figs. 20.15 and 20.12, for conditions during the sea trials and voyage of ship B. The following features may be observed from these curves:-

(1) The fourth harmonic component (which is the first

Fig. 20.13 The semi-amplitudes ΔQ of the harmonic components of shaft torque (expressed as a percentage of mean torque Q) for shallow and deep water. (From Test Series B2-A, draft 30 ft, shaft speed 115 rpm nominal)

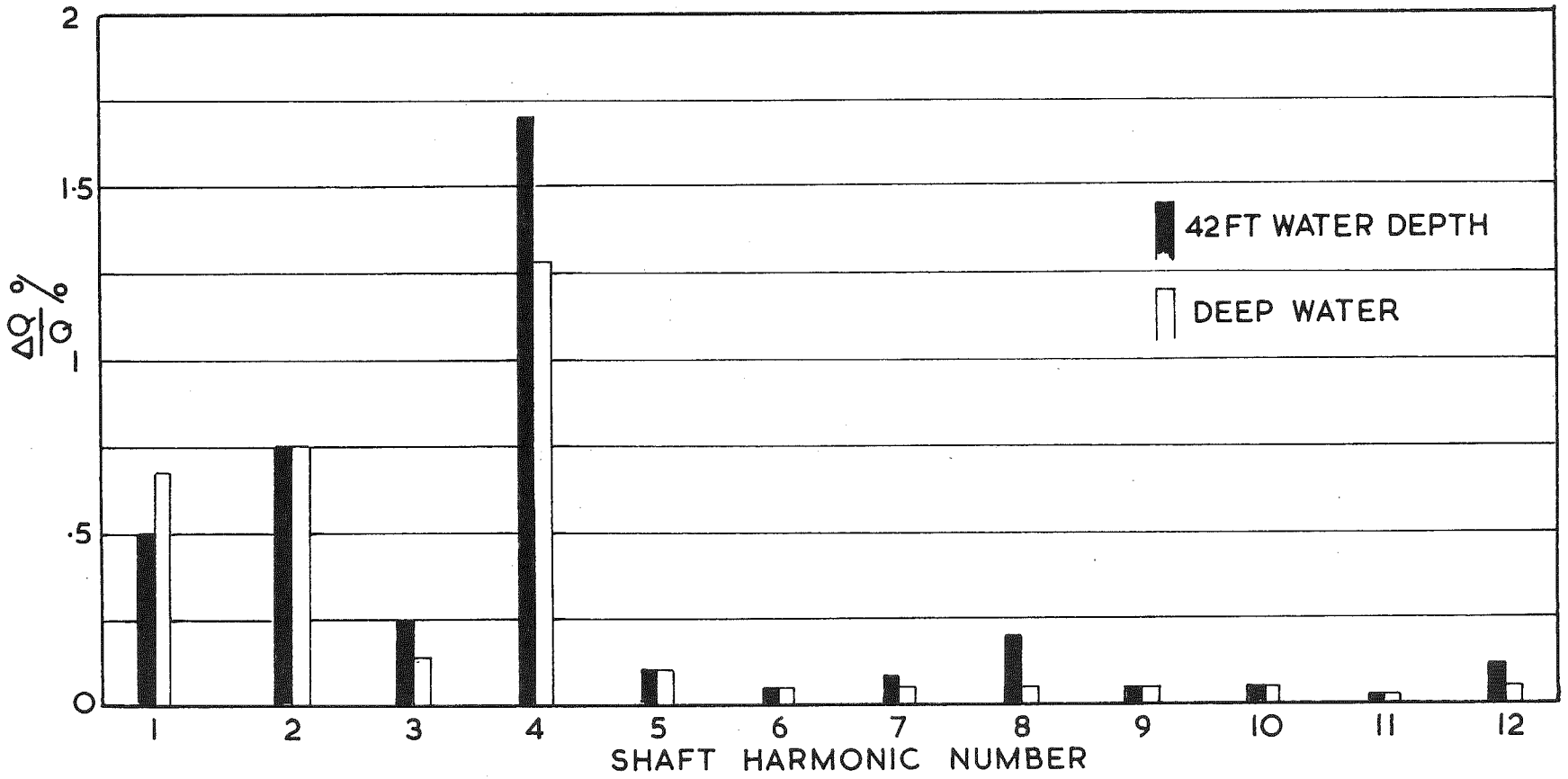
2
1·5
1
·5
0
ΔQ/Q %
42FT WATER DEPTH
DEEP WATER
1
2
3
4
5
6
7
8
9
10
11
12
SHAFT HARMONIC NUMBER

Fig. 20.14 The semi-amplitudes ΔT of the harmonic components of shaft thrust (expressed as a percentage of mean thrust T) for shallow and deep water.

This figure also applies to the applied hydrodynamic thrust, since this is equal to shaft thrust.

(From Test Series B2-A, draft 30 ft, shaft speed 115 rpm nominal)

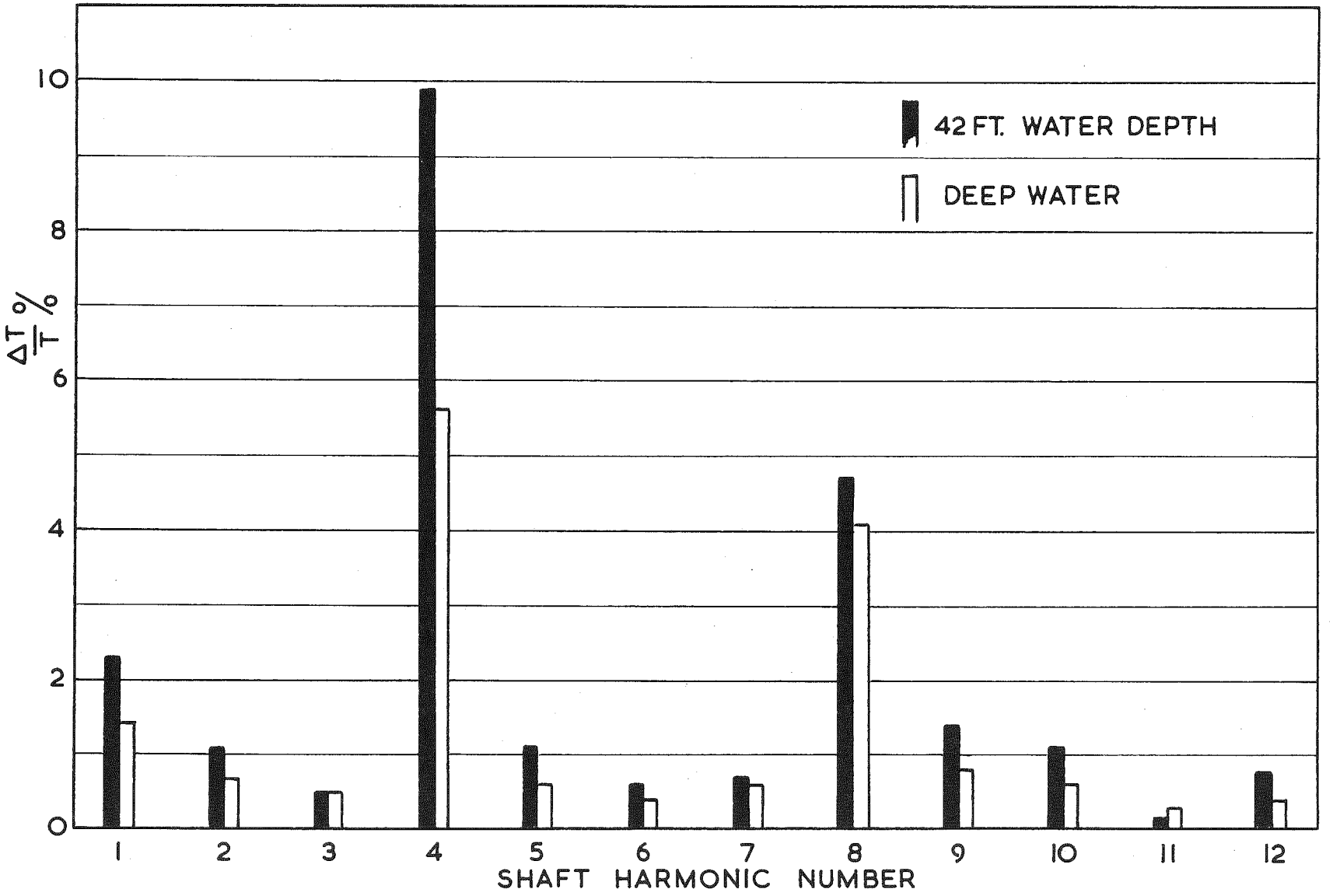
42 FT. WATER DEPTH
DEEP WATER
$\frac{\Delta T}{T}$ %
0
2
4
6
8
10
1
2
3
4
5
6
7
8
9
10
11
12
SHAFT HARMONIC NUMBER

Fig. 20.15 The semi-amplitudes ΔQ of the harmonic components of applied hydrodynamic torque (expressed as a percentage of mean torque Q), for various shaft speeds.
(The draft at which these results were taken was 22.5 ft for Test Series B1 and 30 ft for Test Series B2-B)

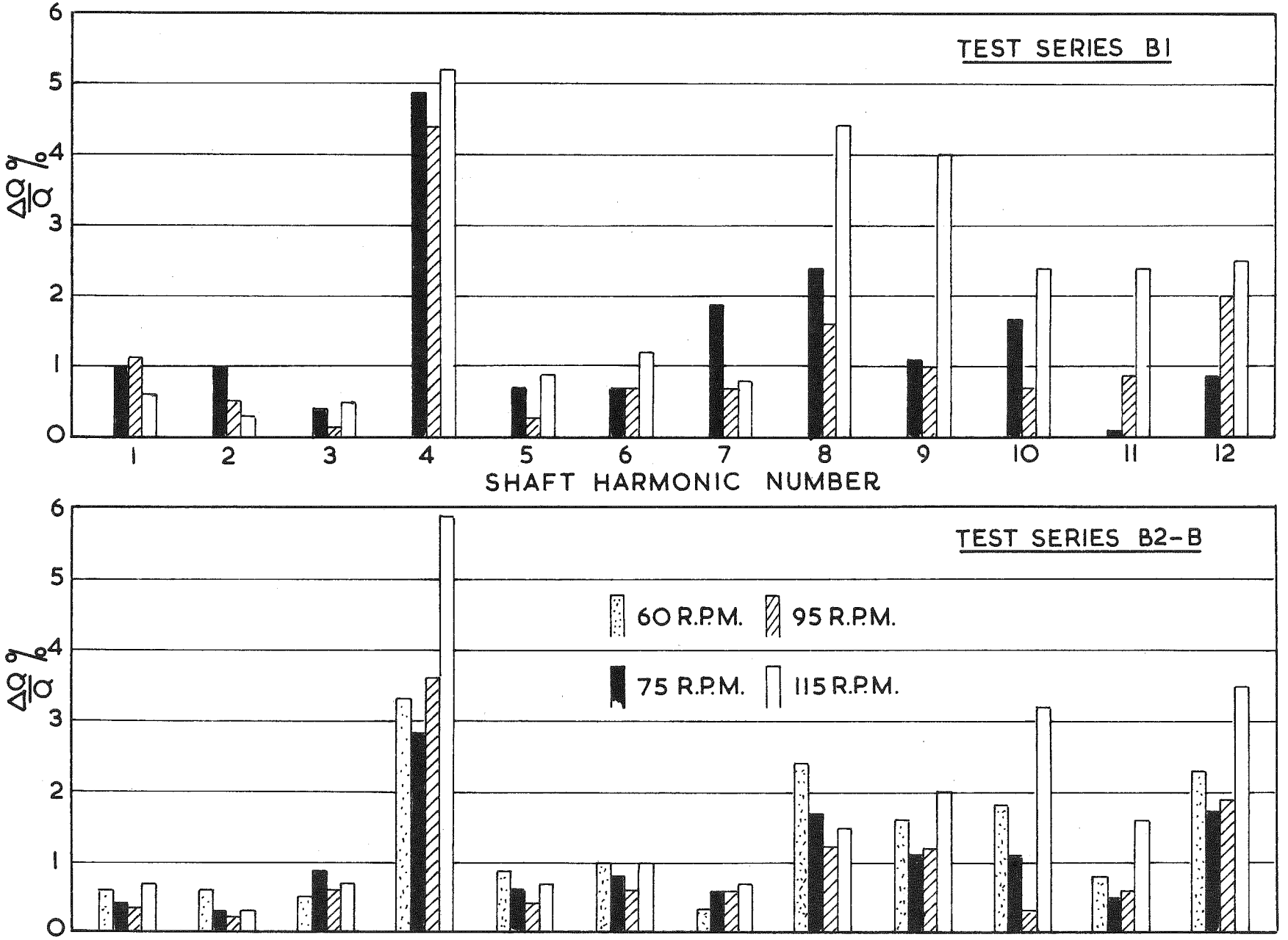
TEST SERIES B1
$\frac{\Delta Q}{Q}$ %
0
1
2
3
4
5
6
1
2
3
4
5
6
7
8
9
10
11
12
SHAFT HARMONIC NUMBER
TEST SERIES B2-B
60 R.P.M.
95 R.P.M.
75 R.P.M.
115 R.P.M.

harmonic of blade frequency) is as would be expected, the dominant component. The eighth harmonic, which might also be expected to be prominent, is significant in both torque and thrust cases (Cf. the shaft torque data in Fig. 20.11, in which the eighth harmonic is suppressed).

(2) In the torque results, the first, second and third harmonics are not as prominent as they were in the case of shaft torque (Fig. 20.11). On the other hand, harmonics 5 to 12 appear much more prominent than would be expected. For these higher harmonics however, the damping assumed in the mobility analysis is probably in some error, and this may partly account for the unusual results. It is likely, however, that the higher harmonics are quite significant. The reason for the difference between the sea trials and the voyage data is probably the same as is given in Section 20.2.2, sub section (2).

(3) The torque results generally show a definite increase in the semi-amplitudes of the components as the shaft speed increases. At the lowest speeds shown, there also appears to be an increase in amplitude.

(4) The applied hydrodynamic thrust results are the same as the shaft thrust results, and the remarks in Section 20.2.2 subsections (4) and (5) also apply.

The effect of sea depth on the torque and thrust components is shown in Figs. 20.16 and 20.14. The curves from which these Figures were abstracted are illustrated by Fig.20.17, which shows

Fig. 20.16 The semi-amplitudes ΔQ of the harmonic components of applied hydrodynamic torque (expressed as a percentage of mean torque Q) for shallow and deep water.
(From Test Series B2-A, draft 30 ft, shaft speed 115 rpm nominal).

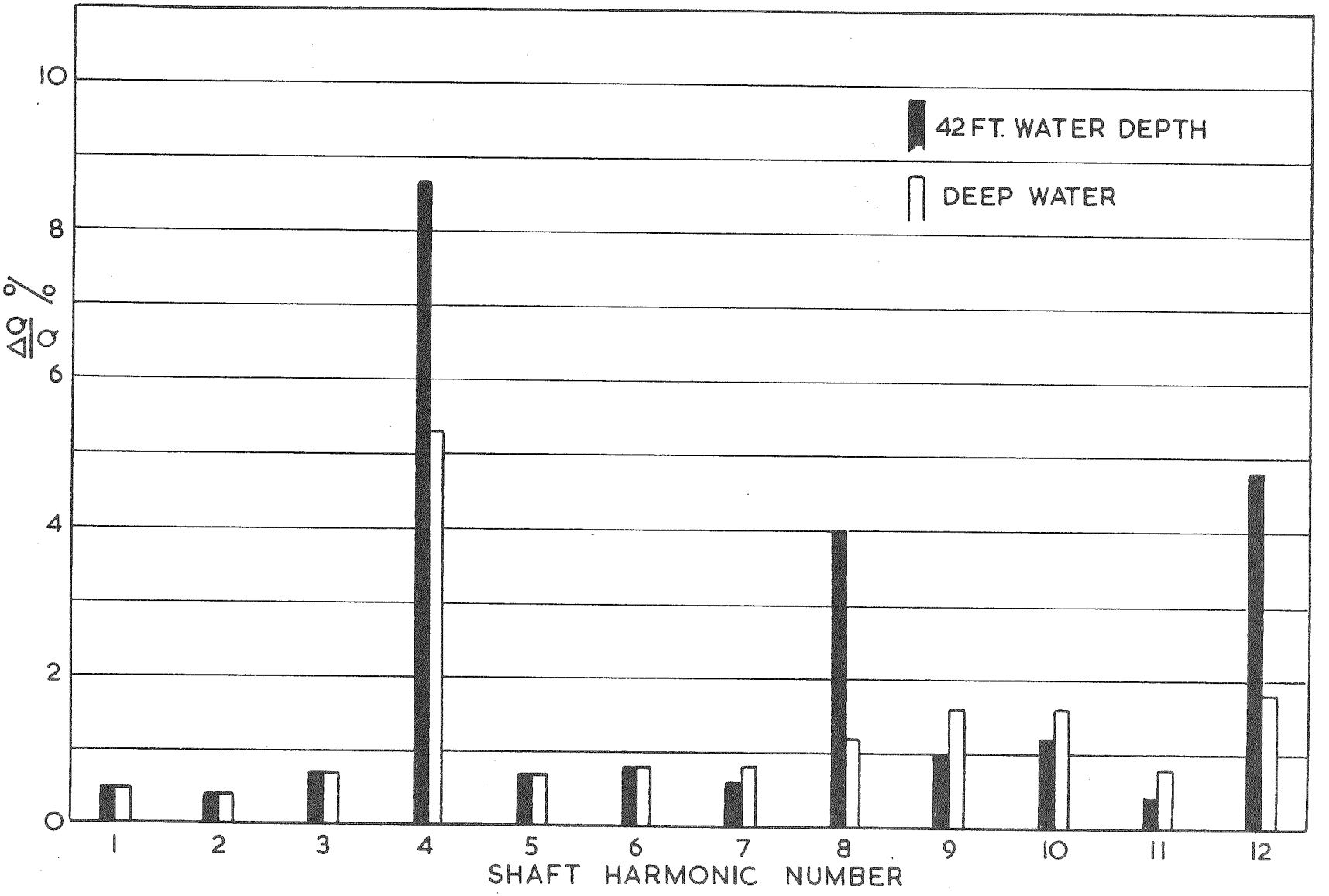
42 FT. WATER DEPTH
DEEP WATER
Δσ/σ %
0
2
4
6
8
10
1
2
3
4
5
6
7
8
9
10
11
12
SHAFT HARMONIC NUMBER

Fig. 20.17 The variation of semi-amplitudes ΔQ and ΔT of the fourth harmonic component of applied hydrodynamic torque and thrust (expressed as a percentage of mean torque and thrust respectively), with depth. (From Test Series B2-A, draft 30 ft, shaft speed 115 rpm nominal).

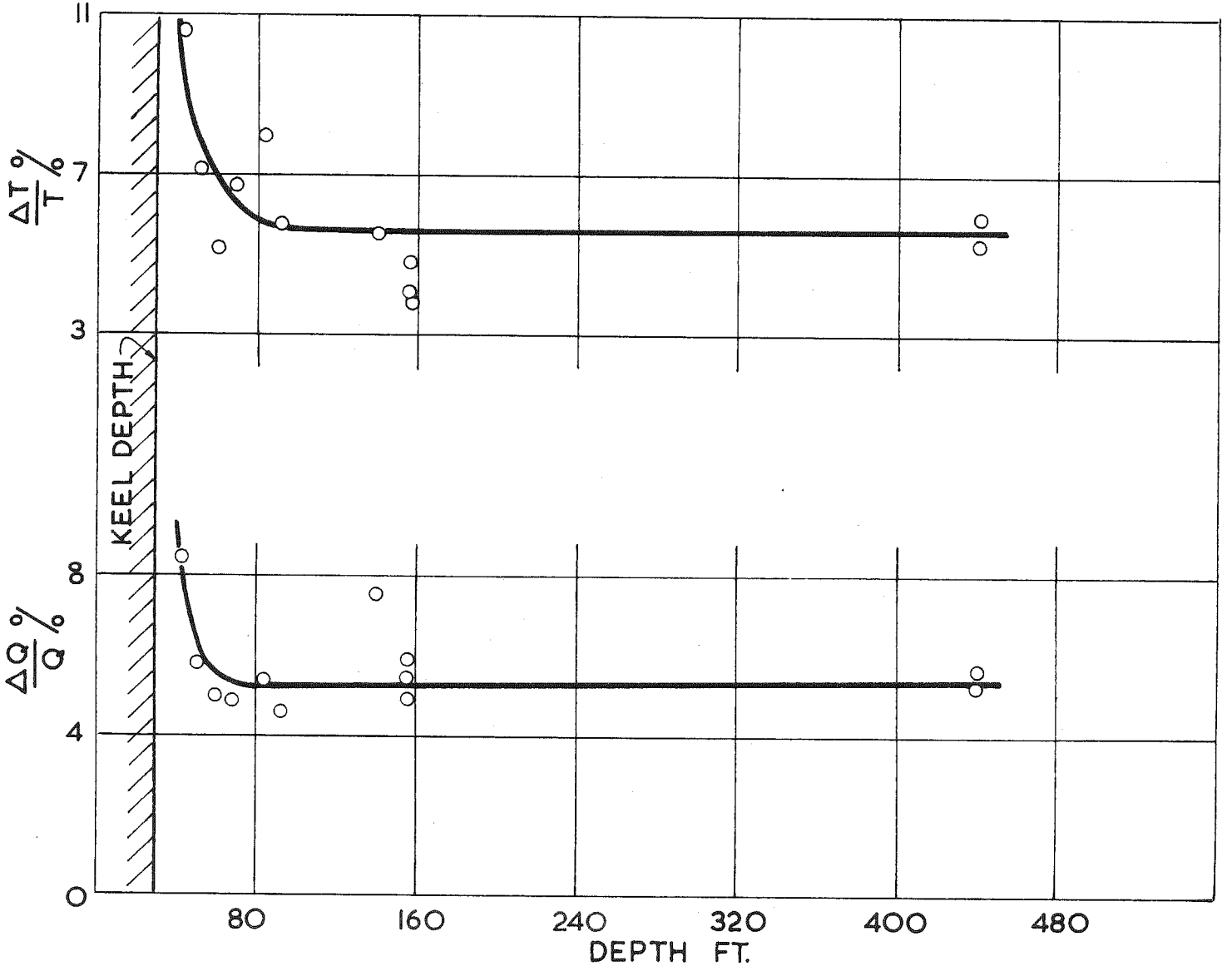
11
7
3
$\frac{\Delta T}{T}$ %
KEEL DEPTH
8
4
0
$\frac{\Delta Q}{Q}$ %
80
160
240
320
400
480
DEPTH FT.

the effect of depth on the fourth harmonic. It will be seen that depth has little effect until the depth under the keel is about three propeller diameters. When the depth under the keel is about two propeller diameters, the curves are beginning to turn sharply upwards. At the very shallow depths there is a marked increase in amplitude.

20.2.4 The Propeller Hydrodynamic Inertia

The hydrodynamic inertia of the propeller, calculated in the manner described in Chapter 18 and Section 20.1.3, are given in Table 20.1. These values are presented as percentages of the mechanical inertia of the propeller. It will be seen from this table that the hydrodynamic inertia varies only over the range 21 to 26 %. This is for a wide variation in operating conditions. The draft varies from 22.5 ft to 30 ft, the ship velocity varies from slow ahead to astern (probably slow), the sea depth varies from 34-96 ft, and the shaft speed varies from slow ahead to slow astern. The propeller amplitude varies from 0.16×10^{-3} to 2.43×10^{-3} radians.

These results reinforce the conclusion given in Chapter 13 (based on model tests), that is, that the hydrodynamic inertia of a propeller is primarily a function of its shape. The effect of amplitude of oscillation, propeller Reynolds number or propeller loading on the hydrodynamic inertia is small.

It is of interest to compare the average value obtained from the full-scale tests with those calculated from the Lewis and Burrill formulae. This comparison is given in Table 20.2.

TABLE 20.1

HYDRODYNAMIC INERTIA OF THE PROPELLER

Test Series	Draft	Ship Velocity	Sea Depth	Amplitude of torque oscillation in tail shaft (Peak-to-peak)	Angular amplitude of propeller oscillation (peak-to-peak)	Hydrodynamic inertia of the propeller as a percentage of the mechanical inertia			Remarks
						Vibration in Mode 1	Vibration in Mode 2	Average of Modes 1 & 2	
	ft	knot	ft	Ton-ft	(radian x10^{-3})	%	%	%	
B1	22.5	very slow	34-50	7.2	2.04	26.7	22.2	24.5	Shaft stopped then rolled slowly forward
B1	22.5	very slow	34-50	2.28	0.65	28.7	24.0	26.4	Shaft just moving forward
B1	22.5	very slow	34-50	1.96	0.55	28.0	23.5	25.8	Shaft stopped then just moving forward
B1	22.5	very slow	34.50	1.64	0.47	23.3	19.3	21.3	Shaft stopped then just moving forward
B1	22	0	34	0.57	0.16	27.3	23.0	25.2	Dock trials - shaft rotating at 3 rpm
B1	22	0	34	1.88	0.54	24.5	20.5	22.5	Dock trials - shaft slowly accelerating through 25 rpm
B1	22.5	11.0	50-70	6.5	1.87	24.0	20.0	22.0	Shaft stopped
B1	22.5	astern (velocity unknown)	50-70	7.8	2.2	28.0	23.5	25.8	Shaft slowing to a stop
B2-A	30	slow	96	6.5	1.87	28.0	23.5	25.8	Shaft just beginning to move ahead
B2-A	30	slow	96	2.03	0.57	23.3	19.3	21.3	Shaft just stopping
B2-A	30	slow	96	7.26	1.96	26.0	21.7	23.9	Shaft slowing down from astern

TABLE 20.1

HYDRODYNAMIC INERTIA OF THE PROPELLER

Contd.

Test Series	Draft	Ship Velocity	Sea Depth	Amplitude of torque oscillation in tail shaft (Peak-to-peak)	Angular amplitude of propeller oscillation (Peak-to-peak)	Hydrodynamic inertia of the propeller as a percentage of the mechanical inertia.			Remarks
						Vibration in Mode 1	Vibration in Mode 2	Average of Modes 1 & 2	
	ft	knot	ft	Ton-ft	(radian x10^{3})	%	%	%	
B2-A	30	slow	96	8.6	2.43	28.7	24.0	26.4	Shaft stopped
B2-A	30	very slow	40-60	1.95	0.55	28.0	23.5	25.8	Shaft just starting to rotate forward
B2-A	30	very slow	40-60	6.4	1.81	28.0	23.5	25.8	Shaft just stopping
B2-A	30	very slow	40-60	4.45	1.26	28.7	24.0	26.4	Shaft rolling slowly astern after stopping
B2-A	30	very slow	40-60	5.42	1.53	27.3	23.0	25.2	Shaft stopping from slow astern, then rolling forward
B2-A	30	very slow	40-60	2.36	0.67	26.0	21.7	23.9	Shaft rolling forward after being stopped
B2-A	30	very slow	40-60	1.81	0.51	24.5	20.5	22.5	Shaft rotating forward slowly
B2-A	30	very slow	40-60	4.17	1.18	28.0	23.5	25.8	Shaft rolling astern, then stopping
B2-A	30	very slow	40-60	3.47	0.98	26.0	21.7	23.9	Shaft rotating astern
							Average =	24.5	

(The Lewis formula is given as equation (12.1) and the Burrill formula as equation (12.5) in Chapter 12). The value used for the propeller mechanical inertia was 4.45×10^5 lb - ft^2, calculated from the propeller drawing.

TABLE 20.2

EXPERIMENTAL AND CALCULATED VALUES OF HYDRODYNAMIC INERTIA

Experimental Average %	Lewis formula %	Burrill formula %
24.5	16.4	17.8

It will be noted that the calculated values are rather lower than the experimental values.

CHAPTER 21

CONCLUSIONS AND RECOMMENDATIONS

21.1 CONCLUSIONS

From the results obtained in the full-scale ship tests, the following conclusions may be drawn:-

(1) There is a greater variation in the harmonic components of torque and thrust from instant to instant, during apparently steady conditions, than is generally realized. This applies to both shaft and applied hydrodynamic torque and thrust. This scatter would appear to be associated with variations in speed, wind, seaway and ship motion, rather than with interchange of energy between modes of vibration of the shaft system.

(2) There are more significant components in the torque and thrust waveforms than are generally realized. The most significant component is generally that at blade frequency. The component at twice blade frequency is often prominent, but the component at three times blade frequency is only significant under certain conditions. The components at one, two and three times shaft frequency are (surprisingly) prominent under many conditions.

(3) The amplitudes of the harmonic components and their distribution with frequency, depends markedly on ship speed, water depth draft, and the degree of fouling of the hull (and also on wind).

(4) There is a pronounced increase in amplitude of the harmonic components as the water depth under the keel decreases below two propeller diameters.

(5) Harmonics above the 12 order of shaft rotational speed are generally insignificant.

(6) Phase angle relationships generally show very poor correlation.

(7) The amplitudes of the components of applied hydrodynamic torque and thrust generally increase with increase of shaft speed. The components of tailshaft torque, for this particular ship, remained practically constant as the speed increased to higher values, due to the dynamic characteristics of the shaft system. The components of tailshaft thrust showed the same trends as in the case of applied hydrodynamic thrust.

(8) Because of the effects discussed in paragraphs (1) (2) (3) (4) (6) above, the difficulties in the way of obtaining precise measurements of harmonic components of torque and thrust for use as a basis of comparison with model tests or calculated results, are greater than previously realized.

(9) The effect of variations in amplitude of oscillation, propeller Reynolds number, and propeller loading on the hydrodynamic inertia of a propeller would appear to be small, over quite wide ranges of these parameters. Estimated values of hydrodynamic inertia for the propeller of the

ore-carrier from the Lewis and Burrill formulae are appreciably lower than the experimental values.

21.2 RECOMMENDATIONS

(1) Since it is absolutely necessary to have reliable, precise values for the amplitudes of the harmonic components of applied hydrodynamic torque and thrust, to form a basis for comparison with the results of model tests and theoretical calculations, it is recommended that further ship testing be carried out.

(2) In further ship tests, a statistical approach will be necessary because of the scatter in the data. This means the collection of even large quantities of data than in the previous tests. It may be advisable to use a spectral analysis approach in the processing of this data. It is therefore recommended that future data be recorded on magnetic tape in the field, either in digital or in analague form. The simplest method would be to record the waveforms by amplitude-modulation of a high-frequency carrier wave. The tapes could subsequently be cut into sections, and these sections formed into loops. The loops could then be run through an (electronic) harmonic analyser, to obtain the harmonic components. An increased tape speed could be used if necessary.

(3) It is recommended that future ship tests be co-ordinated with model tests or theoretical calculations.

(4) It is also recommended that an attempt be made to correlate the existing ship data with model tests or theoretical calculations.

(5) It is suggested that in future ship tests, measurements be made of the fluctuating surface pressures on the afterbody of the hull, to gather some full-scale information on surface forces and moments.

PART VI

RESEARCH ON

LOW - VIBRATION PROPULSION

CHAPTER 22

RESEARCH ON LOW-VIBRATION PROPULSION

22.1 INTRODUCTION

It is apparent, that a stage has been reached in the evolution of the displacement vessel, at which the propeller-excited vibrations are on the point of exceeding (and have exceeded in some cases) the level which can be considered as acceptable. Since the problem is likely to become more serious (see Section 1) it was considered that research directed towards low-vibration propulsion would be worthwhile. Accordingly, at the beginning of 1962, an investigation was begun on possible configurations of propulsion systems for large displacement vessels, which would have inherently lower vibration characteristics than the conventional propeller.

If the propulsion system is to be theoretically vibrationless, there must be no fluctuating forces generated. If the energy transfer in the propulsive unit is to be by rotodynamic means (i.e. by a rotor), then physical reasoning indicates that the following two requirements must be satisfied if there are to be no unsteady forces generated. The first requirement is that the velocity field relative to each blade should not change in magnitude or direction (i.e. the velocity field should be symmetric about the axis). This will mean that the blade forces will then be steady with time. The second requirement, which is in some degree inter-related with the first, is that the net forces due to the blade pressure fields on the boundaries be invariant with time. This can only be achieved with a finite number of rotor blades if the solid boundaries in the proximity of the rotor are symmetrical

around the axis.

These two requirements can be summarised as : symmetry of flow and boundaries, about the axis. Although this ideal may be impossible to achieve in practice, it can be shown that the closer it is approached, the smaller will be the unsteady forces. This applies to both requirements. Enclosing the rotor in a rigid duct for example, since it satisfies the boundary symmetry condition will reduce the unsteady surface forces even though the rotor may remain operating in a non-symmetric flow and be generating considerable unsteady rotor forces.

A number of configurations which wholly or partly satisfy the above requirements have been considered. These fall basically into two groups:

(a) "Open" configurations in which the rotor is relatively distant from solid boundaries, and in which the rotor operates in either a uniform or axially symmetric fluid stream.

(b) "Enclosed" systems in which the rotor is enclosed by axially symmetric boundaries, and operates in an axially symmetric fluid stream. A variant of this type is the rigid duct system mentioned above in which the requirement on axial flow symmetry is relaxed.

The following configurations, which would have inherently low vibration characteristics, were considered:

1. Conventional screw propeller behind a hull with modified after-body.
2. Various configurations with the propeller mounted at or forward of the bow.
3. Various multi-hull configurations in which the propeller

or propellers would operate in more uniform wakes than with the conventional screw system.

(4) A submersible hull consisting of a cigar-shaped main body completely submerged with a narrow streamlined superstructure protruding above the waterline.

(5) A hull with propulsive units in pods on outriggers.

(6) Various forms of internal duct system (hydraulic jet propulsion or hydro-jet)

During 1962 a comparison was made between the characteristics of the various configurations. Some of the criteria which were considered were estimated overall efficiency, vibration level, steering power, off-design performance, fouling deterioration, and damage susceptibility. This preliminary study indicated that although some of the configurations would be suitable for various special-purpose vessels, only the "rigid duct" system showed possibilities as a replacement for conventional propellers on large surface-displacement vessels. Work has been concentrated, therefore, on this configuration, which has been named "hydro-jet" propulsion.

A general analysis of the hydro-jet system has been carried out, which has indicated the significant parameters and their relationship. Subsequently, a project study has been carried out for a 19,000 ton ore-carrier propelled by a dual hydro-jet system, to determine whether a satisfactory compromise could be reached between the hydrodynamic requirements and the structural, machinery, and other requirements of the vessel. The results were sufficiently encouraging

to justify further work, and this project is being continued, by M.R.Hale, who has been engaged on the low-vibration propulsion investigation since its commencement (as a post-graduate student under the supervision of the author). A model ducted-jet system is at present being constructed by Hale for testing in the 18" research water tunnel later in 1964, to determine vibration and performance characteristics. If the results of the model studies show sufficient promise, the construction of a 20 foot self-propelled model of a dual hydro-jet system is contemplated.

22.2 THE VIBRATION CHARACTERISTICS OF A HYDRO JET SYSTEM

One of the propulsive units for a dual "hydro-jet" system (one on each side of the ship) is shown in Fig. 22.1. Flow enters through the intake at station 1, passing along the duct, through the very high specified-speed impeller, through the stator vanes which remove the rotation imparted to the flow by the impeller, and out through the nozzle at station 4. The hub of the stator vanes contains the end-bearing for the tail-shaft. The thrust bearing is mounted inside the hull adjacent to the point at which the tail-shaft passes through the plating. The flow in the upstream section of the duct near the hull, splits to pass around the streamlined tail-shaft fairing before entering the impeller. A torsional isolater is mounted on the tail-shaft adjacent to the thrust bearing. If it is assumed that the duct is completely rigid and that the thrust bearing is fixed rigidly to the duct, then the nett mean force which this closed duct system will impart

Fig. 22.1 Diagrammatic layout of hydrojet system

(water - line section)

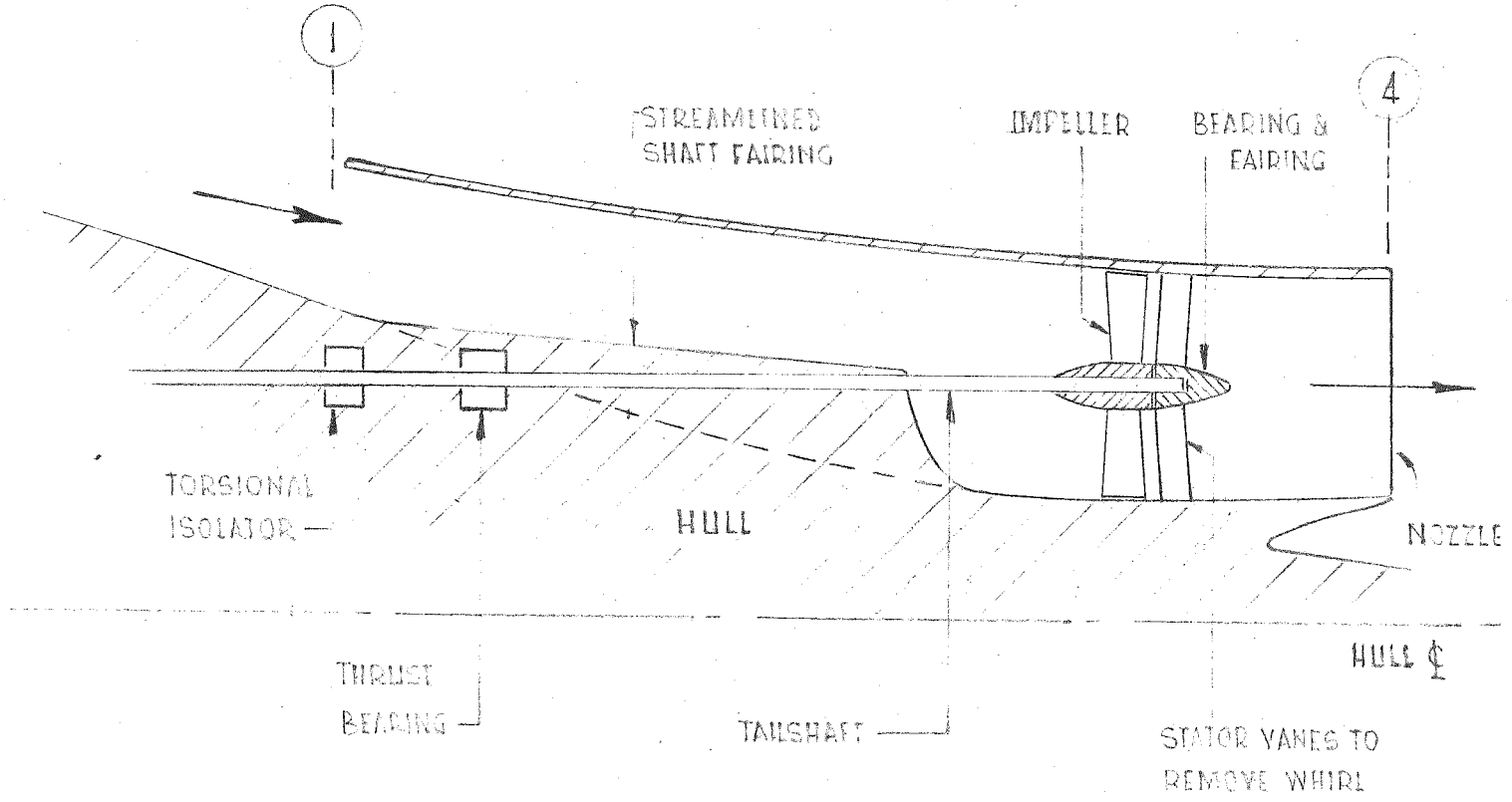
1
4
STREAMLINED SHAFT FAIRING
IMPELLER
BEARING & FAIRING
TORSIONAL ISOLATOR
HULL
NOZZLE
THRUST BEARING
TAILSHAFT
HULL ℄
STATOR VANES TO REMOVE WHIRL

to the hull will be equal to the momentum difference between the flow at stations 1 and 4. The flow at section 1 can be assumed to be steady although not necessarily uniform. The steadiness of the flow at station 4 will depend upon the distance between the impeller and the station. If this distance is sufficiently large, the trailing vortex sheets from the impeller and stator will have mixed to produce a fairly uniform turbulent flow. Although the momentum flux through station 4 will fluctuate about a mean value, the fluctuations will be small in comparison with the mean momentum flux. The thrust force which the duct applies to a ship will therefore be a steady mean force on which is superimposed small fluctuations. There will also be small surface fluctuating forces in the radial directions. The level of these vibrations will be very small, as compared with a conventional screw system. The fluctuating forces applied to the impeller may still be at an appreciable level, however. The use of a suitable torsional isolater in the tail-shaft might be used to reduce the torque fluctuations to a small level.

The above analysis assumes a rigid duct. In this case, the large surface fluctuating forces are to a large extent cancelled within the system. In practice, although the duct may be made very stiff with reinforcing rings etc., the duct deflections will reduce the effectiveness of the internal cancelling.

Information on the vibration characteristics of a ducted system will be obtained later in 1964 by Hale from a pressure survey along the duct surface during the model studies. The torque and thrust

fluctuations in the impeller shaft will be measured by the propeller dynamometer (described earlier in this thesis). As the duct is mounted on strain-gauged supports, the nett force on the duct will also be measured.

22.3 PERFORMANCE OF A HYDRO-JET SYSTEM

Consider the diagrammatic hydro-jet unit shown in Fig. 22.2. The hydrodynamic losses may be divided into two groups:

a. Impeller and stator losses.

b. The losses due to intake, duct, nozzle.

The losses associated with the impeller and stator are accounted for in the impeller efficiency η_E. The intake plus duct plus nozzle losses, which will be termed the ductwork losses, may be expressed as a fraction of the intake kinetic energy, on the basis of a dimensional analysis, i.e.

$$\text{Ductwork losses per unit mass flow} = \xi \left(\frac{V^2}{2}\right)$$

where ξ is termed the loss factor (22.1)

It may then be shown that the performance of the system can be represented by curves such as shown in Fig. 22.3. This figure has been plotted using an impeller-stator efficiency of 0.90, as it has been estimated (see Ref. 22.1) from high specific-speed axial-pump data that this efficiency should be obtainable for the large size impellers here considered. The adverse effect of increase in loss factor ξ on the overall propulsive efficiency is clearly seen. On the

Fig. 22.2 Schematic diagram of hydrojet system

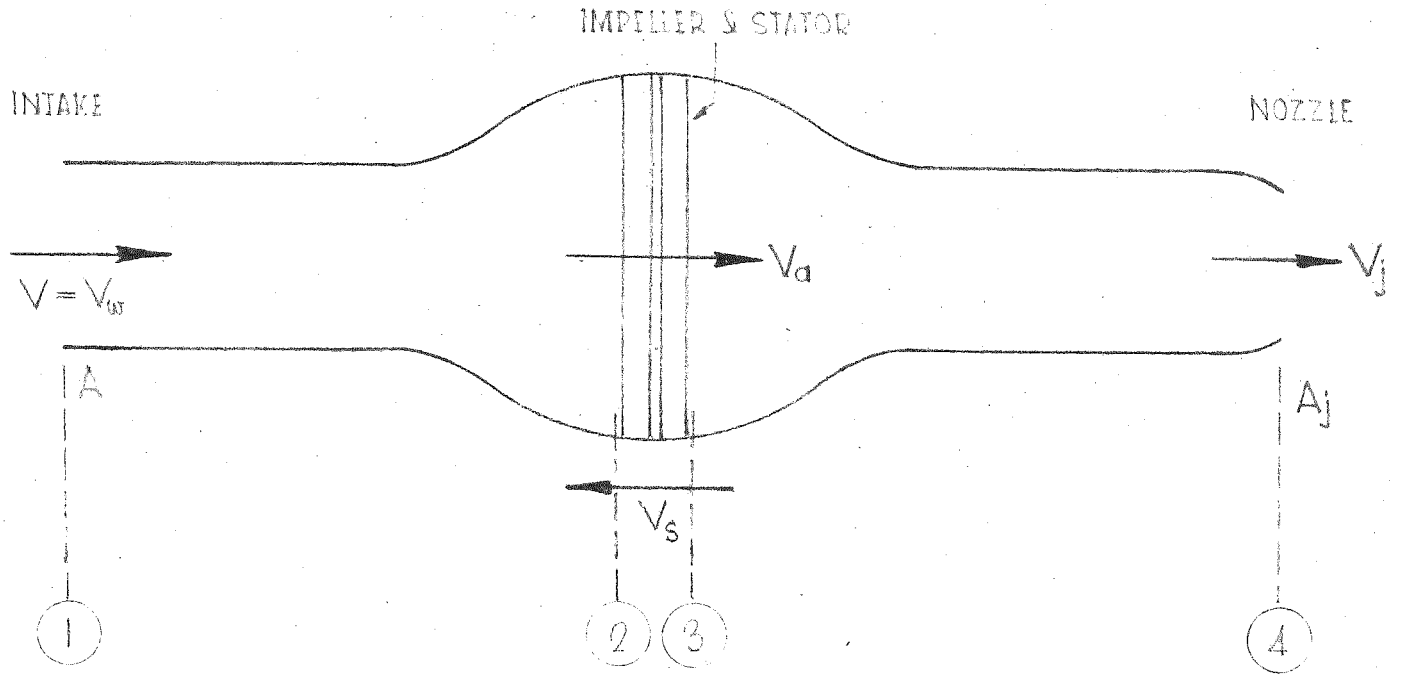
IMPELLER & STATOR
INTAKE
NOZZLE
V = Vw
Va
Vj
A
Aj
Vs
1
2
3
4

Fig. 22.3 Estimated performance of hydrojet unit

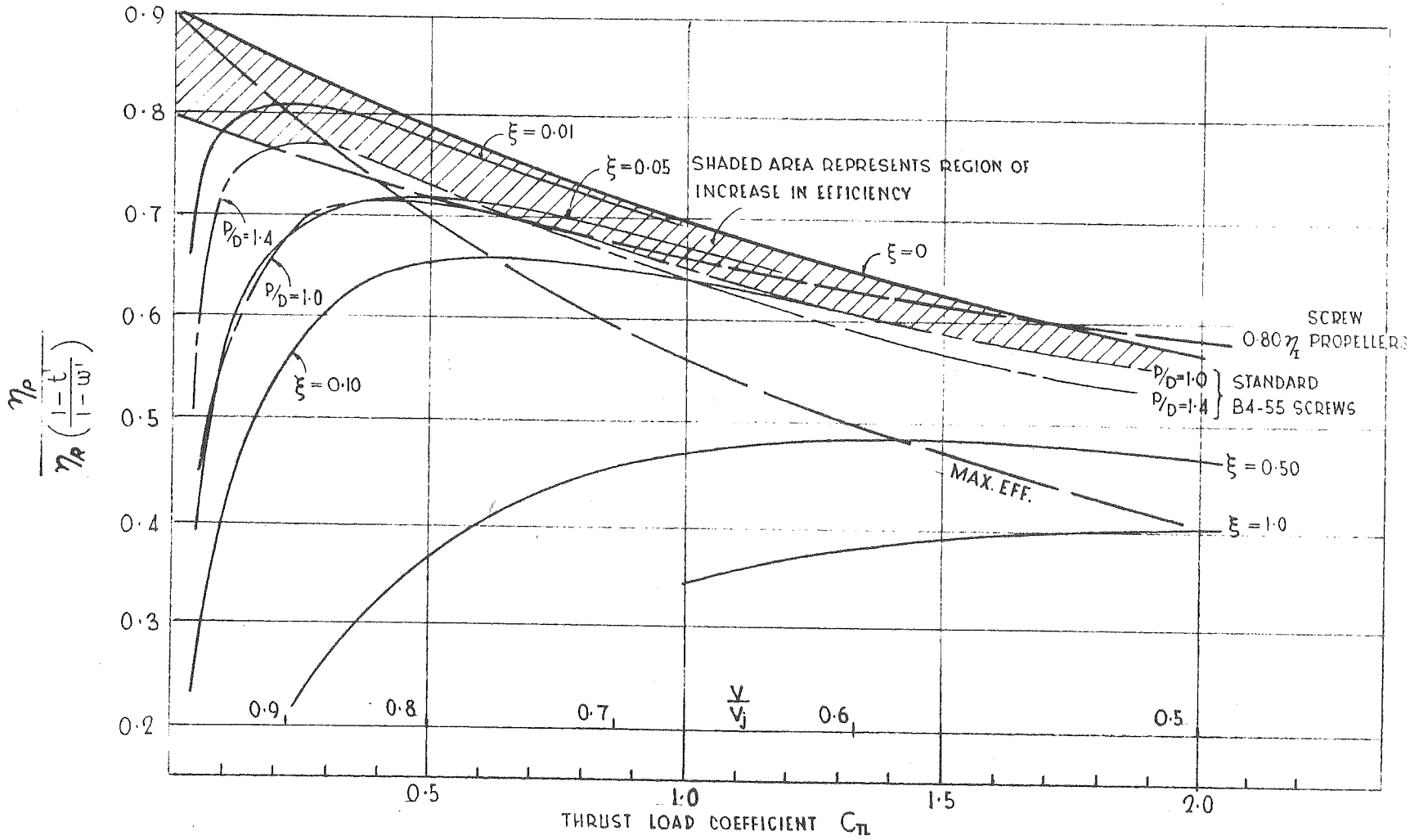

FIG. ESTIMATED PERFORMANCE OF HYDRO-JET UNIT

(An impeller efficiency η_I of 0·90 has been assumed.)

diagram, for comparison, there has been plotted the characteristics of the standard B4-55 Screw Series for pitch diameter ratios of 1.0 to 1.4. The 0.80 x Ideal (Froude) efficiency line for screw propellers has also been plotted on the diagram, as this is often taken in practice as representing the upper limit of efficiency for normal screw operation. It will be seen that the ducted system offers a potential increase in efficiency (particularly at the lower thrust load coefficients) as compared with the screw propeller, provided that the loss factor ξ is kept below about 0.10.

Actually, the performance of the hydro-jet system is more favourable than would appear at a first glance from the diagram. In order to compute the overall propulsive efficiency η_p from the diagram, it is necessary to know the value of the thrust deduction factor t' and the wake fraction w'. The values of thrust deduction and wake fraction will depend upon the ship propulsion-system configuration. The values for screw propulsion are given in the literature. No information of this nature is available for the hydro-jet system. However, it can be deduced that the thrust deduction for the hydro-jet system will be smaller than for the screw configuration, and the wake fraction of the same order as the screw configuration. This means that the hydro-jet efficiency will be more favourable than the shaded area would indicate on Fig. 22.3.

The reason why the thrust deduction is less for the hydro-jet unit is that the low-pressure region on the after-body of the ship caused

by the flow being accelerated into the propeller disc does not exist in the hydro-jet system, outside the duct, to any appreciable extant. Also, any region of slightly reduced pressure forward of the intake is on a surface substantially parallel to the hull axis and hence has only a small component in the direction of motion. (The propulsive thrust is always larger than the resistance of the hull without the propulsion unit, this difference being expressed mathematically by the "thrust deduction factor". The additional resistance associated with the low pressure region is a major component of this difference, for screw propeller ships).

The reason why the wake fraction for the hydro-jet would be of the same order as the screw system is because the intake shape would be made such as to swallow as much low-velocity fluid in the boundary layer as possible.

The results of a more detailed analysis are shown in Fig. 22.4. In this analysis, the ductwork losses have been equated to the frictional loss in the equivalent straight duct. The equivalent straight duct has been defined as a circular duct of cross-sectional area equal to the hydrojet intake area and whose length is such that the duct has a frictional loss equal to the ductwork loss of the hydro-jet unit being considered, at the same intake velocity. Only conditions of operation along the maximum efficiency line in Fig. 22.3 have been considered. The effect of variation of impeller efficiency, however, has been included in this diagram. It will be seen from Fig. 22.4 for example that in order to obtain a value $\eta_{p_{max}} \left(\frac{1-t'}{1-w'}\right)$ equal to 0.75, with an

Fig. 22.4 Optimum characteristics of hydrojet system

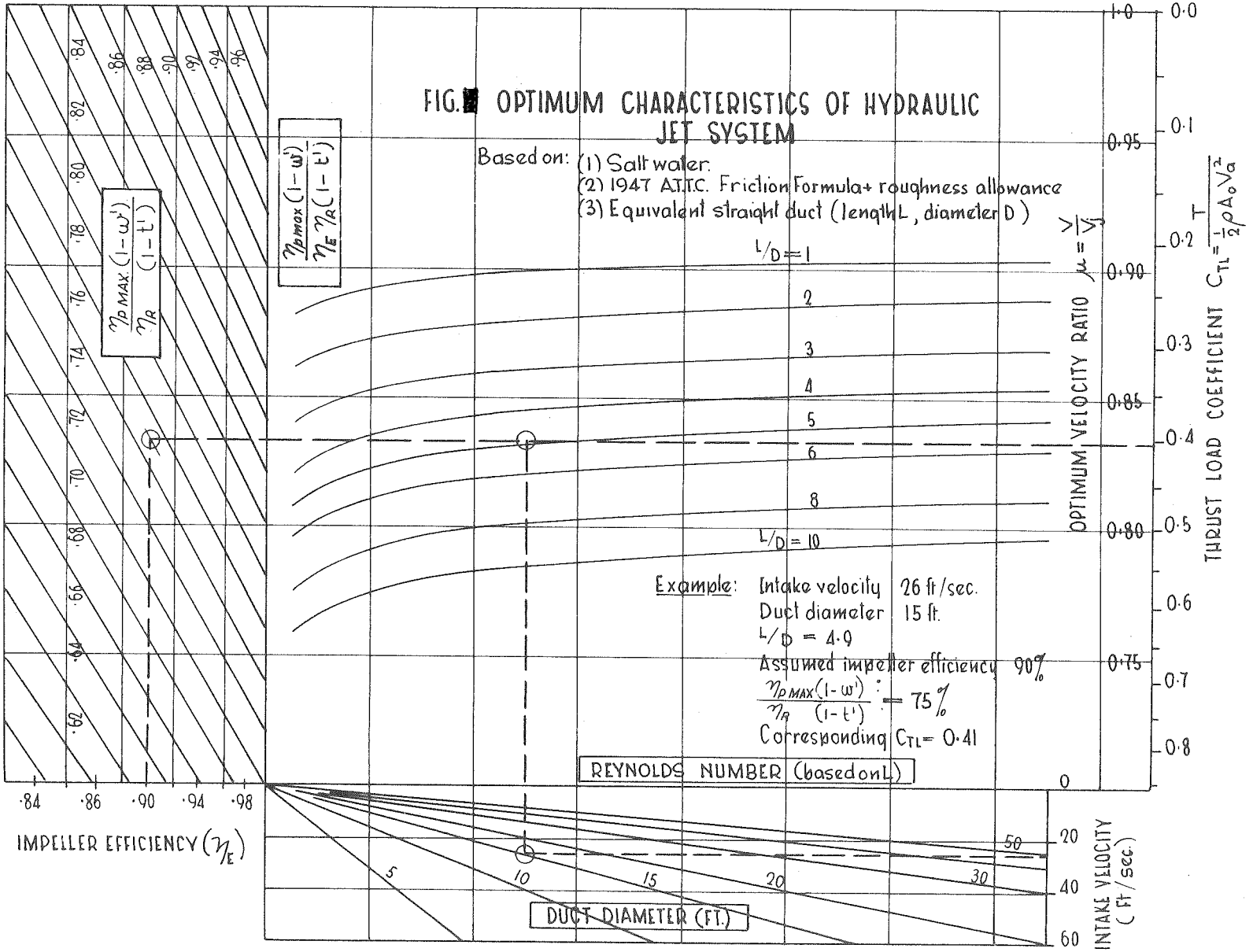
FIG. OPTIMUM CHARACTERISTICS OF HYDRAULIC JET SYSTEM
Based on: (1) Salt water.
(2) 1947 A.T.T.C. Friction Formula + roughness allowance
(3) Equivalent straight duct (length L, diameter D)
$\frac{\eta_{D\,MAX}(1-w')}{\eta_R(1-t')}$
$\frac{\eta_{D\,MAX}(1-w')}{\eta_E\,\eta_R(1-t')}$
L/D = 1
2
3
4
5
6
8
L/D = 10
Example: Intake velocity 26 ft/sec.
Duct diameter 15 ft.
L/D = 4·9
Assumed impeller efficiency 90%
$\frac{\eta_{D\,MAX}(1-w')}{\eta_R(1-t')}$ = 75%
Corresponding C_{TL} = 0·41
REYNOLDS NUMBER (based on L)
5
10
15
20
30
50
DUCT DIAMETER (FT.)
IMPELLER EFFICIENCY (η_E)
·84 ·86 ·88 ·90 ·92 ·94 ·96 ·98
·62 ·64 ·66 ·68 ·70 ·72 ·74 ·76 ·78 ·80 ·82 ·84
OPTIMUM VELOCITY RATIO $\mu = \frac{V}{V_j}$
1·0 0·95 0·90 0·85 0·80 0·75
THRUST LOAD COEFFICIENT $C_{TL} = \frac{T}{\frac{1}{2}\rho A_o V_a^2}$
0·0 0·1 0·2 0·3 0·4 0·5 0·6 0·7 0·8
INTAKE VELOCITY (Ft/sec.)
0 20 40 60

impeller efficiency of 0.90, the length to diameter ratio of the equivalent duct must be about 5.0 for a duct of 15 ft.diameter and an intake velocity of 26 ft/s.

If the configuration of the hydro-jet system approximates to a straight parallel duct, and if the intake and nozzle losses are small, this means that the actual hydrojet duct length will have to be about 5 impeller diameters if the 0.75 value is to be obtained for the diameter and intake velocity quoted. Achieving a value of 0.75 would mean (see Fig. 22.3) that the hydro-jet efficiency would be comparable with that of a screw propeller, for the lower values of thrust load coefficient. The advantage of a plot such as Fig. 22.4 is therefore that it can be used to indicate very rapidly the approximate dimensions of a hydro-jet system for any specified performance. A study of Figs. 22.3 and 22.4 indicates that in order to obtain satisfactory efficiency from a hydro-jet system, the duct length must be comparatively short, less than approximately 5-6 x the impeller diameter.

22.4 A PROJECT STUDY OF A HYDRO-JET SHIP

A project study has been carried out for a 19,000 ton ore-carrier propelled by a hydro-jet system. The primary aim of this study was to determine whether a duct system could be incorporated in such a vessel without causing excessive diffficulties in terms of shape, space, structural requirements, machinery lay-out, steering etc. A number of configurations were considered, but that shown in Fig. 22.5 was the only one which appeared to satisfy all the basic requirements. Although it is difficult

Fig. 22.5 Lines plan of 19,000 ton dual-hydrojet ore - carrier

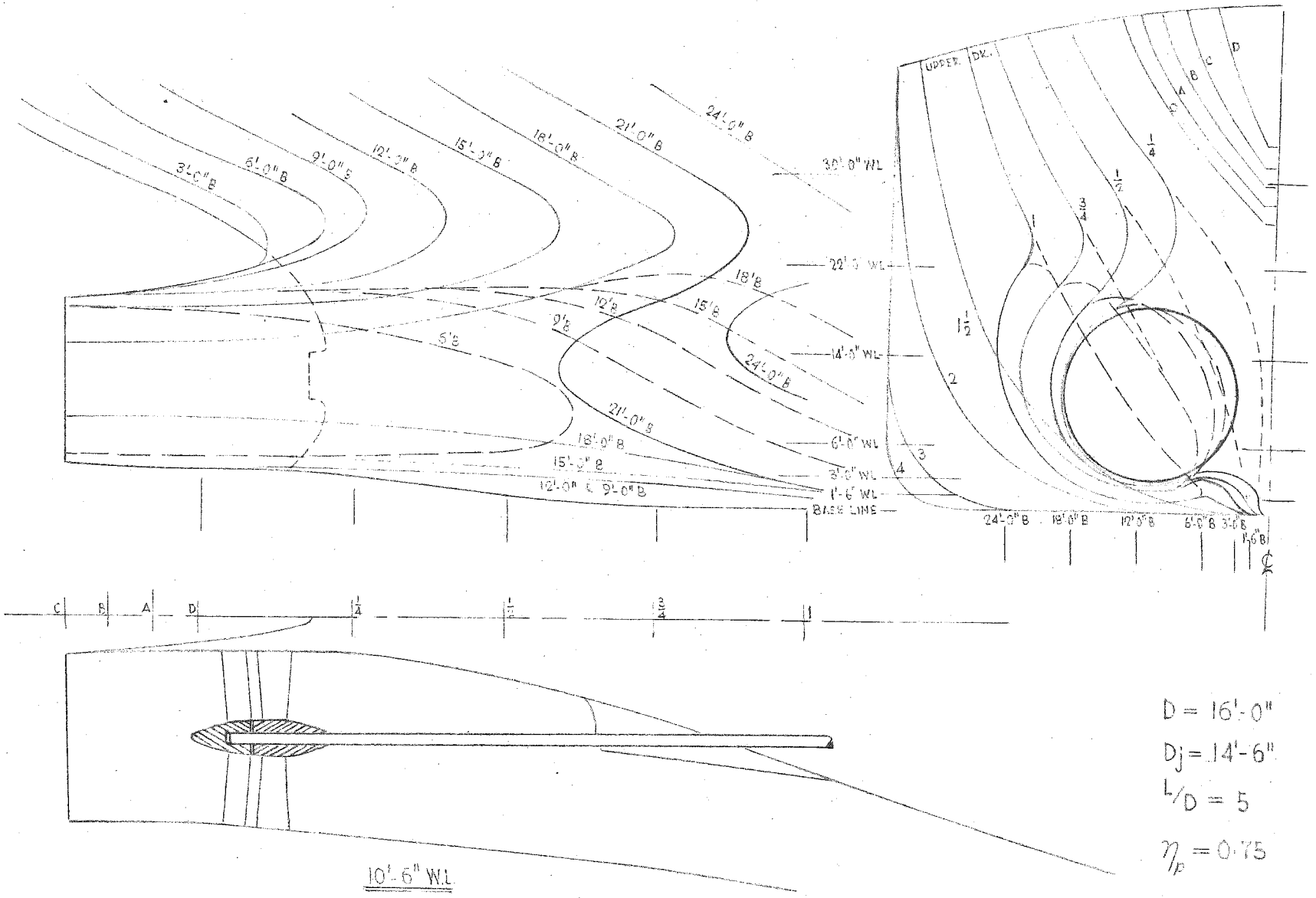

D = 16'-0"

Dj = 14'-6"

L/D = 5

η_p = 0·75

to make an accurate estimation of the thrust deduction and wake fraction which would be applied to such a configuration, conservative values of these factors were estimated and a value for the overall propulsive efficiency calculated. This indicated that an overall propulsive efficiency for the vessel of the order of 75 % might well be obtainable.

Consideration was also given to the problem of steering. Some form of swinging nozzle would appear to have advantages over the rudder immersed in the jet stream, both from the point of view of steering power and efficiency. The effect of fouling on the performance of the vessel was also considered. Although the fouling problem is by no means solved, the success of some of the treatments developed by the U.S.Navy indicate that fouling in the duct may not present insuperable difficulties.

22.5 DEFINITIONS AND SYMBOLS FOR A HYDROJET UNIT

Since the hydrojet unit differs in configuration from a conventional screw propulsion system, it is necessary to redefine certain parameters or coefficients so that they validly apply. A list of the symbols and definitions relevant to this chapter, and the figures therein is given below:-

V = Intake velocity

V_w = Wake velocity at intake

V_s = Ship velocity

A = Area of intake

A_j = Nozzle area

η_E = Impeller efficiency

η_p = Overall propulsive efficiency

$$= \frac{\text{E.H.P.}}{\text{shaft power}} = \frac{R.V_S}{\text{shaft power}}$$

R = Ship resistance (without propulsive unit)

T = Thrust of propulsive unit

t' = Thrust deduction factor defined by $R = T(1-t')$

w' = Wake fraction at intake defined by $V_w = V_s(1-w')$

V_a = Axial velocity through impeller annulus area A_o.

A_o = Impeller annulus area

C_{TL} = Thrust load coefficient

$$= \frac{T}{1/2\rho A_o V_a^2}$$

ρ = Mass density

APPENDIX I

THE STEADY TORQUE AND THRUST CHARACTERISTICS OF THE VARIABLE - PITCH PROPELLER

During the test programme described in Chapter 11, measurements were made of the mean torque and thrust of the variable-pitch propeller, under various conditions of operation. These included both positive and negative thrust regions. The results obtained are shown plotted in dimensionless form in Fig. I.1a and I.1b, for various nominal pitch settings. The dimensionless coefficients used are defined below:-

$$\text{Thrust coefficient } K_t = \frac{T}{\rho N^2 D^4} \qquad (I.1)$$

$$\text{Torque coefficient } K_Q = \frac{Q}{\rho N^2 D^5} \qquad (I.2)$$

$$\text{Advance ratio } J = \frac{V_A}{ND} \qquad (I.3)$$

where

T = thrust

Q = torque

N = rotational speed (Revolution /unit time)

D = propeller diameter

V_A = corrected tunnel velocity (See Appendix II)

ρ = fluid mass density

Fig. I.1 Dimensionless characteristics of the variable-pitch propeller

(a) Thrust coefficient K_t versus advance ratio J

(b) Torque coefficient K_Q versus advance ratio J

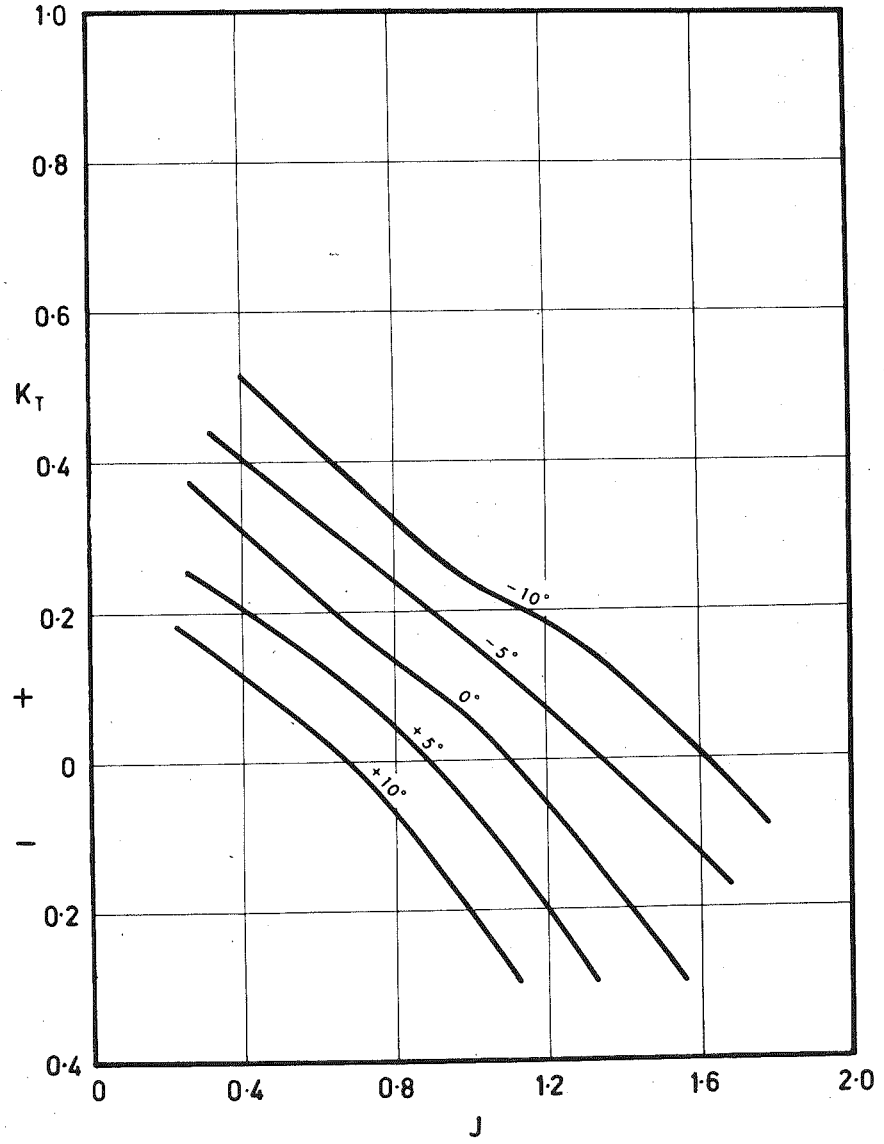
1·0
0·8
0·6
K_T
0·4
0·2
+
0
−
0·2
0·4
0
0·4
0·8
1·2
1·6
2·0
J
−10°
−5°
0°
+5°
+10°

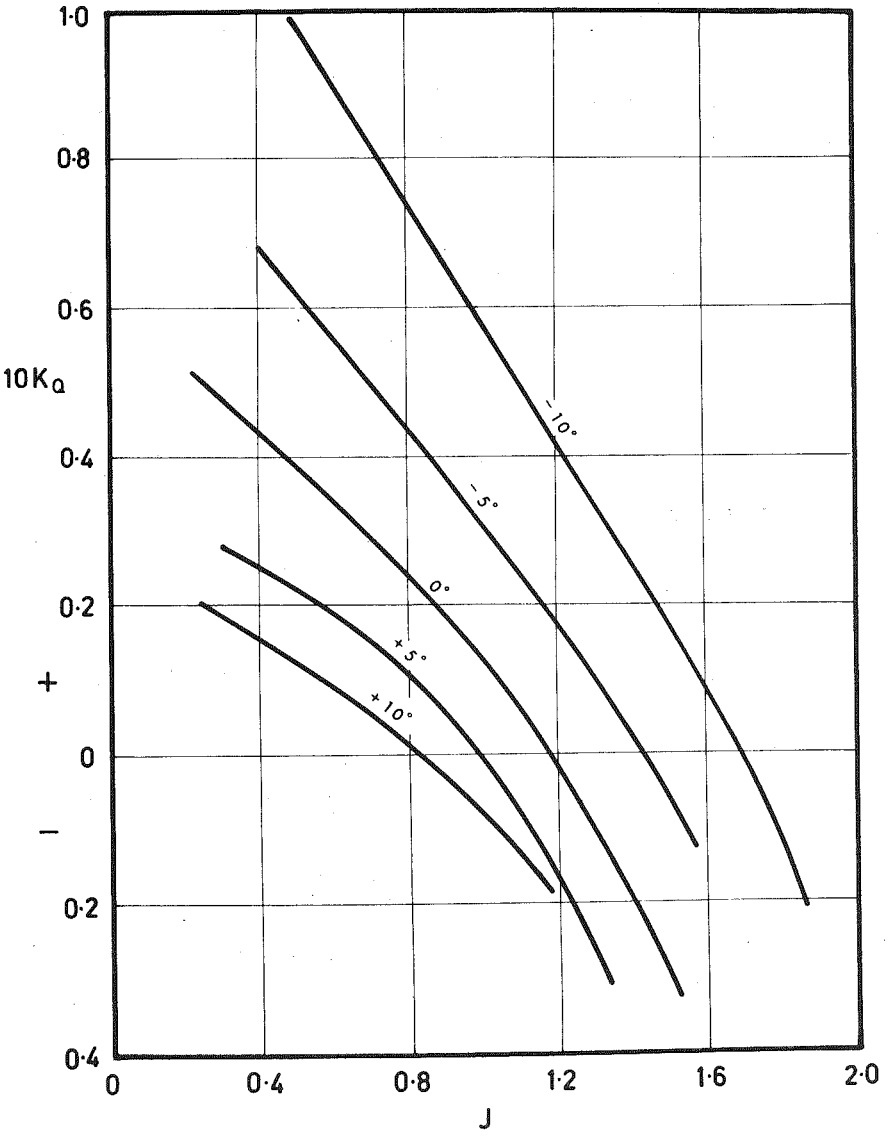
1·0
0·8
0·6
$10K_Q$
0·4
0·2
+
0
−
0·2
0·4
0
0·4
0·8
1·2
1·6
2·0
J
−10°
−5°
0°
+5°
+10°

APPENDIX II

GRAPHICAL CONSTRUCTION FOR PROPELLER REYNOLDS NUMBER

During the experimental work on the dynamometer it was necessary to estimate values of test parameters which would give test runs at approximately equally spaced intervals of advance ratio J, for given values of propeller Reynolds number R_n. At the same time, care had to be taken that the torque Q and thrust T were kept below the maximum allowable values. In addition, the tests had to be within certain ranges of tunnel velocity V and propeller rotational speed N. It was found that these calculations were lengthy and involved considerable trial-and-error, when calculated numerically, but could be speedily performed by using a graphical presentation derived by E.H.Watkins.

The formula for propeller Reynolds Number (at 0.7 radius) is

$$R_n = \frac{1}{\nu}\sqrt{V_A^2 + (0.7\pi DN)^2} \qquad \text{(II.1)}$$

where l = blade width at 0.7 radius

V_A = corrected tunnel velocity

D = propeller diameter

N = rotational speed (revolution/unit tine)

ν = fluid kinematic viscosity

The corrected tunnel velocity V_A is the "open-water" velocity for the propeller, calculated from the tunnel velocity V, by the method given in Ref. 11.9.

For a given propeller and given fluid this equation may be

rearranged as

$$k_1 R_n^2 = k_2 N^2 + V_A^2 \qquad (II.2)$$

where k_1 and k_2 are constants

This is of the form

$$C^2 = A^2 + B^2 \qquad (II.3)$$

This equation can be solved by means of the right-angle-triangle-inscribed-in-a-semi-circle construction shown in Fig. II.1. For a given value of the base C (i.e a given R_n), the value of B (and hence the value of V_A) can be found for any given value of A (i.e for a given value of N), and vice versa. Additional semi-circles of various diameters but with the same centre, drawn on the diagram extend the construction to a range of Reynolds numbers (See Fig.II.2) The common base-line of the semi-circles can (for a given propeller) be marked with a scale indicating the values of Reynolds number. If more convenient, the scale (suitably adjusted) can be marked on half the base line, using the centre as origin, as done in Fig.II.2. Lines of constant N, and of constant V_A, can also be plotted on the diagram as also shown in Fig. II.2. Similarly lines of constant T or Q or other propeller parameter can also be drawn.

The value of advance ratio J is given by

$$J = \frac{V_A}{ND} \qquad (II.4)$$

FIG. II.1 Right - angled triangle construction

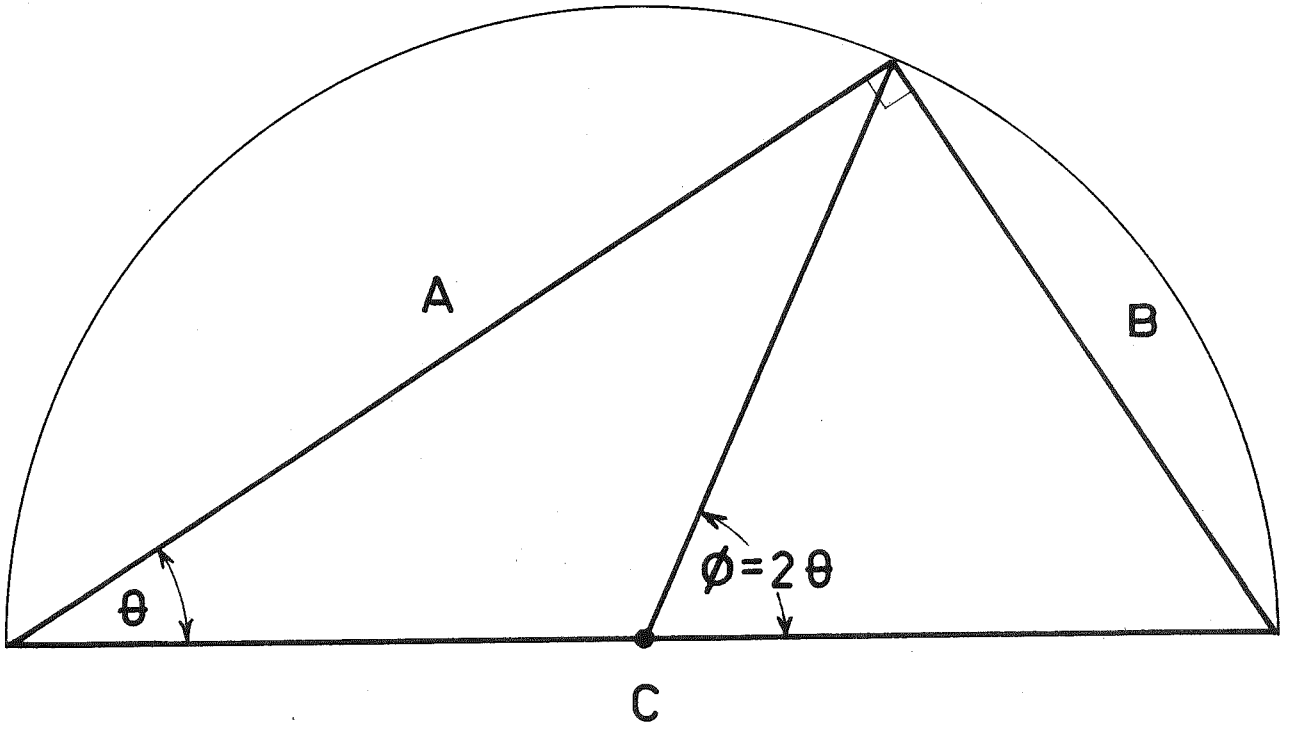
A
B
θ
Ø=2θ
C

Fig. II.2 Diagram relating Reynolds number R to tunnel velocity V and rotational speed N

MB 408 PROPELLER

$$N_{R_{0.7R}} = \text{Chord}_{0.7R} \cdot \frac{(V_a'^2 + [2\pi n \cdot 0.7R]^2)^{\frac{1}{2}}}{\nu}$$

$$3.13 \times 10^4 \cdot (V_a'^2 + [2.44 \cdot \frac{N}{100}]^2)^{\frac{1}{2}}$$

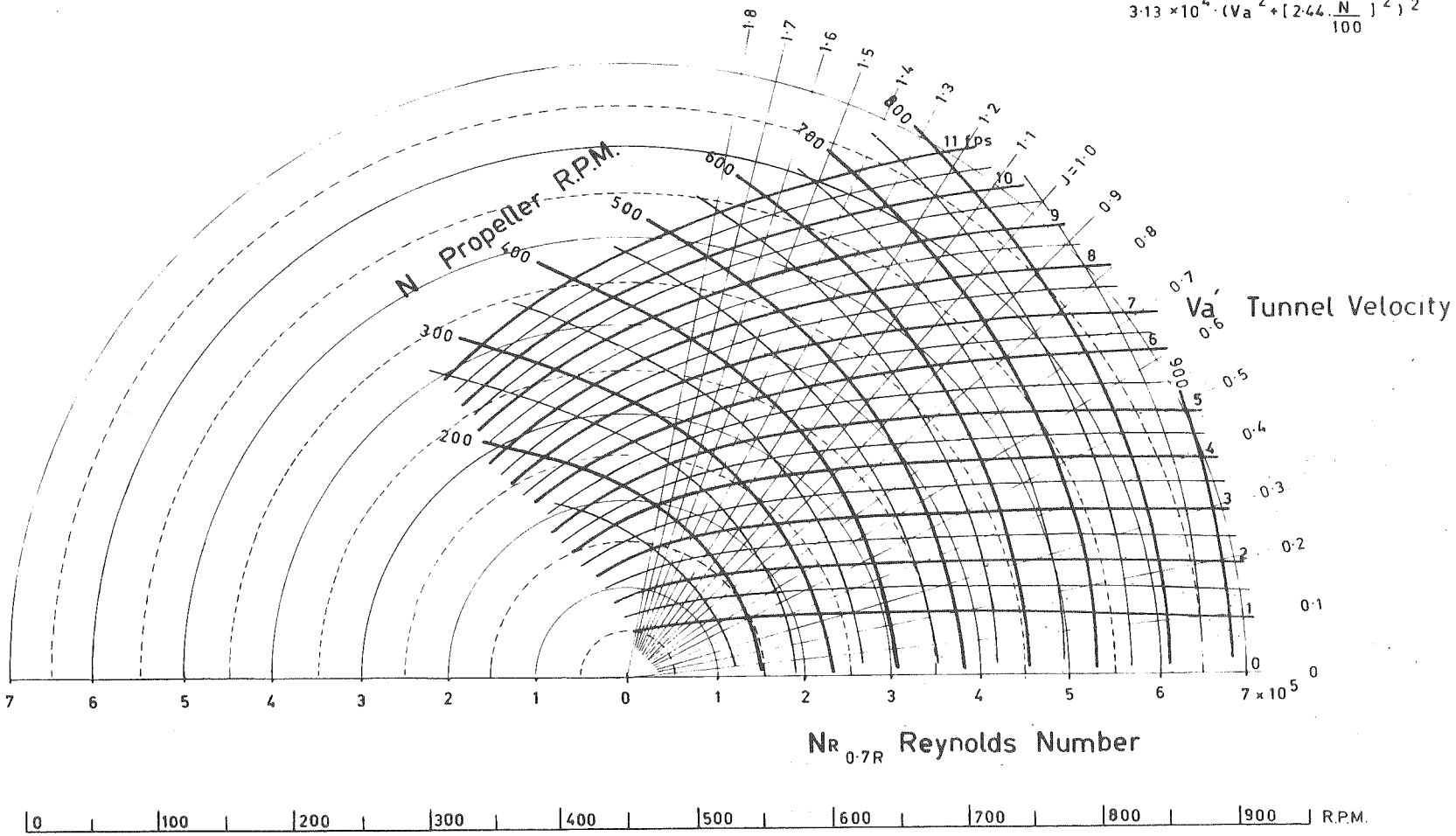

0 | 100 | 200 | 300 | 400 | 500 | 600 | 700 | 800 | 900 R.P.M.

Scale of N for the propeller

This may be written in terms A and B as

$$J = k \frac{B}{A} \qquad \text{(II.5)}$$

From Fig. II.1 this may be written as

$$J = k \tan \Theta \qquad \text{(II.6)}$$

$$\text{or} \qquad J = k \tan \frac{\phi}{2} \qquad \text{(II.7)}$$

The angle which a point on the diagram makes at the centre with the base line is thus related to the corresponding value of J. It should be noted from equation (II.7) that points along a given radius have the same value of J since they have the same value of ϕ. A scale of J values may thus be inscribed around the outer semi-circle, if desired, as is shown in Fig. II.2.

APPENDIX III

DIMENSIONLESS COEFFICIENTS OF TORQUE AND THRUST FLUCTUATIONS

The thrust T of a ship's propeller may be assumed to depend upon the shape parameters a,b,-- of the ship and propeller, the propeller diameter D, the hull roughness k, the shaft speed N, the fluid density ρ, the fluid viscosity μ, and the acceleration due to gravity g.

Thus

$$T = f(a,b,---,D,k,N,\rho,\mu,g) \qquad \text{(III.1)}$$

By dimensional analysis, these variables may be arranged in dimensionless graphs, in the following functional relationship

$$\frac{T}{\rho N^2 D^4} = f_1\left(\frac{a}{D}, \frac{b}{D} ---, \frac{k}{D}, \frac{\rho N D^2}{\mu}, \frac{N^2 D}{g}\right) \qquad \text{(III.2)}$$

Similary, the thrust fluctuations ΔT, whether peak-to-peak values of the thrust waveform, or amplitudes of the harmonic components of the waveform, may be assumed to depend upon the same variables as T does. By dimensional analysis, this relationship may be expressed in the following form:-

$$\frac{\Delta T}{\rho N^2 D^4} = f_2\left(\frac{a}{D}, \frac{b}{D}, ---, \frac{k}{D}, \frac{\rho N D^2}{\mu}, \frac{N^2 D}{g}\right) \qquad \text{(III.3)}$$

By dividing equation III.3 by III.2 is obtained the relationship:-

$$\frac{\Delta T}{T} = f_3 \left(\frac{a}{D}, \frac{b}{D}, --, \frac{k}{D}, \frac{\rho N D^2}{\mu}, \frac{N^2 D}{g}\right) \qquad \text{(III.4)}$$

Equation III.2 may be rearranged as

$$\frac{N^2 D}{g} = f_4 \left(\frac{a}{D}, \frac{b}{D} --, \frac{k}{D}, \frac{\rho N D^2}{\mu}, \frac{T}{\rho N^2 D^4}\right) \qquad \text{(III.5)}$$

Substituting this into III.4, gives

$$\frac{\Delta T}{T} = f_5 \left(\frac{a}{D}, \frac{b}{D}, --, \frac{k}{D}, \frac{\rho N D^2}{\mu}, \frac{T}{\rho N^2 D^4}\right) \qquad \text{(III.6)}$$

If geometrically similar ships or the same ship under different conditions, are only considered, the ratios $\frac{a}{D}$, $\frac{b}{D}$ --- are constants. If the roughness (i.e. the degree of fouling, if the ship has been in the water for sometime) is the same for the conditions considered, the ratio $\frac{k}{D}$ is a constant.

For many fluid phenomena it is known that at high Reynolds numbers, variation of Reynolds number has little effect on dimensionless coefficients which dimensional analysis has shown are strictly functions of Reynolds number. One example of this behaviour, is the relative constancy of the coefficient of friction for pipes and flat plates, at high Reynolds numbers. It may be tentatively postulated, by analogy,

that the Reynolds number term $\frac{\rho N D^2}{\mu}$ in equation (III.6) has little effect on the equation for most operating conditions of ships. This postulate will be proved or disproved by experimental evidence.

For the conditions assumed in the paragraph above, equation III.6 reduces to

$$\frac{\Delta T}{T} = f\left(\frac{T}{\rho N^2 D^4}\right) \qquad \text{(III.7)}$$

or

$$\frac{\Delta T}{T} = f\left(K_t\right) \qquad \text{(III.8)}$$

where K_t is the thrust coefficient $\frac{T}{\rho N^2 D^4}$

In a similar fashion the following expression for the torque fluctuations ΔQ may be derived:-

$$\frac{\Delta Q}{Q} = f\left(K_t\right) \qquad \text{(III.9)}$$

It was found (See Section 20.2.1) that when the results for the peak-to-peak fluctuations ΔT of the thrust waveform from the sea trials results of ship B, were plotted, there was some improvement in correlation as compared with plotting ΔT versus N (See Fig.20.6). When the results for the peak-to-peak fluctuations ΔQ of the torque

waveform, from the sea trials results of ships A and B were plotted, there was a remarkable improvement in correlation as compared with plotting ΔQ versus N (See Fig. 20.5). In the thrust case, the results fell into two groups depending on whether the wind was ahead or astern. In the torque case, curiously the wind made little difference. The results for the two ships in the torque case, fell into two different lines, as would be expected from the different fouling conditions of these vessels (as shown by the differences in resistance constant)

The improvement in correlation when plotting according to equations (III.8) and (III.9) indicates that the postulate about independence from Reynolds number is not too much in error.

It is tentatively recommended, therefore, that the results of future ship tests be plotted in the dimensionless form indicated by equations (III.8) and (III.9).

APPENDIX IV

STEADY - STATE PERFORMANCE OF SHIP B

The steady-state torque characteristics of ship B have already been given in Section 17.7. It was there shown that the torque was given by the following equations:-

Test Series B1

$$Q = 1344\, N^{2.19} \qquad \text{(IV.1)}$$

Test Series B2-B

$$Q = 1006\, N^{2.25} \qquad \text{(IV.2)}$$

where Q is in lbf-ft and N is in radian/second

The equation for Test Series B2-B may also be used for Series B2-A for conditions when the draft was 30 ft and the sea depth was greater than 70-80 ft.

The thrust for the two sets of conditions is given in Fig. IV.1. The values given in the figure for Test Series B2-B may also be used for Series B2-A for conditions when the draft was 30 ft and the sea depth was greater than 70-80 ft.

Fig. IV.1 Thrust characteristics of Ship B.

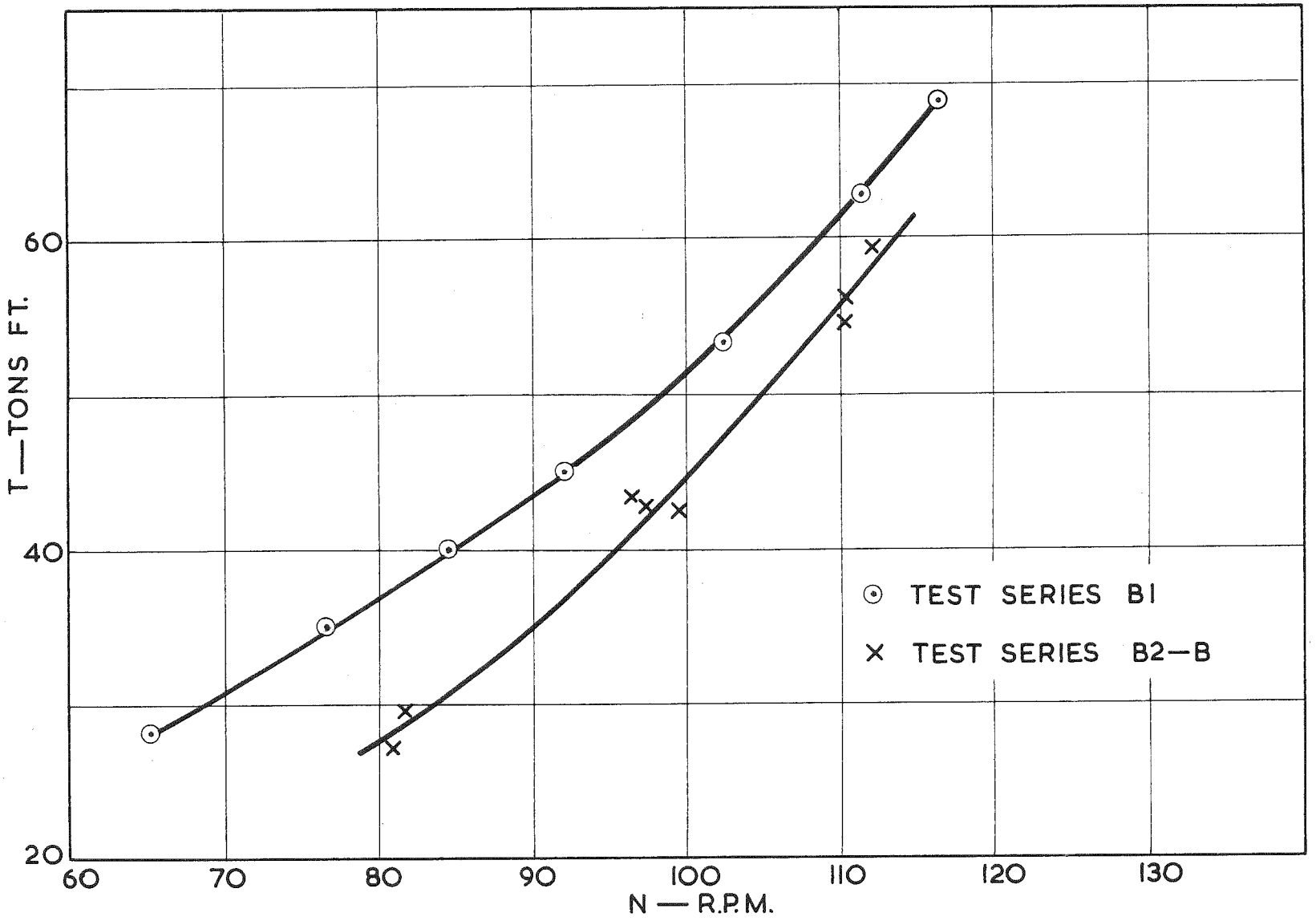
T — TONS FT.
60
40
20
60
70
80
90
100
110
120
130
N — R.P.M.
TEST SERIES B1
TEST SERIES B2—B

APPENDIX V

PUBLICATIONS SUBMITTED AS ADDITIONAL EVIDENCE.

(This appendix is bound as a separate accompanying volume)

BIBLIOGRAPHY

CHAPTER REFERENCE		
0.1	NORRIE, D.H.	"The Towing of Small Ship Models" Bulletin of Mechanical Engineering Education, Vol 3,pp 1-7,1964.
0.2	SEATON, A.J.	"Small Ship Model Resistance Testing" Thesis for Degree of Bachelor of Engineering, University of Adelaide, 1959.
0.3	SIMON,R.	"Experimental Investigation of Resistance and Form Factor for a Ship Model" Thesis for Degree of Bachelor of Engineering,University of Adelaide,1960.
0.4	PANASUNAN	"Further Investigation of Ship Resistance and Form Factor" Thesis for Degree of Bachelor of Engineering, University of Adelaide,1961.
1.1	VOIGT,H.	"Einige neure Erkenntnisse und Erfahrungen bei Schiffsvibrationen" Jarbuch Schiffbautechnische Gesellchaft Vol 47, Feburary 1953. (Translated as "Recent Findings and Emperical Data obtained in the Field of Ship Vibrations", David Taylor Model Basin Translation 268, Feb. 1958.
1.2	-	"Bibliography on Ship Vibrations" Available from business office of Schiffbautechnische Gessellschaft.
1.3	SCHUSTER,S.	"Propellers in Non-Uniform Wakes: A Summary of Published Work" Proceedings 10th International Towing Tank Conference,London,1963.
1.4	LEWIS,F.M.	"Propeller-Vibration Forces" Preprint No.5, Annual Meeting Nov.14-15, 1963, The Society of Naval Architects and Marine Engineers.

1.5 SILVERLEAF,A. MARWOOD, W.J. and BOYLE,H.B. "Some Ship and Model Measurements of Unsteady Propeller Forces" Transactions of the Royal Institution of Naval Architects,1964a.

1.6 NORRIE, D.H and HALE, M.R "Hydrojet Propulsion Research at the University of Adelaide" Engineering, 1964a.

1.7 PANAGAPULOS,E. "Design Stage Calculation of Torsional,Axial and Lateral Vibrations in Marine Shafting" Transactions of the Society of Naval Architects and Marine Engineers, vol. 58, 1950

1.8 HARRIS, C.M. and CREDE, C.E "Shock and Vibration Handbook" (in 3 vols), vol.3, McGraw-Hill, New York, 1961.

1.9 KJAER, V.A. "Vertical Vibrations in Cargo and Passenger Ships" Acta Polytechnica Scandinavia Me 2 (AP 244/1958) Mechanical Engineering series.

1.10 LEWIS, F.M. and TACHMINDJI, A.J. "Propeller Forces Exciting Hull Vibration" Transactions of the Society of Naval Architects and Marine Engineers, vol.62, 1954.

1.11 LEWIS, F.M. "Propeller Vibration" Transactions of the Society of Naval Architects and Marine Engineers, vol.43-44 1935-6.

1.12 KROHN,J. and WERELDSMA, R. "Comparative Model Tests on Dynamic Propeller Forces" International Shipbuilding Progress vol.7, No. 76, Dec.1960.

1.13 VAN MANEN, J.D. and KAMBS,J. "Effect of Shape of Afterbody on Propulsion" Transactions of the Society of Naval Architects and Marine Engineers.

1.14 STRUNTY, PIEN, HINTERTHAN and FICKEN. "Series 60 - The Effect of Variations in Afterbody Shape upon Resistance, Power, Wake Distribution and Propeller Excited Vibratory Forces" Transactions of the Society of Naval Architects and Marine Engineers, vol.68, 1960.

1.15 - "Propellers - Five Blades or Four" LLoyd's Bulletin 100A1, No.7, 1961.

2.1 DAVIES, P.O.A.L. "Some Aspects of the Design of Research Circulating Water Tunnels" Journal of the Institution of Engineers, Australia, vol. 26, No.6, June 1954.

2.2 BATCHELOR, G.K. and SHAW, F.S. "A Consideration of the Design of Wind Tunnel Contractions" Australian Council for Aeronautics Report AC 44, 1944.

2.3 TAYLOR, G.I. and BATCHELOR, G.K. "The Effect of Wire Gauge on Small Disturbances in a Uniform Stream" Quarterly Journal of Mechanics and Applied Mathematics. vol. 2, March 1949.

2.4 WOOD, A.E.R. "The Dynamics of the Adelaide University Water Tunnel" University of Adelaide, Department of Mechanical Engineering, Post-graduate Seminar, Oct. 1954.

3.1 TOSTEVIN, G.M. "Ship Propeller Vibration" Master of Engineering Thesis, University of Adelaide, 1956.

3.2 WATKINS, E.H. "Studies in Marine Propeller Vibrations" Master of Engineering Thesis, University of Adelaide, 1959.

4.1. KU, Y.H. "The Analysis and Control of Non-Linear Systems" Roland Press 1958.

4.2 PEI-SU HSIA "Graphical Analysis for Non-Linear Systems" Institution of Electrical Engineers Preprint M1168 (Measurements Section Paper), 1951.

4.3 TIMOSHENKO, S. "Vibration Problems in Engineering" pp 155-157, 3rd edition, van Nostrand, 1955.

5.1 THOMSON, W.T. "Mechanical Vibrations" p 54, Allen and Unwin, 1950.

5.2 THOMSON, W.T. "Mechanical Vibrations" p 46, Allen and Unwin, 1950.

5.3 THOMSON, W.T. "Mechanical Vibrations" p.45, Allen and Unwin, 1950.

6.1 SAUNDERS, H.E. "Hydrodynamics in Ship Design" p 437, vol. 2. Published by Society of Naval Architects and Marine Engineers (1957).

6.2 BRAHMIG, R. "Experimental Determination of the Hydrodynamic Increase in Mass in Oscillating Bodies" No.11 Schiffbau (June 1940) and No.12 Schiffbau (June 1940) Translated as Translation 118 by David Taylor Model Basin, 1943.

6.3 GUNTZBERGER, H. "Effet Amortisseur de l'helice sur les oscillations de torsion des lignes d'arbes" (Buffer effect of the propeller on the torsional vibrations of line shafting) Bulletin de l'Association Technique Maritime et Aeronautique, vol.39.Paris, 1935.

6.4 BAUMANN, H. "Tragheitsmoment und Dampfung Belasteter Schiffsschrauben" (Damping and Moment of Inertia of Loaded Propellers) Werft-Reederei-Hafen, vol. 20, No.16,1939.

6.5 McGOLDRICK, R.T. "Effect of Entrained Water in the Mass Moment of Inertia of Ship Propellers" Experimental Model Basin (now David Taylor Model Basin) Report 307, July 1931.

6.6 KANE, J.R and McGOLDRICK, R.T "Longitudinal Vibration of Marine Propulsion Shafting Systems" Society of Naval Architects and Marine Engineers, vol.57, 1949.

6.7 LEWIS, F.M. and AUSLAENDER, J. "Virtual Inertia of Propellers" Journal of Ship Research, vol.3, No.4, March 1960.

6.8 THOMSEN "Dynamische Modell-Messingen bei Propeller-Schwingungen" Schiff and Hafen, Feb. 1961.

6.9 BURRILL, L.C and ROBSON, W. "Virtual Mass and Moment of Inertia of Propellers". Transactions of North-East Coast Institution of Engineers and Ship-Builders, Vol.78, 1962.

8.1 JACOBSEN, L.S. "Steady Forced Vibration as Influenced by Damping. An Approximate Solution of the Steady Forced Vibration of a System of One Degree of Freedom under the Influence of Various Types of Damping" Transactions of the American Society of Mechanical Engineers, vol.52, APM-52-15, 1930.

8.2 STREETER, V.L. "Handbook of Fluid Dynamics" Section 10, McGraw Hill, 1961.

11.1 NORRIE, D.H. "Research in Propulsion Vibration at the University of Adelaide" Transactions of Royal Institution of Naval Architects, 1964a

11.2 NORRIE, D.H. "The Research Water Tunnel Facility at the University of Adelaide" Journal of Institution of Engineers, Australia, vol.36, Nos. 1-2, Jan-Feb 1964.

11.3	NORRIE, D.H.	"Strain Gauge Instrumentation for Simultaneous Measurement of Torque and Thrust" Australian Journal of Instrument Technology, vol. 20, No.1,Feb.1964.
11.4	TOSTEVIN, G.M.	"Ship Propeller Vibration" Master of Engineering Thesis 1956, University of Adelaide.
11.5	LERBS, H.W	pp 156-158 of Discussion in Ref.11.6
11.6	MURRAY, A.B. KORVIN-KROUKOVSKY,B.V. and LEWIS, E.V.	"Self-Propulsion Tests with Small Models" Transactions of Society of Naval Architects and Marine Engineers, vol.59,pp129-167, 1951.
11.7	LEAPER, J.L.	Admiralty Research Laboratory (Private communication 25th Nov.1963)
11.8	O'BRIEN,T.P.	"The Design of Marine Screw Propellers" P 41, Hutchinson, 1962.
11.9	WOOD and HARRIS	"Some Notes on the Theory of an Airscrew Working in a Wind Channel. Advisory Committee for Aeronautics R & M 662,1920.
12.1	FOTTINGER,H.	Zeitschrift fur Flugtechnik und Motorluftechiffahrt, p 234, 1912.
12.2	FOTTINGER, H.	"Fortschritte der Stromungslehre im Maschinenbau und Schiffbau" (Advances in the Theory of Flow in Engineering and Shipbuilding) Jahrbuch der Schiffbau-technischan Gessellschaft, vol.25,pp295-344,1924 (Translated as Taylor Model Basin,Translation 48)
12.3	BURRILL, L.C. and BOGGIS, A.C.	"Electronics in Naval Architecture" North-East Coast Institution of Engineers and Shipbuilders.vol.67,1951.

12.4	NORRIE, D.H.	"Marine Propeller Vibration Research at the University of Adelaide" Proceedings of First Australasian Conference on Fluid Mechanics and Hydraulics (Perth 8-13 December 1962) Published by Pergammon Press.
12.5	PRICE, R.I.	"Effect of Entrained Water on Virtual Inertia of Ship Propellers". Naval Engineering Thesis, Massachussetts Institute of Technology, June 1955. (Results partially reproduced in Ref.7)
12.6	GARIBOLDI, R.J.	"Procedure for Torsional Vibration Analysis of Multimass Systems" Buships, Navy Dept. Unclassified Research and Development Report, 371-V-19, Dec.1953.
14.1	STRAHLE, D.G. and DUNNE, L.G.	"Time - Multiplexed Telemetering of Strain-Gauge Bridges using D.C. - Pulse Techniques" Weapon Research Establishment (Salisbury S.A) Rech.Memo.S.A.D.105, July 1958.
15.1	BENETEAU, P.J and MURARI, E.	"D.C.Amplifiers Using Transistors" Electronic Engineering vol.35, No.422 pp 257-259, April 1963.
16.1	HILGER & WATTS LTD.	"Instructions for Use of the Mechanical Digitiser FD8".
17.1	MANLEY, R.G	"Waveform Analysis" Chapman and Hall, 1945.
17.2	-	"Interpolation and Allied Tables" His Majesty's Stationary Office.
17.3	GARIBOLDI, R.J.	"Procedure for Torsional Vibration Analysis of Multimass Systems" Department of the (U.S) Navy, Bureau of Ships, Research and Development Report 371-V-19, December 1953.

17.4 FREBERG,C.R. and KEMLER,E.N. "Elements of Mechanical Vibration" John Wiley, 1943.

17.5 DEN HARTOG,J.P. "Mechanical Vibrations" McGraw Hill, 1947.

19.1 VAN LAMMEREN,W.P.A. "Resistance,Propulsion and Steering of Ships" Technical Publishing Co (Holland),1948.

20.1 SILVERLEAF,A. MARWOOD,W.J, and BOYLE, H.B. "Some Ship and Model Measurements of Unsteady Propeller Forces" Transactions of the Royal Institution of Naval Architects,1964b.

20.2 LEWIS,F.M. and AUSLAENDER,J. "Virtual Inertia of Propellers" Journal of Ship Research, vol.3, No.4, March 1960.

22.1 VAN MANEN,J.D. "Fundamentals of Ship Resistance and Propulsion" Part B, p 120, Netherlands Ship Model Basin, Publication 132a.